Internal erosion in soil hydraulic structures and behavior of eroded soils under complex hydro-mechanical stresses

Bikram Oli

THESE DE DOCTORAT

NANTES UNIVERSITE

ECOLE DOCTORALE N° 602
Sciences de l'Ingénierie et des Systèmes
Spécialité : « *Génie Civil* »

Par

« Bikram OLI »

« Internal erosion in soil hydraulic structures and behavior of eroded soils under complex hydro-mechanical stresses »

Thèse présentée et soutenue à « Saint Nazaire », le « 19 décembre 2023 »
Unité de recherche : GeM-Institut de recherche en génie civil et mécanique- UMR CNRS 6183, F-44600

Rapporteurs avant soutenance :

Jean CÔTÉ Professeur, Université Laval
Eric VINCENS Professeur, École Centrale de Lyon

Composition du Jury :

Président :	Philippe REIFFSTECK	Directeur de Recherche, Université Gustave Eiffel
Examinateurs :	Nadia BENAHMED	Chargée de Recherche, INRAE
	Philippe REIFFSTECK	Directeur de Recherche, Université Gustave Eiffel
Directeur de thèse :	Didier MAROT	Professeur, Nantes Université
Co-encadrants :	Rachel GELET	Maître de Conférences, Nantes Université
	Fateh BENDAHMANE	Maître de Conférences, Nantes Université
Invité		
	Jean-Robert COURIVAUD	Ingénieur Expert, EDF CIH

Abstract

Suffusion is a complex internal erosion mechanism involving the dislodgment, transport and partial filtration of fine particles within granular soils. It poses significant challenges in the maintenance of hydraulic earth-structures. This study analysis the suffusion behavior utilizing a newly developed triaxial permeameter capable of precise control over hydraulic and mechanical conditions. The influence of two important factors on the suffusion behavior is studied: the mechanical stress state and cyclic hydraulic loadings. Regarding the first study, four gap-graded cohesionless soils were subjected to various stress states: oedometric, triaxial isotropic, triaxial compressive and triaxial tensile conditions. The oedometric stress state is historically the reference stress state. A systematic approach was employed to characterize each suffusion phases: initiation, self-filtration, blow-out and steady state, from the temporal evolution of: the hydraulic conductivity, the erosion rate, the cumulative eroded mass and the cumulative expended energy. Notably, the impact of the stress state on the steady state proved limited compared to microstructural effects, although oedometric stress conditions accelerated the blow-out phase through circumferential preferential flow paths. For the second study, complex cyclic hydraulic loadings are studied with respect to piecewise increasing multi-stage hydraulic loadings that are commonly used. Notably, the influence of initiation point of the cyclic loading was found significant.

Résume

La suffusion est un mécanisme d'érosion interne, impliquant le détachement, le transport et la filtration partielle des particules fines dans un sol granulaire. Il génère d'importants problèmes de maintenance pour les structures hydrauliques en terre. Cette étude analyse le phénomène de suffusion grâce à un nouveau perméamètre triaxial, permettant le contrôle précis des chargements mécaniques et hydrauliques. L'influence sur la suffusion de deux facteurs importants est étudiée : l'état mécanique, et les chargements hydrauliques cycliques. En ce qui concerne la première étude, quatre sols lacunaires sont soumis à différents états mécaniques : œdométrique, isotrope triaxial, compression triaxiale et extension triaxiale. L'état œdométrique est l'état de référence dans la littérature. Une approche systématique est utilisée pour caractériser chaque étape du processus de suffusion : l'initiation, l'auto- filtration, le débourrage et l'état permanent ; à partir des évolutions temporelles : de la conductivité hydraulique, du taux d'érosion, de la masse érodée cumulée et de l'énergie cumulée dissipée par l'écoulement. Finalement, l'impact de l'état mécanique sur l'état permanent de la suffusion apparait limité, en comparaison de l'impact de la microstructure. Toutefois l'état œdométrique accélère l'apparition du débourrage, grâce à des chemins d'écoulements préférentiels. Pour la seconde étude, plusieurs chargements hydrauliques cycliques sont étudiés et comparés au chargement hydraulique croissant par palier, couramment utilisé. Le point d'initiation du cycle influence significativement l'initiation du débourrage.

Résume étendu

Contexte général et objectifs

Les ouvrages hydrauliques assurent de nombreuses et importantes missions en termes de production d'hydroélectricité, de protection contre les inondations, de production d'eau potable ou destinée à l'irrigation. Ils permettent également la navigation fluviale ou l'installation d'infrastructures de loisir. Les linéaires de ces ouvrages sont donc très conséquents, ce qui amène le choix du sol comme principal matériau de construction. Toutefois plusieurs études statistiques (ICOLD, 1995 ; Foster et al., 2000 ; Richards et Reddy, 2007) ont mis en évidence l'importance de l'effectif des instabilités que peuvent subir les ouvrages hydrauliques en terre, très majoritairement par érosion externe ou interne. En conséquence, il apparaît nécessaire de caractériser la sensibilité des sols constituant les ouvrages hydrauliques en terre ou leur fondation, vis-à-vis des phénomènes d'érosion et plus particulièrement les phénomènes d'érosion interne. Parmi les quatre mécanismes d'érosion interne, la suffusion apparaît comme l'un des plus complexes, or la majeure partie des essais de suffusion détaillés dans la littérature a été mené sous chargements mécaniques œdométriques et sous sollicitations hydrauliques monotones. Pourtant sur site, les chargements hydromécaniques appliqués aux sols peuvent être très différents. Dans ce contexte, un nouveau dispositif triaxial est développé afin de réaliser des essais de suffusion sous chargements hydromécaniques complexes. Deux études paramétriques sont menées afin d'étudier indépendamment l'influence de l'état mécanique et celle du chemin de chargement hydraulique, tout en s'assurant de la répétitivité des essais.

Revue bibliographique

Le chapitre dédié à la revue bibliographique permet tout d'abord de différencier les quatre mécanismes d'érosion interne (Fell et Fry, 2007) : l'érosion de conduit, l'érosion régressive, l'érosion de contact et la suffusion. Ce quatrième mécanisme mobilise la fraction fine dont certains grains peuvent être détachés par l'écoulement, puis être transportés entre les constrictions de la fraction grossière. Au cours de ce transport, certains grains détachés peuvent être bloqués. L'ensemble de ces processus va entraîner une modification de la distribution granulométrique, mais également de la porosité et de la perméabilité du milieu poreux.

Les principaux paramètres influençant ce processus complexe sont identifiés, notamment la distribution granulométrique. Dans la littérature sont présentés plusieurs critères (US Army, 1953 ; Istomina, 1957 ; Kezdi, 1969 ; Sherard, 1979 ; Kenney et Lau, 1985 ; Burenkova, 1993 ; Li et Fannin, 2008 ; Wan et Fell, 2008 ; Indraratna et al., 2011, 2015 ; Chang et Zhang, 2013b) basés sur la distribution granulométrique et qui proposent un premier criblage quant à la potentielle sensibilité des sols vis-à-vis de la suffusion. Toutefois, ces critères ne considèrent que deux possibilités : sol « stable » ou « instable ». Par ailleurs, l'influence de plusieurs paramètres n'est pas prise en compte, notamment la forme des grains, la densité, la microstructure, l'état mécanique et le chemin de chargement hydraulique. L'influence de ces deux derniers paramètres apparaît particulièrement intéressante à étudier, car les configurations jusqu'alors utilisées lors de

nombreux essais détaillés dans la littérature peuvent être très différentes des configurations sur site. Chang et Zhang (2013a) ont notamment conclu à une influence significative de l'état mécanique sur le gradient de déformation du squelette, avec toutefois une interrogation sur la valeur de ce gradient sous chargement mécanique isotrope. Plusieurs études ont également mis en exergue des différences de développements de la suffusion, en fonction du chemin de chargement hydraulique (Nguyen et al., 2012 ; Luo et al., 2013 ; Rochim et al., 2017 ; Takahashi, 2023) qui sur site peut énormément varier en fonction par exemple, des intempéries ou de la localisation considérée dans l'ouvrage. Or pour la plupart des essais détaillés dans la littérature, la sollicitation hydraulique était systématiquement croissante. Cependant, il convient de souligner que Prasomsri et Takahashi (2021) ont mené des essais sous chargement hydraulique cyclique, ce qui a notamment permis de montrer l'accroissement de la masse érodée avec le nombre de cycles appliqués. Malheureusement, les auteurs n'ont pas comparé leurs résultats avec ceux d'un essai sous chargement monotone et l'amplitude des cycles était constante. Enfin Takahashi (2023) a souligné la complexité du comportement mécanique des échantillons érodés, qui semble être différent lors d'essais de suffusion menés à débit imposé ou à gradient hydraulique imposé. Cette observation suggère que l'état érodé n'est pas précisément défini. Chen and Zhang (2023) ont également réalisé des essais sous chargement hydraulique cyclique, mais les valeurs de gradient hydraulique appliqué étaient très élevées et peu représentatives des valeurs in-situ.

La majeure partie des essais détaillés dans la littérature a été menée à l'aide de perméamètres à paroi rigide (Sherard et al., 1984 ; Kenney et Lau, 1985 ; Skempton et Brogan, 1994 ; Wan et Fell, 2002 ; Ke et Takahashi, 2012b ; Marot et al., 2020 ; …). Cependant avec l'objectif de limiter les écoulements préférentiels entre l'échantillon et la cellule rigide, ainsi que pour contrôler l'état mécanique appliqué à l'échantillon, plusieurs bancs triaxiaux ont également été développés (Bendahmane et al., 2008 ; Chang et Zhang, 2011 ; Ke et Takahashi, 2014b ; Slangen et Fannin, 2017). Les caractéristiques techniques de ces différents dispositifs sont comparées, permettant ainsi d'identifier les principales caractéristiques du nouveau dispositif.

Développement d'un appareillage triaxial modifié

Le dispositif développé repose sur le principe d'une cellule triaxiale, qui est modifiée afin de permettre l'application sur l'échantillon, d'un écoulement vertical descendant et de collecter les grains érodés. La méthodologie expérimentale comporte 4 étapes successives : la saturation, la consolidation, l'érosion puis l'analyse granulométrique post-suffusion par couches. La position verticale du réservoir amont est pilotée automatiquement, afin de contrôler précisément la phase de saturation de l'échantillon, sous écoulement ascendant avec une vitesse de montée de 0.25 mm/min. L'étape de consolidation consiste à appliquer sur l'échantillon, un chemin de contrainte effective jusqu'à atteindre une contrainte effective moyenne de 70 kPa. Par ailleurs, le vérin permet l'application d'une contrainte axiale, aussi bien en compression qu'en extension. La contrainte effective principale est donc verticale ou horizontale, c'est-à-dire parallèle ou perpendiculaire à l'écoulement. Comme le dispositif permet de piloter automatiquement la position du réservoir amont, l'écart de charge hydraulique appliqué à l'échantillon peut être modifié durant toute la phase d'érosion. Le dispositif permet donc de reproduire des fluctuations de charge hydraulique qui peuvent se produire sur site, notamment en raison de variations du

niveau d'eau dans la rivière ou la retenue. Après la phase d'érosion, l'analyse post-suffusion consiste à extraire soigneusement l'échantillon, qui est ensuite congelé puis découpé en quatre couches et à réaliser une inspection visuelle des quatre couches. Chaque couche est ensuite soumise à une analyse de la distribution granulométrique, pour comprendre les effets de la suffusion sur la migration des particules fines. Le dispositif est doté d'un système complet d'instrumentations afin de mesurer au cours du temps : l'écart de pression entre les sections amont et aval de l'échantillon, la pression de confinement, le déviateur de contrainte, les variations du volume de l'échantillon, sa déformation axiale et le débit d'eau injecté. Un code sous Labview a été développé afin d'acquérir automatiquement les données susmentionnées et de suivre continument le gradient hydraulique ainsi que la conductivité hydraulique. Afin de valider la caractérisation du comportement mécanique d'échantillons de sol, réalisée à l'aide du nouveau dispositif, des essais ont également été réalisés avec un banc triaxial du commerce. La bonne concordance des résultats a démontré la fiabilité et la précision du nouvel appareil. Pour la validation de la caractérisation de la sensibilité à la suffusion, les résultats d'un essai avec le nouvel appareil ont été comparés à un test de référence réalisé avec un autre dispositif. Quelques différences dans la masse érodée et l'indice de résistance à l'érosion ont été mesurées. Toutefois elles sont attribuées à des modifications dans la configuration de réalisation des essais. En outre, les évolutions de conductivité hydraulique sont concordantes et le nouvel appareil a reproduit avec succès les différentes phases d'évolution du phénomène de suffusion. En conclusion, l'appareil triaxial modifié développé et sa procédure expérimentale fournissent une plate-forme robuste et efficace pour étudier la suffusion et ses effets sur le comportement mécanique des sols. Par ailleurs, le pilotage automatique du positionnement du réservoir amont améliore l'efficacité et la fiabilité des tests expérimentaux, ouvrant ainsi la voie à des recherches plus approfondies dans le domaine de l'ingénierie géotechnique.

Influence de l'état mécanique sur l'initiation et le développement de la suffusion

Afin de caractériser l'influence de l'état mécanique sur la suffusion, 25 essais ont été réalisés sur des mélanges sable-gravier, donc à distribution lacunaire et comprenant 15%, 25%, 35% ou 40% de sable. Cette investigation a impliqué quatre états de contraintes spécifiques : compression triaxiale isotrope, compression triaxiale, extension triaxiale et œdométrique. L'analyse des résultats a porté sur l'ensemble du processus de suffusion et permet d'aboutir à plusieurs conclusions clés. Premièrement, pour optimiser la répétitivité de préparation des échantillons, il convient de piloter précisément l'accroissement progressif de la charge hydraulique, au cours de la phase de saturation. Deuxièmement, quatre étapes au cours du processus de suffusion sont identifiées : l'initiation, l'auto-filtration, le débourrage et l'état d'équilibre. Selon l'approche de Skempton et Brogan (1994), l'initiation est caractérisée par une augmentation initiale de la conductivité hydraulique. L'auto-filtration est marquée par une réduction de la conductivité hydraulique et du taux d'érosion. Le débourrage entraîne une augmentation de la conductivité hydraulique et du taux d'érosion, tandis que l'état d'équilibre de suffusion est atteint lorsque que la conductivité hydraulique est stabilisée et que le taux d'érosion décroit. Chaque phase peut être caractérisée par un ou plusieurs paramètres spécifiques. Conformément aux approches détaillées dans la littérature, l'initiation est représentée par le gradient hydraulique critique ou la vitesse

critique de Darcy (Côté, 2010). L'amplitude de l'auto-filtration est définie par la variation de la conductivité hydraulique en relatif par rapport à sa valeur initiale. Le débourrage est défini par le point d'inflexion de la courbe masse érodée cumulée versus énergie cumulée dissipée. A ce point d'inflexion, la sollicitation hydraulique peut être caractérisée par l'une ou l'autre des deux grandeurs suivantes : le gradient hydraulique de débourrage ou l'énergie cumulée dissipée de débourrage. Enfin l'état d'équilibre de suffusion peut être caractérisé par quatre facteurs : le pourcentage de masse érodée par rapport à la masse initiale de fines, l'indice de résistance à l'érosion, la vitesse de Darcy ou la déformation axiale.

Pour la phase d'initiation, les résultats soulignent tout d'abord la difficulté de mesurer le gradient hydraulique critique d'initiation en condition d'extension triaxiale. Cette observation nous conduit à favoriser les essais suivant les trois autres états mécaniques. Il convient aussi de noter que pour les quatre sols étudiés, l'effet de l'état mécanique sur le gradient hydraulique critique est très limité. En ce qui concerne la vitesse critique de Darcy, la prédiction proposée par Côté (2010) s'avère être du bon ordre de grandeur, bien que systématiquement plus grande que la valeur mesurée.

Pour la phase d'auto-filtration, la microstructure a une influence prédominante. Lorsque les particules fines ne remplissent que très partiellement l'espace poral compris dans la fraction grossière (microstructure dite « underfilled »), l'amplitude de l'auto-filtration est limitée. A l'inverse, lorsque les grains de la fraction grossière flottent entre les particules fines (microstructure dite « overfilled »), l'amplitude de l'auto-filtration est légèrement amplifiée. Pour la microstructure intermédiaire (en transition entre « underfilled » et « overfilled »), il y a manifestement compétition entre les processus de détachement et de filtration localisée qui engendre un accroissement de l'auto-filtration. Pour la valeur utilisée du déviateur vis-à-vis de sa valeur au pic, l'état mécanique ne semble pas avoir un effet systématique pour les quatre microstructures testées. Toutefois en condition œdométrique, les chemins d'écoulement circonférentiels raccourcissent le développement de l'auto-filtration.

Pour la phase de débourrage, les valeurs de gradient hydraulique de débourrage, comme celles de l'énergie de débourrage sont plus faibles pour la microstructure dite « underfilled ». Pour cette même microstructure, le débourrage semble insensible à l'état de contrainte en raison du rôle secondaire des particules fines dans la transmission des forces de contact inter-grains. L'effet de l'état mécanique apparaît plus marqué lorsque les particules fines et les particules grossières contribuent conjointement aux chaines de force. En conditions œdométriques, les chemins d'écoulement circonférentiels atténuent l'amplitude des paramètres de débourrage.

Pour la phase d'état d'équilibre de tous les sols testés, l'influence de l'état de contrainte sur l'indice de résistance à l'érosion semble limitée. Toutefois en conditions œdométriques, la vitesse de Darcy est plus faible que pour les autres états mécaniques. Cet état mécanique induit donc une conclusion légèrement conservative. Enfin, la valeur de l'indice de résistance à l'érosion est légèrement plus élevée pour la microstructure « underfilled » en comparaison des deux autres types de microstructure. Cette microstructure est donc classée légèrement plus résistante, mais cette classification relative est probablement due à la valeur plus faible de l'indice de vides inter-grossier.

Influence de chargements hydrauliques complexes sur l'initiation et le développement de la suffusion

Ce chapitre est consacré à l'étude de l'influence de différents chargements hydrauliques cycliques sur la suffusion d'un mélange sable-gravier contenant 25% de sable. Sont étudiés les effets : du gradient hydraulique d'initiation du cycle, de l'amplitude du cycle et enfin du nombre de cycles de chargement. Un essai nommé MHL est également réalisé sous gradient hydraulique croissant par paliers, sans cycle. L'analyse comparative de tous les résultats obtenus permet de tirer les conclusions suivantes :

1. Lorsque le gradient hydraulique d'initiation du cycle i_0 est égal à 2,5, les valeurs testées de l'amplitude du cycle (Δi = 1,1 et 2,1) n'ont pas d'influence significative sur les quatre phases de suffusion (initiation, auto-filtration, débourrage et état d'équilibre).

2. Dans cette étude, le nombre de cycles est égal à un ou deux. Pour deux valeurs différentes de gradient hydraulique d'initiation du cycle, les résultats des tests montrent que le nombre de cycles a une influence limitée sur le processus de suffusion.

3. Quatre valeurs de gradient hydraulique d'initiation du cycle (i_0 = 1,5, 2,5, 4 ou 5) ont été utilisées dans l'étude. Les résultats révèlent que pour le sol testé, lorsque i_0 est inférieur ou égal à 4, l'influence du cycle sur le processus de suffusion est limitée. Cependant, si le cycle démarre avec un gradient hydraulique d'initiation i_0 supérieur à 4, une augmentation de la masse perdue cumulée par unité de volume est observée, même pendant la phase décroissante du cycle. En outre, il convient de noter que, même si la puissance maximale atteinte avant la phase décroissante du cycle reste la même (c'est-à-dire $6{,}5*10^{-2}$ W), la croissance de la masse perdue dépend de la puissance minimale atteinte. Concrètement, si la puissance *minimale* atteinte pendant le cycle P_{min} est de $2{,}5*10^{-2}$ W, l'augmentation de masse perdue est du même ordre de grandeur que celle des autres tests. Cependant, l'augmentation de masse perdue devient bien plus significative si la puissance minimale atteinte pendant le cycle P_{min} est de $4*10^{-2}$ W.

4. Une attention particulière devrait être accordée à l'approche basée sur les gradients hydrauliques critiques, i_{HC} et i_{MVE}. Le gradient i_{HC} correspond au gradient lors d'une forte augmentation de la conductivité hydraulique, tandis que i_{MVE} correspond au point d'inflexion de la courbe de masse perdue cumulée par unité de volume versus l'énergie dissipée cumulée par unité de volume. Notamment, pour les essais cycliques réalisés avec un gradient hydraulique d'initiation i_0 égal à 5, les valeurs de i_{HC} et i_{MVE} sont inférieures à celles de l'essai MHL, qui est réalisé sous gradients hydrauliques croissant par palier, sans cycle. Autrement dit, cette méthode interprétative suggère que le sol présente une plus grande résistance en l'absence de cycle, c'est-à-dire à partir des résultats du test MHL.

5. Par rapport aux essais cycliques, l'indice de résistance à l'érosion est légèrement inférieur pour l'essai MHL. En conséquence, la classification de la susceptibilité à la suffusion basée sur le test MHL est légèrement conservatrice.

Conclusion et perspectives

Le principal objectif de cette thèse étant d'étudier l'influence de chargements hydromécaniques complexes sur le processus de suffusion, un dispositif triaxial spécifique a été développé afin de contrôler précisément lors des essais, les conditions de chargements hydrauliques et mécaniques. Ainsi, la position du réservoir amont est pilotée et l'appareil permet également d'appliquer une contrainte axiale en compression ou en extension. Les tests de validation ont confirmé la fiabilité et la précision de l'appareil, ce qui en fait un outil précieux pour l'étude du comportement de la suffusion dans des conditions contrôlées de contrainte et de chemin de chargement hydraulique.

Quatre mélanges de sable-gravier ont été soigneusement préparés (avec des teneurs en sable de 15 %, 25 %, 35 % et 40 %). Les investigations ont été réalisées sous différents états de contraintes : œdométrique, triaxiale isotrope, compression triaxiale (avec la contrainte principale dans la direction verticale) et extension triaxiale (avec la contrainte principale dans la direction horizontale). De plus, une attention particulière a été accordée afin d'assurer une bonne répétabilité de la procédure expérimentale, qui a été validée en comparant l'évolution temporelle de la conductivité hydraulique, du taux d'érosion, de la masse perdue cumulée et l'énergie dissipée cumulée.

Tout au long de ce travail, une approche systématique a été rigoureusement utilisée pour caractériser de manière exhaustive les diverses phases du processus de suffusion. Cette caractérisation est principalement fondée sur l'évolution temporelle de la conductivité hydraulique et du taux d'érosion. Quatre phases ont ainsi été identifiées : initiation, auto-filtration, débourrage et état d'équilibre. L'initiation de la suffusion est identifiée grâce à une augmentation légère mais marquée de la conductivité hydraulique (Skempton et Brogan, 1994). Par la suite, la deuxième phase met en évidence un phénomène d'auto-filtration, caractérisée par la réduction du taux d'érosion qui peut être concomitante à une réduction de la conductivité hydraulique. L'amplitude de l'auto-filtration est quantifiée par la variation relative de la conductivité hydraulique. La troisième phase se manifeste par une nette augmentation du taux d'érosion, qui peut être suivie d'une augmentation marquée de la conductivité hydraulique. Appelée « débourrage », cette phase est principalement attribuée au détachement et au transport de particules solides. Le débourrage est mieux défini au point d'inflexion de la courbe masse cumulée versus énergie cumulée dissipée. Dans la quatrième et dernière phase, la conductivité hydraulique converge vers la stabilité, tandis que le taux d'érosion connaît une tendance à la baisse. Ce comportement peut s'expliquer par la présence d'une ou plusieurs voies d'écoulement préférentiel créées par le processus d'érosion, aboutissant finalement à un état d'équilibre. Cet état d'équilibre peut être caractérisé par plusieurs paramètres pertinents tels que la déformation axiale finale, l'indice de résistance à l'érosion, la vitesse de Darcy et le pourcentage de masse perdue.

Pour certains essais menés en conditions œdométrique, isotrope ou déviatorique en compression, un gradient hydraulique d'initiation unique de 0,2 a été mesuré, ce qui indique que le gradient hydraulique critique est peu influencé par l'état de contrainte. Cependant, dans un état d'extension triaxiale, l'initiation telle que définie par Skempton et Brogan (1994) n'a pas pu être observée. Dans ce contexte, les états de compression triaxiale, contrainte isotrope ou œdométrique doivent être privilégiés pour mesurer les paramètres relatifs à l'initiation (gradients hydrauliques critiques ou

vitesses critiques de Darcy). L'auto-filtration est amplifiée pour les microstructures de types intermédiaires, c'est à dire comprises entre les microstructures dites « underfilled » et « overfilled ».

Des différences notables sont apparues lors de la comparaison des tests effectués dans des états de contrainte œdométrique et de compression triaxiale. La phase d'auto-filtration est plus courte dans la configuration œdométrique, permettant un débourrage plus précoce. Par ailleurs, l'analyse détaillée des distributions granulométriques post-suffusion et des coupes transversales a révélé que l'état de contrainte œdométrique favorise les écoulements préférentiels circonférentiels, ce qui entraîne un délai raccourci pour atteindre le débourrage. Cet état de contrainte s'accompagne donc d'une caractérisation légèrement plus conservative. Enfin, l'influence de l'état de contrainte sur l'état d'équilibre de la suffusion a été explorée, révélant pour tous les sols testés, une sensibilité bien plus limitée que l'influence de la microstructure.

L'étude approfondie de l'influence de chargements hydrauliques cycliques sur le processus de suffusion a fourni des informations précieuses pour les pratiques d'ingénierie. Un résultat significatif est le rôle joué par le gradient d'initiation du chargement cyclique i_0. Pour le sol testé et l'état de contrainte choisi, si i_0 est inférieur à 4, l'influence du cycle est très limitée. Par contre si i_0 est supérieur à 4, un comportement de type endommagement est observé, c'est-à-dire que le débourrage se produit pour un gradient plus faible que l'essai de référence réalisé sans cycle, y compris lors de la phase décroissante du cycle. L'étude exploratoire de l'influence de l'amplitude du chargement cyclique Δi a révélé que les deux amplitudes testées (1,1 à 2,1) n'exerçaient pas d'influence significative sur l'ensemble du développement de la suffusion. Par ailleurs, l'influence du nombre de cycles de chargement (1 ou 2) apparaît également limitée.

La communauté scientifique compare principalement le comportement mécanique d'échantillons de sol non érodés à celui de leurs homologues érodés, sans tenir compte du degré d'érosion de ces matériaux (Chang et Zhang, 2011 ; Chang et al., 2014 ; Ke et Takahashi, 2014a, 2014b, 2015 ; Mehdizadeh et al., 2017 ; Mehdizadeh, 2018). Une considération importante dans ce contexte est la définition de paramètres pour caractériser chaque phase du processus de suffusion, améliorant ainsi la comparaison mécanique post-suffusion pour différents degrés de suffusion. De plus, l'homogénéité post-suffusion de chaque échantillon doit être caractérisée avant d'effectuer un essai mécanique post-suffusion, car le degré d'hétérogénéité peut affecter l'interprétation de l'essai mécanique. A ce jour, il n'existe aucune norme concernant le choix de la grille ou du tamis de sortie placé à l'extrémité aval de l'éprouvette. Souvent, cette ouverture est choisie pour permettre le détachement des particules les plus fines et retenir les plus grosses. Or sur site, les conditions de sortie des particules érodées peuvent être extrêmement variables. Par conséquent, la suffusion devrait probablement être analysée pour une gamme représentative d'ouvertures de sortie, qui pourraient être calculées à partir de la taille moyenne de constriction (Seblany et al., 2021). De plus, il convient de faire très attention à cette ouverture, lors de la caractérisation mécanique post-suffusion, car une augmentation de la contrainte déviatorique peut provoquer l'extrusion d'une partie de l'échantillon à travers cette grille. En outre, les recherches futures devraient se concentrer sur l'analyse des paramètres liés à la suffusion qui doivent être discutés en fonction la taille de l'échantillon, du chemin de chargement hydraulique et de l'orientation de l'écoulement par rapport

à la gravité. En d'autres termes, il convient d'évaluer le caractère intrinsèque de ces paramètres, ou du moins de préciser clairement leur domaine de validité. De telles investigations permettraient une utilisation plus éclairée de ces paramètres dans les lois de comportement (Kodieh et al., 2021 ; Gelet et Marot, 2022). Jusqu'à présent, les tests de répétabilité sont rarement effectués et sont principalement utilisés pour vérifier la validité d'une procédure expérimentale donnée. Cependant, les tests de répétabilité peuvent également être utilisés pour mesurer l'ampleur de la variation ou de la dispersion d'un ensemble de paramètres. La communauté scientifique gagnerait à proposer une standardisation des tests de suffusion. Une telle norme permettrait (i) une meilleure comparaison entre plusieurs études, (ii) une mise en service rigoureuse de nouveaux appareils et (iii) pourrait servir de référence pour valider des lois de comportement. Par ailleurs la réalisation d'un benchmark expérimental permettrait la constitution d'une base de données qui pourrait être publiée en libre accès et plusieurs méthodes d'interprétation pourraient être proposées (Marot et Bowman, 2022). Concernant l'influence des chemins de chargement hydrauliques cycliques sur le comportement global de la suffusion, les résultats obtenus restent exploratoires, de sorte qu'une grande variété de configurations reste à explorer. Par exemple, les résultats obtenus doivent être confirmés pour d'autres pourcentages de fins et d'autres états de contrainte. L'effet d'endommagement, lié au chargement hydraulique cyclique (exprimé en gradient hydraulique ou en puissance dissipée par l'écoulement) doit être confirmé par des essais complémentaires. Enfin, les essais de laboratoire sont souvent réalisés en quelques heures alors que sur site, les sols peuvent être soumis à des sollicitations sur plusieurs jours. Par conséquent, la validité des observations devrait être confirmée par la réalisation de tests à long terme.

En se concentrant sur ces objectifs de recherche, les études futures peuvent faire progresser considérablement la compréhension du processus de suffusion et contribuer au développement de procédures standardisées pour améliorer la cohérence et la fiabilité des protocoles de test de suffusion. Ces perspectives visent collectivement à améliorer la rigueur et la cohérence de la recherche dans ce domaine, produisant à terme des informations plus fiables et plus complètes sur le comportement hydromécanique couplé des sols suffusifs.

Acknowledgement

I would like to begin by expressing my profound gratitude to Prof. Jean-Claude Badoux and Prof. Ramesh Kumar Maskey for their unwavering support and guidance, which ignited and nurtured my passion for research. Their mentorship has been pivotal in shaping my academic journey.

My deepest appreciation goes to my thesis supervisors, Didier Marot, Rachel Gelet, and Fateh Bendahmane, who have played an instrumental role in shaping the trajectory of my research and have provided me with invaluable guidance, expertise, and unwavering support throughout this academic journey. I would also like to extend my appreciation to the External Supervisory Committee Members, Prof. Benahmed Nadia and Prof. Luc Sibille, for their valuable remarks and suggestions.

I am profoundly grateful to the companies EDF and VERBUND for their generous financial support, and to the management from Capacités SAS, which has been instrumental in advancing my research endeavors. Their funding has truly made a difference. I extend my heartfelt thanks to Laurence Guihéneuf and Claire Lemoine from Capacités SAS for their indispensable administrative and technical support. Their contributions have been essential to the success of this work. I also want to acknowledge Philippe Leroy for his valuable technical contributions.

For their friendship and day-to-day support, I thank my friends: Motu & Chotu, Sandip, Subash, Bishal, Remun, Satendra, Kaichi, Golthay, Duday, Ghale, Chiku, Biplov, Abiral, Rishab, GCT, Anil, Pratik, Pramod, Poshan, Tilak, Aashish, Anupama, Ranju, Deepa, Bibek, Anish, Binita, Aakash, Aagana, Aashutish, Pratiksha, Sumi, Ajeena, Sunita, Bhawana, Ganesh, Nitesh, Mahesh, Khumay, Zahidul Karim, Shila, Vinamasu Hiroyuki, Andronikis, Hammad, Ahmed, Seong-Hoon Hwang, Luisa, Lee, Patrycja, Estifanos Addisu, Nuhamin, Lina, Abubakar, Mahdi, Amina, Lisa, Aty, Hikmatullah, JK, Giress, Paul, Mhamad Ali Ahmad, Theo, Yameng, Junior, Karim, Gayelle, Youssef, Jack, Remy, Bouba, Lara, Ali, Khodor, Mohamed, Timothee, Nadin, Mahmoud, Shadi, Raid, and Maryam.

To my wife, Suzu, I offer special thanks for her enduring support, her patience, and her ability to infuse humor into even the most challenging and stressful moments of this doctoral pursuit. Long-distance hardships were made bearable through her unwavering presence.

Lastly, my gratitude goes to my parents and family for their unwavering love, encouragement, and belief in my abilities. Their support has been the bedrock upon which I built this academic achievement. I am profoundly grateful to all of you for being an integral part of this significant chapter in my life.

Bikram OLI
Saint-Nazaire, France
December 2023

Table of content

List of figures

List of tables

List of symbols

α	Stress-reduction factor
$\lvert\Delta k\rvert / k_{ini}$	Normalized hydraulic conductivity variation
Δh	Hydraulic head drop (m)
Δi	Cyclic gradient amplitude
Δk	Difference in hydraulic conductivity (k) between self-filtration phase extremes
Δm	Resolution of load cell / mass balance
ΔP	Pressure drop between upstream and downstream sections (Pa)
Δt	Hydraulic loading step duration
Δz	Height of the soil layers
D'_{15}	Diameter of coarse fraction such that 15% by weight of soil is finer than this size
D_{60}	Diameter of particles such that 60% by weight of the particle sizes are finer than this size
D^c_{c35}	Controlling constriction size of the coarser fraction
d	Base particle diameter (mm)
d_0	Pore element diameter
d'_{85}	Diameter of fine fraction such that 85% by weight of soil is finer than this size
d_5	Diameter of particles such that 5% by weight of soil is finer than this size
d_{20}	Diameter of particles such that 20% by weight of soil is finer than this size
d_{90}	Diameter of particles such that 90% by weight of soil is finer than this size
e	Void ratio
E_{flow}	Expended energy by seepage flow
E_{HC}	Cumulative expended energy per unit volume corresponding to the strong increase in hydraulic conductivity
E_{MVE}	Cumulative energy per unit volume to the turning point of cumulative lost mass vs cumulative expended energy curve
E_{RE}	Cumulative expended energy per unit volume corresponding to the strong increase in erosion rate
F	Percentage of mass passing corresponding to the size D

F_{md}	Initial dry mass of fine content
g	Gravity acceleration (m/s^2)
γ_d	Dry unit weight of soil (N/m^3)
γ_s	Unit weight of soil particles (N/m^3)
γ'	Submerged unit weight of soil (N/m^3)
γ_w	Submerged unit weight of water (N/m^3)
ρ	Density (kg/m^3)
ρ_d	Dry Density (kg/m^3)
G_r	Gap ratio (d_{max}/d_{min})
H	The percentage of mass passing between the particle size D and 4D
H/F	Stability index (-)
I_α	Suffusion resistance index
i_c	Critical hydraulic gradient for heaving (m/m)
i_{cr}	Critical hydraulic gradient for suffusion (m/m)
i_{HC}	Hydraulic gradient corresponding to the strong increase in hydraulic conductivity
i_{MVE}	Hydraulic gradient corresponding to the turning point of cumulative lost mass vs cumulative expended energy curve
i_{RE}	Hydraulic gradient corresponding to the strong increase in erosion rate
i_{SB}	Critical hydraulic gradient to the first increase of hydraulic conductivity (Skempton and Brogan 1994)
i_u	Minimum hydraulic gradient value within the cycle
k	Hydraulic conductivity (m/s)
k_{ini}	Initial hydraulic conductivity
L	Specimen Length
M_{eroded}	Total lost mass during test (gm)
n	Global porosity
O_{50}	Average capillary tube diameter in the coarser fraction (mm)
P	Fine content % with size smaller than 0.063 mm
P_{flow}	Power expended by seepage flow
p'	Mean effective stress
Q	Fluid flow rate (m^3/s)

S^*	Critical fines content
v	Darcian flow velocity (m/s)
V_{onset}	Darcy velocity corresponding to the suffusion onset (cm/s)
$\lvert\epsilon_{z,\,steady}\rvert$	Axial strain at steady state
σ'_{b0}	Effective stress at the bottom soil layer (kPa)
σ'_{t0}	Effective stress at the top soil layer (kPa)
σ'_{vm0}	Mean vertical effective stress in middle layer (kPa)
$\bar{\sigma}'_{vm}$	Normalized mean vertical effective stress
φ	True friction angle

Chapter 1

1 Introduction

1.1 General introduction

Internal erosion is a recognized prominent causal factor contributing to failures in earthen hydraulic structures such as embankment dams, dikes and levees. Consequently, the safety of these structures requires a detailed understanding of these internal erosion phenomena. Internal erosion is usually classified into four distinct categories: concentrated leak erosion, backward erosion, contact erosion and suffusion (Fell and Fry, 2007). The specific objective of this research centers on investigating suffusion, which encompasses a sequential process involving the detachment and migration of fine particles through the pores of coarser particles, alongside partial filtration within the soil matrix, driven by the in-situ seepage flow.

1.2 Engineering significance and context

Earthen hydraulic structures serve a crucial role in managing and controlling stream discharge to mitigate the risk of flooding. As the demand for water increases due to technological advancements and human needs, these structures have also evolved to fulfill additional purposes like navigation, hydroelectricity generation, irrigation and flood management. Despite their advantages in terms of availability and cost-effectiveness due to the use of earthen materials, these structures are susceptible to internal erosion, a significant challenge driven by the energy-laden water they retain, which ultimately threatens their integrity. The data obtained from ICOLD (1995) and depicted in Table 1.1 provides compelling evidence regarding the contrasting vulnerability of dams constructed with loose material compared to their counterparts made of concrete or masonry. The statistics provide clear evidence that dams constructed using loose materials are more prone to susceptibility and risk. These vulnerabilities are primarily attributed to a lack of knowledge regarding filter design and the management of seepage flow, which is believed to be the leading cause of these serious incidents.

Table 1.1 Number of failure/year/dams in the world (excluding China) from 1970 to 1990, ICOLD (1995)

Type of Dam	Number of dams	Number of failures	Number of failures per 100,000 years*dams
Concrete or masonry	5,500	2	2
Loose material	16,500	26	9

Richards and Reddy (2007) revealed that approximately half of dam failures were caused by internal erosion. Additionally, their research, which incorporated data from Lane (1935), Jones

(1981) and findings from the National Performance of Dams program, indicated that nearly one-third of piping failures could be attributed to the classic phenomena of backward erosion or suffusion.

The historical frequencies of embankment dam failure, as derived from Foster et al., (1998; 2000) and ICOLD (2015), provide valuable insights into failures and accidents in embankments of large dams constructed between 1800 and 1986. The analysis excludes Japan (pre-1930) and China, as shown in Table 1.2 and Table 1.3. The reported rate of failures due to internal erosion is two per 10,000 dams per year, highlighting its significant contribution to approximately 50% of embankment dam failures, which is equivalent to failures caused by overtopping during floods. Comparatively, the percentage of failures attributed to sliding failures due to static and seismic instabilities is lower. The data indicates that out of 11,192 embankment dams, around 147 (approximately 1 in 76) have experienced failure or accidents related to internal erosion. Moreover, two-thirds of all failures and half of the accidents occurred during the initial filling or within the first five years of operation, emphasizing the importance of internal erosion study in earthen hydraulic structures.

Table 1.2 Embankment dam failure statistics cited from Foster et al., (1998 and 2000) and ICOLD (2015)

Failure Mechanism	Erosion		Embankment Sliding	
Mode of Failure	Internal Erosion	External Erosion (Overtopping)	Static Instability	Seismic Instability
% Globally	46 %	48 %	4 %	2 %

Table 1.3 Historical Frequencies of Embankment Dam Failure and accidents: Insights from Foster et al., (1998 and 2000) and ICOLD (2015), Excluding Japan (pre-1930) and China

Case	Total	In Dam	Around Conduits or wall
Internal Erosion Failures	36	19	17
Internal Erosion Accidents	75	52	23
Seepage accidents with no detected erosion	36	30	6
Total no. of failures and accidents	147	101	46
Population of Dams	11192	11192	5596
Historical Frequency for Failures and Accidents	0.013	0.009	0.00822
Proportion of Failures and Accidents on First Fill	36%		
Proportion of Failures and Accidents after First Fill	64%		
Historical Frequency for First Fill	-	0.0032	0.003
Historical Frequency after First Fill	-	0.0058	0.0052
Historical annual frequency after first fill	-	$2.20 * 10^{-4}$	$2.00 * 10^{-4}$

Brown and Gosden (2008) found that among the 2,500 registered dams in the United Kingdom, a substantial portion (60%) of the reported accidents were associated with internal erosion. Additionally, the study indicated that an average of two serious accidents per year were attributed to this specific factor. France has an impressive infrastructure in place to combat floods and facilitate transportation and hydroelectricity. Fry and Bonelli (2012) state that the country boasts an extensive network of flood protection dikes spanning over 9,000 km, alongside 8,000 km of navigation canals and 1,000 km of hydroelectric canals. Notably, the cumulative length of the dikes is approximately 13 times the largest dimension of France's territory. Additionally, Fry et al., (2012) reported that between February 2010 and April 2012 (within 26 months), there were 23 instances of internal erosion failures out of 44 in small water retaining structures and 3 failures out of 8 in large dams. The frequency of failure was found to be approximately one per year (Fry et al., 2012).

Engemoen and Redlinger (2009) along with Engemoen (2011) conducted a comprehensive analysis of 220 embankment dams to examine internal erosion incidents for the U.S. Bureau of Reclamation. Their study revealed that approximately 45% of the dams had experienced accidents. Among these incidents, one led to complete failure, 53 were attributed to particle transport, while excessive seepage or sand boil occurrences were observed for the remaining incidents. The accidents were distributed, with nine taking place in the embankment, 70 in the foundation and others occurring around the conduits. Remarkably, this investigation highlighted that dams demonstrating overall successful performance were still susceptible to internal erosion accidents, which could potentially arise at any point during the dam's service life. The incidents mentioned above from various locations worldwide indicate that internal erosion plays a significant role in the failure of hydraulic structures. These incidents highlight the extent of vulnerability associated with such structures and emphasize the need for further research to address this issue effectively.

Suffusion is a complex phenomenon characterized by the selective erosion of fine particles within a matrix of coarser particles, driven by seepage flow. This process involves three simultaneous processes: detachment, transport and partial filtration of the fine particles. The migration of fine particles induces significant local changes in density, porosity, permeability and mechanical behavior, impacting both micro and macro soil structural behaviors. These changes can ultimately lead to detrimental consequences, such as the formation of sinkholes, settlements, or structural failure. Although several researches have been undertaken to explore different aspects of internal erosion, such as the susceptibility of soil materials, criteria for filter design and threshold hydraulic gradients, understanding the individual phases of suffusion under complex stress conditions and their impact on the soils' mechanical behavior remains challenging. Moreover, the potential influence of the stress state on suffusion-related parameters has not been thoroughly understood.

This thesis is positioned in the fields of geotechnical and hydraulic engineering, with a primary focus on earthen structures, including dams, dikes and levees concerning the phenomenon of suffusion. The research aims to address critical concerns related to material susceptibility and suffusion characterization but also the effect of the stress-state, of the microstructure effect and of the hydraulic loading path. By providing valuable insights into the suffusion behavior, the study will contribute to the improvement of design practices and the implementation of enhanced safety measures for earthen structures subjected to complex stress and hydraulic conditions.

1.3 Objectives and scope

Considering the significant impact of internal erosion on the failure of earth structures, this research attempts to investigate suffusion, a strongly coupled hydro-mechanical phenomenon, on a gap-graded cohesionless soil using a newly developed modified tri-axial apparatus. The key concerns of the industrial and scientific community involve evaluating the material susceptibility of various structures, characterizing the suffusion process, identifying risk zones and estimating the mechanical consequences associated with suffusion events. To address some of these vital aspects, the research study is designed with the following specific objectives:

- Develop a modified tri-axial chamber capable of conducting successive experimental steps, including saturation, consolidation, erosion and post-suffusion analysis
- Investigate the initiation and development of suffusion under complex stress states to understand the underlying mechanisms
- Examine the influence of complex hydraulic loading on the suffusion process to gain insights into its behavior under different hydraulic conditions

Most of the suffusion tests described in the literature have been carried out under hydro-mechanical loading conditions that may not be representative of in-situ conditions. The developed modified tri-axial chamber incorporates the inflow and the collection of eroded soil particles. The successive steps: saturation, consolidation and erosion analysis are realized in the device, which ensures minimal sample disturbance. The hydraulic loading system is fully automated and multi-stage gradients can be applied precisely as per the requirement.

The outcome of this research will deliver a comprehensive study of suffusion under complex mechanical stress states and hydraulic loading paths. This study aims to provide several parameters for characterizing each phase of suffusion, implications for engineering practice and results that can be used in future numerical modeling studies.

1.4 Thesis outline

This doctoral thesis is structured into six chapters, each of which is briefly described below:

Chapter 1: Introduction

This chapter introduces the research topic, presenting the background and the context of the study. It outlines the engineering implications of the research, emphasizing the significance of understanding suffusion in geotechnical and hydraulic engineering. The chapter defines the objectives and scope of the research and provides a roadmap for the thesis outline.

Chapter 2: Literature review

In this chapter, a comprehensive literature review is conducted, focusing on internal erosion mechanisms and more specifically on suffusion. In addition, suffusion parameters are examined, including susceptibility based on geometric criteria, initiation and development based on hydraulic loads. The influence of various parameters on suffusion, such as particle shape, relative density, microstructure, stress state and hydraulic loading path, is also discussed.

Chapter 3: Development of a modified triaxial-apparatus

This chapter describes the development of the modified triaxial apparatus specifically designed to experimentally investigate suffusion under various complex stress states thanks to an automated control of the applied hydraulic load. The components of the triaxial cell, the confining and axial loading system, automatic seepage control, collection/effluent tank, instrumentation and data acquisition system are presented in detail. The suffusion test procedure is outlined to ensure reproducibility and accuracy of results.

Chapter 4: Influence of the stress state on the initiation and development of suffusion

Chapter 4 investigates the influence of various stress states on the initiation and development of suffusion. Also, four gap-graded soils are tested to assess the influence of the microstructure (underfilled, in transition and overfilled) on the observed behavior. The experimental investigation details the methodology, the testing program (tri-axial tests and top cap validation) and the computation of key parameters, such as the hydraulic conductivity, the erosion rate, energy and the eroded mass. The chapter characterizes the four phases of suffusion and provides a comparative analysis of both stress states and fines percentage on suffusion parameters, with implications for engineering practices.

Chapter 5: Influence of complex hydraulic loadings on the suffusion process

This chapter explores the influence of several complex hydraulic loading paths on suffusion, such as multi-staged increasing, decreasing and re-increasing in hydraulic heads referred to as cycles. The research objectives are defined and the testing program is outlined. The impact of the cycle starting point, cycle size and the number of cycles on suffusion is investigated. Findings are discussed and their implications for engineering practices are presented.

Chapter 6: Conclusions and perspectives

The final chapter summarizes the key findings of this work and draws conclusions. It emphasizes the implications of the study for engineering practices. Future perspectives and recommendations, including the need for benchmark tests for suffusion, are provided.

Chapter 2

2 Literature review

The section provides an overview of internal erosion mechanisms in hydraulic structures. It highlights the various forms of erosion, including concentrated leak erosion (piping), backward erosion, contact erosion and suffusion. Suffusion, in particular, is the primary focus of this thesis, given its potential risks and consequences for hydraulic structures. Understanding and addressing suffusion is vital for ensuring the stability and safety of these structures, making further research in this area crucial.

2.1 Overview of internal erosion mechanisms

Internal erosion is generally defined as the process involving the migration of soil particles from within or from the foundation of earthen water-retaining hydraulic structures. This phenomenon is initiated when the hydraulic forces exerted by the water flowing through an earth dam surpass the ability of the soils in the dam and its foundation to withstand these forces, specifically when the hydraulic force surpasses the contact forces between the soil particles, as outlined by the International Commission on Large Dams (ICOLD, 2015). The most significant hydraulic loads typically occur during floods. This occurrence has the potential to alter the soil structure and mechanical behavior, leading to either gradual or rapid failure consequences. Garner and Fannin (2010), further elaborate that the initiation of internal erosion relies on the alignment of three critical conditions as shown in Figure 2.1 :

- Material susceptibility: This refers to the erodibility of fine particles relative to the grain or constriction size present in the soil matrix.
- Critical stress condition: It involves the contribution of fine particles in force chains, playing a role in providing primary or secondary support for the coarse particles.
- Critical hydraulic load: This represents the required seepage flow necessary to overcome the effective stresses acting on the fine particles.

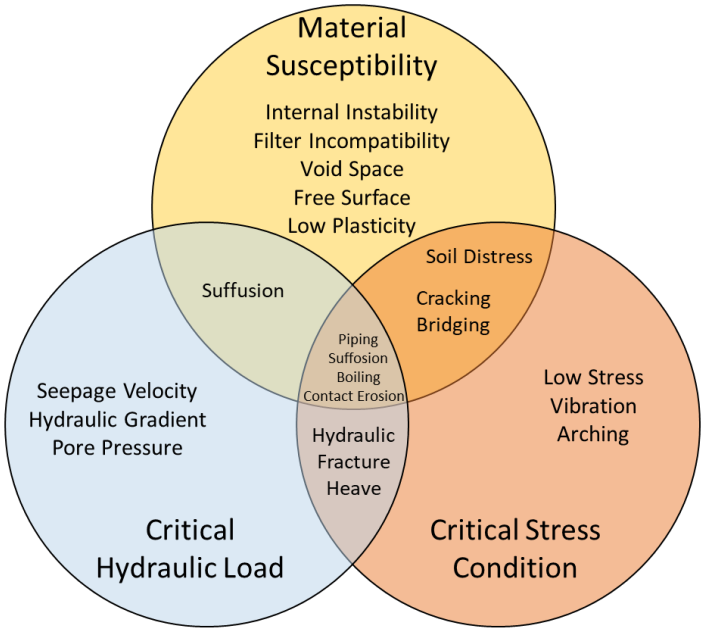

Figure 2.1 Venn Diagram showing internal erosion mechanisms dependent on a combination of material susceptibility, stress and hydraulic load (Garner and Fannin, 2010)

The process of internal erosion is typically categorized into four phases (Foster and Fell, 2001):

1. Initiation of erosion (particle detachment): this phase involves the initial detachment of soil particles, marking the beginning of the erosion process
2. Continuation of erosion (inadequate particle retention): in this phase, the erosion process continues due to insufficient retention of particles within the soil structure
3. Progression of erosion (continuous particle transport and pathway enlargement): during this phase, soil particles are continuously transported and the erosion pathway expands, leading to further erosion
4. Initiation of a breach: the final phase represents the point where erosion has progressed to the extent that it initiates a breach or failure in the structure

More recently, Fell and Fry (2007) have categorized internal erosion into four distinct phenomena as shown in Figure 2.2:

1. Concentrated leak erosion(piping); i.e. the water flows through a crack, a hole, or a hollow, thus eroding the walls.
2. Backward erosion, i.e. the water flow erodes the surface of the soil from where it comes, thus causing a backward erosion of this exit surface.
3. Contact erosion (ex. between gravel and silt), i.e. the water flows through a very permeable soil, thus eroding a fine soil at the interface.
4. Suffusion (volume erosion), i.e. the outflow erodes the small grains through the pores of the coarser grains.

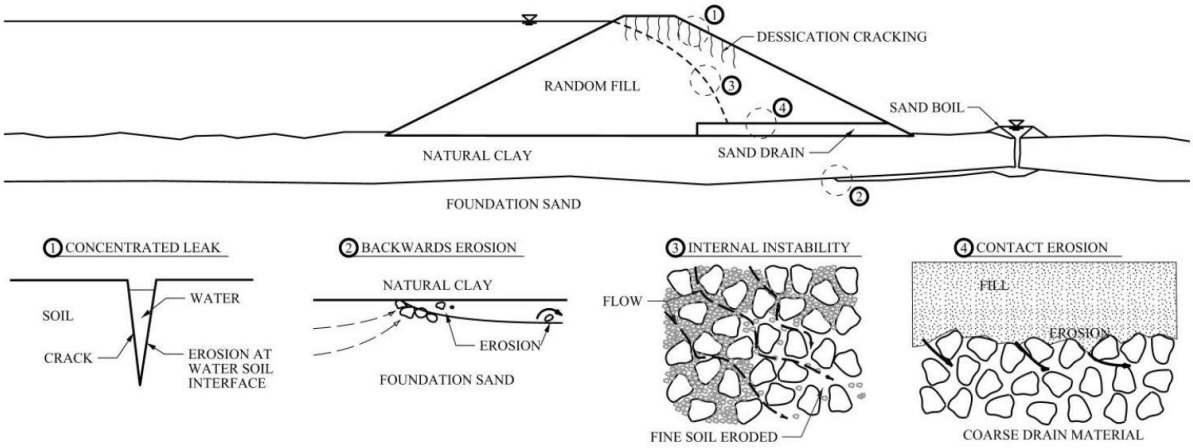

Figure 2.2 Classification of internal erosion (Robbins and Griffiths, 2018))

These phenomena are now presented in turn (ICOLD, 2015) to provide further useful details such as soils' characteristics or typical observed onsite disorders.

Concentrated leak erosion

In certain types of soils, such as plastic soils, unsaturated silt, silty sand and silty sandy gravel, openings or cracks can be formed due to various factors like differential settlements, freezing and thawing, desiccation cracks, flow through gaps, external disturbances caused by animals, or hydraulic fracturing caused by low stresses around conduits. When water leaks through these openings, it can erode the sides of the gaps, giving rise to what is known as "concentrated leaks" (ICOLD, 2015). If the concentrated leak erosion continues to progress, it can lead to the formation of a pipe-like pathway for the flowing water. This gradual development of a pipe is a consequence of the ongoing concentrated leak erosion process.

Backward erosion

As the name suggests, "backward erosion" occurs from the downstream toe of the embankment and progresses upstream in sandy embankment foundations. Eventually, it reaches the reservoir through a circular channel, often referred to as "piping." Backward erosion involves the detachment of soil particles at the exit of the erosion path in non-plastic soils. Two types of backward erosion have been identified:

1. Backward erosion piping: This involves the formation of shallow pipes in the opposite direction of the flow beneath an embankment, leading to sand boils. It typically occurs during floods, where sand layers are covered by a cohesive material. The progression of backward erosion piping creates a network of small channels and if these channels reach the reservoir or river, a pipe is formed (ICOLD, 2015).

2. Global backward erosion: This refers to the failure or collapse of soil above or around a backward erosion piping site. When the collapse is upward, sinkholes or near vertical cavities are formed. As a consequence, sub-vertical sinkholes or sloughing and unravelling may occur on the downstream face (ICOLD, 2015).

Contact erosion

"Contact erosion" is a form of internal erosion where selective erosion of fine particles occurs at the interface with a coarser layer, resulting from the flow passing through the coarser layer. This phenomenon is commonly observed along the contact between different-sized particles, such as silt and gravel. As contact erosion progresses, it can lead to the development of sinkholes and pipes within the embankment core (ICOLD, 2015), posing a significant risk to the stability of hydraulic structures. For flood management purposes, silt levees are often layered upon the gravel foundation along rivers and this has raised concerns in France, as noted by Beguin et al., (2012) and Bonelli (2013).

Suffusion

In the literature, different terms and definitions have been used to describe the process of "suffusion". According to Wan and Fell (2008), suffusion refers to the movement of finer soil particles through constrictions between larger soil particles caused by seepage forces. On the other hand, Moffat et al., (2011) introduced two distinct processes: "suffusion" (erosion without volume change) and "suffosion" (erosion with volume change) to characterize internal instability. For consistency in this report, the term "suffusion" is adopted based on ICOLD (2015). It defines suffusion as the transportation of fine particles through the pores of coarser particles in internally unstable, gap-graded, or broadly graded non-plastic soils when the seepage force is sufficient to push the fine particles.

The phenomenon of suffusion involves selective erosion of the fine fraction within the matrix of coarser particles, leading to local changes in permeability, seepage velocities, gradient, porosity, grain size distribution and strength. Although suffusion is a slow kinetic process, substantial transportation of fines can result in the formation of sinkholes, settlements and possibly mechanical failure. Suffusion poses a significant maintenance issue to hydraulic structures stakeholders. As outlined in the ICOLD (2015) guidelines, three essential criteria have to be satisfied:

i. **Geometric criterion**: the fine soil particles must be smaller in size than the constrictions between the coarser particles, which form the basic soil structure.

ii. **Stress criterion**: the amount of finer soil particles must be limited so that they do not completely fill the voids among the coarser particles. If there are excess finer particles, the coarser particles will not form the essential soil structure but rather remain dispersed within the matrix of fine soil particles.

iii. **Hydraulic criterion**: the third criterion is related to the pore water velocity according to Fell and Fry (2013), whereas Garner and Fannin (2010) considered the variations in pore water pressure and Marot et al., (2011; 2016) advocate the power dissipated by the flow. So, the hydraulic load through the soil matrix must exert enough force to overcome the stresses acting on the particles from the surrounding soil and to transport the finer soil particles through the constrictions between the larger particles.

2.2 Suffusion parameters

2.2.1 Suffusion susceptibility based on geometric criteria

The evaluation of a soil's susceptibility to suffusion can be determined based on its Particle Size Distribution (PSD). The ideal consideration pertains to the geometry of pore channels or pathways, where fine particles can move through the smallest constrictions without clogging. However, due to the complexities involved in measuring the pores' network, PSD is often favored.

The field of geometric criteria for assessing suffusion susceptibility has been extensively explored in the existing literature, with researchers employing a variety of empirical, experimental and computational methods. Notable studies in this area include research conducted by (U.S. Army, 1953; Istomina, 1957; Kezdi, 1969; Sherard, 1979; Kenney and Lau, 1985; Burenkova, 1993; Indraratna, Raut and Khabbaz, 2007; Li and Fannin, 2008; Indraratna, Nguyen and Rujikiatkamjorn, 2011; Chang and Zhang, 2013b). From this vast body of research, the most commonly used methods for assessing suffusion susceptibility are presented below:

U.S. Army (1953) and Istomina (1957) criteria

These two criteria for classifying soils as internally stable are determined based on the coefficient of uniformity (C_u), which is calculated as the ratio of the particle diameter corresponding to 60% passing (D_{60}) to the particle diameter corresponding to 10% passing (D_{10}):

- A soil is considered internally stable if $C_u < 20$ (U.S. Army, 1953)
- Suffusion does not occur when $C_u < 10$ in sandy gravel soils ((Istomina, 1957).
- $C_u > 20$ indicates a high likelihood of suffusion, while $10 \leq C_u \leq 20$ represents a transitional condition.

Kezdi's (1969) and Sherard's (1979)

The Kezdi (1969) and Sherard's (1979) methods are also based on split-gradation into fine and coarser fractions and aim to assess the potential instability of granular soils. Both of these methods are founded on the classical retention criterion for granular filters, which were originally proposed by Terzaghi (1939).The soil gradation is internally stable if $(D'_{15}/d'_{85}) \leq 4$ for Kezdi's method and $(D'_{15}/d'_{85}) < 5$ for Sherard's method. The definition of D'_{15} is the diameter of coarse fraction which corresponds to the size with 15 % by weight of the range of particle sizes being smaller and d'_{85} is the diameter of fine fraction with 85 % by weight being smaller as shown in Figure 2.3.

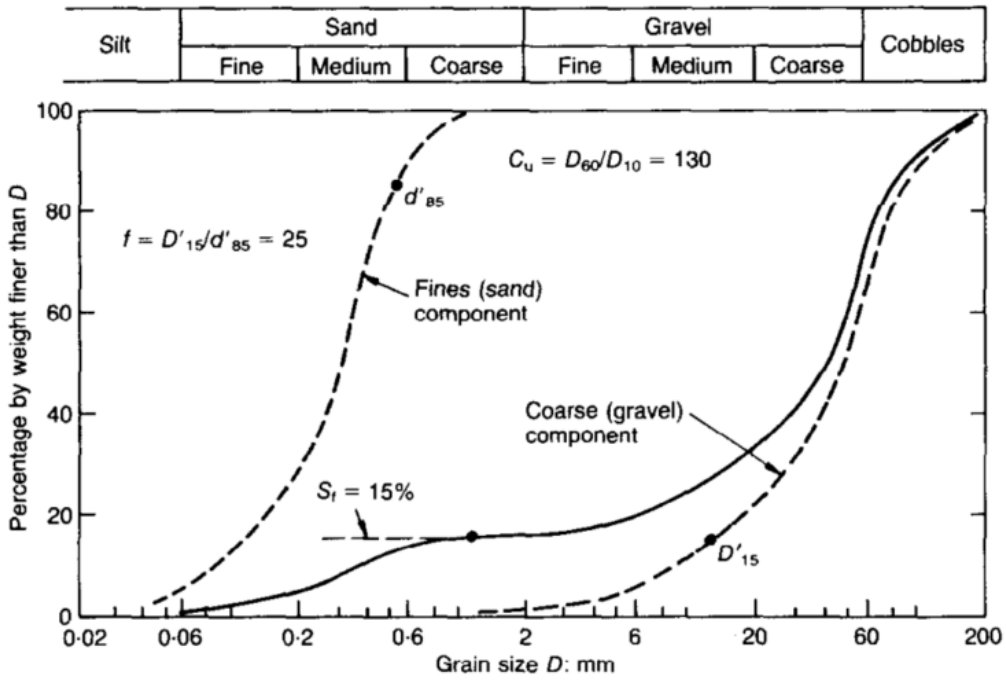

Figure 2.3 Definitions of D'_{15} and d'_{85} based on Kezdi's (1969) and Sherard (1979) methods cited from Skempton and Brogan (1994)

Kenney and Lau's method (1985 and 1986)

The Kenney and Lau (1985) method was developed through experimentation to assess the potential for instability in cohesionless sands and gravel fractions. Their approach introduces the concept of stable versus unstable gradations, based on a stability index denoted as (H/F), which is calculated from the grain size distribution of coarse-grained soil. H represents the percentage of mass passing between the particle size D and 4D, while F denotes the percentage of mass passing corresponding to the size D. The computation range is selected from the finer end of the gradation curve, ranging from 0 to a maximum of 20% for soils with widely-graded (WG) material and 30% for soils with narrowly graded (NG) material. In 1985, they initially proposed a criterion for internal instability, stating that (H/F) should be less than 1.3. This criterion was applicable for narrowly graded soils with $F \leq 30\%$ and $C_u \leq 3$, as well as widely graded soils with $F \leq 20\%$ and $C_u > 3$. However, in 1986, a revised stability index $(H/F)_{min}$ of less than one indicates that a soil is potentially internally unstable. The illustration in Figure 2.4, adopted from Rönnqvist and Viklander (2015), depicts the Kenney-Lau method.

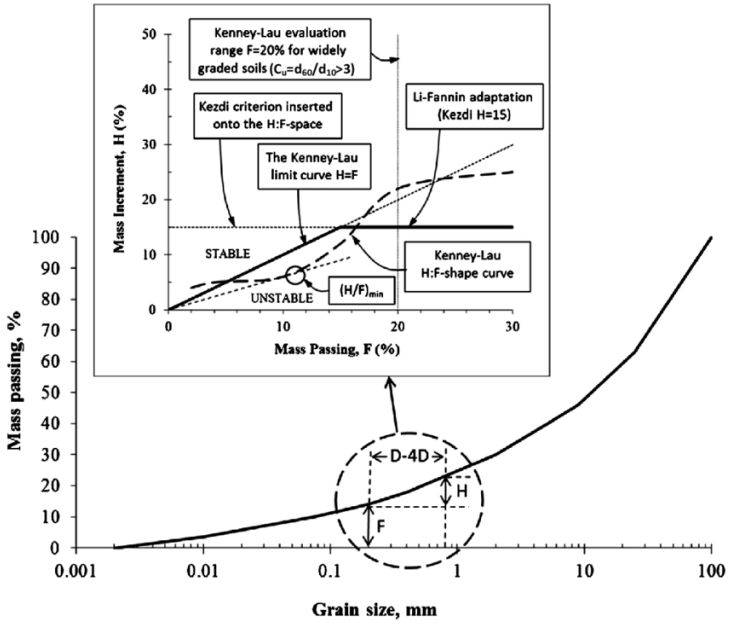

Figure 2.4 Kenney-Lau method adopted from Rönnqvist and Viklander (2015)

Burenkova's method (1993)

Burenkova (1993) presented a geometric criterion for assessing the internal stability of cohesionless sand-gravel soils, based on laboratory testing results. The criterion relies on conditional factors of uniformity, $h' = d_{90}/d_{60}$ and $h'' = d_{90}/d_{15}$. Figure 2.5 illustrates materials susceptible to internal instability, with distinct boundaries defining "suffusive soils" from "non-suffusive soils." Zones I and III correspond to suffusive compositions, while Zone II represents non-suffusive compositions and Zone IV pertains to artificial soils. The boundary for Zone II (non-suffusive) is defined by the following condition:

$$0.76 \log(h'') + 1 < h' < 1.86 \log(h'') + 1$$

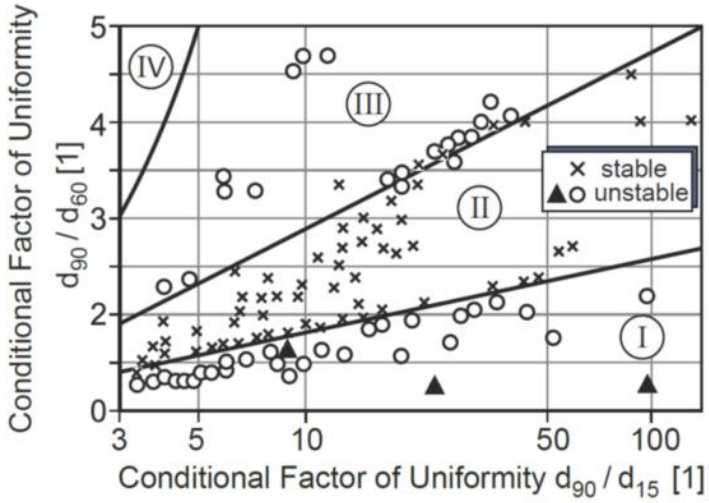

Figure 2.5 Materials susceptible to internal instability proposed by Burenkova (1993)

Li and Fannin (2008)

Li and Fannin (2008) conducted an extensive review of two methods, namely Kezdi (1969) and Kenney and Lau (1985, 1986) and aimed at assessing the susceptibility of materials to internal instability. While recognizing some conservatism in both methods, Li and Fannin proposed a novel hybrid threshold to determine material susceptibility by combining the limit value of Kenney and Lau with that of Kezdi. Their proposal involves utilizing Kenney and Lau's criterion when F < 15% and switching to Kezdi's criterion for F values greater than 15%. In other words, a soil is classified as potentially unstable when it is gradation has a ratio of $(H/F)_{min}$ less than 1 for F values below 15%, or when the value of H is below 15% for F values ranging from 15% to 30%.

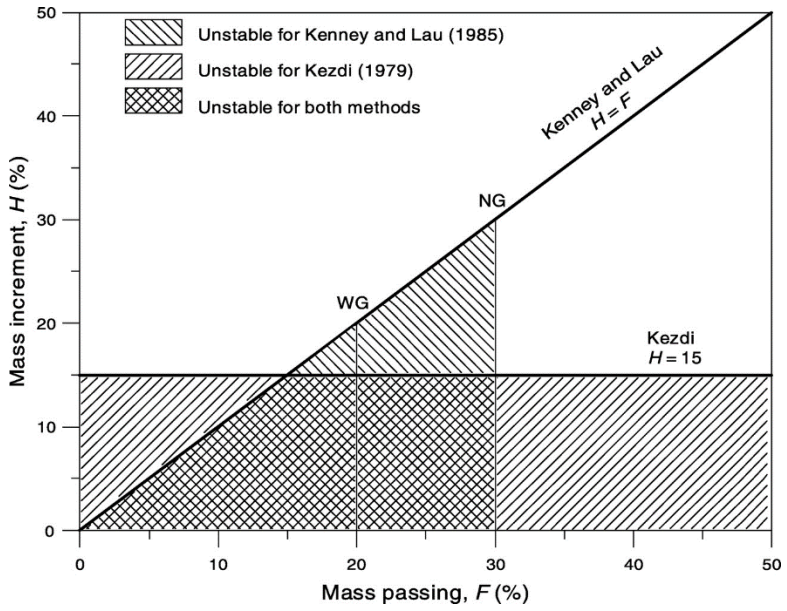

Figure 2.6 Review of two criteria (Li and Fannin, 2008)

Wan and Fell's method (2008)

From the Burenkova's method, Wan and Fell (2008) proposed enhanced techniques to predict the internal instability of sand-gravel soils with silty and clayey fines. However, it is worth noting that the proposed method is not suitable for gap-graded soils. The approach involves calculating two shape parameters, namely d_{20}/d_5 and d_{90}/d_{60}, which are then compared to established boundaries representing stable, unstable and transition zones, as illustrated in Figure 2.7.

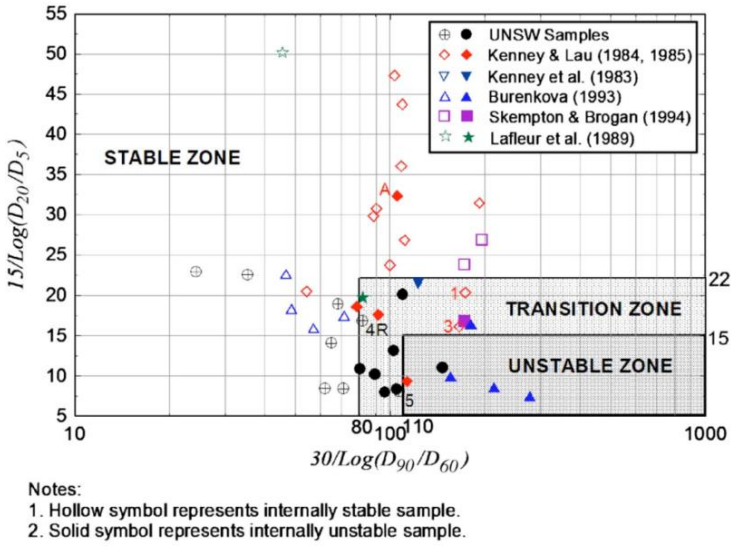

Figure 2.7 Enhanced method for assessing internal instability proposed by (Wan and Fell (2008)

Indraratna's et al., method (2011, 2015)

Indraratna et al. (2011) proposed a criterion to evaluate the potential internal instability of suffusive soils, building upon concepts introduced by Kenney and Lau (1985) and Indraratna et al., (2007). The proposed method relies on two key parameters: D^c_{c35} representing the controlling constriction size of the coarser fraction and d^f_{85} indicating the representative particle size of the finer fraction *by surface area*. They established distinct boundaries for assessing the internal stability of soils based on the ratio D^c_{c35} / d^f_{85}:

- If $D^c_{c35} / d^f_{85} > 0.82$, the soil is classified as internally unstable
- If $D^c_{c35} / d^f_{85} < 0.73$, the soil is classified as internally stable
- If $0.73 \leq D^c_{c35} / d^f_{85} \leq 0.82$, the soil falls within transition zones

Building on their earlier research, Indraratana et al., (2015) conducted laboratory hydraulic tests on granular soil samples with varying relative density. They devised a technique that integrated particle size distribution (PSD) with relative density to effectively distinguish between internally stable and unstable samples. Hence, the "internal stability" of each sample was also influenced by their compaction level. The division point, determined based on the $(H/F)_{min}$ ratio, followed the approach proposed by Kenney and Lau. The researchers then combined this PSD with the optimized constriction size distribution (CSD) criterion, introduced by Indraratna et al., (2007), to evaluate the effectiveness of the filter component in retaining the base soil. If the ratio $D^c_{c35} / d^f_{85} \geq 1$, the soil is internally stable, as illustrated in Figure 2.8.

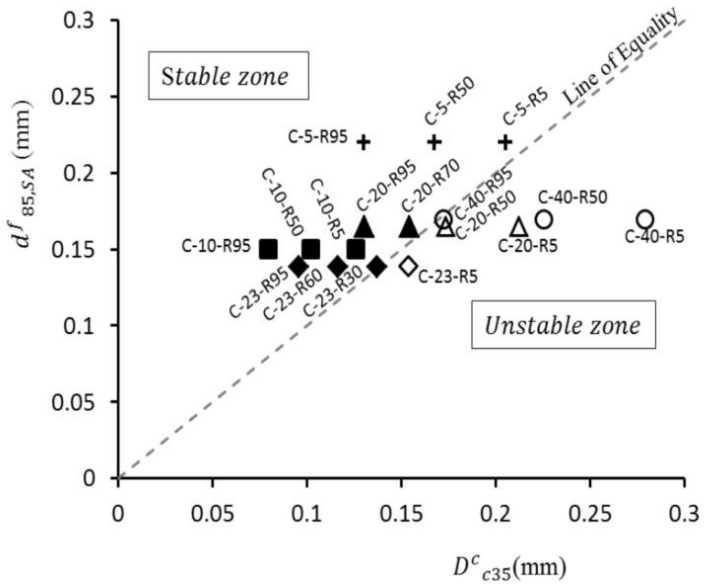

Figure 2.8 Potential Internal instability proposed by Indraratna et al., (2015) where solid symbols represents stable and hollow symbols unstable

Chang and Zhang's method (2013b)

Chang and Zhang (2013b) conducted a study to explore additional control variables for assessing internal stability in various types of soil gradations, including well-graded and gap-graded soils. They introduced fine content P (content smaller than 0.063 mm) and gap ratio G_r as new factors to consider in determining internal stability and controlling parameters. For well-graded soils, the influential parameters for internal stability were found to be $(H/F)_{min}$, as proposed by Kenney and Lau (1985) and the fine content P. On the other hand, for gap-graded soils, the gap ratio (G_r) and fine content P were identified as key factors.

In well-graded soil gradations as shown in Figure 2.9:

- For fine content (P) less than 5%, the internal stability criterion is $(H/F)_{min} > 1.0$: internal stability
- For $5\% \leq P \leq 20\%$ the criterion is $(H/F)_{min} > -(1/15)\ P + 4/3$: internal stability for low plasticity soils
- For $P > 20\%$: the soil is considered stable

In gap-graded soil gradations as shown in Figure 2.10:

- For $P < 10\%$, the internal stability criterion is $G_r < 3.0$, indicating internal stability
- For $10\% \leq P \leq 35\%$, the criterion is $G_r < 0.3P$, indicating internal stability for medium plasticity soils
- For $P > 35\%$, the soil is considered stable

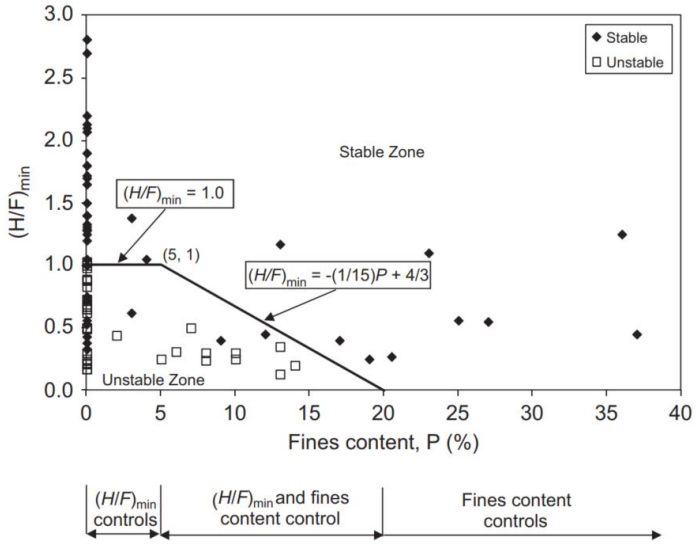

Figure 2.9 Geometric criteria for well-graded soils proposed by Chang and Zhang (2013b)

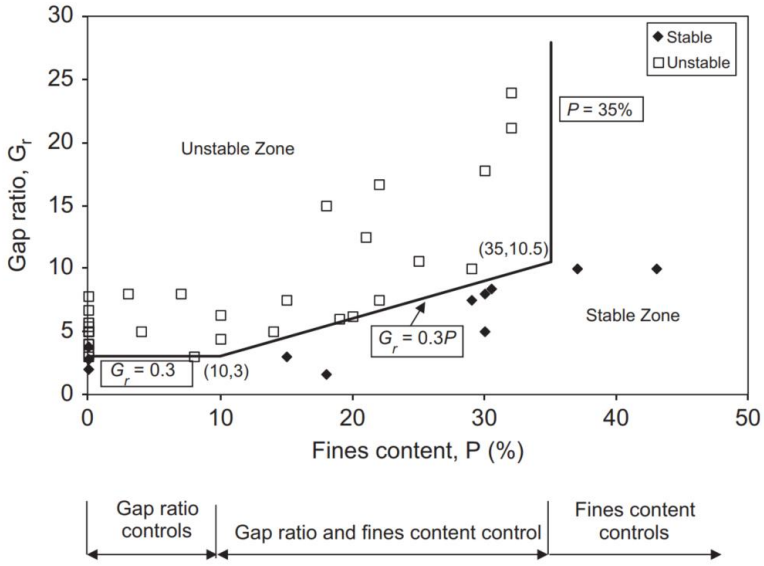

Figure 2.10 Geometric criteria for gap-graded soils proposed by Chang and Zhang (2013b)

The assessment of soil suffusion susceptibility, which relies on various geometric criteria, involves shape analysis of the Particle Size Distribution (PSD). However, the use of simplistic index values and binary categorization into stable and unstable soils may oversimplify the complexities of suffusion susceptibility. Real-world scenarios involve multiple site-specific factors, such as hydraulic loading path, stress conditions and environmental changes, which can significantly influence soil behavior. Relying solely on existing databases to classify soils as stable or unstable poses a risk of overlooking critical nuances that play a crucial role in determining internal stability.

Table 2.1 presents an overview of the most commonly utilized geometric screening tools.

Table 2.1 Overview of different geometric internal stability criteria

Methods	Year	Internal stability criteria
U.S. Army	1953	$Cu < 20$
Istomina	1957	$C_u \leq 10$: internally stable ; $10 \leq C_u \leq 20$: transitional $C_u \geq 20$: internally unstable
Kezdi	1969	$(D'_{15}/d'_{85})_{max} \leq 4$: internally stable
Sherard	1979	$(D'_{15}/d'_{85})_{max} \leq 4$ to 5 : internally stable
Kenney and Lau	1985 & 1986	$(H/F)_{min} \geq 1.3$: internally stable (1985) $(H/F)_{min} \geq 1.0$: internally stable (1986)
Burenkova	1993	$0.76 \log(h'') + 1 < h' < 1.86 \log(h'') + 1$: non-suffusive
Wan and Fell	2008	$30/\log(D_{90}/D_{60}) < 80$ or $15/\log(D_{20}/D_5) > 22$ and $30/\log(D_{90}/D_{60}) > 80$: internally stable
Li and Fannin	2008	$(H/F)_{min} < 1$ for $F \leq 15\%$, or $H < 15\%$ for $15 \leq F \leq 30\%$: internally Unstable
Indraratna et al.,	2011	$D^c_{c35} / d^f_{85} > 0.82$: internally unstable $D^c_{c35} / d^f_{85} < 0.73$: internally stable $0.73 \leq D^c_{c35} / d^f_{85} \leq 0.82$: transitional zones
Chang and Zhang	2013	Well-graded: $P < 5\%$ and $(H/F)_{min} > 1.0$: internally stable $5\% \leq P \leq 20\%$ and $(H/F)_{min} > -(1/15)P + 4/3$: internally stable for low plasticity soils $P > 20\%$: internally stable
		Gap-graded: $P < 10\%$ and $G_r < 3.0$: internally stable $10\% \leq P \leq 35\%$ and $G_r < 0.3P$: internally stable for medium plasticity soil $P > 35\%$: internally stable
Indraratna et al.,	2015	$D^c_{c35} / d^f_{85} \geq 1$: internally stable

2.2.2 Suffusion initiation: critical hydraulic gradients

Terzaghi (1925) observed that the critical hydraulic gradient (i_c) for sand materials under upward flow conditions is typically approximately equal to unity (1). This critical hydraulic gradient causes a reduction of effective stresses to zero, resulting in a phenomenon known as heaving or sand boiling and theoretically obtained as the ratio between the density of the submerged soil and the density of water. However, Skempton and Brogan (1994) conducted tests on unstable sandy gravel and observed a segregation piping process occurring at hydraulic gradients significantly lower than those predicted by classical theory, typically ranging from about one fifth to one third of the critical gradient. This deviation was attributed to the ability of sand particles to pass freely through the pores of the gravel, with a significant portion of the effective stress being borne by the primary skeleton of the gravel. Consequently, Skempton and Brogan (1994) introduced the stress-reduction factor (α) as a means to quantify the influence of fine particles within the soil matrix and represent the fraction of applied effective stresses. The proposed expression for the critical hydraulic gradient for suffusion in sand soils i_{cr} is given as:

$$i_c - i_{cr} = \alpha \frac{\gamma'}{\gamma_w} \tag{2-1}$$

$$\alpha = \frac{\sigma'_f}{\sigma'_c} \tag{2-2}$$

In which σ'_f and σ'_c are the effective stresses acting on fine and coarse particles, respectively. The parameter α varies within a range from nearly zero to one, reflecting the contribution of fine particles to the force chain.

Furthermore, Wan and Fell (2008) conducted observations on internally unstable soils and noted that erosion onset occurred at hydraulic gradients lower than the classical critical gradient. This additional finding further underscores the deviation from classical predictions regarding critical hydraulic gradients in certain soil conditions. Ke and Takahashi (2012b) introduced a distinction between two critical hydraulic gradients: one representing the critical hydraulic gradient for soil stability, as originally proposed by Terzaghi to describe the heaving phenomenon and the other being the critical hydraulic gradient for internal erosion. The latter refers to the point at which a slight outward rush of fine particles is observed and corresponds to the inflection point in the hydraulic gradient and upward seepage flow velocity relationship curve. Their findings align with the observations made by Skempton and Brogan, indicating that on gap-graded soils, the onset of erosion occurs at values ranging from one fifth to one third of the critical hydraulic gradient for soil stability.

Building upon these experimental findings, a unified approach is proposed to incorporate the influence of effective stress for estimating the critical hydraulic gradient that triggers the onset of internal erosion. This approach utilizes the grading curve and considers the stress reduction factor, α. To accomplish this, a hydromechanical envelope is established, representing the relationship between the critical hydraulic gradient and normalized effective stress. This concept is grounded in the notion of stress reduction within finer particles and is validated through experimental observations. From this vast body of research, the most commonly used methods for assessing critical hydraulic gradient using a hydromechanical approach are presented below:

Li (2008) proposed that α depends on the shape of soil gradation curve and general correlation with geometric indices (D'_{15}/d'_{85}) and (d'_{85}/O_{50}) were established. Where d'_{85} is grain diameter for which 85% of the grains by weight of the fine soil are smaller, D'_{15} is grain diameter for which 15% of the grains by weight of the coarse soil are smaller and O_{50} is the average capillary tube diameter in the coarser fraction (mm). The hydro-mechanical envelope for the internally unstable soil is expressed as (Li, 2008, pp. 190–191):

$$i_{cr} = \frac{\alpha}{1-0.5\alpha}\left(\bar{\sigma}'_{vm} + 0.5\frac{\gamma'}{\gamma_w}\right),\ \bar{\sigma}'_{vm} = \frac{\sigma'_{vm}}{\gamma_w \Delta z}\quad ,\sigma'_{vm} = \frac{1}{2}(\sigma'_{t0} + \sigma'_{b0}) \tag{2-3}$$

where $\bar{\sigma}'_{vm}$ is the normalized mean vertical effective stress, Δz is the height of the soil layer, σ'_{t0} and σ'_{b0} are the effective stress at the top and bottom soil layer respectively. The critical hydraulic gradient is determined to be directly proportional to the normalized mean vertical effective stress. By integrating the geometric indices with the hydromechanical index (α), it becomes possible to predict the initiation of suffusion, a process crucial for understanding the onset of internal erosion in soils.

Indraratna and Radampola (2002) put forth a mathematical formulation designed to calculate the critical hydraulic gradient necessary for initiating base particle movement within a filter. This expression for the critical hydraulic gradient is founded on the dimensions of the pore elements and the base particles. When the base particle diameter (d) is smaller than the pore element diameter (d_0), the critical hydraulic gradient is determined as follows:

$$i_{cr} = \frac{2}{3\gamma_w}\frac{d.\delta s}{(d^2+0.375d_0^2)}(\gamma')[cos \propto (f) + sin \propto] \tag{2-4}$$

where $\propto$ is a shape coefficient of the filter soil, f denotes the friction coefficient of the base material and γ'represents the submerged unit weight.

Moffat and Fannin (2011) conducted erosion tests on cohesionless soils under different consolidation stresses and found that the critical hydraulic gradient increased with an increase of the mean effective stress. They proposed a linear hydromechanical relation governing the internal stability of these soils, where either an increase in hydraulic gradient or a decrease in effective stress could trigger the initiation of internal instability. This implies that both the hydraulic load and the effective stresses play significant roles in causing internal erosion. Building on this research, Li and Fannin (2012) developed an empirical envelope (Eq.2-5) to assess the internal instability of cohesionless soils:

$$i_{cr} = \alpha\left(\frac{\sigma'_{to}}{\gamma_w \Delta z} + \frac{\gamma'}{\gamma_w}\right) = \alpha\left(\frac{\sigma'_{vmo}}{\gamma_w \Delta z} + 0.5\frac{\gamma'}{\gamma_w}\right) \tag{2-5}$$

where σ'_{to} represents the vertical effective stress at the top of specimen when i = 0, Δz is the thickness of soil specimen, $\sigma'_{vmo}$is the mean vertical effective stress in the middle of soil layer ($\sigma'_{vmo} = \sigma'_{to} + 0.5\rho' g \Delta z$) and α is the stress reduction factor.

Moffat and Herrera (2015) presented a theoretical model which utilizes momentum balance equations and considers three components: water, finer soil fraction and coarser soil fraction to determine the hydromechanical boundary of internally unstable soils under vertical seepage. The model considers several parameters such as the vertical effective stress σ_v', the soil porosity n^f, the true friction angle between coarse and fine fractions ϕ_u and the proportion of effective stress transmitted to the finer fraction G^*. The estimation of the true friction angle (ϕ_u) for the tested materials is acknowledged as a challenging endeavor. The derived equations to estimate the critical hydraulic gradient are as follows:

$$\text{For downward flow}: i_{cr} = \frac{G^*}{\gamma_w \Delta z}(\sigma_v' \tan(\phi_u) + \Delta\sigma_v') - \frac{n^f \rho_f g}{\gamma_w}$$

$$\text{For upward flow}: i_{cr} = \frac{G^*}{\gamma_w \Delta z}(\sigma_v' \tan(\phi_u) + \Delta\sigma_v') + \frac{n^f \rho_f g}{\gamma_w} \quad (2\text{-}6)$$

In the study conducted by the authors, measurements of the geometric stress reduction factor, G*, were performed by substituting the critical hydraulic gradient (i_{cr}) and other relevant parameters from experiments into Equation (2-6). This procedure led to the determination of a unique G* value for each soil type, with the assumption that G* remains independent of stress levels. It was also postulated that, for soils with known grain size distribution curves and effective stress distributions, an appropriate G* value could be selected from graphical representations (Figure 2.11) and subsequently employed in conjunction with Equations (2-5) to estimate the critical hydraulic gradient (i_{cr}) governing internal instability.

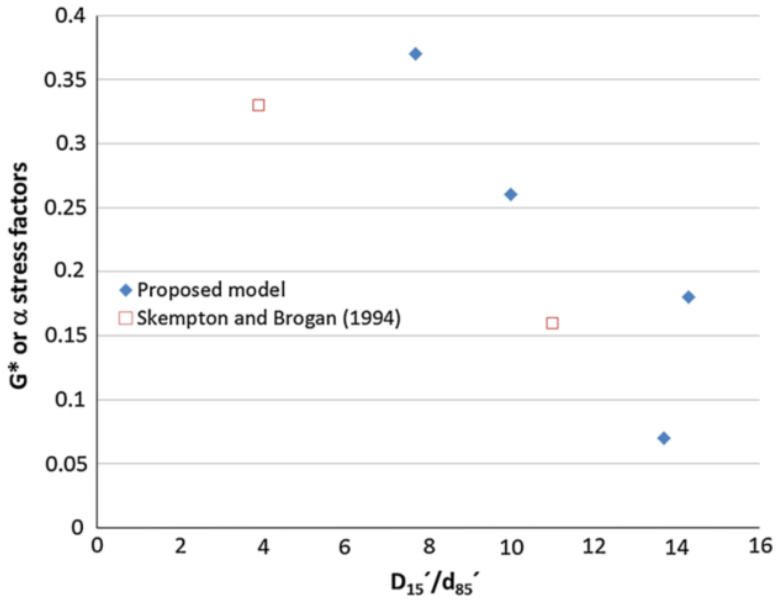

Figure 2.11 Nomogram for Predicting G Using Moffat and Herrera's (2015) Proposed Model*

In the scientific literature, the definition of a critical hydraulic gradient has been defined in various ways, reflecting the complexity of soil erosion processes. Notably, different authors have associated the critical hydraulic gradient with distinct erosion-related phenomena. As previously expounded upon, Terzaghi (1925) associated it with the formation of sand boils, whereas Skempton and Brogan (1994) delved into the phenomenon of segregation piping. Indraratna and

Radampola (2002) directed their attention toward the filtration of base soil and Moffat and Fannin (2011) centered their investigation on the internal instability of cohesionless granular soils. It is crucial to highlight that these varying definitions often represent different stages or aspects of the overall erosion process. Some authors define it in terms of an increase in permeability, while others relate it to local particle movement or variations in local hydraulic gradients. Such diversity in definitions can lead to confusion and underscores the need for more comprehensive and integrated approaches to defining critical hydraulic gradients. This complexity in defining critical hydraulic gradients highlights the intricate nature of suffusion initiation in soils under hydraulic loading. Multiple factors, including the presence of fine particles, grain diameter ratios, pore and fine particle dimensions, effective stress and stress conditions, influence these critical thresholds. Consequently, this research underscores the importance of considering both hydraulic loading and stress states to accurately assess soil internal instability.

While previous research has contributed significantly to our understanding, further investigations are needed to elucidate the interplay between hydraulic and stress-related factors comprehensively. Table 2.2 provides a summary of critical hydraulic gradients for granular soils, offering a snapshot of the diverse definitions and emphasizing the need for a unified and nuanced approach to studying these critical thresholds

Table 2.2 Summary of expression of critical hydraulic gradient for granular soils

References	Criterions
Skempton and Brogan (1994)	$i_c - i_{cr} = \alpha \frac{\gamma'}{\gamma_w}$
Indraratna and Radampola (2002)	$i_{cr} = \frac{2}{3\gamma_w} \frac{d.\delta s}{(d^2 + 0.375 d_0^2)} (\gamma')[cos \propto (f) + sin \propto]$
Li (2008)	$i_{cr} = \frac{\alpha}{1 - 0.5\,\alpha} (\bar{\sigma}'_{vm} + 0.5\,\gamma'/\gamma_w)$
Li and Fannin (2012)	$i_{cr} = \alpha \left(\frac{\sigma'_{vmo}}{\gamma_w \Delta z} + 0.5 \frac{\gamma'}{\gamma_w} \right)$
Moffat and Herrera (2015)	For downward flow : $i_{cr} = \frac{G^*}{\gamma_w \Delta z} (\sigma'_v \, tan(\phi_u) + \Delta\sigma'_v) - \frac{n^f \rho_f \, g}{\gamma_w}$ For upward flow : $i_{cr} = \frac{G^*}{\gamma_w \Delta z} (\sigma'_v \, tan(\phi_u) + \Delta\sigma'_v) + \frac{n^f \rho_f \, g}{\gamma_w}$

where: γ': submerged unit weight of soil, γ_w: unit weight of water, α: stress reduction factor, a: shape factor of the filter soil; d_0: pore element of diameter, d: base particle diameter, f: coefficient of friction of the base material, $\bar{\sigma}'_{vm}$: normalized mean vertical effective stress, σ'_{vm0}: mean vertical effective stress in the middle of soil layer, Δz: thickness of soil specimen, G^*: indicate geometric-based stress reduction factor, $\Delta\sigma'_v$ represents the variation of effective stress σ'_v, ϕ_u denotes the true angle of friction between particles of finer and coarser fractions, n^f represents fine fraction volume ratio (i.e. percentage of e/S_f with e the void ratio and S_f is finer fraction by mass (%)) ; ρ_f represents unit density of fine fraction.

2.2.3 The suffusion resistance index I_α

The suffusion resistance index is an alternative tool developed to evaluate the likelihood of suffusion occurring in hydraulic structures. Unlike the geometric criteria, which remain useful as first screening tools, this index is measured experimentally. This index determines the material's resistance to suffusion on a dedicated scale and provides a more detailed information than a bimodal 'stable' or 'unstable' classification. Unlike the critical hydraulic gradients, this index is obtained at the end of the suffusion process. In addition, it is based on three distinct measures: the amount of eroded particles, the in-situ differential pressure and the flow rate.

Marot et al., (2016) conducted a dedicated experimental study on suffusion to address the absence of a comprehensive erosion susceptibility classification. The study involved a diverse range of soil types and employed a modified triaxial permeameter. To evaluate suffusion susceptibility, the authors introduced an innovative energy-based method. Extensive testing on twelve soil specimens demonstrated the method's effectiveness in evaluating susceptibility for both cohesionless soils and clayey sand. Furthermore, the method yielded consistent classifications for suffusion tests conducted under varying hydraulic and stress conditions. The approach emphasizes the significance of the flow power in assessing suffusion, considering variations in pressure gradient and flow rate. The instantaneous flow power P_{flow} is expressed in watts as:

$$P_{\text{flow}} = (\gamma_w \, \Delta z + \Delta P) \, Q \tag{2-7}$$

where,

Q = Fluid flow rate (m^3/s)

γ_w= Specific weight of water (N/m^3)

ΔP = Pressure drop between upstream and downstream sections (Pa)

Δz = Difference in elevations between sections (m)

The direction of flow (upward or downward) is represented by the sign of Δz and in the case of horizontal flow, the total flow power simplifies to $\Delta P * Q$. Nguyen et al., (2012) showed the significant impact of hydraulic loading path on suffusion development and introduced the concept of energy expended by the seepage flow E_{flow} through the time integration of the instantaneous power. The cumulative loss dry mass (in kg) throughout the suffusion process characterizes the soil's response, accounting for mass lost during specimen preparation. Marot et al., (2016) suggested determining the cumulative expended energy and the cumulative loss dry mass at the end of the suffusion process. This final state is obtained when the hydraulic conductivity stabilizes and the erosion rate decreases and is referred to as the steady state. This steady state can be used to gauge suffusion susceptibility thanks to the erosion resistance index I_α:

$$I_\alpha = -\log\left(\frac{\text{Cumulative loss dry mass}}{E_{\text{flow}}}\right) \tag{2-8}$$

Based on I_α values, the authors proposed six categories of suffusion susceptibility, ranging from highly erodible to highly resistant. For instance, highly erodible for $I_\alpha < 2$; erodible for $2 \leq I_\alpha < 3$; moderately erodible for $3 \leq I_\alpha < 4$; moderately resistance for $4 \leq I_\alpha < 5$; resistant for $5 \leq I_\alpha < 6$; highly resistant for $I_\alpha > 6$. This classification provides a valuable framework to assess and

categorize the potential susceptibility of soils to suffusion. Zhong et al., (2018) further challenged the proposed suffusion susceptibility classification by applying the same method to various specimen sizes. Again, the method's effectiveness was demonstrated in evaluating the same susceptibility for a given soil irrespective of the specimen's size.

2.3 Parameters influencing suffusion

2.3.1 Effect of particle shape

Particle shape is a crucial aspect that may be characterized by three scales: sphericity, roundness and smoothness. Sphericity determines how closely a particle resembles a perfect sphere based on its width, length and height ratio, while roundness measures the smoothness or sharpness of its corners and edges. Smoothness, on the other hand, refers to the evenness of the particle's surface. The work of Kolbuszewski and Frederick (1963) demonstrates that higher angularity of particles leads to increased limiting porosities. Moreover, Marot et al., (2012) conducted experiments on three different samples with varying grain size distribution and angularity, revealing that an increase in the angularity of coarse fraction grains improves suffusion resistance. Despite the significant impact of particle shape on granular soil behavior, its investigation concerning internal erosion remains limited. This underscores the importance of considering particle shape to understand the whole suffusion process more comprehensively.

2.3.2 Effect of relative density

Relative density serves as a key factor in determining whether a soil is internally stable or unstable. Its influence is essential in understanding and characterizing the behavior of fine particles within the soil mass. Several research studies (Ahlinhan and M. Achmus, 2010; Gaucher et al., 2010; Ke and Takahashi, 2012a, 2012b; Indraratna et al., 2015; Chen et al., 2019) have shown that higher relative density is associated with increased stability, while lower relative density is linked to internal instability. The resistance index also increases with the density (Le et al., 2018).

In Mehdideh's (2018, p. 133) research, the back-calculation of α from Ke and Takahashi's (2012b) experiments demonstrated that the relative density has only a minor impact on the migration of fine particles in gap-graded soils with high values of $(D'_{15}/d'_{85})_{max}$. For soils exhibiting such high values, the fine particles remain loosely packed within the pores of the coarse skeleton, with limited contact (inactive fine particles), making the relative density largely insignificant in influencing particle behavior. Conversely, according to Ke and Takahashi (2012b), when the relative density of specimens with the same fine content is increased, it leads to a larger critical hydraulic gradient for internal erosion as shown in Figure 2.12. This indicates that higher relative density enhances the resistance against internal erosion's initiation. The combined findings emphasize that the impact of relative density on particle behavior and internal erosion varies depending on the specific characteristics of the soil and the fine particle content.

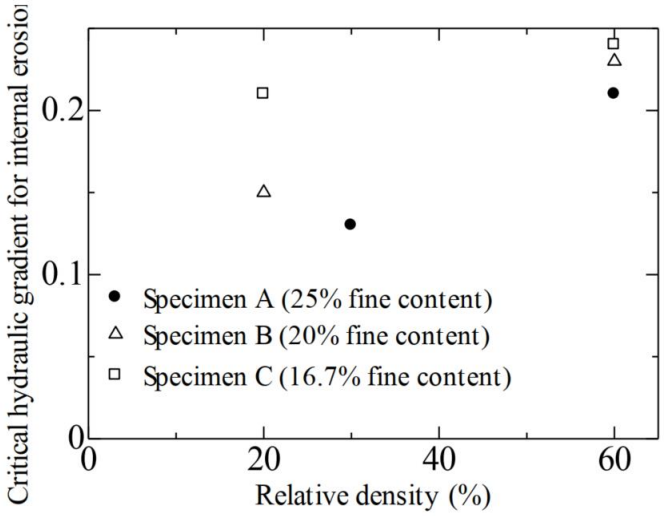

Figure 2.12 Relation between relative density and critical hydraulic gradient by Ke and Takahashi (2012b)

Shire et al., (2014) used Discrete Element Modeling (DEM) to investigate internal instability in broadly-graded cohesionless soils. Their research revealed that relative density plays a substantial role in shaping stress distribution within a critical finer fraction, specifically between 24% and 35%. Based on their findings, Shire et al., (2014) concluded that soils with a fine fraction greater than or equal to 25% can effectively improve stability by increasing in-situ relative density. Conversely, for soils with fine fraction less than 25%, densification efforts would not lead to a significant enhancement in stability.

Indraratna et al., (2015) studied well-graded soils using constriction size distribution and found that relative density significantly impacted samples with lower uniformity coefficient C_u. Their research also revealed that increasing the relative density reduced the quantity of erodible fines, highlighting its role in controlling internal instability and erosion susceptibility.

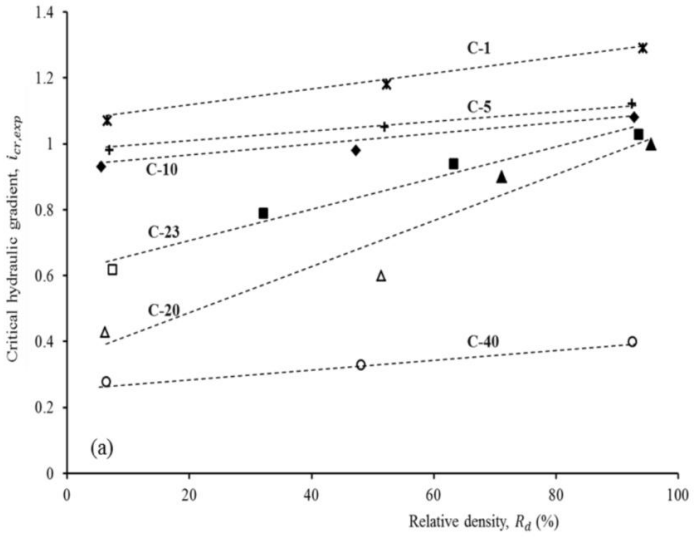

Figure 2.13 Relation of critical hydraulic gradient with relative density by Indraratna et al., (2015)

2.3.3 Effect of the microstructure (underfilled, in transition, overfilled)

In general, understanding the role of fine content in a binary mixture (i.e. gap-graded) is vital for accurately predicting soil behavior and suffusion susceptibility. Engineers should carefully assess the impact of fine particles on compressibility, permeability, shear strength and plasticity to make informed decisions during construction and design. According to ICOLD (2015, p. 135), Kenney and Lau (1985, 1986) discovered that for a soil to be susceptible to suffusion, the percentage of finer fraction should be smaller than the available void space. Their research indicated that this percentage should range between 20% of the total soil for well-graded soils and 30% for narrow-graded soils. However, Wan and Fell (2004, 2007) challenged this notion, proposing that theoretically, the percentage could be as high as 40%. Nonetheless, their experimental data revealed that for broadly graded soils, the percentage was between 22% and 33%, while for gap-graded soils, it ranged from 29% to 38%.

Various researchers in the literature have reported that the variation in fine content has an impact on the microstructure. Skempton and Brogan (1994) introduced two key parameters. The first parameter highlights the presence of a critical fines content, denoted as S^*, below which the fines in a gap-graded material cannot effectively fill the voids within the coarse component. In practical scenarios, the range of S^* is expected to lie within narrow limits, around 29% for loose packing or approximately 24% for dense packing. On the other hand, the second parameter points out that when the fines content, represented as S_{max}, exceeds approximately 35%, the coarse particles tend to remain suspended or "float" within a matrix of fines. Based on these parameters: when the fine content FC < S*, the soil exhibits an "underfilled" fabric; when $S^* < FC < S_{max}$, the fabric is considered in "transition" or "filled"; and when $FC > S_{max}$, the fabric is described as "overfilled." Subsequent research using the Discrete Element Method (DEM) by Shire et al., (2014; 2016) further validated the concept and emphasized that the suffusion susceptibility of transitional soil can be influenced by the relative density. Specifically, they found that an increase in relative density should lead to improved stability. However, in cases where the soil is underfilled, densification does not significantly impact the suffusion susceptibility.

Thevanayagam et al., (2002) and re-investigated by Thevanayagam (2007) presented an effective classification system aimed at identifying the microstructure of binary soil mixtures with different levels of fines content C_F as shown in Figure 2.14. For coarse grain soil mixtures (a), they observed three distinct microstructural configurations:

Case i. Fines are fully confined within the voids of the coarse grains

Case ii. Fines are confined and partially in contact with the coarse grains

Case iii. Fines are confined and act as separators between the coarse grains

For fine grain soil mixtures (b), two microstructural patterns were identified:

Case iv-1. Coarse grains are fully dispersed within the fine grain soil matrix

Case iv-2. Coarse grains are partially dispersed and serve as reinforcing elements within the soil matrix

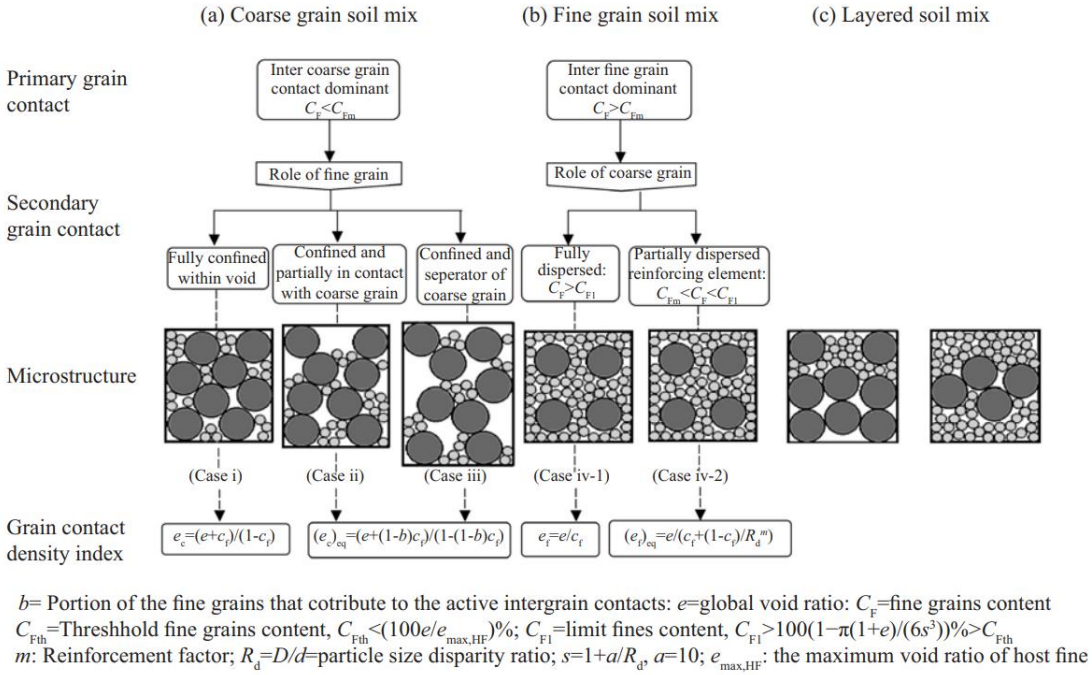

b= Portion of the fine grains that cotribute to the active intergrain contacts: e=global void ratio: C_F=fine grains content
C_{Fth}=Threshhold fine grains content, $C_{Fth}<(100e/e_{max,HF})\%$; C_{F1}=limit fines content, $C_{F1}>100(1-\pi(1+e)/(6s^3))\%>C_{Fth}$
m: Reinforcement factor; $R_d=D/d$=particle size disparity ratio; $s=1+a/R_d$, a=10; $e_{max,HF}$: the maximum void ratio of host fine

Figure 2.14 Intergranular soil mix classification by Thevanayagam et al., (2002)

In the microstructure analysis, researchers identified four distinct cases (Figure 2.14). In cases i, ii and iii, the fine content falls below a threshold value C_{Fth} and the primary soil skeleton is predominantly composed of coarse grain soil. In case i, fine particles are entirely confined within the pore spaces, not actively contributing to the soil structure but acting as fillers instead. Case ii demonstrates fine particles being confined and partially in contact with coarser grains, thereby adding secondary reinforcement. In case-iii, fines act as separators between the coarse grains. However, in case iv-2, the fine content exceeds the threshold fine content C_{Fth} but remains below the limit fine content C_{F1}. In this particular scenario, the soil structure becomes partially dispersed and carries a minor portion of effective stresses. Conversely, in case iv-1, the soil structure is predominantly composed of fine particles, with the coarse particles fully dispersed within the matrix of fine grains, carrying a major portion of effective stresses. A category where coarse and fine grains form a fully layered system is commonly observed in contact erosion, as shown in Figure 2.14 (c).

Ke and Takahashi (2014a) conducted an extensive investigation into suffusion characteristics and its mechanical implications using a series of soil specimens with varying fines content percentages (15%, 25% and 35%). These specimens represented distinct microstructural compositions and were subjected to various stress states. The study elucidates the crucial role played by the initial fines content in shaping soil packing behavior and, consequently, exerting a significant influence on hydromechanical responses. In specimens featuring lower fines content, fine particles were observed to preferentially occupy voids among coarser grains and remain locked within these voids during the erosion process. In contrast, specimens with higher fines content exhibited fines acting as separators between coarser grains. Notably, the study emphasizes that the presence of larger voids among coarser grains in specimens with higher initial fines content contributes significantly to increased fines loss during suffusion. Consequently, soils characterized by higher initial fines

content exhibit more pronounced suffusion effects, highlighting the intricate interplay between fines content, microstructure and soil behavior.

Prasomsri and Takahashi (2020) investigated the contribution of non-plastic fines to seepage-induced suffusion susceptibility in gap-graded sands. Their results showed that the initial fines content significantly affected the onset and progression of suffusion. Underfilled soils experienced self-filtering and suffusion at relatively low hydraulic gradients. Overfilled soils were susceptible to *suffosion*, seepage-induced failure, or internal stability at higher hydraulic gradients. Undrained compression tests on these eroded specimens revealed that suffusion caused soil loosening and increased contractive behavior, while suffosion resulted in a more dilative behavior at large strain level.

Prasomsri et al., (2021) found that fines content played a crucial role in determining the onset of suffusion in gap-graded sands. Underfilled soils, with fines content below 30%, exhibited vulnerability to suffusion at relatively low hydraulic gradients. Transitional soils, containing fines ranging from 30% to 35%, showed suffusion at larger critical hydraulic gradients. On the other hand, overfilled soils, with fines content exceeding 35%, displayed either suffusion or internal stability, but required higher hydraulic gradients for erosion initiation.

2.3.4 Effect of the stress state

The behavior of soils within hydraulic embankment structures is intrinsically linked to the stress states they experience. These stress states encompass a wide spectrum, including conventional compressive stress, undesired extension stress arising from arching effects and the hydro-mechanical stress associated with rigid body behavior, commonly represented as the oedometric stress state. Importantly, the oedometric stress state has been extensively employed in the development of criteria based on grain size. Despite these advancements, the potential influence of various stress states on parameters relevant to suffusion, a phenomenon that can significantly affect the stability of embankment structures, remains an area of inquiry that demands comprehensive elucidation.

In the realm of suffusion research, a notable aspect is the concentration of existing literature on exploring the mechanical consequences of stress states, with a lesser emphasis on understanding the onset and progression of suffusion. For instance, investigations by researchers such as Moffat and Fannin (2006, 2011), Bendahmane et al., (2008), Luo et al., (2013; 2020), Chang and Zhang (2013a) and Ke and Takahashi (2014a) have predominantly delved into discerning the conditions that lead to instability onset through controlled stress manipulation. These efforts have yielded key findings, which are synthesized and presented in the subsequent sections.

Moffat and Fannin (2006, 2011): The study conducted by Moffat and Fannin in 2006 aimed to explore the onset of seepage-induced instability in a specific granular material composed of glass beads. The research sought to better understand the hydromechanical relationship between effective stress and hydraulic gradient, particularly in the context of materials that exhibit potential instability when subjected to slurry mixing and discrete deposition techniques. The authors employed a rigid-wall permeameter for their experimental setup and maintained unidirectional seepage flow under head-controlled hydraulic loading conditions. Notably, the average initial

gradient across the specimen was consistently around one for all conducted tests. It is essential to emphasize that throughout their investigation, only the vertical effective stress was considered in the analysis of effective stress. The findings of Moffat and Fannin's study suggest the presence of a potential relationship between the vertical effective stress and the critical hydraulic gradient that triggers instability within the glass beads material.

In a subsequent investigation conducted by Moffat and Fannin in 2011, their research was expanded to include core zone samples (C-20 and C-30) and samples from the immediate downstream transition zone (T-0 and T-5) of the W.A.C Bennett Dam. This study aimed to establish a hydromechanical relationship for four widely graded grain size distributions with varying fine content (0%, 5%, 20% and 30% fines with a particle size lower than 74 μm), under conditions of unidirectional seepage flow using a permeameter configuration. The localized onset of instability was characterized by a significant decrease in the local hydraulic gradient, triggered by an increase in hydraulic conductivity or a reduction in effective stress. The corresponding reduction in the local hydraulic gradient value is referred to as the critical hydraulic gradient, marking the termination of the test. Multiple tests were conducted for the four fine content series, varying the effective stress to delineate unstable stress-gradient zones. The development of minimum and maximum envelopes was based on measured scattered values of critical gradients (see Figure 2.15). The findings postulate that the spatial variation of effective stress and hydraulic gradient plays a crucial role in determining the location where particle migration instability initiates. The hydromechanical paths for the four different fine content tests revealed distinctive characteristics for each of the four soils tested. However, a linear trend emerged, showing an increase in critical hydraulic gradient with rising effective stress within the stress-gradient space, as depicted in Figure 2.15. The most stable samples were identified as core samples C-20 and C-30, respectively, in ranking, while the least stable samples were identified as transition zone samples T-5 and T-0.

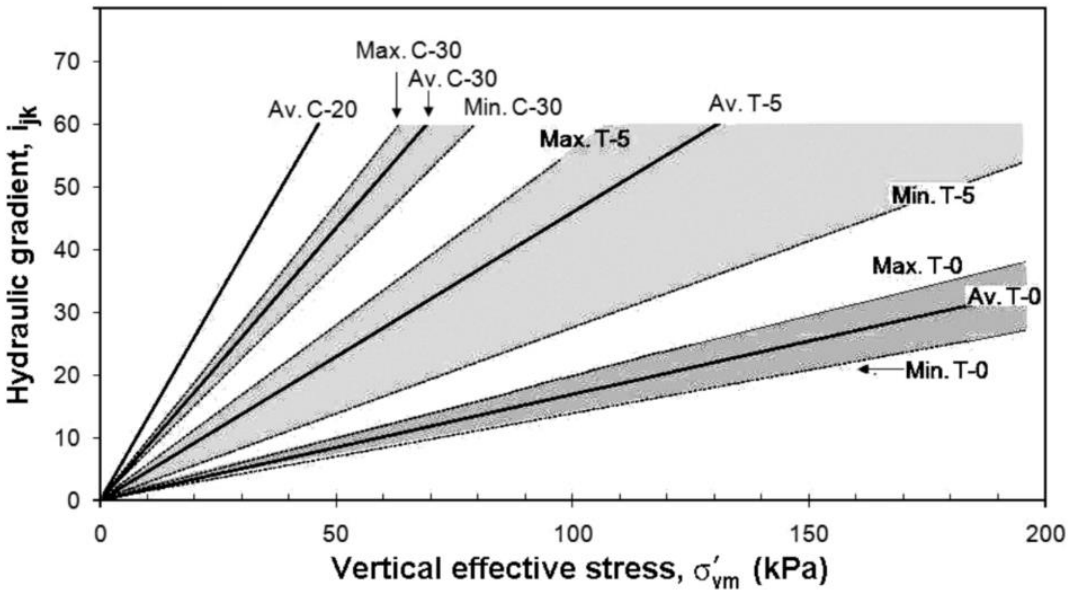

Figure 2.15 Hydromechanical boundaries in stress-gradient space by Moffat and Fannin (2011)

Bendahmane et al., (2008) examined suffusion tests by subjecting clayey sand specimens to isotropic confining pressure. Their research revealed that in the context of clayey sand, the rate of suffusion decreases when the confining pressure is increased indicating that an increase in the effective stress causes an increase in the soils' resistance to suffusion.

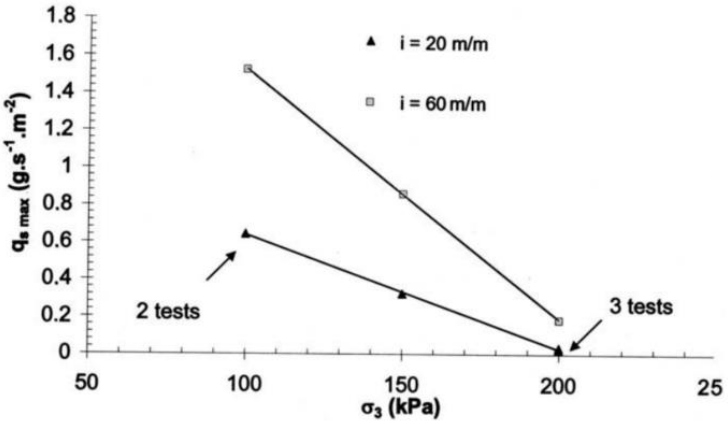

Figure 2.16 The influence of confining pressure on erosion rate, as studied by Bendahmane et al., (2008)

Luo et al., (2013) investigated the hydro-mechanical effects on suffusion using a partially penetrated cut-off wall setup. Their research focused on a gap-graded sandy gravel material with an underfilled soil microstructure, characterized by a fine content of approximately 18%. The primary emphasis in Luo et al.,'s study was on the influence of stress state on suffusion, specifically confining stress, with no consideration of axial load effects. The study introduced the concept of the penetration ratio, defined as the ratio of the cut-off wall's height to the specimen's dimensions. To identify suffusion-induced failure in the specimen, the researchers monitored abrupt increases in flow velocity and eroded mass. It is essential to note that this investigation primarily concentrated on the initiation phase of suffusion. In other words, it aimed to pinpoint the critical suffusion hydraulic gradient by observing particle migration and minimal eroded mass, without delving into the parameters governing suffusion development in detail. The study revealed a linear relationship between the critical suffusion hydraulic gradient and confinement stress, as illustrated in Figure 2.17.

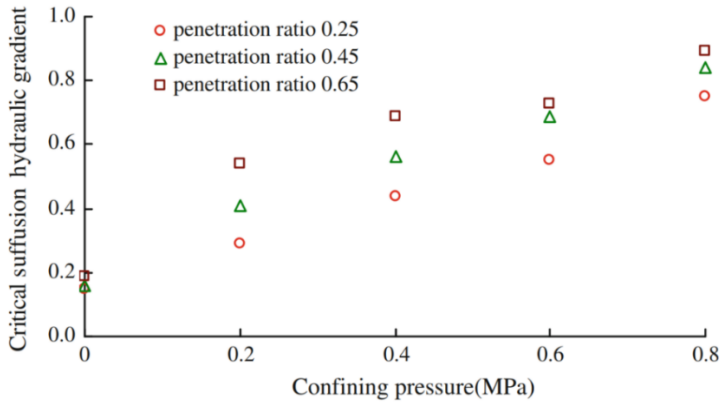

Figure 2.17 Relation between confining pressure and critical suffusion hydraulic gradient by Luo et al., (2013)

In a subsequent study conducted by Luo et al., (2020), the researchers conducted a comparative investigation into the impact of deviatoric stress on four distinct soils, each characterized by a fine content ranging from 15% to 25%. Notably, their analysis was limited to the initiation phase of suffusion. An intriguing outcome of this study was the observation of a non-linear relationship between the critical hydraulic gradient and deviatoric stress. Furthermore, the choice to adopt a specific pore-opening size of 4 mm in the experiments may have significantly influenced both the initial stages and subsequent development of suffusion. This choice gains particular significance when considering that the minimum size of coarse grains typically falls around 1 mm. Consequently, it can be anticipated that the selected pore-opening size plays a pivotal role in shaping suffusion behavior, given its potential to influence the detachment of both fine and coarse particles. This, in turn, results in a complex microstructure, especially under the application of deviatoric stress.

Chang and Zhang (2013a) comprehensive laboratory experiments on internal erosion in soils under diverse stress conditions revealed distinct erosion stages and critical gradients associated with initiation, skeleton deformation and failure. Notably, the initiation hydraulic gradient, under compression stress, increased with the shear stress ratio but decreased near shear failure, while soils under triaxial extension stress exhibited higher initiation gradients at the same porosity. Interestingly, isotropic stress states lacked a skeleton-deformation gradient, suggesting that the maximum applied gradient did not reach the development phase due to reduced force chain buckling as shown in Figure 2.18. Consequently, under isotropic stress, the skeleton-deformation gradient was postulated to be much higher than in compression or extension stress states. Additionally, the inconsistency in hydraulic loading paths i.e. post-initiation phase added complexity to their findings, contributing valuable insights into stress state's critical role in suffusion behavior.

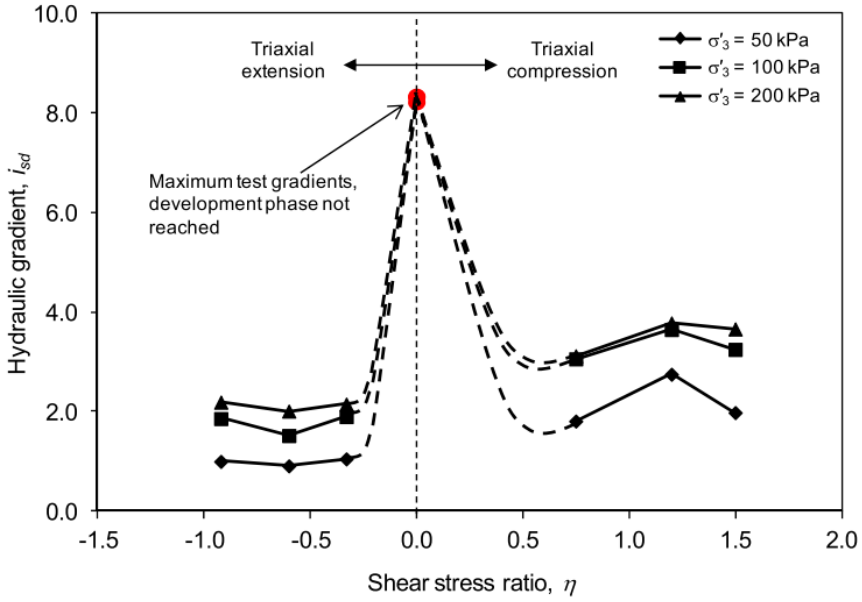

Figure 2.18 Skeleton-deformation hydraulic gradient vs. Shear stress ratio (Chang and Zhang, 2013a)

Ke and Takahashi (2014a) dedicated study investigated the influence of effective stress on suffusion. They conducted constant-flow-rate controlled seepage tests on specimens with an initial fines content of 35%, subjecting them to three different effective confining pressures (50 kPa, 100 kPa and 200 kPa). Their findings revealed that specimens subjected to the highest confining pressure (200 kPa) exhibited significantly less pronounced increases in hydraulic conductivity, cumulative fines loss and volumetric strain compared to those tested under the lowest applied confining pressure (50 kPa). This observation strongly suggests that higher effective confining pressure effectively mitigates suffusion development, aligning with findings from a previous study by Bendahmane et al., (2008).

Liang et al., (2017) explored the influence of isotropic and anisotropic stress conditions on critical hydraulic gradients associated with particle movement during suffusion experiments. They defined the Low Critical Hydraulic Gradient (LCHG) as the hydraulic gradient at which the observable movement of fine particles initiates. Furthermore, they introduced the High Critical Hydraulic Gradient (HCHG), which signifies the hydraulic gradient at which global erosion, distinct from local erosion, occurs during the experiments. The determination of HCHG involved averaging the hydraulic gradients observed in the current erosion step and the preceding step. This comprehensive study, conducted with 36 specimens containing 20% fines and employing a gradient-controlled seepage mechanism, revealed notable trends. Under isotropic stress conditions, critical hydraulic gradients appeared to increase with confining stress, whereas under anisotropic stress conditions, critical hydraulic gradients exhibited a non-linear relationship with deviatoric stress as shown in Figure 2.19.

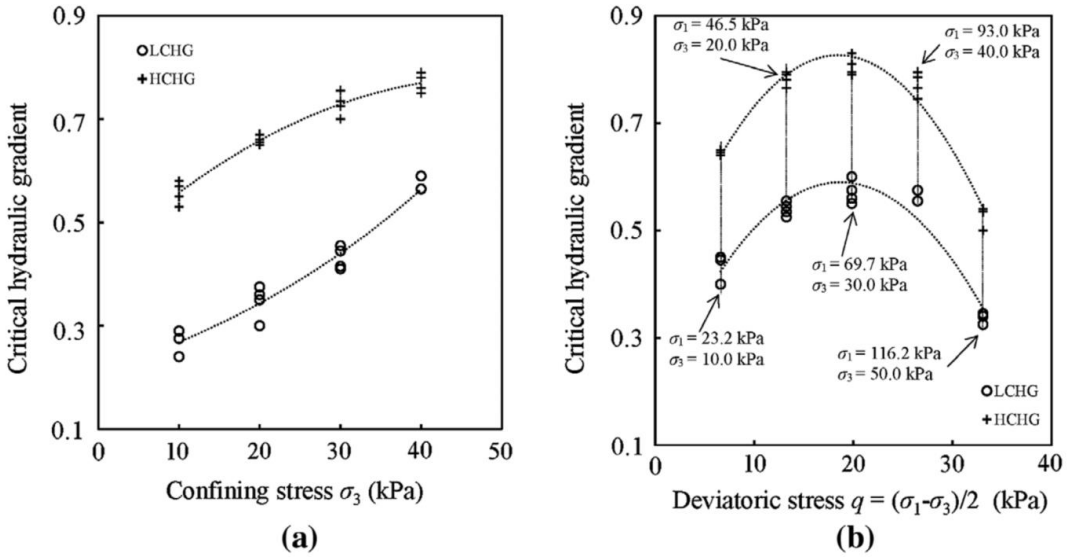

Figure 2.19 Stress states influence on critical hydraulic gradients: (a) under isotropic and (b) anisotropic by Liang et al., (2017)

A conclusive synthesis of the existing research reveals several key insights regarding the influence of stress states on suffusion behavior. It is evident that an increase in confining stress generally leads to a higher critical hydraulic gradient, indicating increased soil resistance to suffusion, albeit with potential variations depending on specific soil characteristics. However, a limited number of studies have delved into the detailed impact of stress state variations, including isotropic, compressive and tensile states, on suffusion behavior. Furthermore, there is a notable absence of

comparative studies involving the oedometric stress state, despite its extensive use in proposing suffusion susceptibility classifications and criteria. Fewer still have explored the combined effects of stress state and fines content. Most studies primarily focus on the initiation phase, with limited parameters characterizing the influence of stress state on the broader suffusion development process. These gaps underscore the need for further experimental investigations to comprehensively understand the interplay between stress states and fines content throughout the entirety of the suffusion process.

It is imperative to recognize that challenges arise when comparing these findings with earlier research due to inherent variations in soil types (ranging from underfilled to in transition and overfilled), seepage directions (downward or upward) and the application of diverse hydraulic loads. These variations significantly influence both the initiation and development of suffusion, necessitating caution in direct comparisons. An essential consideration lies in the definition and characterization of different phases of suffusion, as the mechanical consequences are assessed at varying degrees of suffusion in different studies. Establishing clear and consistent definitions for each phase of suffusion is paramount to facilitate accurate comparisons across multiple studies addressing the mechanical consequences of suffusion.

2.3.5 Effect of the hydraulic loading path

Researchers have explored different approaches to evaluate the effect of the hydraulic history on the suffusion process, employing either flow rate control or hydraulic gradient control. For example, Ke and Takahashi (2014b, 2014a), Slangen and Fannin (2017), Mehdizadeh et al., (2017), Mehdizadeh (2018) and Nguyen et al., (2019) successfully employed flow rate control in their studies. On the other hand, Sail et al., (2011); Chang and Zhang (2011; 2013b, 2013a), Chang et al., (2012) ; Rochim et al., (2017) ; Zhong et al., (2018) and Marot et al., (2020) opted for hydraulic gradient control. Fewer studies compared the significant influence of these types of hydraulic loading path on the suffusion process and the related parameters (Nguyen et al., 2012; Rochim et al., 2017; Prasomsri and Takahashi, 2021; Takahashi, 2023). Some key conclusions are summarized below.

Nguyen et al., (2012) characterized the erodibility of clayey sand and performed either flow-rate-controlled or hydraulic-gradient-controlled tests. Flow rate-controlled tests showed a hydraulic conductivity which is firstly decrease and subsequently increasing, while gradient-controlled tests led to a sole decrease of the hydraulic conductivity due to filtration effects. Thanks to the energy-based approach and to the erosion resistance index, the obtained classification of erosion processes was identical for hydraulic gradient controlled tests and for flow rate-controlled tests.

Luo et al., (2013) observed that a long-term large hydraulic head, in comparison with short-term experiments, resulted in increased eroded mass and reduced the hydraulic gradient needed for substantial suffusion development in their hydraulic gradient-controlled erosion tests.

In the study conducted by Rochim et al., (2017), a comprehensive investigation into the intricate processes underlying suffusion development unveiled the involvement of detachment and partial filtration within the porous network, resulting in notable variations in hydraulic conductivity and interstitial pressure dynamics. Central to the analysis of suffusion initiation lies the determination

of the critical hydraulic gradient. However, a pivotal finding from their research emphasizes that the nature of hydraulic loading can profoundly modify the critical hydraulic gradient, thus altering the conditions under which suffusion occurs. This observation underscores the multifaceted nature of suffusion, arising from the interplay of detachment, transport and filtration processes, all contingent upon the history of hydraulic loading. To comprehensively explore these interdependencies and the suffusion development, Rochim et al., advocate for a systematic approach involving the incremental increase of hydraulic gradients until hydraulic conductivity stabilizes. Moreover, it is imperative to independently characterize both the hydraulic loading and the ensuing erosion, encompassing the computation of two critical parameters: the energy dissipated by water seepage and the cumulative loss of dry mass.

The study conducted by Prasomsri and Takahashi (2021) offers valuable insights into suffusion development under the influence of multiple seepage conditions and isotropic stress states. It is essential to note that their experimental system was designed such that the measured flow rate and gradient were direct responses to the imposed pressure from the inlet tank, creating a cyclic pressure regime ascending from 400 kPa to 430 kPa and descending back to 400 kPa at a controlled rate of 2 kPa/min. The hydraulic loading history during these imposed pressure cycles is graphically represented in Figure 2.20 (a) and the repetition of this hydraulic loading sequence is defined as the multiple seepage conditions. It is noteworthy that the development of hydraulic conductivity during the descending and ascending phases of the seepage cycle was not analyzed due to the pronounced fluctuations in the cyclic seepage loading. However, it is imperative to acknowledge that the cyclic seepage flow characteristics, encompassing both loading and unloading phases of hydraulic loading, could significantly influence the outcomes of seepage tests, thus warranting further investigation, as aptly suggested by the authors. Their research findings highlight that suffusion induced a non-destructive response, exhibiting as seepage-induced eroded soil mass without notable volume changes but with observable alterations in hydraulic conductivity. Furthermore, suffusion-induced local clogging of detached particles resulted in discernable variations in discharge velocity and hydraulic gradient. This observation underscores the critical importance of considering both flow and gradient dynamics when evaluating the complex hydraulic loading history and its implications in suffusion phenomena assessment.

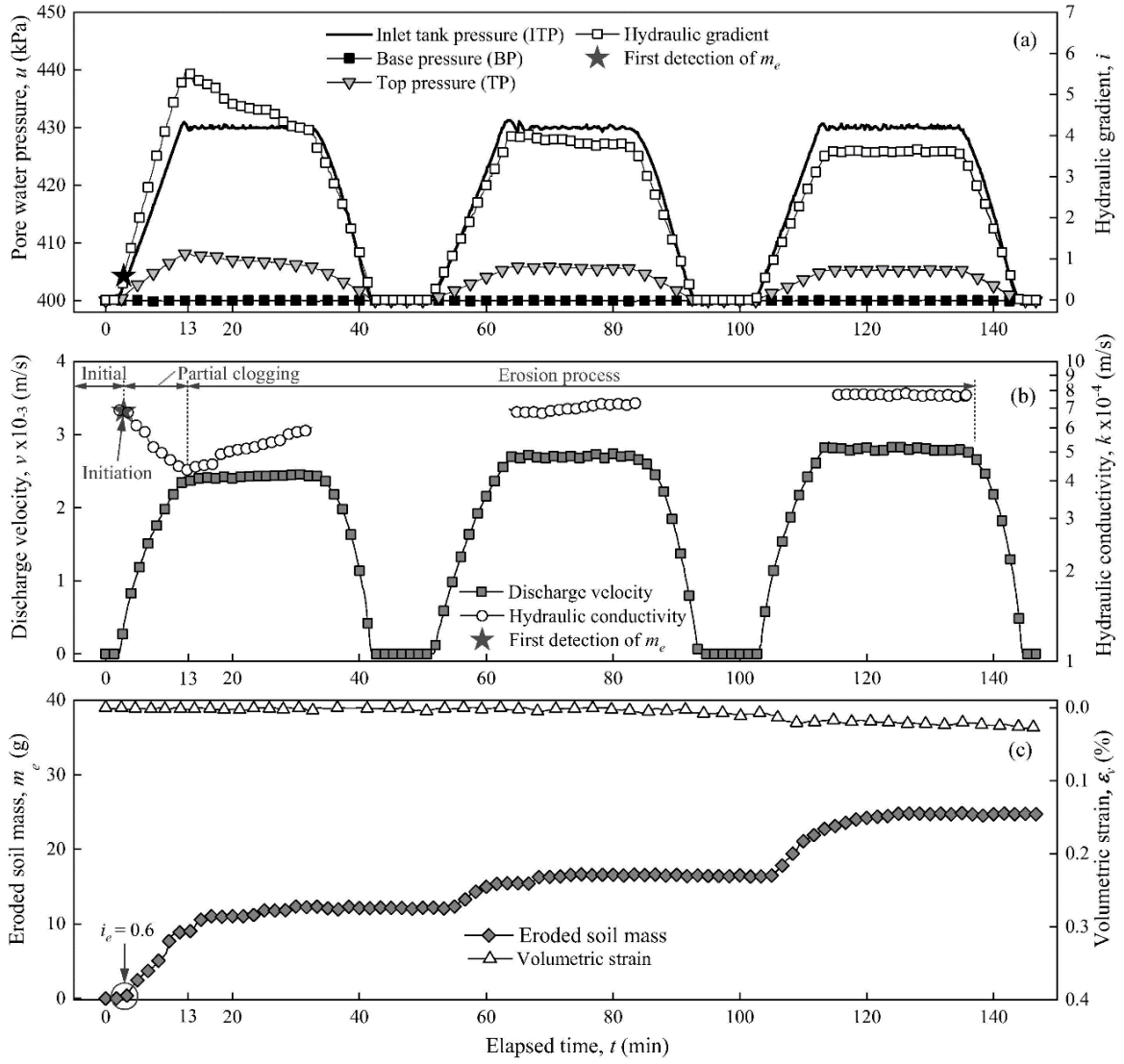

Figure 2.20 Seepage test scheme and results for sample WE_NE3 (Prasomsri and Takahashi, 2021)

Xu et al., (2022) conducted a series of carefully designed tests, encompassing various hydraulic paths such as monotonic stepwise loading, cyclic reversal subsequent to monotonic loading and direct cyclic loading. Their meticulous experimentation revealed a notable trend: cyclic hydraulic gradient reversals had the effect of significantly intensifying the erosion process, even when the mean hydraulic gradients remained consistent. Intriguingly, microscopic analysis further unveiled a reduction in clogging within the soil matrix during cyclic reversals, a phenomenon that seemingly paradoxically facilitated overall erosion. It is noteworthy that the selected gap-graded binary mixture in this study represents an overfilled microstructure, characterized by a substantial fine content of 35%. Additionally, it is important to acknowledge that the duration of reversal gradients appears very quick, exceeding what would typically be observed in real-world scenarios such as embankment dams and dikes. On the other hand, the effect of hydraulic loading frequency on internal erosion is not investigated.

Chen and Zhang (2023) study explores suffusion development under cyclic hydraulic gradients, with a focus on the influence of mean hydraulic gradient and cyclic gradient amplitude in a gap-graded soil containing 35% fine content. Their findings reveal significant impacts on erosion, driven by the initial grain size distribution and cyclic gradient patterns. Cyclic seepage promotes the loss of fine particles, resulting in increased hydraulic conductivity, particularly within internally unstable soil. Notably, a large initial hydraulic gradient (i = 9) accelerates observable erosion, with tests reaching gradients as high as 41 (see Figure 2.21). However, this level of gradient is rarely encountered in real-world field scenarios and may introduce potential heterogeneity-related influences on the outcomes, beyond the sole effect of cyclic hydraulic loading paths. The increase in cyclic gradient amplitude (Δi) initially enhances hydraulic conductivity but stabilizes at a constant value over time. As reported, erosion is most pronounced in the first cyclic stage and diminishes in subsequent stages, even with an increase in mean hydraulic gradient.

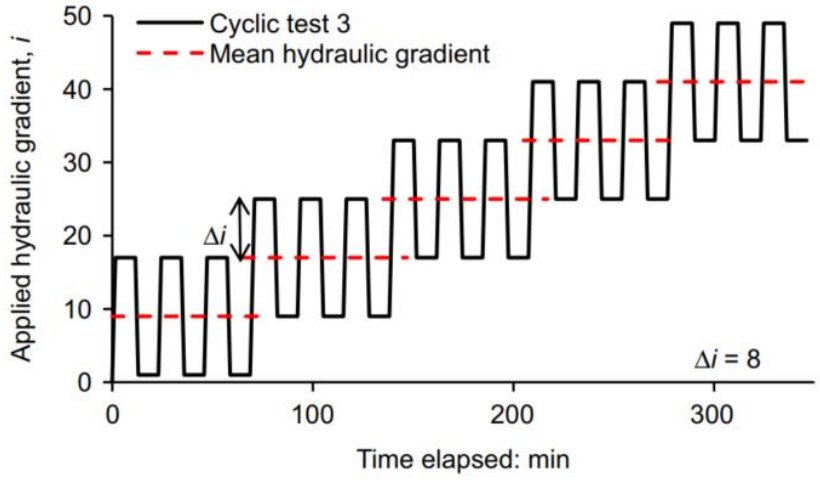

Figure 2.21 Schematic representation of cyclic hydraulic loading test setup by Chen and Zhang (2023)

Furthermore, in the comparison study conducted by Takahashi (2023), distinct effects of seepage control methods on soil behavior during erosion were highlighted. Flow velocity control significantly altered the soil structure, causing a considerable loss of fines and densification and resulting in larger reductions in undrained strength. In contrast, tests under hydraulic gradient control led to a more uniform erosion pattern in the cross-sectional direction, resulting in smaller fines loss but making the soil more fragile and leading to smaller reductions in undrained strength. With the objective of following the development of all suffusion phases (detachment, transport and filtration, which in particular depend on the history of hydraulic loading), tests must be realized by increasing the applied hydraulic gradient, which should be carried on until the stabilization of the hydraulic conductivity (Marot et al., 2016; Rochim et al., 2017; Takahashi, 2023).

2.4 Devices for experimental investigation on suffusion

The study of suffusion has undergone progressive phases of device development. Initially, the assessment of internal stability involved the use of simple rigid wall permeameters (Sherard et al., 1984). These permeameters relied on visual inspection of eroded mass, geometrical criteria and particle size distribution analysis. However, they lacked the capability to measure influential parameters such as the pore pressure, the axial deformation and the erosion rate. Subsequent advancements led to the development of modified rigid wall permeameters, which incorporated pressure ports to measure pore water pressure, hydraulic conductivity, axial deformation and erosion rate. Despite advancements in seepage control and eroded mass measurement, these modified permeameters still did not incorporate a comprehensive loading system. In contrast, the third phase of devices, known as modified triaxial permeameters, addressed the issue of preferential seepage at the interface of the rigid wall and the specimen, significantly impacting the volumetric erosion mechanism. These devices featured improved axial loading systems and a better control over stress states. This section provides a detailed overview of the pivotal role played by experimental devices in advancing suffusion research. The accomplishments and innovative features of these devices are presented, highlighting the significant advancements in suffusion research.

2.4.1 Rigid wall permeameters

The evolution of devices designed to measure the susceptibility of materials to internal erosion has witnessed substantial advancements throughout the years. Initially, early devices, as described by Sherard et al., (1984) and Kenney and Lau (1985), adopted a basic rigid wall configuration. These early setups had limited control over the assessment of seepage and erosion susceptibility, relying primarily on mass loss measurements and subsequent particle size distribution analysis following erosion.

As the field progressed, improved versions of rigid wall permeameters were developed to enhance the study of material susceptibility. These advancements included the refinement of seepage control systems, the incorporation of piezometers to measure local pore pressure along the specimen and the determination of flow rates for calculating hydraulic conductivity, as demonstrated by Skempton and Brogan (1994) and Ke and Takahashi (2012b). These improvements were further complemented by measurements of mass loss and post-suffusion particle size distribution analysis, as observed in studies such as Lafleur et al., (1989), Sterpi (2003), Wan and Fell (2004).

It is notable that in most experimental tests, seepage flow was directed downward, leveraging gravity to aid in the recovery of eroded particles. However, some devices also incorporated upward seepage flow directions, as evidenced by experiments conducted by Tanaka and Toyokuni (1991) and Ke and Takahashi (2012b). Additionally, in certain cases, both upward and downward seepage directions were employed, as exemplified by the studies conducted by Garner and Sobkowicz (2002), Moffat and Fannin (2006) and Moffat and Fannin (2011). Furthermore, some devices allowed for the alteration of seepage flow direction to the horizontal plane, as seen in studies by Ahlinhan and Achmus (2010), Pachideh and Hosseini (2019) and Marot et al., (2020).

Despite these advancements, it is worth noting that most of these studies did not apply vertical stress, with some relying on nominal top loads (Kenney and Lau, 1985; Åberg, 1993). Nevertheless, certain experimental setups incorporated axial loading systems, enabling the measurement of axial loads at either the top (Li, 2008) or both the top and bottom of the specimen(Moffat and Fannin, 2006; Sail et al., 2011). This additional feature provided a more comprehensive understanding of material behavior under varying stress conditions.

One notable advantage of rigid wall permeameters is their capacity to provide external visualization of the specimen. This feature allows for the utilization of external methods such as X-ray topography to measure local density Sibille et al., (2015) and monitor microstructure evolution during testing, as effectively demonstrated by Nguyen et al., (2019). However, it is essential to acknowledge that these setups may lack control over confinement stress, potentially preferential flow affect the local density and overall permeability.

In summary, the evolution of devices for measuring material susceptibility to internal erosion has progressed from simple rigid wall configurations with limited control to more advanced setups that incorporate seepage control, stress monitoring and flow rate measurements. These advancements have significantly contributed to the understanding of material behavior in the context of internal erosion. However, challenges associated with controlling preferential flow remain a prominent area of interest and concern within this field of study. For reference, the general configurations of rigid wall permeameters adopted by various researchers are illustrated from Figure 2.22 to Figure 2.25.

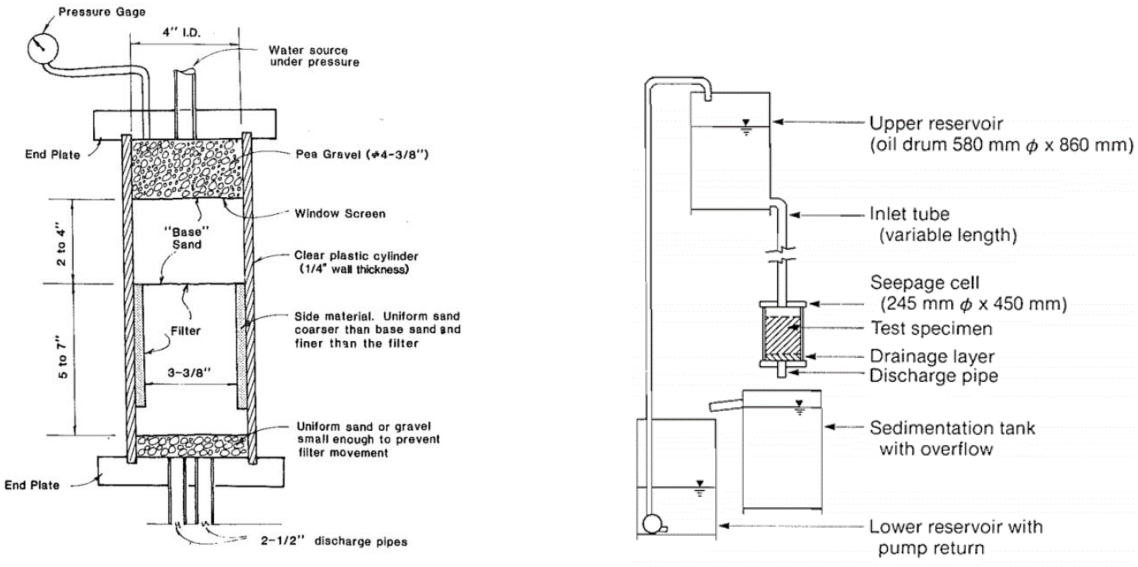

[a] *[b]*

Figure 2.22 Rigid wall permeameters configuration by [a]Sherard et al., (1984) and [b] Kenney and Lau (1985)

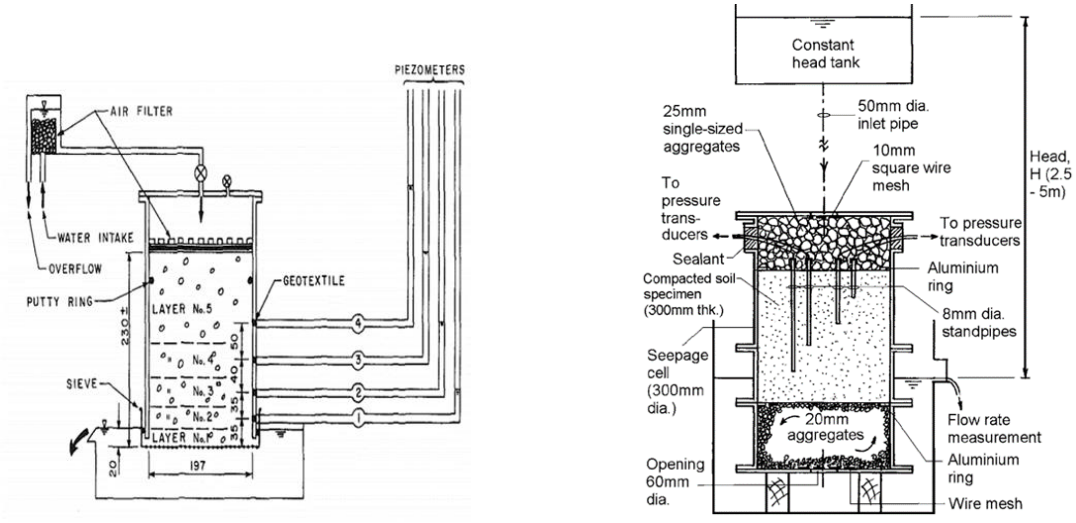

[a] *[b]*

Figure 2.23 Rigid wall permeameters configuration by [a] Lafleur et al., (1989) and [b] Wan and Fell (2008)

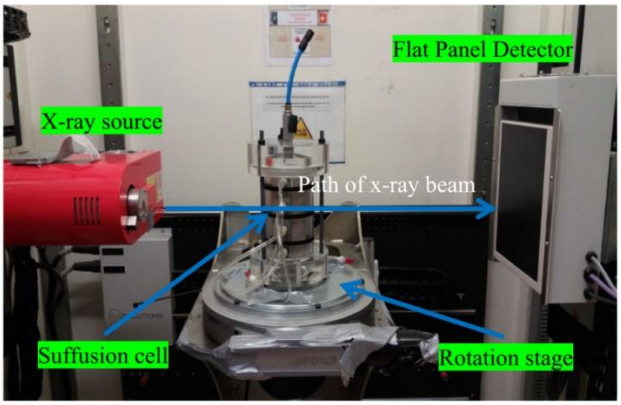

Figure 2.24 Rigid-wall permeameter configuration with X-ray chamber by Nguyen et al., (2019)

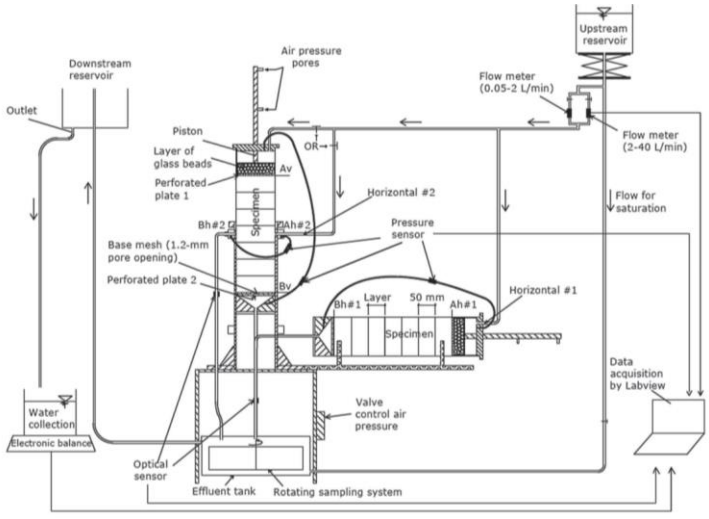

Figure 2.25 Multidirectional flow apparatus for suffusion susceptibility testing (Marot et al., 2020)

2.4.2 Modified triaxial permeameters

The development of devices for investigating material susceptibility to internal erosion has led to the creation of modified triaxial permeameters with innovative features aimed at overcoming challenges associated with preferential seepage flow paths. These advanced devices offer enhanced control over stress states and seepage conditions, enabling comprehensive investigations into the suffusion process. Additionally, modified triaxial permeameter has capability to incorporate the measurement of flow rates, eroded mass, axial and volumetric deformation. Several researchers have contributed to the refinement and utilization of these modified triaxial permeameters over the years, each building upon the work of their predecessors:

One such notable advancement was introduced by Bendahmane et al., (2008), who addressed concerns regarding preferential seepage paths affecting erosion initiation. They developed an experimental device that eliminated preferential flow, allowing for controlled stress states and the measurement of flow rates and eroded mass. Marot et al., (2009; 2012) and Nguyen et al., (2012) utilized the same modified triaxial permeameter device to study changes in hydraulic conductivity, water flow rate, particle angularity and erodibility during suffusion. Marot et al., (2011) introduced an innovative optical sensor integrated into the device, enabling real-time monitoring of fine solid particle concentrations during fluid flow experiments. Expanding on the device's capabilities, Marot et al., (2016) investigated both suffusion and global backward erosion processes using the originally designed device. The general configuration of device is shown in Figure 2.26

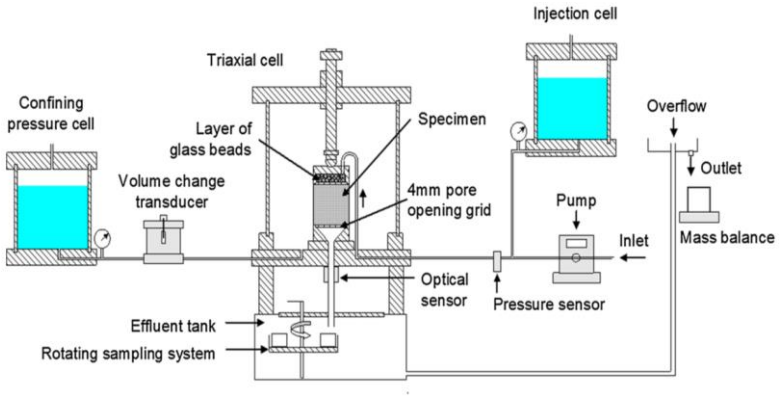

Figure 2.26 Device configuration for internal erosion study by Marot et al., (2016)

Shwiyhat and Xiao (2010) conducted preliminary studies on the mechanical characteristics of sandy soil impacted by suffusion, adapting the triaxial cell to allow seepage and eroded soil particles to exit the specimen into an effluent tank. This modification facilitated the measurement of erosion rates, as later utilized by Xiao and Shwiyhat (2012) to investigate the influence of suffusion on instability onset.

Chang and Zhang (2011) developed a stress-controlled erosion apparatus, providing independent control over hydraulic gradient and stress state and computed radial deformation from planar deformation observed on digital photographs (Figure 2.27) . Chang and Zhang (2013a) conducted extensive laboratory tests on internal erosion initiation and development under various stress conditions using the same device. The modified triaxial permeameter served a significant role in studies conducted by Chang et al., (2012) and Chang et al., (2014), allowing for successive

experiments on saturation, consolidation, erosion and the mechanical consequences of eroding non-plastic fine particles. Chen et al., (2016) investigated post-erosion stress-strain behavior, aligning their results with the findings from Chang and Zhang's study in 2011. Furthermore, Chen and Zhang (2023)conducted preliminary laboratory tests on the device to study the development of internal erosion and changes in hydraulic conductivity under one-way cyclic seepage, along with the post-erosion stress-strain behavior.

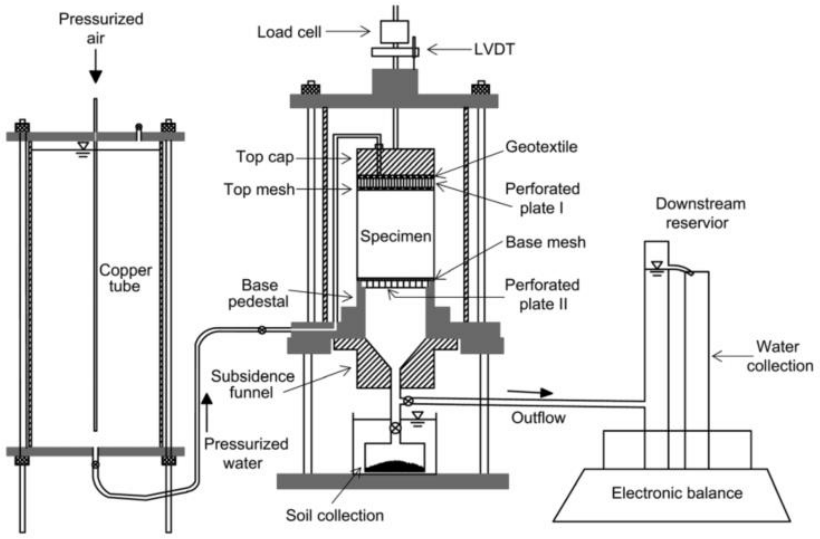

Figure 2.27 Schematic of modified triaxial apparatus by Chang and Zhang (2011)

Ke and Takahashi (2014b) developed a new modified triaxial permeameter that enabled the study of eroded soils within a single test duration. This innovation incorporated a continuous monitoring system to measure eroded soil mass and focused on investigating the drained and undrained behavior of gap-graded non-cohesive soils. The volumetric deformation is deduced from the local measurement of three pairs of strain gauges. Subsequent studies by Ke and Takahashi (2015), Ouyang and Takahashi (2015) and Ke et al., (2016) utilized the same modified triaxial permeameter to investigate various aspects of suffusive cohesionless soil and internal erosion. Furthermore, Prasomsri and Takahashi (2020, 2021) utilized a revised version of the device initially developed by Ke and Takahashi (2014b) as depicted in Figure 2.28

Another innovative development is the double-wall triaxial cell, initially conceptualized by Bishop and Donald (1961) and further refined by Slangen (2015), Slangen and Fannin (2017), McClelland (2020) and Ataii and Fannin (2022), enabled both triaxial and modified triaxial permeameter tests. This innovative design allowed for the indirect measurement of specimen volume change by monitoring the fluid surrounding the specimen. Eroded mass during the test could be collected and quantified, following a methodology adapted from the work of Ke and Takahashi (2014b). The schematic representation of device is shown in

These advanced devices have significantly expanded the capabilities of researchers in the field of internal erosion, enabling more comprehensive studies and providing valuable insights into the suffusion process.

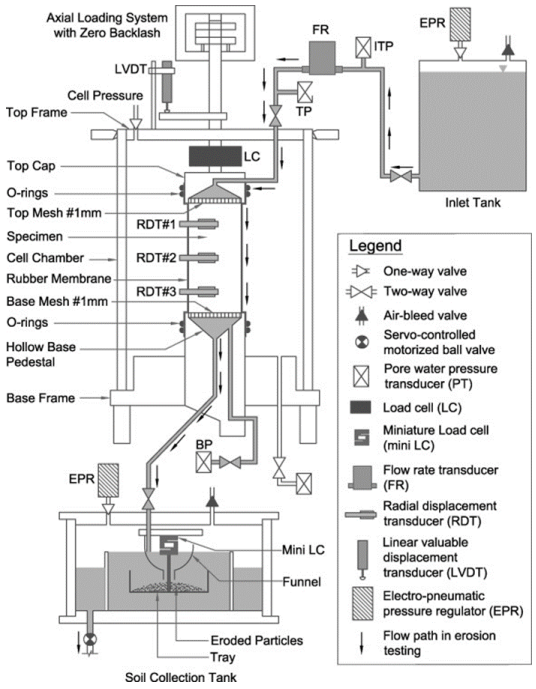

Figure 2.28 Device configuration (originally adapted from Ke and Takahashi, 2014b) used in Prasomsri and Takahashi (2021).

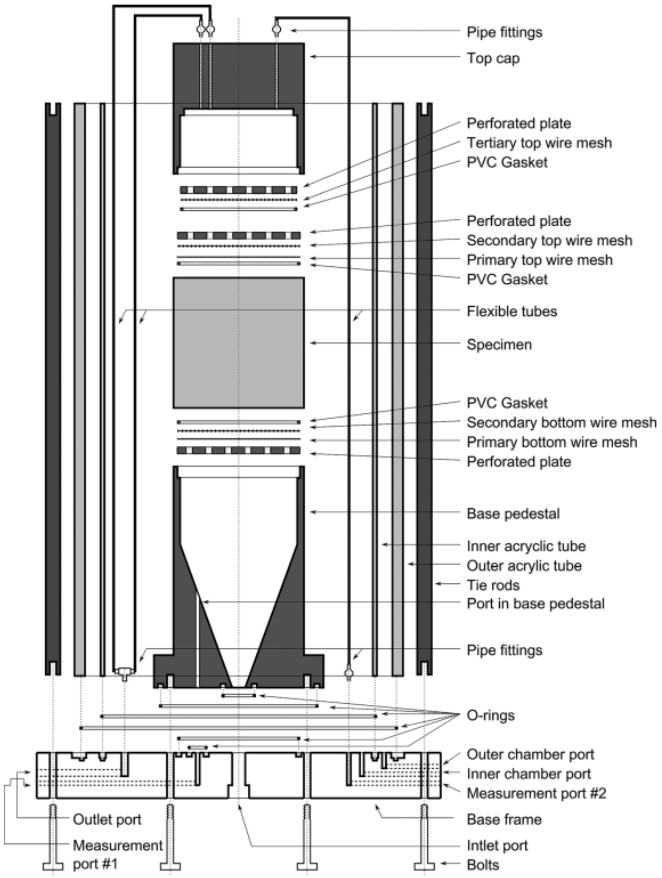

Figure 2.29 Modified triaxial-cell with double-walled design by Slangen and Fannin (2017)

2.4.3 Measurement capabilities

Seepage measurement system

The seepage control and measurement in suffusion studies can take two distinct principle: differential head control across the specimen or flow control. In a head-controlled seepage system, the differential head across the specimen is either held constant from the upstream reservoir or applied in multiple stages, with the resulting induced flow rate being measured. On the other hand, a flow-controlled seepage system maintains a constant flow rate, with the resulting differential head across the specimen being measured. The principle of head control is widely applied in rigid wall permeameter testing, as demonstrated by Sherard et al., (1984), Kenney and Lau (1985), Åberg (1993), Lafleur et al., (1989), Tanaka and Toyokuni (1991) and Moffat and Fannin (2006), with some exceptions in studies by Skempton and Brogan (1994) and Nguyen et al., (2019). In the case of modified triaxial tests, head-controlled seepage systems are predominantly adopted, as seen in studies by Bendahmane et al., (2008), Marot et al., (2009; 2012; Marot et al., 2016), Chang and Zhang (2011), Luo et al., (2013), Slangen and Fannin (2017), Li et al., (2020), Prasomsri and Takahashi (2020, 2021) and Ataii and Fannin (2022). Notably, Ke and Takahashi (2014a, 2014b) and Mehdizadeh et al., (2017) have opted for flow-controlled seepage systems. It is important to note that while rigid wall permeameters enable the measurement of both local and global hydraulic gradients, modified triaxial permeameters are restricted to the measurement of the global hydraulic gradient.

The choice of seepage control system in suffusion studies is a multifaceted decision that depends on research objectives, soil behavior and practical experimental setup. Recent research by Takahashi (2023) suggests that flow-controlled tests can significantly alter soil structure, resulting in increased fines loss and densification, while head-controlled seepage systems lead to more uniform cross-sectional erosion but render the soil fragile. This underscores the complexity of seepage control system selection in suffusion studies, with trade-offs to consider.

Mass measurement

In evaluating the critical aspects of erosion rate measurement techniques, it becomes evident that variations exist in measurement methodologies across different devices. One significant factor influencing the measurement of eroded mass lies in the direction of seepage flow. Gravity and flow direction dynamics play a crucial role in settling and measuring eroded mass. Notably, in scenarios with upward flow direction, eroded mass measurement is not typically prioritized by investigators, as observed in studies by Skempton and Brogan (1994), Tanaka and Toyokuni (1991) and Slangen and Fannin (2017). However, exceptions do exist, with some cases measuring eroded mass in both flow directions , as demonstrated by Li et al., (2020).

Two distinct eroded mass measurement capabilities are commonly employed within the scientific community: discrete and continuous, each characterized by unique effluent tank concepts. Chang and Zhang (2011) employ a detachable container allowing for discrete measurements, while Marot et al., (2016) employ a submersed rotational configuration with eight distinct collection buckets, also utilizing discrete measurements. Continuous measurements were first introduced by Ke and Takahashi (2014b) and the eroded mass measurement cell had a load resolution of 0.015 g. It is noteworthy that the pressure distribution induced by frequent opening and closing of the solenoid

valve can significantly impact real-time monitoring in continuous measurements. Mehdizadeh et al., (2017) employ a continuous measurement system with a high load resolution of 10 g, while Ataii and Fannin (2022) further enhance resolution to 2 g, eliminating pressure distribution in the original Ke and Takahashi (2014b) design. Prasomsri and Takahashi (2021) emphasize an accuracy level of ±0.1g in their measurements. It is crucial to critically assess that during the initiation phase, recorded information may be accurate; however, during the development of suffusion when flow rates are high, the noise introduced by flow and the opening and closing of flow becomes a significant concern. It is imperative to submerge highly sensitive load sensors to achieve accuracy, but paradoxically, these sensors can record noise generated by turbulence during the development phase of suffusion. Therefore, it is essential to emphasize the necessity for accurate measurement capabilities in devices used for studying suffusion mechanisms and erosion rate measurements.

Stress and strain measurements

The stress measurement capabilities of different generations of devices vary significantly, particularly between rigid wall permeameters and modified triaxial permeameters. Rigid wall permeameters typically lack the capacity to apply axial loads, with some resorting to nominal loads or vibration at the specimen's top (Kenney and Lau, 1985; Wan and Fell, 2008), while also lacking control over confinement stress (Moffat and Fannin, 2006). In contrast, modified triaxial permeameters universally offer control over both axial and confinement stresses, providing versatility in stress paths, including triaxial compression (Li et al., 2020; Luoet al.,2020), extension (Chang and Zhang, 2013a), anisotropic and isotropic stress states (D. Chang and Zhang, 2011; Liang et al., 2017, 2019). The stress capabilities of these devices have been widely utilized to investigate the mechanical responses of suffusion, including drained monotonic compression tests on post-suffusion specimens (Chang and Zhang, 2013a; Ke and Takahashi, 2014a, 2015) and post-suffusion undrained triaxial compression tests (Xiao and Shwiyhat, 2012; Ke and Takahashi, 2014b; Ouyang and Takahashi, 2015; Mehdizadeh, Disfani, et al., 2017; Prasomsri and Takahashi, 2020). However, only a limited number of devices possess the capability to maintain an extension stress state, with a focus on studying internal instability (Chang and Zhang, 2013a). This underscores the critical role of advanced measurement capabilities in suffusion research.

Modified triaxial permeameters offer the added capability of measuring specimen deformation, typically achieved by monitoring axial and volumetric changes. Axial strain is commonly quantified using high-precision displacement sensors like LVDT and LPOT, while various techniques are employed to assess volumetric deformation. These include photogrammetry (Chang and Zhang, 2011; Mehdizadeh et al., 2017; Nguyen et al., 2019), strain gauge-derived methods (Luo et al., 2013; Ke and Takahashi, 2014a, 2014b), monitoring inflow and outflow volumes (Xiao and Shwiyhat, 2012), assessing cell water variations (Li et al., 2020) and tracking volume changes in double-walled triaxial chambers (Slangen and Fannin, 2017; McClelland, 2020; Ataii and Fannin, 2022). The recent updates by Ataii and Fannin (2022) offer high accuracy (±0.05 cm^3 or 0.01% of the specimen volume) and address limitations of conventional methods (e.g., pore water variation) in suffusion tests. However, from both experimental setup and economic perspectives, other techniques (e.g., cell water variation, photogrammetry) still maintain their capability to

measure volumetric deformation with reliable accuracy, provided errors are minimized. This emphasizes the importance of selecting the most suitable technique based on the specific research requirements and constraints.

2.4.4 Synthesis on device development

The evolution of suffusion experimental devices has significantly improved our understanding of its impact on soil behavior. Initially, simple rigid wall permeameters lacked crucial measurements like pore pressure and erosion rate. Modified versions incorporated pressure ports, but a comprehensive loading system was still lacking. The breakthrough emerged with the development of modified triaxial permeameters, addressing seepage issues and providing a better stress control. This versatile device enabled an improved study of suffusion's effects on soil properties, erosion and behavior under varying stress states. It proved invaluable in deepening our comprehension of internal erosion. The characteristics of each device presented in this section are summarized in Table 2.3 .

Table 2.3 Synthesis on devices' development

References	Apparatus	Material	Specimen Dimension *D x L [mm]*	Flow direction	Hydraulic loading path	Stress Control Degree	Measurements				Remarks
							Eroded Mass	Axial Deformatio	Volumic deformation	B-value	
Sherard et al., (1984)	Simple rigid wall	Sand and gravel	101.6 x (50.8 to 101.6)	DF	HGC	0	No	No	No	No	Double layered base and filter material: Filter Criterion recommended
Kenney and Lau (1985)	Simple rigid wall	Sand and gravel	125/240 /550 x 860	DF	HGC	1	No	No	No	No	Assessing the potential internal stability
Åberg (1993)	Rigid wall	sand and gravel	190 x 133	DF	HGC	1	No	No	No	No	Challenges filter criteria and presents a mathematical model
Lafleur et al., (1989)	Rigid wall	Clay, sand and gravel	150 x 150	DF	HGC	0	Yes	No	No	No	Self-filtration is related to gradation curve profile and soil broadness coefficient (O'_F/do).
Tanaka and Toyokuni (1991)	Rigid wall	Sand	151 x 385	UF	HGC	0	No	No	No	No	Explore hydraulic failure in multi-layered sands
Skempton and Brogan (1994)	Rigid wall	Sand and gravel	139 x 155	UF	Multi-stage: FVC	0	No	No	No	No	Emphasize the necessity of considering both soil gradation and the role of fine particles in stress transfer
Wan and Fell (2004b, 2008)	Rigid wall	Clay, silt, sand and gravel	300 x (250 to 300)	DF	HGC	0; 1	No	No	No	No	Geometric method was proposed for evaluating the internal stability of broadly graded soils
Moffat and Fannin (2006)	Rigid wall	Spherical Beads	279 x 450	DF	HGC	2	No	Yes	No	No	Suggesting a potential connection between effective stress and the critical hydraulic gradient that initiates instability

Bendahmane et al., (2008)	Modified Triaxial	Clay and sand	50 x 50	DF	HGC	3	Yes	No	No	Yes	Influence of confinement stress on imitation and response on erosion rate
Marot et al., (2009, 2011, 2012, 2016)	Modified Triaxial	Sand and kaolin mix	50 x 50	DF	CH; FVC and HGC	3	Yes	No	No	Yes	Parametric study on influence of internal flow; insights into assessing the susceptibility of gap-graded soils to suffusion
Shwiyhat and Xiao (2010, 2012)	Modified Triaxial	Clayey sand	51 x 102	DF	HGC	3	Yes	Yes	Yes	> 0.95	Suffusion parameter study; Higher strength after erosion for well-graded soil; weaker for poorly graded soil
Chang and Zhang (2011)	Modified Triaxial	Sandy gravel	100 x 100	DF	Multi-stage: HGC	3	Yes	Yes	Yes	≈ 0.85	The soil's stress-strain behavior shifts from dilative to contractive following erosion
Sail et al., (2011)	Rigid wall	Glass beads	280 x 600	DF	Multi-stage: HGC	2	Yes	Yes	No	No	Suffusion causes settlement, increased pressure and localized blowout, leading to significant specimen deformations
Luo et al., (2012)	Modified Triaxial	Sandy gravel	100 x 100	DF	Gradual increasement: HGC	3	Yes	Yes	Yes	No	The long-term large hydraulic head led to more severe and likely suffusion failures compared to short-term experiments
Ke and Takahashi (2014b)	Modified Triaxial	Bianry sand mix	70 x 150	DF	FVC	3	Yes	Yes	Yes	> 0.95	Effective confining pressure resulted in less extensive suffusion and larger initial fines content experienced more erosion
Slangen and Fannin (2017)	Modified Triaxial	Glass beads	10 x 10	UF	Multi-stage: HGC	3	No	Yes	Yes	> 0.95	Enables the measurement of specimen volume change during multistage seepage flow
Mehdizadeh et al., (2017)	Modified Triaxial	Binary sand mix	75 x 150	DF	FVC	3	Yes	Yes	Yes	> 0.93	The initial strain-hardening behavior transformed into limited deformation flow behavior due to internal erosion

Rochim et al., (2017)	Rigid wall	Sand and gravel	50 x 100	DF	Multi stage: HGC and FVC	0	Yes	No	No	No	Significant influence of historical hydraulic loading on the critical hydraulic gradient value
Nguyen et al., (2019)	Rigid wall	Binary sand mix	70 x 140	DF	Multi-stage: FVC	0	No	Yes	Yes	No	Complexity of suffusion process makes it challenging to interpret post-erosion mechanical consequence
Marot et al., (2020)	Rigid wall	Sand and gravel	80 x 500	DF	Multi stage: HGC	2	Yes	No	No	No	Suffusion susceptibility was primarily influenced by the more resistant soil under perpendicular flow and by the less resistant soil under parallel flow
Li et al., (2020)	Modified Triaxial	Silt, sand and gravel	200 x 400	UF; DF	HGC	3	Yes	Yes	Yes	Yes	Uniform post-erosion particle sizes had slightly higher peak stress, highlighting the need for homogeneity in erosion-related mechanical studies
Prasomsri and Takahashi (2020, 2021)	Modified Triaxial	Bianry sand mix	70 x 150	DF	HGC	3	Yes	Yes	Yes	> 0.95	Suffusion loosens and contracts soil; suffosion increases dilatation at higher strains; Eroded soil is weaker and more contractive than non-eroded
This study (2023)	Modified Triaxial	Sand and gravel	100 x 200	DF	Multi-stage: HGC	3	Yes	Yes	Yes	≈ 0.85	Study suffusion initiation and development under complex stress and analyze its behavior with varying hydraulic conditions

Note :

UF : upward Flow
DF : Downward Flow
FVC : Flow velocity control
HGC : Hydraulic gradient control

0 : Zero stress applied
1 : Nominal stress applied
2 :Axial stress applied
3 :Triaxial stress

2.5 Summary

The literature review chapter is the cornerstone of this thesis, illuminating the central concept of internal erosion mechanisms in hydraulic structures. It defines the diverse forms of internal erosion, including concentrated leak erosion, backward erosion, contact erosion and the central focus of this thesis, suffusion. This comprehensive overview underscores the complexity of internal erosion phenomena, justifying the necessity for specialized investigation.

Suffusion, characterized by the movement of fine soil particles through constrictions between larger soil particles, stands as a gradual yet impactful kinetic process. Its potential to alter permeability, seepage velocities, density, grain size distribution and strength raises serious concerns about hydraulic structure stability. The ICOLD (2015) guidelines provide essential criteria encompassing geometric, stress and hydraulic factors, forming the foundation for assessing and mitigating suffusion risks, aligning perfectly with the objective of developing a modified triaxial chamber capable of successive experimental steps.

The "Suffusion parameters" section delves deeply into the complexities of assessing suffusion susceptibility and understanding its initiation and development under the influence of geometric conditions, mechanical and hydraulic loads. Geometric criteria, primarily based on Particle Size Distribution (PSD), offer valuable insights into soil stability, although the complexity of real-world scenarios necessitates a more detail approach beyond simple binary categorizations i.e. stable or unstable. Understanding the interaction between hydraulic and mechanical stresses plays a pivotal role in understanding suffusion behavior. Existing methodologies have limitations, underlining the need for a comprehensive understanding of factors influencing suffusion, a goal that this research strives to achieve.

The exploration of the effect of various stress states has been particularly insightful, with findings indicating a significant relationship between effective stress and the critical hydraulic gradient, a pivotal factor in soil erosion initiation. The diverse approaches and outcomes emphasize the necessity of considering both the percentage of fines and the stress state to accurately assess the suffusion susceptibility of soils, shedding light on the complex and interrelated nature of suffusion behavior.

The diverse approaches to evaluating hydraulic loading history, either through flow velocity control or hydraulic gradient control, have been discussed, highlighting the need for an informed approach to comprehensively characterize each suffusion’s phases. This recognition of the research conducted by different authors reveals valuable information on the alterations in soil structure, hydraulic conductivity and mechanical behavior due to suffusion under varying loading conditions.

A significant step forward remains the modified triaxial permeameter, a breakthrough device that allows researchers to study suffusion in a more controlled manner. It enables the exploration of suffusion effects on soil behavior and mechanical properties, facilitating the investigation of erosion initiation, development and the behavior of eroded soils under different stress states. It is versatility and capability to conduct successive experiments on saturation, consolidation, erosion and shearing prove invaluable in gaining a deeper understanding of internal erosion and capturing the internal erosion response.

This literature review chapter establishes a pivotal foundation for the subsequent chapters of this thesis, presenting a comprehensive overview of the current state of knowledge in the field of suffusion behavior within hydraulic structures. The combined synthesized findings and the identification of existing gaps in this domain lay the essential groundwork for the experimental and analytical endeavors that will follow. Armed with this extensive knowledge, this thesis is dedicated to the development of a modified triaxial chamber and the in-depth investigation into the initiation, development and intricate behavior of suffusion under the influence of complex stress states and varying hydraulic loading conditions. Overall, this chapter contributes to the advancement of knowledge in the domain of internal erosion in hydraulic structures, setting the stage for the comprehensive investigations to come.

Chapter 3

3 Development of modified triaxial apparatus

The objective of this study is to investigate and characterize the initiation and development of suffusion, as well as its effects on the mechanical behavior, under various mechanical conditions and representative hydraulic loadings. These loadings include scenarios such as a progressive increase in the upstream water level, a flood event, or consecutive elevations of the upstream water level. To achieve this objective, the development of an advanced automated device is necessary. The stress state applied to the specimen follows the principles used in triaxial tests. In order to accommodate the erosion mechanism, modifications were made to the top cap and base pedestal of the triaxial chamber. Specifically, the top plate of the triaxial cell was designed to allow water injection, while the base pedestal was adapted to enable the collection of eroded soil particles. These modifications were essential in order to inject the inflow of water, to measure the applied difference of head and capture the eroded soil particles during the experiment.

The experiment consists of several successive steps: saturation, consolidation, erosion and post-suffusion analysis. All of these steps can be conducted using the developed device. The system enables tests to be performed based on the controlled head principle and it is fully automated. A general view of the new triaxial erodimeter device is shown in Figure 3.1. Moreover, the eroded mass from the specimen is collected in the effluent tank located at the bottom.

3.1 Modified triaxial cell

3.1.1 Modified top and bottom cap

Stainless steel was selected as the material for the fabrication of the top and bottom plates, considering that these components come into contact with water. The top cap of the device consists of a 55 mm thick hollow cylinder, which is filled with a 25 mm thick layer of gravel. This gravel layer serves two purposes: to uniformly diffuse the injected flow and to reduce the impact of the jet, as suggested by Ke and Takahashi (2014a). Positioned right below the gravel layer is a 1.2 mm mesh size filter. Finally, the bottom of the top cap is sealed with a 5 mm thick stainless-steel plate that has a pore opening size of 6 mm (Figure 3.2). By incorporating this layer, the smooth flow of water through the system is maintained.

The top cap of the device is equipped with three nozzles: two for injection purposes to control the inflow and one pressure port for measuring the upstream pressure. In addition, there are three small ports situated at the top of the top cap, serving as an air release valve during the saturation phase. To prevent any potential migration of fine particles during the saturation process, a 80 μm upstream filter mesh is carefully placed between the top cap and the specimen when the test is

initiated. This mesh acts as a barrier, ensuring that fine particles are retained within the specimen and do not pass through to the top cap. Moreover, this mesh is preferred over filter paper to make saturation phase easier.

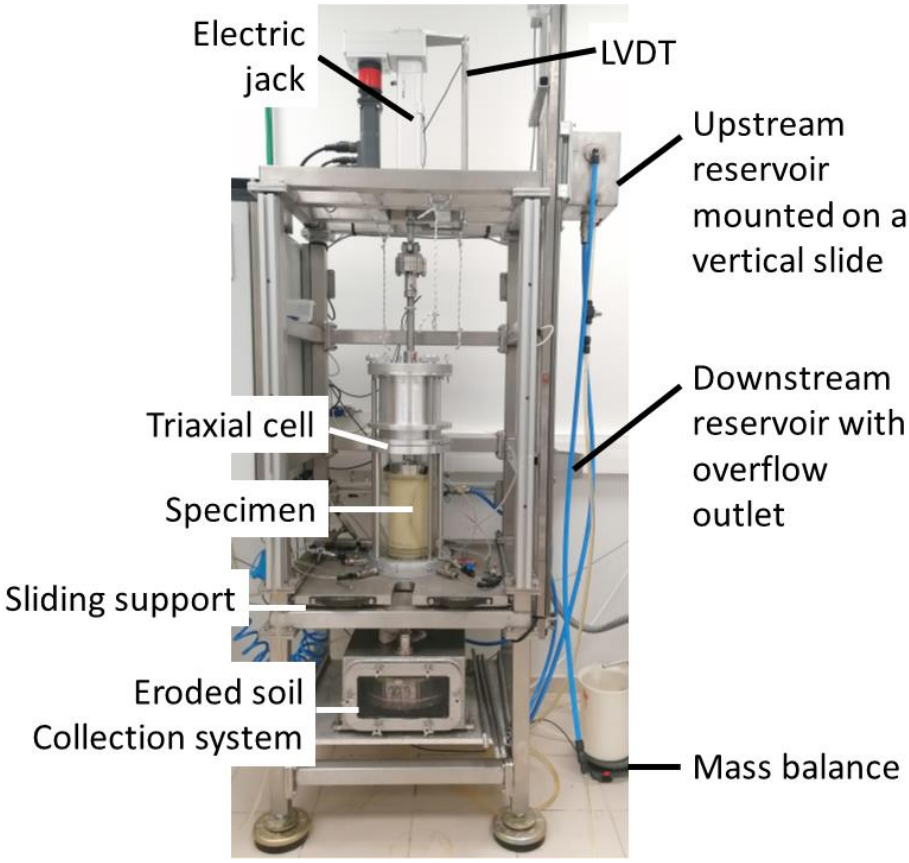

Figure 3.1 Annotated photographs of new device

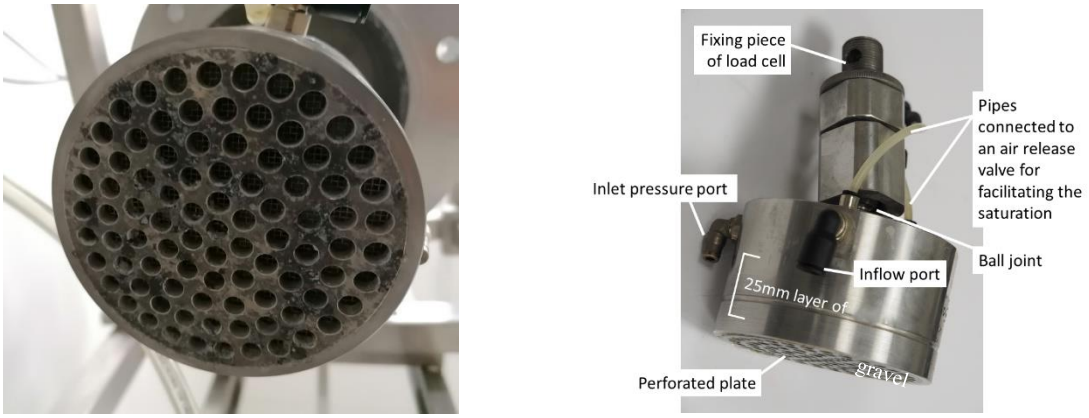

[a] [b]

Figure 3.2 Modified top cap: [a] top view and [b] side view

The base pedestal is designed with a conical-shaped funnel to effectively guide the eroded particles into the collection unit and minimize particle deposition. A small pipe with a 2 mm diameter is connected to a pressure port at the base pedestal to measure the outlet pressure using the differential pressure sensor. At the top of this funnel, a 5 mm thick stainless-steel plate with a 6 mm pore size opening is positioned. A mesh is placed at the interface between the specimen and this plate, acting as a downstream filter. The pore opening of the mesh is selected based on the smallest particle size of the coarse fraction or constriction size. For this particular study, the downstream mesh has a pore opening of 1.2 mm as shown in Figure 3.3.

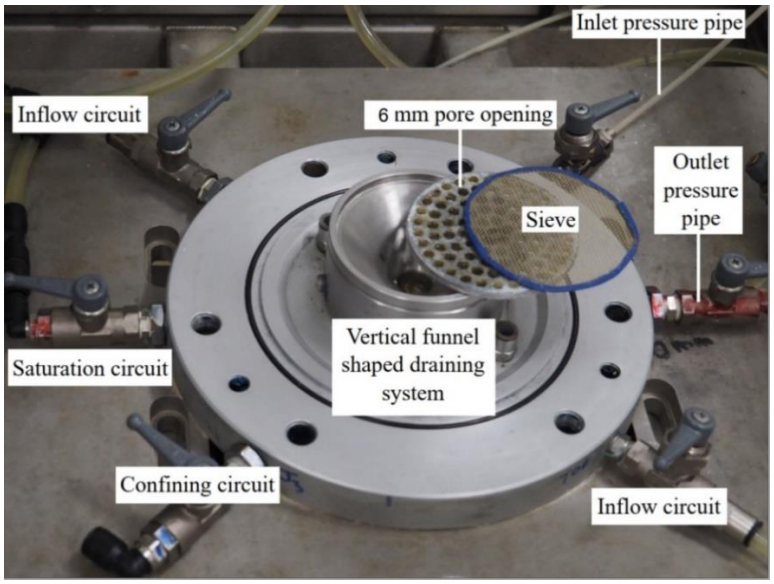

Figure 3.3 Modified base pedestal: port description and configuration of outlet chamber (mesh, plate and funnel).

3.1.2 Cylindrical cell

The cylindrical cell is made of acrylic and supported by rods around the circumference as shown in Figure 3.4. Its inner diameter is 170 mm, while its height is 340 mm.

3.2 Confining and axial loading system

The generation of cell pressure in the system relies on an air/water interface, which is controlled by an air pressure regulator. To accurately measure the volume change of the cell fluid and, consequently, the specimen volume change, including during seepage flow injection, an automatic volume change apparatus (± 0.05 ml) is employed.

For the axial loading system, an electric jack and a loading rod are used. At the end of the loading rod, a submersible load cell is securely attached to measure the axial force. To ensure proper alignment and connection between the top cap and the load cell, a specially designed component

consisting of two coaxial solid cylinders is employed. These solid cylinders can be interlocked together using a pin, as depicted in Figure 3.4.

To monitor the axial strain of the specimen, a Linear Variable Differential Transducer (LVDT) sensor is employed. This sensor measures the displacement of the jack, providing accurate data on the specimen's axial strain, as illustrated in Figure 3.1.

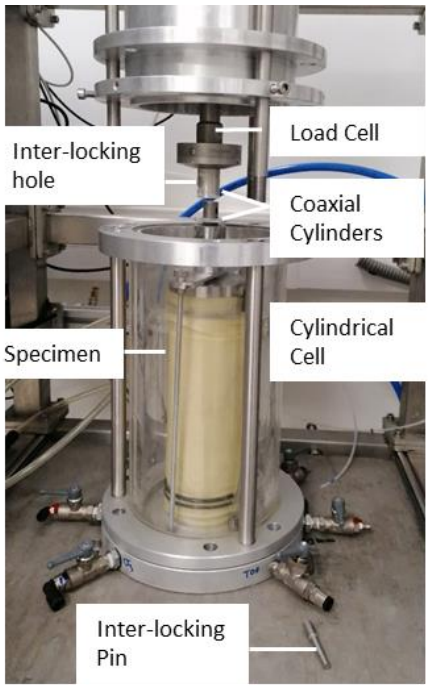

Figure 3.4 Cylindrical cell and axial load connection

3.3 Automatic seepage control system

The hydraulic gradient in the experiment is automated by vertically driving the mobile reservoir, allowing for a maximum vertical elevation of 1300 mm above the specimen top. In real-world scenarios, hydraulic loading on embankments and their foundations constantly varies due to factors such as rainfall, floods, evaporation and reservoir filling or emptying. To accurately replicate these fluctuations in a laboratory setting, an automated water supply system is crucial.

The water supply system is designed to either maintain a constant hydraulic gradient or vary it according to a predetermined pattern by adjusting the flow rate. Previous studies by Ke and Takahashi (2014b); Slangen and Fannin (2017); Mehdizadeh et al., (2017) have successfully controlled the flow rate, while Sail et al., (2011), Chang and Zhang (2011), Rochim et al., (2017) and Zhong et al., (2018) have conducted experiments using controlled multi-stage hydraulic gradients. Suffusion involves the interdependent processes of detachment, transportation and filtration, all of which are influenced by the history of hydraulic loading. To better observe the whole development of the suffusion process, Rochim et al., (2017) evidenced that a multistage hydraulic gradient should be preferred to a single stage one or imposed flow rate. Therefore, for

the erosion phase, it has been determined that applying multi-stage hydraulic loadings is necessary to effectively study suffusion.

To ensure precise control over the hydraulic loading path, the upstream reservoir is mounted on a vertical slide, as depicted in Figure 3.5. This configuration allows for continuous vertical movement of the reservoir at a travel speed ranging from 1 mm/min to 5 mm/min. The vertical motion of the reservoir is achieved using a timing belt and a controlled step motor equipped with a gear mechanism. With a specimen height of 200 mm, this setup enables the application of hydraulic gradients ranging from 0 to 8. The precise control of the vertical movement of the reservoir provides the flexibility to replicate a wide range of hydraulic loading conditions and facilitates the precise examination of the effects of different hydraulic gradients on the erosion process.

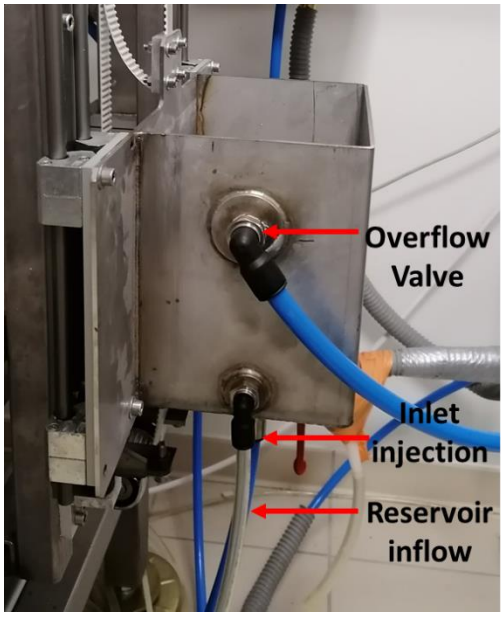

Figure 3.5 Mobile reservoir mechanism

3.4 Effluent Tank

The main objective of the collection system is to effectively collect eroded particles and discharged water while enabling simultaneous measurement of the eroded particle weight and maintaining a constant back-pressure for specimen saturation. Overcoming challenges such as achieving continuous weight measurement, preserving back-pressure and mitigating the influence of inlet flow required careful design considerations.

In the pursuit of achieving continuous mass measurements, difficulties appeared during my master's thesis work (Oli, 2020), where the desired accuracy could not be reached with the newly developed collection system. To get around this, modifications were introduced to the rotation collection unit. Specifically, the number of buckets was increased from 8 to 16, as shown in Figure 3.6. This adaptation doubled the precision of the eroded mass measurements. Despite this improvement, it's crucial to acknowledge that the measurement of eroded mass remains intermittent, resulting in periodic erosion rate measurements.

Although Marot et al., (2011) introduced the concept of an optical sensor for continuous measurements, this sensor may not be used to measure sand and gravel eroded particles. The rapid settling of eroded sand does not allow a proper calibration for several solid concentration, and hence does not provide an accurate value for the eroded mass. While calibration is feasible with clay and silt particles, given their turbidity and longer settling times, the persisting challenge with sand prevents the use of an optical sensor for continuous mass measurements.

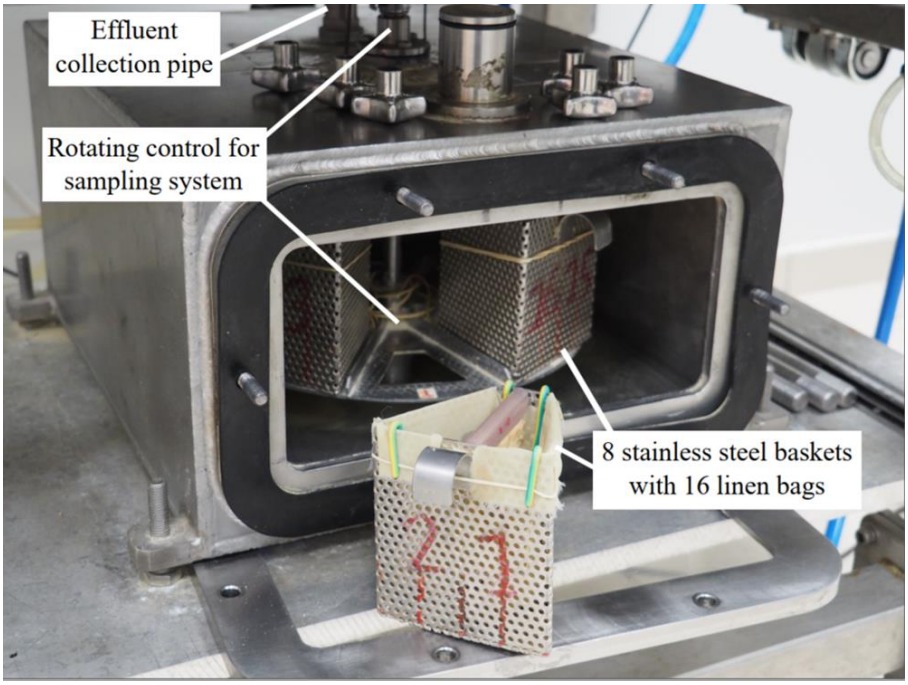

Figure 3.6 Effluent tank

In Appendix A, the effluent tank's performance and limitations are extensively examined. This includes detailed investigations on load cell perturbation and noise, delay tests and the impact of inflow conditions. The appendix provides comprehensive insights into the design, functionality and experimental findings, enhancing our understanding of the effluent tank's capabilities.

3.5 Instrumentation and data acquisition system

3.5.1 Instrumentation

The instrumentation used in the study includes several devices to measure different parameters accurately. These instruments are as follows:

- A differential pressure transducer was employed to measure the differential pore water pressure within a range of 0 to 25 kPa. It provides a high accuracy of ± 0.2 % in pressure measurement. These measurements, combined with specimen length, enable the computation of the hydraulic gradient with an impressive accuracy of 0.04.
- A mass balance was utilized to measure the seepage flow rate with a precision of 1 cm^3/s. This instrument ensures accurate measurement of the flow rate.

- An LVDT (Linear Variable Differential Transducer) sensor was employed to measure the axial strain of the specimen. It has a maximum measurement range of 100 mm and offers an accuracy of 0.25 %.
- A travel linear transducer was used to measure the volume change of the specimen. With an accuracy of ± 0.05 cm^3, this device provides precise measurement of specimen volume change.
- A pressure transducer was utilized to measure the confining pressure, with a maximum capacity of 1000 kPa. It offers an accuracy of ± 0.2 % in pressure measurement.
- A submersible load cell was employed to measure the axial force acting on the specimen. It has a maximum capacity of 64 kN and provides an accuracy of 0.05 % in force measurement.

3.5.2 Data acquisition system

An accurate and precise automated data acquisition system is essential in modern engineering applications, enabling reliable and efficient experimental testing. In this study, a customized LabVIEW platform was developed to effectively monitor and control various physical parameters during the data acquisition phase. LabVIEW, a visual programming language developed by National Instruments, facilitates seamless communication between instruments and a computer. The data acquisition system comprises four key components: physical input/output signals and sensors, Data Acquisition (DAQ) devices, driver software and a software application. The developed code has been tailored to meet the specific requirements of this experiment.

The LabVIEW code enables the acquisition of analog input signals from a range of sensors, including load sensors, flow sensors, LVDT sensors for axial strain, mass balance sensors for mass flow rate and three pressure transducers (pore pressure, differential pressure and confinement pressure). The code also incorporates automatic control of the vertical elevation of the upstream reservoir using user-defined parameters for displacement increments and durations. It includes functionality to insert pauses when the target velocity is below 1 mm/min, ensuring precise alignment with the desired ramp and step pattern. Using the LabVIEW code, the time evolutions of key parameters such as hydraulic gradient, hydraulic conductivity, injected flow rate, specimen volume variation, axial strain and deviatoric stress can be automatically plotted. The acquired data is securely stored in a text output file after each test, ensuring its safe preservation for subsequent analysis. The developed LabVIEW code, along with the calibration process for input/output sensors and signals, is thoroughly explained and documented in Appendix B .

3.6 Device validation

The developed modified triaxial apparatus underwent a rigorous validation process to ensure its proper functioning and reliability. Two types of tests were performed for this purpose: a mechanical test and a suffusion test. The specimens used in these tests had consistent dimensions of 200 mm in height and 100 mm in diameter. The mechanical test aimed to assess the mechanical properties of the soil and compare them with those obtained from a standard triaxial device operated by different researchers. By conducting this comparison, the performance of the modified apparatus was evaluated in terms of its ability to replicate similar mechanical behavior to the

standard device. On the other hand, the suffusion test focused on characterizing the initiation and development of suffusion process. Through these thorough validation tests, the functionality and effectiveness of the modified triaxial apparatus were evaluated, providing confidence in its suitability for further experimentation and research in the field of geotechnical engineering.

3.6.1 Mechanical test validation

Under drained conditions, three specimens of Fontainebleau sand were subjected to testing. Two of the specimens, with diameters of 50 mm and 100 mm, were tested using a standard triaxial device, while the third specimen was tested using the newly developed device. The setup of the developed device and the sheared specimen can be seen in Figure 3.7. Test results are presented in Figure 3.8, depicting the relationship between deviatoric stress and axial strain and volumetric strain and axial strain.

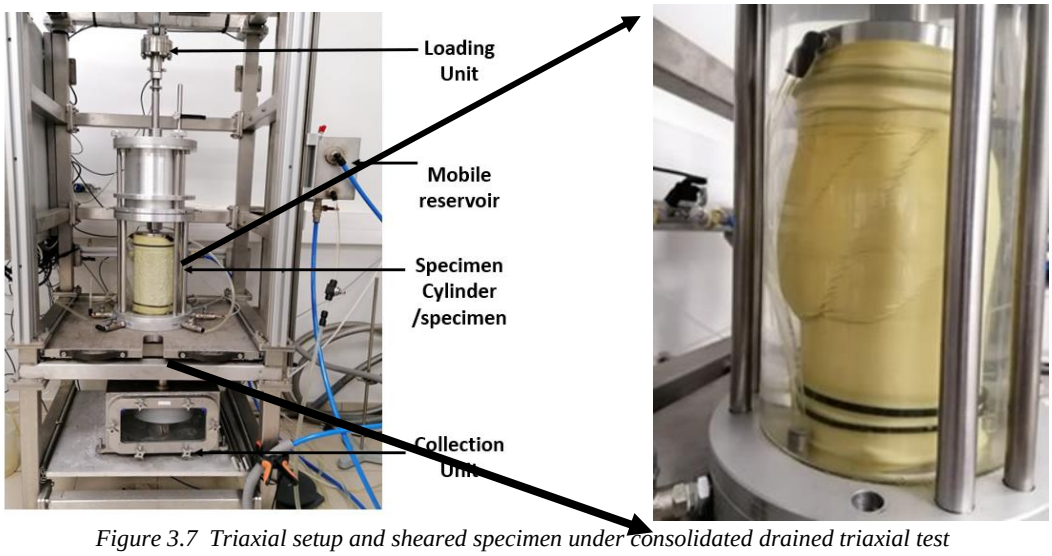

Figure 3.7 Triaxial setup and sheared specimen under consolidated drained triaxial test

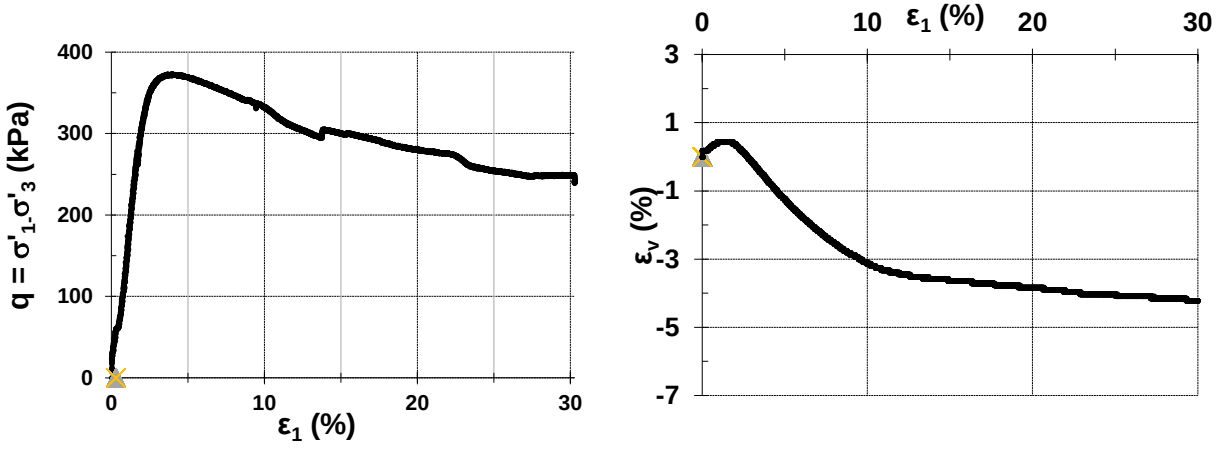

[a] [b]

Figure 3.8 [a] Stress-strain curve and [b] volumetric variation, for the triaxial compression test

The results of the mechanical tests showed good agreement between the developed device and the standard triaxial device in terms of the measured mechanical properties, such as cohesion (c) and friction angle (φ). This successful validation of the new device in mechanical testing demonstrates its reliability and effectiveness. The corresponding values are presented in the Table 3.1.

Table 3.1 Mechanical properties of consolidated drained test

Configuration	Diameter [mm]	Cohesion c [kPa]	Angle of friction φ
Standard tri-axial	50	0	41°
	100	0	41°
Developed Device	100	0	41°

3.7 Suffusion test validation

The reproduction of suffusion test conditions presented a unique challenge, requiring a careful comparison between the suffusion validation test (B90-a_R4) and a reference test (B90-a Rochim et al., 2017). In order to validate the suffusion phenomena, four repeat tests were conducted. The test material, referred to as B, is a gap-graded cohesionless soil consisting of 25% sand S1 and 75% gravel G3, both sourced from Sablière Palvadeau in France. This specific composition was chosen to accurately represent the desired characteristics for the testing purposes. The Table 3.2 below highlights the similarities and differences between these two tests, providing valuable insights into the suffusion validation process.

Table 3.2 General comparison on test conditions

Specification	B90-a Rochim (2017)	B90-a_R4
Specimen dimensions (Diameter x Height)	50 mm x 50 mm	100 mm x 200 mm
Pore opening of downstream sieve (mm)	4	1.2
Initial dry density (kN/m^3)	17.39	17.39
Initial water content at preparation (%)	7.8	4
Specimen preparation	Single layer static compaction	Multilayer moist tamping
Applied hydraulic gradient	0.1 - 6	0.1 - 3
CO_2 injection duration (min)	5	10
Saturation duration (hours)	12	14 (velocity 1 mm/min)
Erosion duration (min)	180	140

Validation Result

Figure 3.9 illustrates the consistent trend in the time evolution of hydraulic conductivity for both the B90-a_R4 test and the test conducted by Rochim et al. (2017). However, it is noteworthy that the B90-a_R4 specimen exhibits a higher permeability, leading to an increase of the energy expended by the seepage flow. Consequently, the erosion resistance index (I_α) obtained for the B90-a_R4 test was 3.28, while for Rochim et al. (2017) it was 2.93. The observed discrepancy in the initial hydraulic conductivity values can be attributed to differences in specimen diameters, with the B90-a_R4 specimens' diameter begin twice the one used by Rochim et al. (2017). Recall that our specimens measure 100 mm in diameter and 200 mm in height, while those tested by Rochim et al. (2017) are 50 mm in diameter and 50 mm in height.

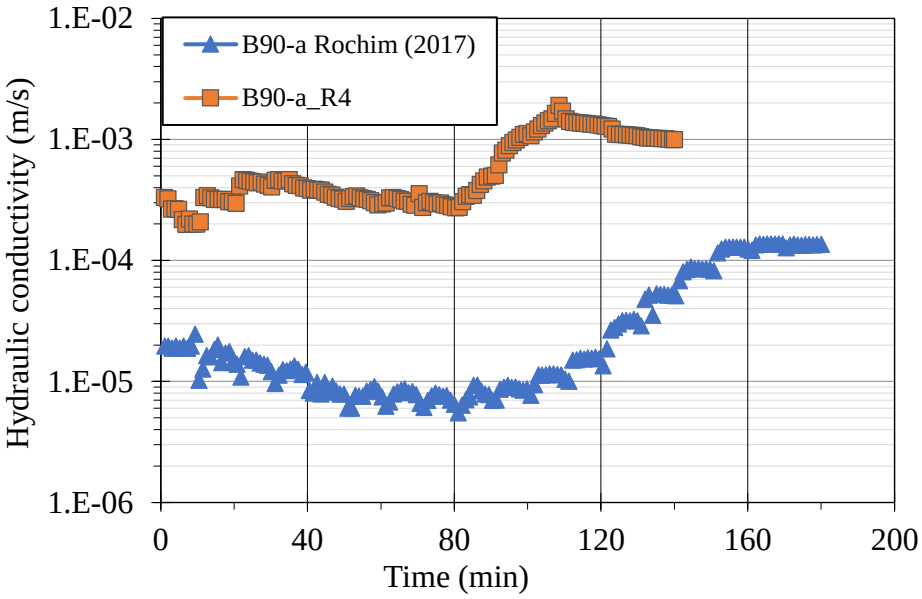

Figure 3.9 Temporal evolution of hydraulic Conductivity: A comparative analysis

During the saturation phase, the B90-a_R4 test demonstrated a 1.8% loss of fine particles relative to the initial fine content, while Rochim et al. (2017) measured a 0.01% in fine content. Precisely replicating the percentage of mass loss proves challenging due to the diameter of the specimen section, where a larger diameter results in greater particle loss for the same volume. The higher loss of fine particles in the B90-a_R4 test leads to an increase in effective porosity. Despite a similar trend, the higher effective porosity in the B90-a_R4 test results in a higher initial hydraulic conductivity compared to Rochim et al.'s study.

To assess the commissioning of the new device with the B90-a_R4 test against the reference test B90-a_Rochim (2017), the work of Zhong et al. (2018) should be considered. Zhong et al. (2018) illustrated the substantial impact of the saturation velocity during the saturation step on particle loss and initial hydraulic conductivity for the same soil. Illustrated in Figure 3.10, their findings presented a range of particle loss percentages (0.7% to 2.5%) and corresponding initial hydraulic conductivity values (3.38 10^{-5} m/s to 5.6410^{-3} m/s). The reference test B90-a_Rochim (2017) is marked on this graph with a blue arrow and the new test with an orange one. While, Rochim et al. (2017) measured a rather low particle loss percentage (0.01%) and an initial hydraulic conductivity

of 1.95*10^{-5} m/s; with the new device, the measured initial hydraulic conductivity is 3.3 10^{-4} m/s. In fact, this increase falls within the range reported by Zhong et al. (2018), which validates the suffusive soil response in terms of hydraulic conductivity. This demonstrates the capability of the new device to assess initial hydraulic conductivity within a reasonable range, in line with previous research.

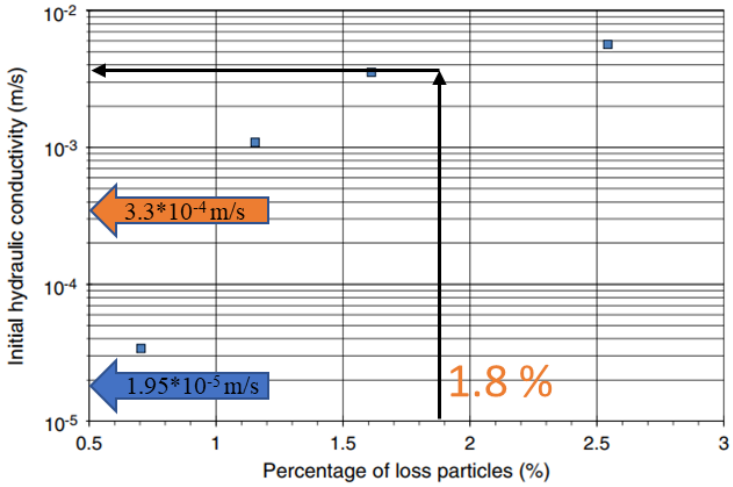

Figure 3.10 Influence of the loss of particles during saturation step (Zhong et al., 2018)

3.8 Suffusion test procedure

Sample preparation is an essential phase in the experimental procedure for suffusion testing. The uniformity of the soil specimen in terms of void ratio, saturation and grain size distribution is crucial for obtaining accurate and reliable results in erosion tests, as well as in any other soil test. Heterogeneity in the specimen, as discussed by Nguyen et al., (2019) can lead to discrepancies in the test results even under similar testing conditions. Therefore, ensuring a homogeneous and consistent specimen is imperative for achieving accurate and meaningful outcomes in suffusion experiments.

In the literature, several methods have been proposed for preparing uniform soil specimens particularly to triaxial test. These methods include the undercompaction method Ladd (1978), moist tamping method (Frost and Park, 2003; Bradshaw and Baxter, 2007), slurry method (Kuerbis and Vaid, 1988; Carraro and Prezzi, 2008) and pulviation method. For this research, the under-compaction moist tamping technique, originally introduced by Ladd (1978) and enhanced by Frost and Park (2003) was selected. It minimizes the segregation of soil particles during sample preparation and ensures specimens with maximum uniformity throughout their height.

The test specimens, with a diameter of 10 cm and height of 20 cm, were prepared by compacting four layers of soil at an optimum water content of 4%. Each layer had a height of 5 cm. The dry density of the specimens was set at 17.39 kN/m^3. To prevent any collapse, the specimens were carefully wrapped with a membrane using a gentle suction technique, as depicted in Figure 3.11.

The aspect ratio of the specimens, maintaining a dimension ratio of 1:2, followed the guidelines outlined in ASTM D47667-04 for triaxial tests.

[a] [b]

Figure 3.11 [a] Specimen positioning under bottom pedestal and [b] Gap Graded Palvadeau soil

Test procedure

Following the sample preparation step, the experimental procedure consists of four stages performed sequentially: saturation, consolidation, erosion and post-suffusion gradation.

1. Saturation:

The cell pressure was maintained at 20 kPa to prevent sample collapse and CO_2 was injected at a slow rate to replace any pre-existing air and dissolve during saturation. The presence of CO_2 bubbles at the outlet was verified by connecting the air release valve of the top cap to a pipe dipped in a thin water layer. Extensive experimental tests were conducted to determine the optimal saturation rate that minimizes mass loss prior to the erosion phase. It was observed that higher saturation rates resulted in increased mass loss. To ensure a cautious experimental approach, the saturation rate is set at an average of 0.25 mm/min. This involves an initial rate of 1 mm/min for one minute, followed by a three-minute pause, resulting in an average of 0.25 mm/min. By adopting this value, the loss of fine particles during the saturation stage is minimized, enhancing stability and low eroded mass during the critical early phases of sample saturation.

The degree of saturation is assessed through the Skempton coefficient $B = \Delta u / \Delta\sigma_3$, where Δu is the measured overpressure induced by a corresponding increase in confining pressure $\Delta\sigma_3$ (ASTM D4767-88). In a standard triaxial test (ASTM D7181-11), B-values greater or equal to 0.95 indicate fully saturated specimens. Yet, using the ASTM norm without any care on suffusive soils would imply applying backpressure and manipulating the effluent collection pipe and inflow circuit, potentially inducing uncontrolled pressure variations and microstructure disturbances. To mitigate such perturbations and prevent microstructure damage before the erosion phase, the B-value measurement was conducted on a dedicated (i.e. sacrificed) specimen with 25% fine content. The

recorded value was 0.85; however, this measurement may be underestimated due to the presence of large dead volumes at the top and bottom caps, suggesting that the actual degree of saturation might be higher.

2. Consolidation:

Following the achievement of the desired saturation phase, the specimen, configured in a triaxial arrangement, underwent a consolidation process to attain a mean effective stress level of 70 kPa. Confining pressure was gradually applied at a rate of 1 kPa/min. A constant effective stress path was selected for all the test to investigate the influence of stress conditions. Under isotropic stress conditions, the specimen reached the state of erosion phase once the confining stress was incrementally elevated to the predetermined stress level. During the triaxial compression or extension tests, the axial stress underwent incremental increments or decrements at a rate of 1 kPa/min until reaching the desired stress magnitude. The vertical stress was meticulously regulated using a jack mechanism and a specialized program, ensuring the precise and accurate application of stress throughout the testing procedures.

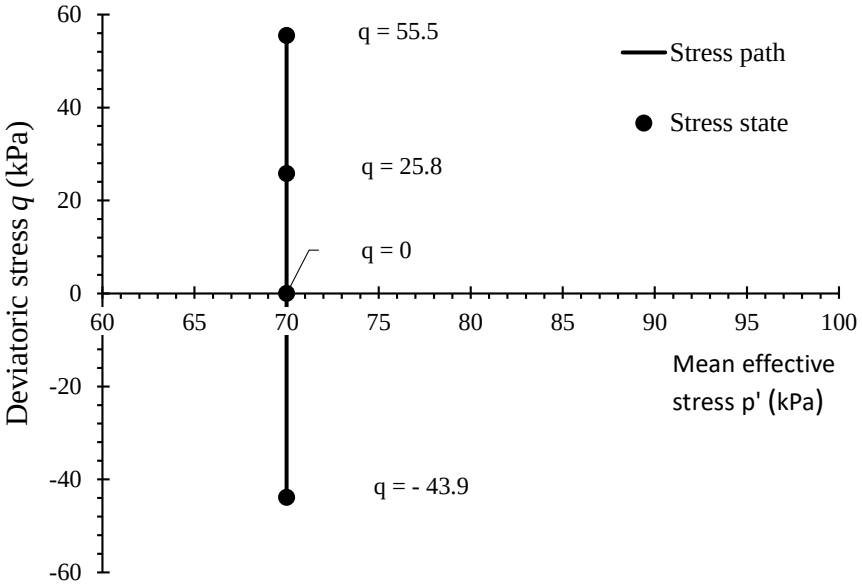

Figure 3.12 Mechanical loading condition

3. Erosion:

Suffusion was initiated by applying a controlled multi-stage hydraulic gradient to all specimens. Specimens were subjected to a downward flow by imposing a multistage hydraulic gradient, with the first stage equal to 0.1 (see Figure 3.13). The suffusion test during device commissioning revealed a distinctive erosion rate profile, indicating rapid erosion of fine particles within the initial 2 to 3 minutes after applying the hydraulic load. In addition to this period, a settling time was necessary for accurate particle collection. Therefore, each hydraulic gradient stage remained constant for 10 minutes, providing sufficient time to capture all the eroded particles.

To explore alternative testing durations, this settling time was extended to 20 minutes during the device commissioning phase. Yet, the erosion rate equilibrium was reached within the 10-minute duration so that this value was chosen to optimize the test duration. It's crucial to note that the suitability of the 10-minute settling duration depends on the soil type. Cohesive soils, in particular, may require a different optimal duration due to their specific material characteristics. Establishing a predefined time step adjusted to the soil's properties and the erosion testing configuration is essential to ensure that, for a given applied hydraulic gradient, the settling duration aligns with erosion rate equilibrium, considering inherent variations in soil behavior and erosion response.

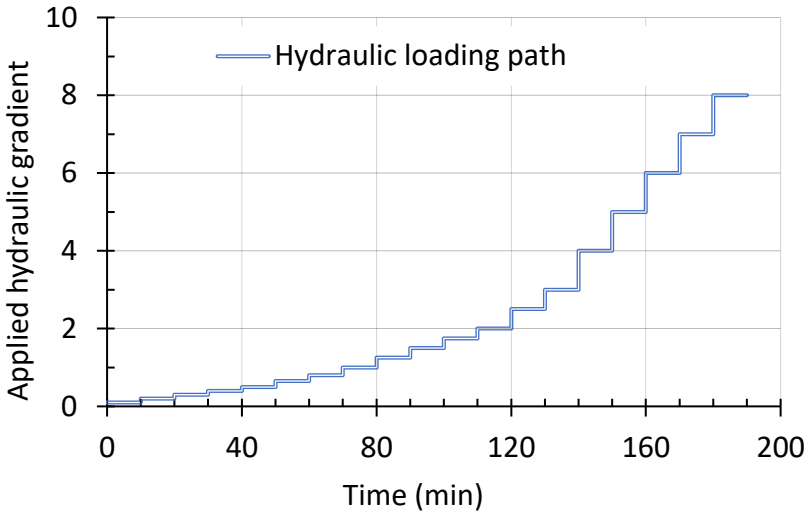

Figure 3.13 Multi-stage hydraulic loading during erosion stage

4. Post-suffusion gradation:

After completing the erosion phase, the sample was carefully extracted and frozen to facilitate visual inspection of the four layers. Each layer was then oven-dried at 105 °C for 24 hours and sieved for further analysis.

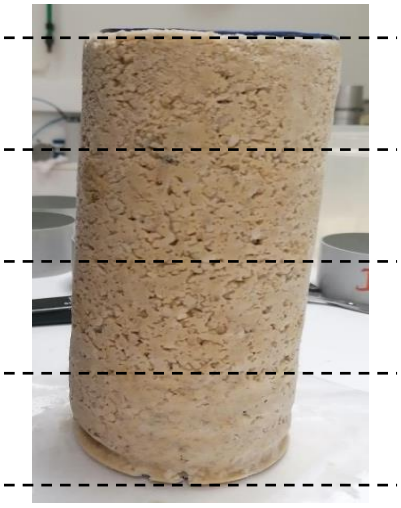

Figure 3.14 Frozen post-suffusion specimen

3.9 Summary

This thesis chapter presents the development of a modified triaxial apparatus with the primary objective of investigating and characterizing suffusion, as well as its effects on the mechanical behavior of soil under various hydraulic loadings. The apparatus was designed to incorporate modifications to the top cap and base pedestal of the triaxial chamber, enabling the inflow of water and collection of eroded soil particles during the experiment. These modifications were essential to simulate and study the suffusion mechanism accurately.

The experimental process involves several successive steps, including saturation, consolidation, erosion and post-suffusion analysis. All of these stages can be conducted using the advanced automated device. The system operates based on the controlled hydraulic loading and is fully automated, ensuring precise control and monitoring of the test parameters throughout the experiments. A schematic diagram of the new triaxial erodimeter device is provided, depicting its overall configuration.

During the saturation phase, an optimal saturation rate of 0.25 mm/min was determined, minimizing the loss of fine particles and promoting stability during the initial sample saturation. The consolidation step involves applying a constant effective stress path to the sample until reaching a mean effective stress of 70 kPa, ensuring proper preparation for the subsequent erosion phase.

The erosion phase is a crucial part of the experiment, as suffusion mechanisms are best observed and characterized under multi-stage hydraulic gradients. The automated water supply system allows for precise control of the hydraulic loading path, replicating real-world hydraulic loading fluctuations encountered in embankments and foundations due to factors such as rainfall, floods, evaporation and reservoir filling or emptying.

After the erosion phase, the post-suffusion analysis involves carefully extracting the sample and conducting a visual inspection of the four layers. Each layer is then subjected to further analysis, including oven-drying and sieving, to understand the effects of suffusion on fine particle migration.

To ensure accurate and reliable data acquisition during the experiments, the apparatus is equipped with a comprehensive instrumentation system. Various devices, such as differential pressure transducers, mass balances, LVDT sensors and submersible load cells, are used to measure parameters such as pore water pressure, seepage flow rate, axial strain, specimen volume change and axial force acting on the specimen. The data acquisition system, developed using the LabVIEW platform, enables real-time monitoring and visualization of key parameters during the tests, providing essential insights for subsequent analysis.

The apparatus was thoroughly validated through mechanical and suffusion tests. The mechanical test validation involved comparing the mechanical properties of soil specimens tested using the modified apparatus and a standard triaxial device operated by different researchers. The results showed good agreement, demonstrating the reliability and accuracy of the new apparatus in mechanical testing.

For suffusion test validation, the apparatus was compared with a reference test and consistent trends were observed in the time evolution of hydraulic conductivity. The differences in eroded

mass and erosion resistance index were attributed to variations in testing conditions and setup. However, the new apparatus successfully replicated the suffusion phenomena, confirming its capability for accurate assessment of initial hydraulic conductivity and specimen preparation.

In conclusion, the developed modified triaxial apparatus and its experimental procedure provide a robust and effective platform for studying suffusion and its effects on soil behavior under different hydraulic and mechanical conditions. The findings from this research contribute to the understanding of suffusion mechanisms, enabling better-informed geotechnical engineering practices related to erosion and soil stability. The advanced automated device, along with its comprehensive data acquisition system, enhances the efficiency and reliability of experimental testing, opening avenues for further research in the field of geotechnical engineering.

Chapter 4

4 Influence of the stress state on the initiation and development of suffusion

Suffusion, although a process characterized by a slow kinetic, does not pose an immediate breach threat when noticed on a dam (Courivaud, 2023). However, it raises questions about potential outcomes over time, like sinkholes, settlement or leakage. Researchers have recognized that suffusion is influenced by various factors, such as the micro-structure, the stress state and hydraulic loading conditions. This understanding comes from a comprehensive body of research (Garner and Fannin, 2010; Liang et al., 2017; Rochim et al., 2017; Wautier, Bonelli and Nicot, 2019; Prasomsri and Takahashi, 2020; Seblany et al., 2021). In addition, the role of fine particles and the load that they carry depends on the fine content (Sibille et al., 2015; Prasomsri and Takahashi, 2021). If fine particles do not fill the voids among the coarser particles, drag forces may displace them. Favorable flow and constriction sizes allow fine particles to move through the solid soil structure. Some displacements, however, may be geometrically blocked Indraratna et al., (2015). These displacements modify local pores, constrictions, porosity, permeability and hydraulic load. Thus, soil micro-structure and hydraulic load are strongly linked and suggest that suffusion is complex mechanism

4.1 Introduction and objectives

The soil within embankment hydraulic structures can undergo diverse stress conditions, including the usual compressive state, the undesired extension stress state due to arching (Kulhawy and Duncan, 1972; Soroush and Pourakbar, 2022) and the hydro-mechanical effects from solid bodies, which are identified as the oedometric stress state. These stress states hold significant implications, particularly for parameters related to suffusion, yet their impact is not fully understood. Previous research, as outlined in section 2.3.4 has demonstrated how different stress conditions influence erosion rates and mechanical responses (Moffat and Fannin, 2006, 2011; Bendahmane et al., 2008; Luo et al., 2013; Ke and Takahashi, 2014a; Liang et al., 2017). For example, it has been observed that increasing the confining stress tends to reduce the erosion rates in sandy clay specimens (Bendahmane et al., 2008). Researchers have also noted variations in initiation and deformation hydraulic gradients under different stress conditions, with isotropic stress leading to more pronounced gradients compared to other states (Chang and Zhang, 2013a). However, the study of stress effects on different soil types and hydraulic load conditions adds complexity to the comparison. Until now, the scientific community has primarily focused on characterizing suffusion through the definition of critical hydraulic gradients (Chang and Zhang, 2013a; Liang et al., 2017; Luo et al., 2020). This paradigm can be traced back to early findings concerning sand boiling, which involved upward flow experiments (Terzaghi, 1939; Skempton and Brogan, 1994). While

these critical thresholds have found utility in earthen hydraulic structural analysis, it is important to exercise caution when applying them commonly due to scale effects and the influence of hydraulic loading history (Rochim et al., 2017).

Alternatively, field-applicable solutions could be established through coupled hydro-mechanical modeling of specific embankments (Gelet et al., 2021), similar to finite element analyses used for slope stability (Griffiths and Fenton, 2004). These models require the development and validation of behavior laws capable of describing the development of suffusion (Kodieh et al., 2021; Gelet and Marot, 2022). Therefore, exploring more integrated definitions of suffusion-related parameters and investigating the influence of stress states on these parameters is essential.

The primary objectives of this chapter are to explore suffusion phases under complex stress states, define parameters characterizing each phase and analyze the impact of various stress states on these parameters. To achieve this, the modified triaxial apparatus presented in Chapter 3, is employed for suffusion tests, allowing precise control over hydraulic gradient, confining pressure and deviatoric stress. Four stress states, i.e. triaxial isotropic, triaxial compression, triaxial tension and oedometric, are investigated to gain a comprehensive understanding of the initiation and development of internal erosion. Throughout, a special attention is given to repeatability tests.

4.2 Experimental investigation

4.2.1 Testing material and methodology

Gap-graded soils serve as crucial constituents in the construction of embankment dikes and their characteristics can vary based on their grading. We may also highlight that widely graded soils can undergo gap-grading during construction due to the segregation of particles. To study the soil responses under controlled conditions in the laboratory, several particular gap-graded mixtures, suspected to be prone to suffusion, are prepared. These mixtures combine a well-graded fine sand (referred to as P-S1) with a uniformly-graded coarse gravel (referred to as P-G3) sourced from the Sablière Palvadeau quarry in France (Figure 4.1). This study involves the testing of four distinct gap-graded soils, with varying percentages of sand (P-S1), 15%, 25%, 35% and 40% and named soils A, B, C and D. This sand is considered as the fine fraction with respect to the coarse gravel (P-G3). This approach allows us to explore the potential influence of four fine percentages on the initiation and the development of the suffusion process.

Grain-size-based criteria, while not exhaustive, often serve as a preliminary screening tool for initial assessment. In pursuit of ensuring a measurable suffusion process in this experimental study, a rigorous evaluation of internal stability is conducted for gap graded soil mixtures. Employing geometric criteria, this assessment is facilitated by well-established methods drawn from contemporary scientific literature.

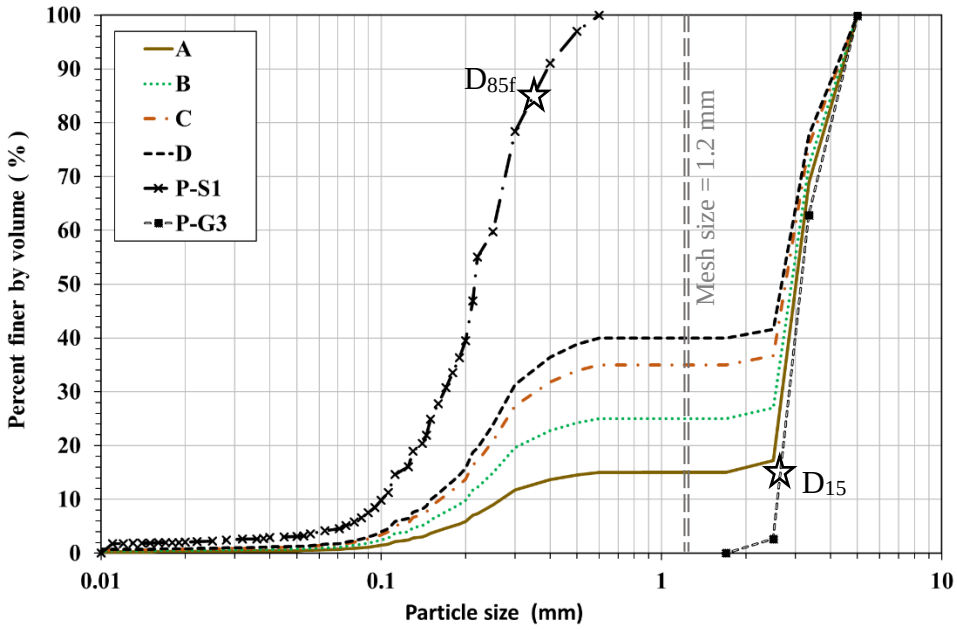

Figure 4.1 Particle size distribution of tested soils

Table 4.1 Physical properties and suffusion susceptibility potentials of the four tested soils

Physical Property	Soil A	Soil B	Soil C	Soil D
Percentage of sand (%)	15	25	35	40
Percentage of particles < 0.063 mm	0.624	1.040	1.456	1.664
Gap Ratio (G_r)	2.833	2.833	2.833	2.833
Coefficient of Uniformity (C_u)	11.927	15.539	18.486	19.497
$d_{15}/\ d_{85}$	0.143	0.061	0.052	0.050
$(H/F)_{min}$	0.053	0.041	0.030	0.026
$D(H/F)_{min}$ (mm)	0.488	0.535	0.573	0.582
Kezdi (1979) [$(D_{15c}/D_{85f})_{max}$] i.e. $7.59 \geq 4$	U	U	U	U
Kenney and Lau's (1985) criterion	U	U	U	U
Wan and Fell's (2008) criterion	/	/	/	/
Chang and Zhang's (2013b) criterion	S	S	S	S

Notes: P = percentage of particle smaller than 0.063 mm; $G_r = d_{max}/d_{min}$ (d_{max} and d_{min}: maximal and minimal particle sizes characterizing the gap in the grading curve); C_u = uniformity coefficient; d_{15} and d_{85} are the particle diameters in which 15% and 85% respectively of the weighed soil is finer for gap graded soil mixture; D_{15c} is the particle diameter in which 15% of weighted coarse particles is finer; D_{85f} is the particle diameter in which 85% of weighted fine particles is finer; F and H are the mass percentages of the grains with a size, lower than a given particle diameter d and between d and $4d$ respectively; $D(H/F)_{min}$ is the corresponding diameter with the minimum value of ratio H/F; U = unstable; S = stable. / = method not relevant for the considered soil.

Drawing insights from criteria established by the U.S. Army (1953) and Isotomia (1957), centered around the uniformity coefficient C_u, the chosen soil gradation showcases internal stability, as it is calculated C_u remains below 20. However, when considering the guidelines set forth by Kezdi (1969) and Sherard (1979), grounded in classical retention criteria for granular filters, the selected soil gradation exposes internal instability. This is evident in the computed D_{15c}/D_{85f} ratio, which stands at 7.59, surpassing both Kezdi's $D_{15c}/D_{85f} \geq 4$ and Sherard's $D_{15c}/D_{85f} \geq 5$ benchmarks for stable gradation. Furthermore, based on Chang and Zhang's (2013b) criterion, the gradation closely approaches the stability limits. Building upon the findings of Prasomsri et al., (2021), it is anticipated that the soil with 15% sand content exhibits underfilled characteristics, while the 40% sand content soil is expected to display overfilled attributes. The remaining two gradations are assumed to fall close to the transition between these two microstructural states. Table 4.1 summarizes the properties of the tested soils selected to span a representative range of suffusion susceptibilities and microstructures, contributing to a comprehensive understanding of the investigated phenomenon.

Choice of downstream filter mesh based on the soil gradation

In this experimental setup, the downstream filter mesh (Figure 4.1), is strategically chosen to the opening of 1.2 mm. This choice prevents larger coarse grains from migrating while allowing all fine grains to pass through. Skempton and Brogan (1994) proposed using the minimum value of the H/F ratio to distinguish between fine and coarse fractions. However, Marot et al. (2009) highlighted that a downstream filter with a pore opening matching the maximum diameter of the fine fraction can hinder suffusion development due to a geometric filtration effect driven by arching. This effect intensifies as more detached particles reach the mesh simultaneously, leading to a potential overestimation of the soil resistance towards suffusion. To address this, the authors recommend identifying the pore opening using the maximum H/F ratio that follows the second minimum value. Applying this method to our tested soils, validates the selection of a 1.20 mm pore opening, optimizing conditions for our suffusion study.

Specimen Labelling

The labeling of specimens follows a standardized format: **X_LT_R**. Here's a concise breakdown of each element:

- **X** represents the 4 distinct gap graded soils, A, B, C and D, with different fine content (%) (Figure 4.1).
- **LT** signifies the loading type based on the deviatoric stress value. For example, LT = 25.8 referrers to a test realized under the positive deviatoric stress of q = 25.8 kPa. In the same vein, LT = - 43.9 referrers to a test realized under the negative deviatoric stress of q = -43.9 kPa. Finally, LT = "oedo" referrers to an oedometric configuration.
- **R** indicates the test repeatability.

This systematic approach ensures that each specimen's label encapsulates its composition, loading conditions and test characteristics. Here the phrase "Oedometric" have distinct boundary conditions compared to triaxial tests. In oedometric testing, the specimen is placed within a membrane supported by a mold without applying confining or deviatoric stress, while in triaxial tests, stress is controlled based on the desired stress state.

Specimen preparation and methodology

The process of preparing specimens involves a systematic three-step approach: production, installation and saturation. To ensure reproducibility, a specific procedure is followed. Initially, a mixture of sand grains and gravels, with a moisture content of 4%, is thoroughly prepared. The chosen moisture content is optimized based on practical experience, recognizing that a higher water content percentage could disrupt the cohesion between fine and coarse particles, leading to segregation. Conversely, a lower moisture content may prove insufficient for the homogeneous mixing of fine content during the sample preparation process.

During specimen installation, a membrane is placed within a steel mold using a slight vacuum and the steel mold is securely connected to the base pedestal. Subsequent compaction is completed through moist tamping, achieving the target dry density of 1739 kg/m³. Previous studies and experiential knowledge gained from working with the soil B at this specific density indicated that it neither falls into the dense nor loose category, making it suitable to triggering suffusive behavior. Given our research objective to investigate the initiation and the development of suffusion under several stress states, the decision to keep the dry density constant allows us to focus on other influential parameters. The specimens used in all tests conducted in this study have consistent dimensions, with a diameter of 100 mm and a height of 200 mm. During the compaction process, the soil is compacted in four layers, each with a thickness of 50 mm, utilizing Ladd's (1978) under-compaction technique to ensure precise control. The alternative approach would have been to take another control parameter, such as for example the relative density.

In both oedometric and triaxial configuration, the top cap is attached to the specimen. In triaxial, a low confining stress of 20 kPa is applied to prevent seepage between the membrane and the specimen. The saturation phase initiates by gradually injecting carbon dioxide for approximatively 20 minutes. Once air is replaced by the carbon dioxide, the dissolution of gas bubbles in water favors a good saturation. Subsequently, tap water is systematically injected at a controlled rate of 0.25 mm/min. This saturation speed is carefully chosen to replicate an initial reservoir impounding rate and to ensure a methodically cautious approach to experimentation. This saturation process extends for approximately fourteen hours, until water begins to seep out through the top cap. The ultimate saturation ratio was verified by measuring the B coefficient, which was estimated to approximately 0.85, on a dedicated specimen, thereby anchoring the quality of the saturation process.

In oedometric tests, the consolidation phase is absent, but the erosion phase is conducted using a membrane-supported mold without applying confining or deviatoric stress to the specimen. Conversely, in triaxial tests, the primary distinction lies in the consolidation phase, as the erosion phase and post-suffusion gradation follow similar procedures to the oedometric configuration, despite differing boundary conditions, as described in section 3.8. During the consolidation phase for each triaxial specimen, the confining stress is incrementally raised at a rate of 1 kPa/min. The core objective of this procedure is to ensure that the induced hydraulic gradient consistently remains below the designated initial value for the multi-stage hydraulic loading path, a value specifically set at 0.1.

For specimens subjected to triaxial compression or extension stress conditions, the axial stress is systematically increased or decreased at a rate of 1 kPa/min, progressing up to the desired stress

threshold. The vertical stress component is automatically regulated through a jack mechanism, thanks to a dedicated program. Throughout the stages of specimen saturation, consolidation and pre-suffusion shearing, all soil losses are captured within a dedicated linen bag. A multistage hydraulic gradient is applied to the specimen and is quantified through computations involving the differential pressure head and the specimen's height. At several chosen hydraulic loading stage, eroded soil is collected via a soil collection system which enables the study the erosion rate time evolution. The volume of outflow is continuously recorded to provide precise insights into variations in hydraulic conductivity throughout the erosion process. The hydraulic conductivity is quantified thanks to computations involving the hydraulic gradient and the flow rate, by using the initial value of the section. The axial and volumetric deformations of the specimen during the erosion process were recorded using a Linear Variable Differential Transducer (LVDT) sensor and an electronic volume change apparatus, respectively. The overall visual representation of the testing apparatus is illustrated in Figure 4.2.

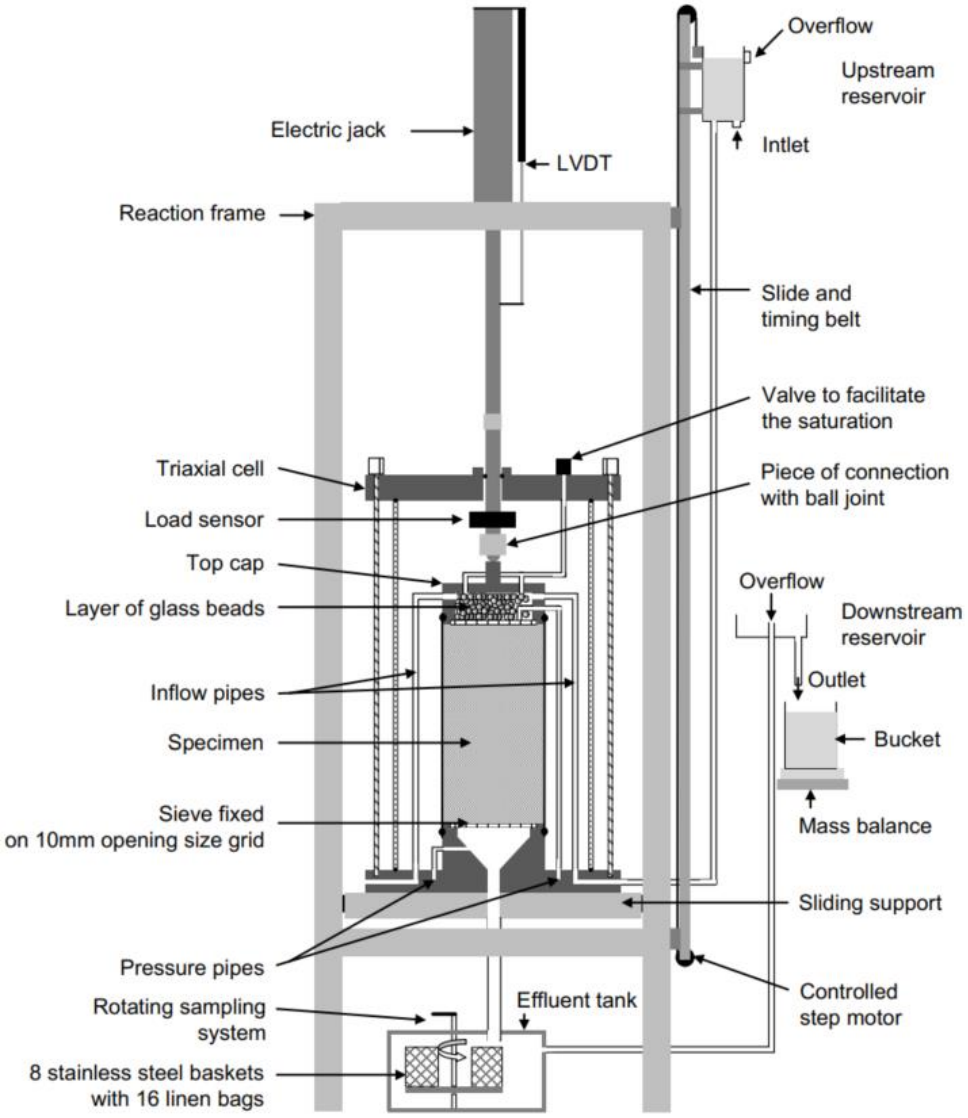

Figure 4.2 General configuration of the experimental bench

4.2.2 Computation of parameters (hydraulic conductivity, erosion rate, energy and eroded mass)

The computation of the hydraulic conductivity is based on the Darcy' formula,

$$K = \frac{Q}{S * i} \tag{4-1}$$

where Q is the flow rate (m^3/s), i stands for the hydraulic gradient (m/m) and S represents the cross-sectional area for flow (m^2). Likewise, the determination of the erosion rate ($kg/m^2/s$) takes the form:

$$\dot{m} = \frac{m_{eroded}}{S*\Delta t} \tag{4-2}$$

in which m_{eroded} corresponds to the mass of fine particles eroded during the duration Δt. As presented section 2.2.3, the comprehensive expression for the total flow power P_{flow} is expressed in watts (W) as follows:

$$P_{\text{flow}} = (\gamma_w \Delta z + \Delta P)\, Q \tag{4-3}$$

where γ_w is the specific weight of water (N/m^3), ΔP is the pressure drop between upstream and downstream sections (Pa) and Δz is the difference in elevations between upstream and downstream sections (m).

The energy expended due to seepage flow E_{flow} is the time integral of the instantaneous power P_{flow}. The cumulative loss dry mass (in kg) throughout the suffusion process characterizes the soil's response, accounting for mass eroded during the test and the mass lost during the saturation, consolidation and pre-suffusion shearing stages. Marot et al. (2016) highlighted that the end of the suffusion process reaches a state of equilibrium, named as "steady state", when the hydraulic conductivity becomes stable and the erosion rate diminishes. This state of equilibrium serves as a reference point to quantify the suffusion susceptibility thanks to the erosion resistance index I_α that is defined by the ratio of the cumulative loss dry mass over the energy expended by the flow, when both are computed at this "steady state" point:

$$I_\alpha = -\log\left(\frac{\text{Cumulative loss dry mass}}{E_{\text{flow}}}\right) \tag{4-4}$$

Based on I_α values, the study proposed six categories of suffusion susceptibility, ranging from highly erodible to highly resistant. For instance, highly erodible for $I_\alpha < 2$; erodible for $2 \leq I_\alpha < 3$; moderately erodible for $3 \leq I_\alpha < 4$; moderately resistance for $4 \leq I_\alpha < 5$; resistant for $5 \leq I_\alpha < 6$; highly resistant for $I_\alpha > 6$.

4.2.3 Testing program

The study conducted a dedicated test program to fill the existing knowledge gaps mentioned in Chapter 2. In prior studies, as noted by Chang and Zhang (2013a) and Marot et al., (2020), it was acknowledged that both the primary stress orientation and/or the direction of the fluid flow within a material can be either parallel or perpendicular with respect to the gravitational acceleration. These conditions can be observed in scenarios involving earth hydraulic structures, such as reservoir filling, floods, segregation, arching and the presence of intersecting pipes.

Beyond the flow direction, a material's stress state can take on various forms, including oedometric, compressive triaxial (where the major stress axis is vertical), isotropic, or even tensile triaxial (with the major stress axis being horizontal).

To study the kinetics of suffusion under such various stress conditions, a comprehensive series of suffusion tests was carried out. These tests encompassed four distinct stress states while maintaining a consistent downward flow direction. The four deviatoric stresses tested in this study are illustrated in Figure 4.3 : q = 55.5, 25.8, 0.0, -43.9 kPa; along with their corresponding shear stress ratios $\eta = q/p'$. Notably, all specimens were first isotropically consolidated and then a target deviatoric stress was applied, establishing a mean effective stress of p' = 70 kPa, which was subsequently held constant to underscore the role of deviatoric stress q.

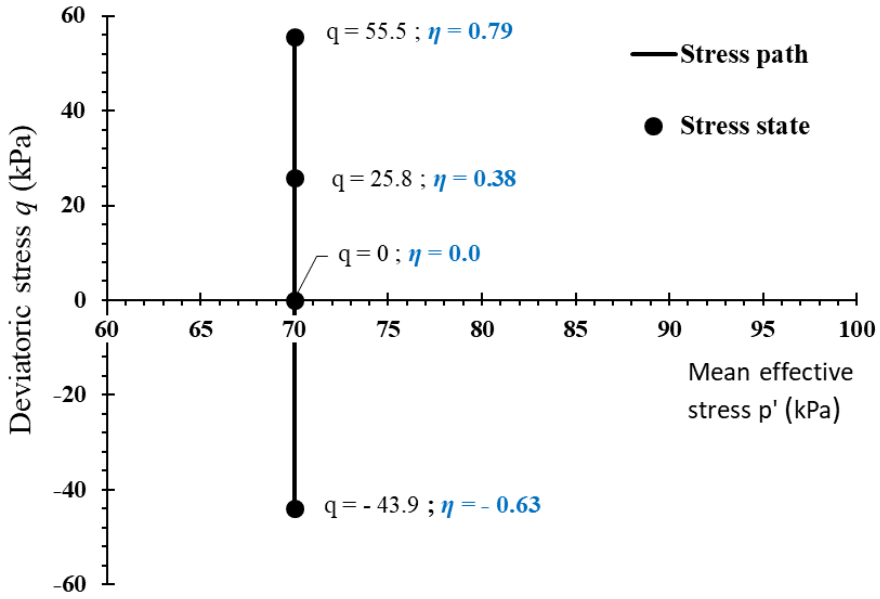

Figure 4.3 Triaxial stress states for internal erosion testing

Table 4.2 summarizes the stress states used for this testing program. To provide a more comprehensive understanding, we conducted conventional drained triaxial compression tests to quantify the peak deviatoric stress, indicated as q_{peak}. The results yielded recorded q_{peak} values of 279.0 kPa, 233.0 kPa, 217.0 kPa and 230.6 kPa, for the following fine content percentages 15%, 25%, 35% and 40%, respectively. Hence, the stress level for each soil and each stress state q / q_{peak} is presented in Table 4.3. The maximum stress level being around 25% suggest that, at these

applied stresses level, no shear bands were formed, a fact of considerable consequence as such bands could substantially modify the flow network. Stress-strain and volumetric-strain curves of the drained tests can be found in Figure_Appx. C.5 and Figure_Appx. C.6 for completeness.

Table 4.2 Summary of the testing program

Applied stress state	Confining pressure (kPa)	Deviatoric stress q (kPa)	Mean effective stress p' (kPa)	Shear stress ratio $\eta = q/p'$
Triaxial compressive high	51.5	55.5	70	0.79
Triaxial compressive low	61.4	25.8	70	0.37
Triaxial isotropic	70	0	70	0
Triaxial tensile	84.6	-43.9	70	-0.63
Oedometric	/	0	/	/

In both triaxial and oedometer conditions, the specimens utilized in this study maintain consistent dimensions, with a diameter of 100 mm and a height of 200 mm. In the context of oedometric tests, the process involves placing the specimen within a cylindrical mold and supporting it using a membrane. A minor axial stress of 3.84 kPa is applied solely through the weight of the top cap. It is important to note that this method does not involve any additional consolidation steps.

Following the preparation phase, all specimens undergo the same hydraulic loading path, as illustrated in Figure 4.4. The goal is to observe the successive suffusion phases. To achieve this, a multi-stage hydraulic gradient loading path is chosen (Rochim et al., 2017). This path is selected with the aim of reaching the steady state of suffusion, i.e. when the hydraulic conductivity stabilizes and the erosion rate decreases.

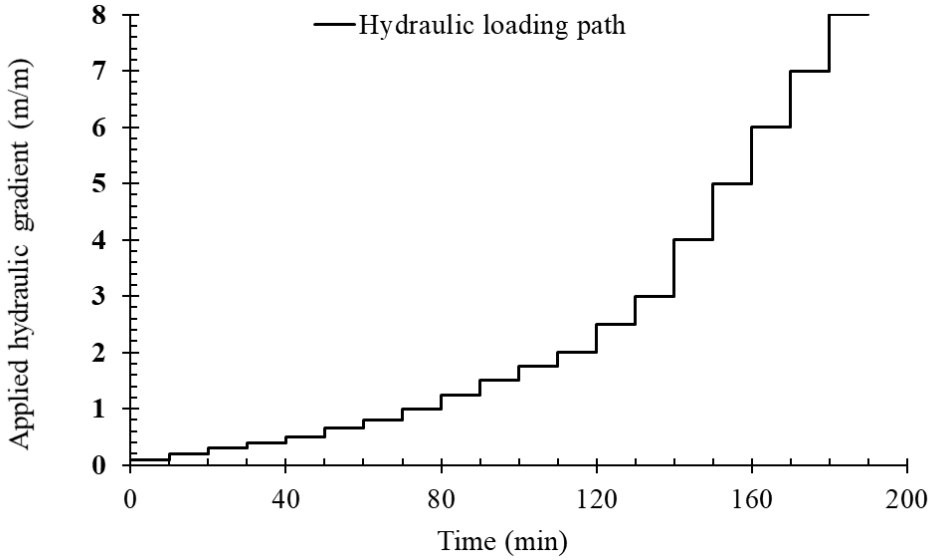

Figure 4.4 Temporal evolution of the applied multi-stage hydraulic gradient

Table 4.3 Properties of tested specimens

Specimen	Percentage of deviatoric stress (%)	Sand Lost mass during specimen preparation (%)	Dry unit weight		Intercoarse Void ratio (e_c)	Void ratio (e)
			Pre-suffusion state (kN/m³)	Post-suffusion state (kN/m³)	Pre-suffusion state (-)	Pre-suffusion state (-)
A_55.5	19.89	0.66	16.77	16.67	0.85	0.57
A_25.8	9.25	1.15	16.89	16.73	0.83	0.55
A_0	0.00	1.02	16.57	16.43	0.87	0.58
A_oedo	0.00	0.73	16.48	16.38	0.88	0.59
B_55.5	23.79	4.55	17.27	16.65	1.03	0.52
B_25.8	11.06	3.28	17.03	16.30	1.06	0.54
B_0	0.00	5.45	16.83	15.94	1.09	0.56
B_-43.9	18.82	9.18	16.31	15.41	1.15	0.61
B_oedo	0.00	1.68	16.99	16.36	1.07	0.55
B_55.5_R1	23.79	5.91	17.05	16.44	1.06	0.54
B_25.8_R1	11.06	4.19	16.91	16.09	1.08	0.55
B_0_R1	0.00	4.14	16.77	15.99	1.05	0.56
B_-43.9_R1	18.82	5.16	16.50	15.74	1.13	0.59
B_-43.9_R2	18.82	6.04	16.48	15.62	1.13	0.59
B_-43.9_R3	18.82	3.10	16.59	15.72	1.12	0.58
C_55.5	25.55	4.86	17.28	16.32	1.34	0.52
C_25.8	11.88	6.62	16.85	15.76	1.40	0.56
C_0	0.00	6.05	16.7	16.01	1.43	0.57
C_-43.9	20.21	10.58	16.27	15.25	1.49	0.61
C_oedo	0.00	8.00	16.40	15.14	1.47	0.60
D_55.5	24.07	6.22	17.18	17.16	1.55	0.53
D_25.8	11.19	5.75	16.85	16.39	1.60	0.56
D_0	0.00	7.73	16.31	15.36	1.69	0.61
D_-43.9	19.04	7.60	16.36	15.00	1.68	0.60
D_oedo	0.00	15.58	15.71	14.64	1.79	0.67
D_25.8_R1	11.19	9.35	16.86	16.76	1.60	0.56

Notes: Percentage of deviatoric stress is the ratio of the deviatoric stress applied during the suffusion test over the peak deviatoric stress measured during a conventional drained triaxial shear test; Percentage of lost mass during specimen preparation is equal to the ratio of sand mass loss during saturation and consolidation steps over the initial mass of sand of the specimen; Intercoarse void ratio (e_c) is defined as the ratio of the sum of the volume of fine grains (v_f) and the volume of voids (v_v) to the volume of coarse grain (v_c) within a soil mass; Void ratio (e) is the ratio of the volume of voids (v_v) to the volume of solids (v_s).

Furthermore, a permeability test was conducted on the individual components of the binary soil mixture: 100% sand and 100% gravel. The primary objective of this undertaking was to establish a foundational understanding of the potential range of hydraulic conductivity within these components. Since, the permeability of the sand alone is, on average, $4.02*10^{-4}$ m/s; it lies within the range of $1*10^{-8}$ to $5*10^{-6}$ m/s and is classified as a "Silty sands" (SM) by the Swiss Standard

SN 670 010b. Similarly, the permeability of the gravel alone is, on average, $2.69*10^{-2}$ m/s. Since this value lies within the range of $5*10^{-4}$ to $5*10^{-2}$ m/s, it corresponds to a "Well graded gravel" (GW), as specified by Swiss Standard SN 670 010b.

Additionally, Table 4.3 presents tabulated values for void ratios at the pre-suffusion state, offering insights into the fabric of the soil before suffusion occurs. The pre-suffusion intercoarse void ratio is defined as the proportion of voids and fine grain volumes relative to the volume occupied by coarse grains. This ratio plays a crucial role in understanding the soil's characteristics before the suffusion process. Importantly, the larger the percentage of fines, the larger the intercoarse void ratio. Further details and descriptions of the tabulated properties will be provided in a later section.

4.3 Characterization of the four phases of suffusion

Suffusion related parameters are now introduced to characterize the whole suffusion process that can be decomposed into, at most, four phases:

1. **Initiation phase**: At the outset of the erosion process, fine particles begin to erode, resulting in an increase in hydraulic conductivity.
2. **Self-filtration phase**: As the process continues, a self-filtration phase emerges. During this phase, both the hydraulic conductivity and the erosion rate start to decrease.
3. **Blow-out phase**: Subsequently, the system enters the blow-out phase. In this stage, a significant quantity of fine particles is washed away and strong increase in hydraulic conductivity is observed, leading to the dominance of preferential flow paths in the overall flow pattern.
4. **Steady state phase**: Finally, the process settles into a steady state. During this phase, the specimens achieve a steady hydraulic conductivity, causing the erosion of fines to gradually taper off, i.e. the rate of erosion decreases.

To illustrate the suffusion phases, two reference tests, B_0 and B_0_R1, were chosen, with B_0_R1 being the repeatability test. The analysis focuses on the temporal evolutions of the suffusion kinetics in specimens containing 25% sand, under isotropic stress conditions (q = 0 kPa). The methodology systematically assesses the temporal changes in hydraulic conductivity (Figure 4.5), erosion rate (Figure 4.6) and cumulative eroded mass in relation to the expended energy (Figure 4.7). For the initiation phase, a critical parameter, the initiation gradient (i_{SB}), is identified using the approach proposed by Skempton and Brogan (1994). This involves detecting a slight increase in hydraulic conductivity, as shown in Figure 4.5. The exact time of this occurrence and the corresponding hydraulic gradient are determined along the hydraulic loading path to establish the magnitude of i_{SB}.

In addition, for the blow-out phase, six key parameters are identified, each designated by specific subscripts: i_{HC}, i_{RE} and i_{MVE} are hydraulic gradients corresponding to the increase of the hydraulic conductivity, the erosion rate and the evolution of the cumulative eroded mass in relation to the expended energy, respectively. Similarly, E_{HC}, E_{RE} and E_{MVE} are the corresponding energies. Upon detecting a significant increase in hydraulic conductivity, the corresponding hydraulic gradient (i_{HC}) and its energy (E_{HC}) are pinpointed by referring to the exact time in the hydraulic loading path (refer to Figure 4.4 and Figure 4.5). Similarly, parameters i_{RE} and E_{RE} are derived from the time evolution of the erosion rate. The final set of parameters, i_{MVE} and E_{MVE}, is determined by

analyzing the evolution of cumulative eroded mass in relation to expended energy (see Figure 4.7). This method employs the double tangents method, similar to load-settlement curves. These phases will be further defined in the subsequent section.

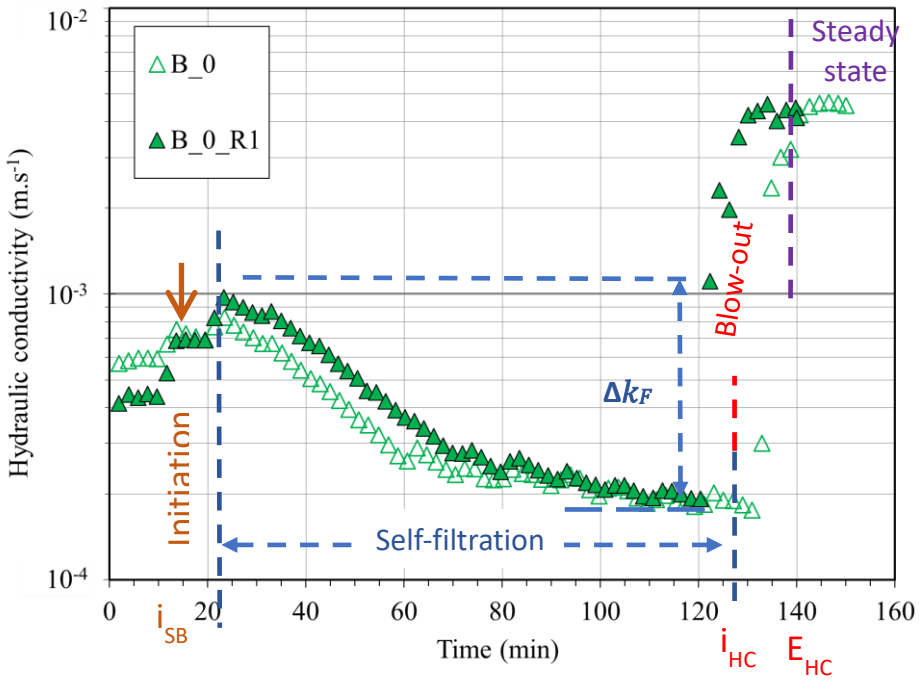

Figure 4.5 Time evolution of hydraulic conductivity for tests B_0 and B_0_R1

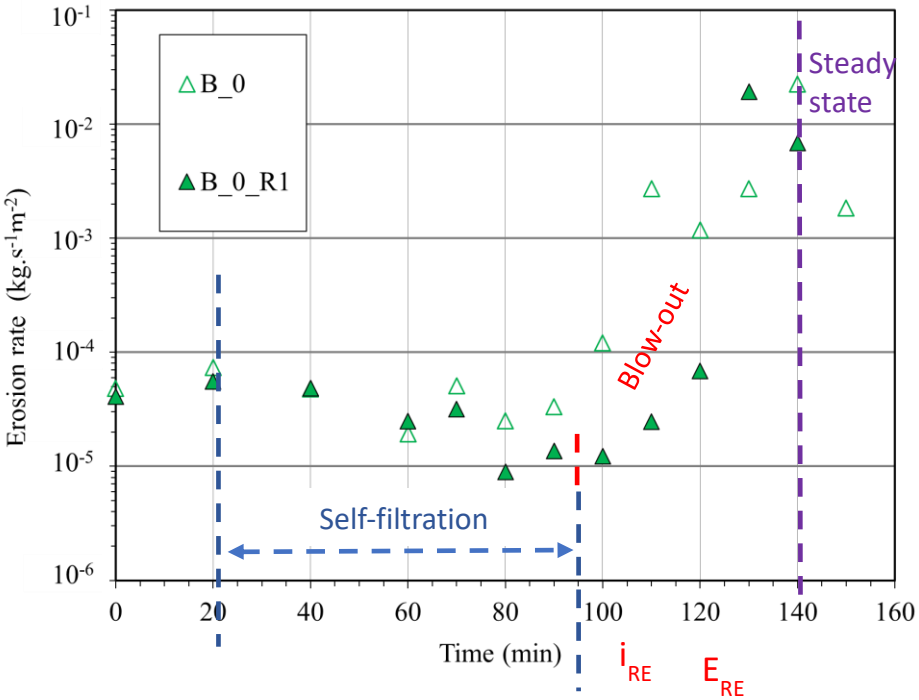

Figure 4.6 Time evolution of erosion rate for tests B_0 and B_0_R1

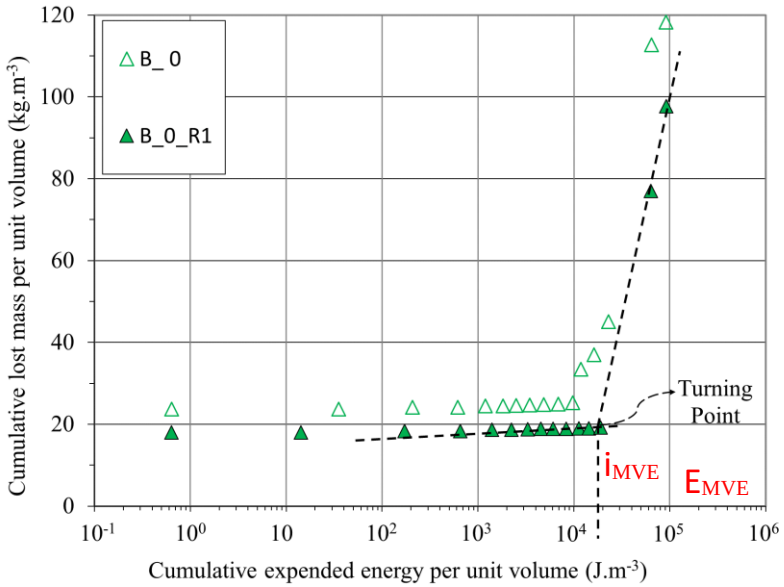

Figure 4.7 Cumulative lost mass versus cumulative expended energy for tests B_0 and B_0_R1

4.3.1 The initiation phase

During the initiation phase, the methodology established by Skempton and Brogan (1994) is employed to characterize the onset of suffusion. For both tests B_0 and B_0_R1, an increase in hydraulic conductivity arises upon the application of the hydraulic loading path at t = 11 minutes. This increase in hydraulic conductivity serves as a key indicator for detecting the initiation of the suffusion process. The corresponding hydraulic gradient is quantified through the hydraulic loading path, termed as i_{SB}. Based on the time indicator and the hydraulic loading path (Figure 4.4), the critical hydraulic gradient is identified as $i_{SB} = 0.2$ for both tests. Nonetheless, the erosion rate may decrease slightly during this phase.

4.3.2 The self-filtration phase

The second phase of the suffusion process is distinguished by a simultaneous decrease in both hydraulic conductivity and erosion rate. In this stage, the normalized difference between maximum and minimum hydraulic conductivity, relative to the initial value, quantifies the amplitude of the self-filtration. Specifically, for B_0, the normalized variation $|\Delta k_F| / k_{ini}$ amounts to 1.129. Notably, the onset of self-filtration is typically detected earlier through the hydraulic conductivity time evolution than that of the erosion rate. Conversely, the end of the blow-out phase shows the opposite pattern. These observations likely arise from the spatial heterogeneity of suffusion. Self-filtration occurs as a consequence of multiple fine particle blockages within the specimen. Considering that the outlet sieve size is greater than the characteristic constriction size at the bottom of the specimen, it is reasonable to anticipate that these blockages will be initially be resolved at the lower part of the specimen (Seblany et al., 2021).

4.3.3 The blow-out phase

The blow-out phase is characterized by an increase of both the hydraulic conductivity and the erosion rate. From 90 min, the erosion rate strongly increases followed by the increase of the hydraulic conductivity at t = 130 min for test B_0 and 120 min for test B_0_R1. This contrasts with the earlier observation of the self-filtration phase, where the onset is typically detected earlier through hydraulic conductivity compared to the erosion rate. The onset of the blow-out phase can be defined through three distinct approaches: (i) by monitoring the rise in the erosion rate, (ii) by tracking the increase in hydraulic conductivity or (iii) by focusing on the inflection point of the cumulative mass versus cumulative expended energy curve as illustrated in Figure 4.7. By adopting approach (i), we identify the corresponding hydraulic gradients, denoted as i_{RE}, equal to 1.25 and 1.75 for tests B_0 and B_0_R1, respectively. These values correspond to expended energy, referred to as E_{RE} and equal to 4.9 kJ.m-3 and 14.3 kJ.m^{-3}, respectively. Conversely, with the second approach (ii), the associated hydraulic gradient values, referred to as i_{HC}, are determined as 3.00 and 2.50, while the respective expended energy values, denotes E_{HC}, are 25.9 kJ.m^{-3} and 22.5 kJ.m^{-3}. As previously discussed, the onset of the blow-out phase is observed earlier in erosion rate. Consequently, adopting the conservative approach of prioritizing eroded mass over hydraulic conductivity in defining the blow-out's onset is practical, but given the low measurement frequency using the evolution of erosion rate over time does not allow for an accurate blow-out's detection. Hence, since the hydraulic conductivity alone falls short in characterizing the blow-out phase, focusing on the overall response, represented by the eroded mass and the expended energy, is an interesting alternative to characterize the blow-out phase. Thus, approach (iii) emerges as the favored method for characterizing the blow-out onset. This entails focusing on the inflection point of the cumulative mass versus cumulative expended energy curve, as illustrated in Figure 4.7. At this inflection point, we define the corresponding hydraulic gradient, i_{MVE}, 1.75 and 2.5 for B_0 and B_0_R1, respectively, alongside the cumulative expended energy per unit volume, $\bar{E}_{MVE}$, equal to 9.8 kJ.m^{-3} and 18.9 kJ.m^{-3}, respectively. This approach is influenced by the method employed to estimate pre-consolidation pressure (Holtz, Kovacs and Sheahan, 1981) and favors an overall approximation.

4.3.4 The steady state

The fourth and final phase is characterized by a steady hydraulic conductivity and a gradual decrease in erosion rate, known as the steady state. For B_0 and B_0_R1, the steady state is observed at t = 140 and 130 min, respectively. Alike the concept of "critical state soil mechanics", it seems worthwhile to characterize this steady state of suffusion with an open mind, i.e. by several parameters. We propose to focus on the percentage of eroded mass in relation to the initial sand mass $M_{eroded}/M_{ini,FC}$, the erosion resistance index I_α, the steady Darcy velocity $v_{F,steady}$ and the steady axial strain $\varepsilon_{z,steady}$.

4.3.5 The particular case of triaxial tensile tests

The time evolution of hydraulic conductivity and erosion rate, illustrated in Figure 4.8, distinctly highlights the substantial variability in suffusion kinetics under the influence of tensile triaxial stress conditions. Notably, there is an absence of the initial initiation phase, directly indicating the

commencement of the self-filtration phase where the hydraulic conductivity undergoes a steady decline before the blow-out's initiation. Despite the absence of initial phase, the latter three suffusion phases remain consistently observable. However, the blow-out initiation occurs over a wide range of hydraulic gradients.

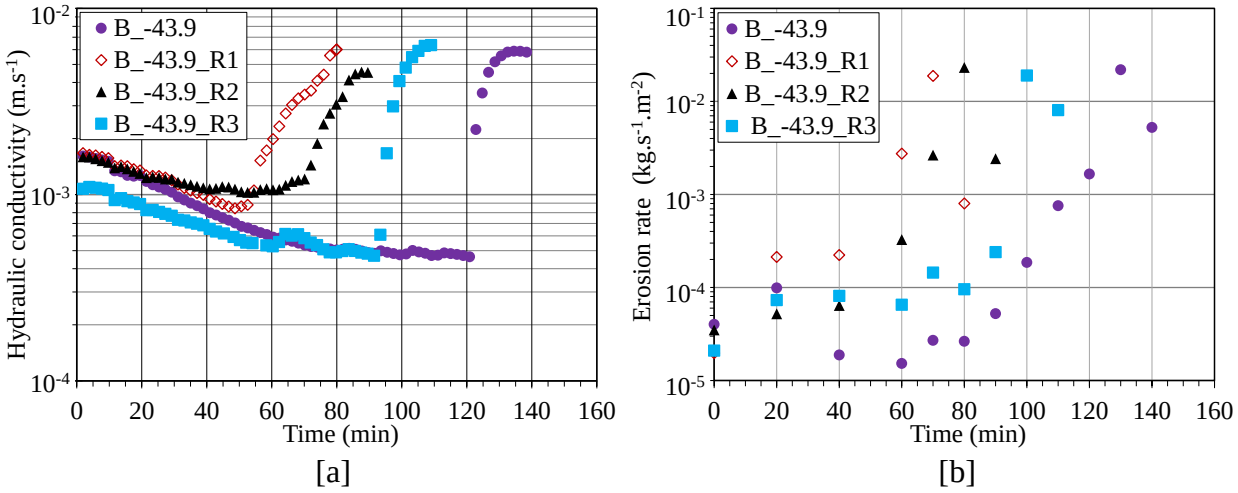

Figure 4.8 Time evolution of hydraulic conductivity [a] and erosion rate [b], for soil B under tension stress state (q=-43.9)

Chang and Zhang (2013a) provide valuable insights into pore behavior based on stress conditions. In triaxial extension cases, pores predominantly elongate radially, perpendicular to the flow direction. Conversely, under compressive stress states, pores tend to elongate vertically as shown in Figure 4.9 .

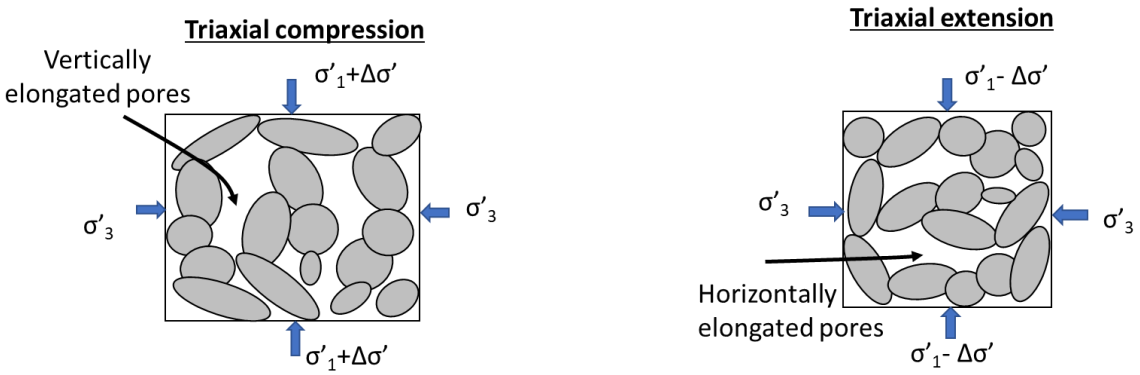

Figure 4.9 Comparison of elongated pores under triaxial compression and extension state

This differentiation is pivotal: when pores and constrictions enlarge parallel to the flow direction, stress-free fine grains can be dislodged, causing a minor increase in hydraulic conductivity at the start of suffusion tests. In contrast, under tensile deviatoric stress conditions, pores and constrictions elongate perpendicular to the flow. This configuration promotes a tortuous flow path so that the detached grains are prone to self-filtration, leading to reduced hydraulic conductivity. This self-filtration-induced localized overpressure can potentially trigger localized blow-out, as observed by Sail et al., (2011). Moreover, the tension-induced stress state introduces a rivalry between suffusion's pursuit of sub-vertical preferential flow paths and the stress state's resistance

through horizontal force chains. This competition emphasizes the importance of local instabilities, which could be responsible for the variability in blow-out initiation that has been observed.

4.3.6 Repeatability tests

The results presented in Figure 4.5 to Figure 4.8 indicate a good initial repeatability, as observed by focusing on the *initial* values of the hydraulic conductivity and the erosion rate. This comparison established the good repeatability of the specimen's preparation, saturation and consolidation. Notably, the initial hydraulic conductivity primarily depends on factors such as the total mass lost during saturation and consolidation phases, which may vary between tests and thereby explains the marginal divergence in initial hydraulic conductivity between specimens (Zhong et al., 2018). This clarification provides insight into the slight variance observed in the initial hydraulic conductivity between the B_0 test and its corresponding repeatability counterpart, B_0_R1, quantified at $5.78*10^{-4}$ m/s and $4.45*10^{-4}$ m/s, respectively.

Meanwhile, the suffusion kinetics' repeatability was assessed by comparing the time evolutions of both the hydraulic conductivity and the erosion rate. As observed in Figure 4.5 to 4.7, the overall time evolutions are very much alike and the repeatability is fairly good for all oedometric and compressive triaxial stress states. On the other hand, the repeatability regarding the suffusion kinetics is not as good for tensile triaxial stress states (Section 4.3.5).

Considering the thorough evaluation of repeatability and the identification of distinct phases, the parameters characterizing suffusion have been systematically identified and are concisely presented in Table 4.4. These values will be further commented in the following sections. Finally, due to the lower repeatability obtained under tensile triaxial stress conditions, we recommend to favor compressive triaxial, isotropic, or oedometric stress states to measure suffusion related parameters.

Table 4.4 Suffusion related parameters of tested specimens

Specimen identity	Onset	Initial hydraulic conductivity	Self-filtration	Blow-out		Steady state			
	i_{SB}	k_{ini}	$\lvert\Delta k_F\rvert / k_{ini}$	i_{MVE}	E_{MVE}	$M_{eroded}/M_{ini,\ FC}$	I_α	$v_{F,\ steady}$	$\lvert\epsilon_{z,\ steady}\rvert$
	(-)	***10^{-3}** m/s	(-)	(-)	(kJ/m^3)	(%)	SI	(cm/s)	(-)
A_55.5	*	10.0	0.049	0.3	4.5	4.88	3.6	0.59	0.03
A_25.8	*	9.75	0.283	0.3	3.9	7.77	3.7	0.55	0
A_0	*	10.6	0.023	0.3	7	6.68	3.4	0.57	0
A_oedo	*	10.3	0.087	0.3	6	4.81	3.7	0.59	0
B_55.5	0.2	0.68	0.987	1.5	11	19.27	2.6	0.5	0.15
B_25.8	0.2	0.52	0.762	1.25	6.5	21.1	2.6	0.5	0.26
B_0	0.2	0.58	1.129	1.75	10.9	27.21	2.8	0.5	0.25
B_-43.9	*	1.6	0.497	1.75	12	29.96	2.7	0.51	0.2
B_oedo	0.2	0.46	0.973	0.8	4	17.12	2.4	0.38	0.2
B_55.5_R1	0.2	0.42	1.059	1.75	11	20.46	2.7	0.4	0.1
B_25.8_R1	0.2	0.72	1.254	1.5	13.4	23.77	2.7	0.48	0.12
B_0_R1	0.2	0.44	1.755	2.5	18.9	22.47	2.9	0.5	0.2
B_-43.9_R1	*	1.65	0.283	0.65	3	23.08	2.1	0.5	0.05
B_-43.9_R2	*	1.59	0.054	0.65	4	26.13	2.2	0.38	0.1
B_-43.9_R3	*	1.09	0.387	1.25	5	22.41	2.5	0.46	0.39
C_55.5	0.2	0.06	0.796	6	40	27.99	2.7	0.54	2.85
C_25.8	0.2	0.09	0.734	5	37.6	29.09	2.9	0.54	1.69
C_0	*	0.21	0.464	5	40.6	18.24	2.9	0.56	0.25
C_-43.9	*	0.41	0.125	7	45	23.17	2.9	0.56	1.78
C_oedo	*	0.30	0.012	1	3	29.66	2.1	0.31	0.1
D_55.5	0.3	0.08	0.273	4	13	★	★	★	★
D_25.8	*	0.12	0.117	5	30.4	40.59	2.5	0.39	11.83
D_0	*	0.08	0.022	3	11	45.17	2.3	0.53	10.2

D_-43.9	*	0.10	0.592	5	15	24.34	2.4	0.38	1.57
D_oedo	*	0.21	0.158	2.5	12	46.19	2.3	0.46	6.73
D_25.8_R1	*	0.08	0.003	3	10.9	41.24	2.0	0.44	16.43

Notes: i_{SB} = the critical hydraulic gradient corresponding to the first increase of hydraulic conductivity (Skempton and Brogan 1994); $|\Delta k_F| / k_{ini}$ = the normalized hydraulic conductivity variation; i_{MVE} = the hydraulic gradient corresponding to the turning point of the curve, cumulative lost mass vs cumulative expended energy; E_{MVE} = the cumulative expended energy per unit volume corresponding to the turning point of the curve cumulative lost mass per unit volume vs cumulative expended energy per unit volume; $M_{eroded}/M_{ini,FC}$ = the percentage of total lost mass with respect to the initial mass of sand; I_α = the erosion resistance index (Marot et al., 2016); $v_{F,steady}$ = the Darcy velocity at the steady state; $|\epsilon_{z,\ steady}|$= the axial strain at the steady state. * = not observed. ★ = could not be measured.

Table 4.5 Repeatability identification based on initial hydraulic conductivity

Compared tests	$\frac{\Delta k_{ini}}{k_{ini}}$ [%]
B_55.5 & B_55.5_R1	38.24
B_25.8 & B_25.8_R1	38.46
B_0 & B_0_R1	24.14
B_-43.9 & B_-43.9_R1	31.88
D_25.8 & D_25.8_R1	33.33

Table 4.5 presents variations in initial hydraulic conductivity values, measured on soils B and D, at several stress states. Each time, the variation between the first test and its repetition is considered. The rang of variation for the initial hydraulic conductivity is lower than 38.46%. Due to the intrinsic sensitivity of the hydraulic conductivity, we will assume that two tests are adequately similar for initial hydraulic conductivity variations below 50%, thereby indicating the repeatability of the initial microstructure

4.4 Effect of the stress state on suffusion

4.4.1 Effect of the stress state on the initiation

The onset gradients, corresponding to the first increase in hydraulic conductivity (Skempton and Brogan, 1994), are detailed in Table 4.4 for the four mixtures across various stress states: oedometric, isotropic triaxial (q = 0 kPa), compressive triaxial (q = 25.8 and 55.5 kPa) and tensile triaxial (q = -43.9 kPa).

It is crucial to emphasize that in certain cases, such as underfilled (soil A) and overfilled (soil D) microstructures, the critical hydraulic gradients could not be ascertained due to either a consistently stable hydraulic conductivity (e.g., A_oedo) or an initially decreasing hydraulic conductivity (e.g., B_-43.9). The declining scenario is frequently witnessed during tensile triaxial stress states, in contrast with the observations of Chang and Zhang (2013a), whose study demonstrated a measurable onset critical hydraulic gradient for all stress conditions. This discrepancy is likely attributable to the rather large gap-ratio of their soil, G_r = 7.9, which promotes an increasing permeability upon the loss of fine particles. This discrepancy also finds its roots in the variances of soil composition – Chang and Zhang examined soils with a 35% fine content and a gap ratio of 7.9, whereas soil A (with 15% fine content , Figure 4.10) and soil D (with 40% fine content, see Figure 4.11) do not exhibit the onset of suffusion, indicating the substantial influence of the fine content and the soil's microstructure.

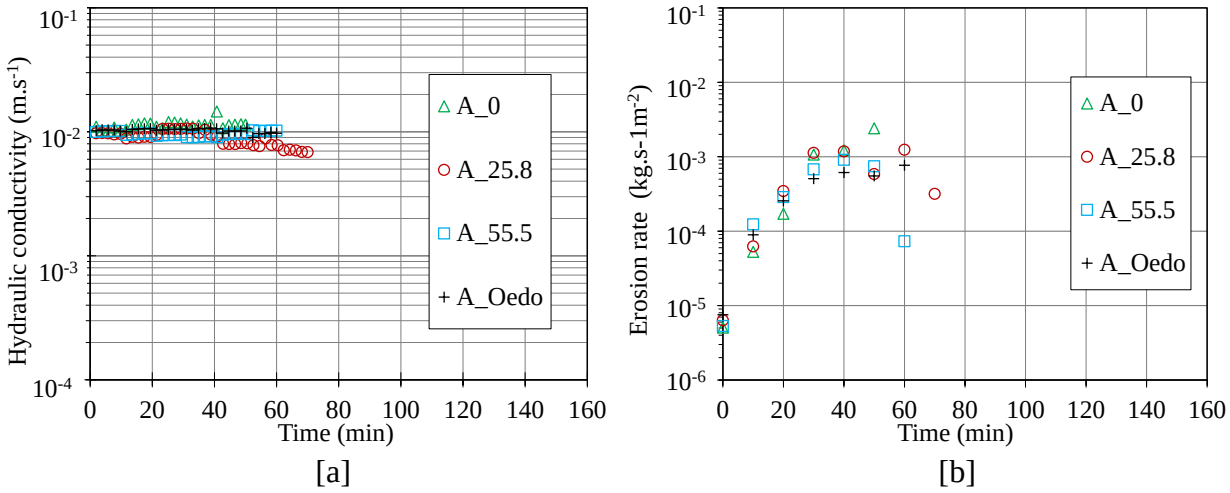

Figure 4.10 Time evolution of hydraulic conductivity [a] and erosion rate [b], for soil A under different stress state

Notably, soil B (Figure 4.12 & Figure 4.13) and some tests on soil C, endowed with a transitional microstructure, exhibit distinct phases of suffusion, alongside an observable onset. In cases where measurement is impossible, the impact of the stress state on the critical hydraulic gradient is minimal. Soil B, for instance, consistently maintains a critical hydraulic gradient of 0.2 across varying stress states as derived from the Figure 4.12.

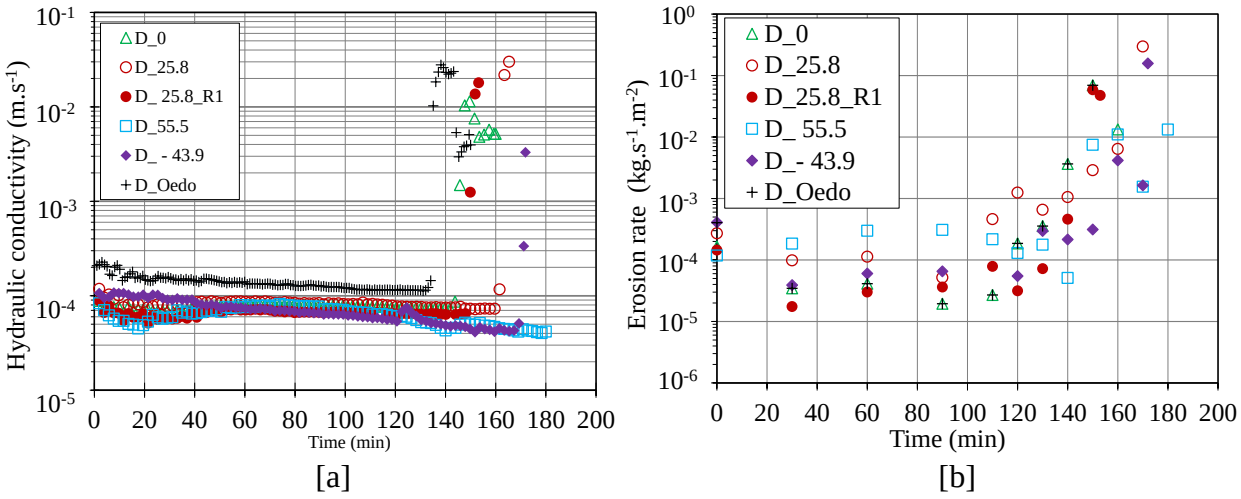

Figure 4.11 Time evolution of hydraulic conductivity [a] and erosion rate [b], for soil D under different stress state

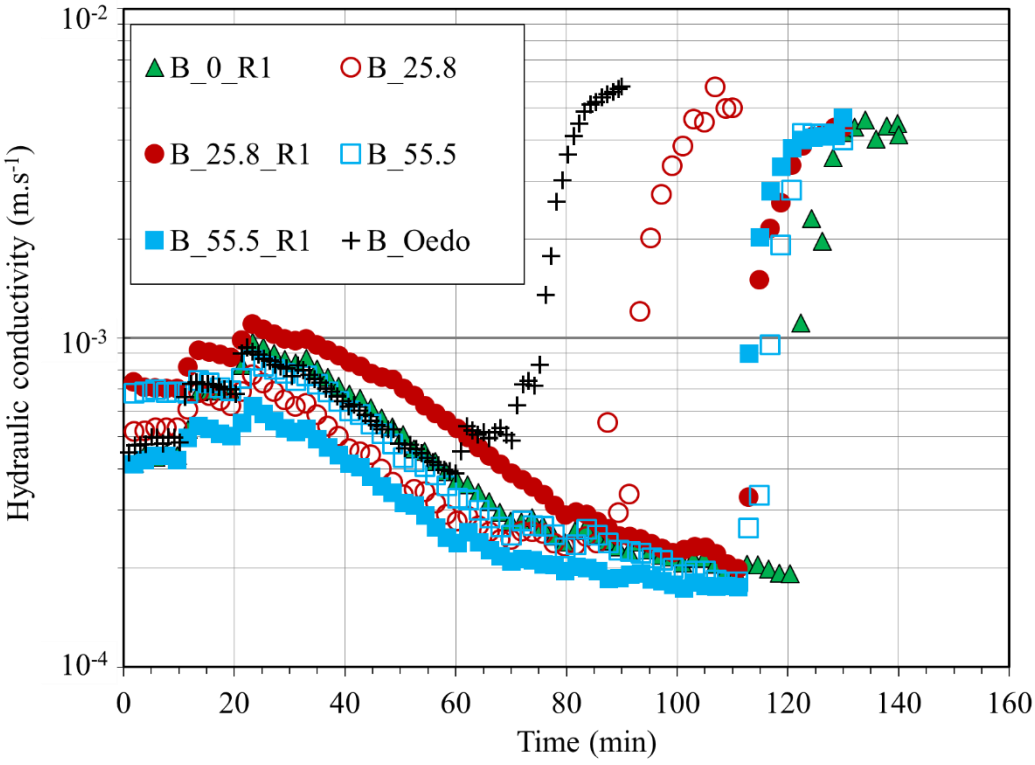

Figure 4.12 Time evolution of hydraulic conductivity, for soil B and different stress states

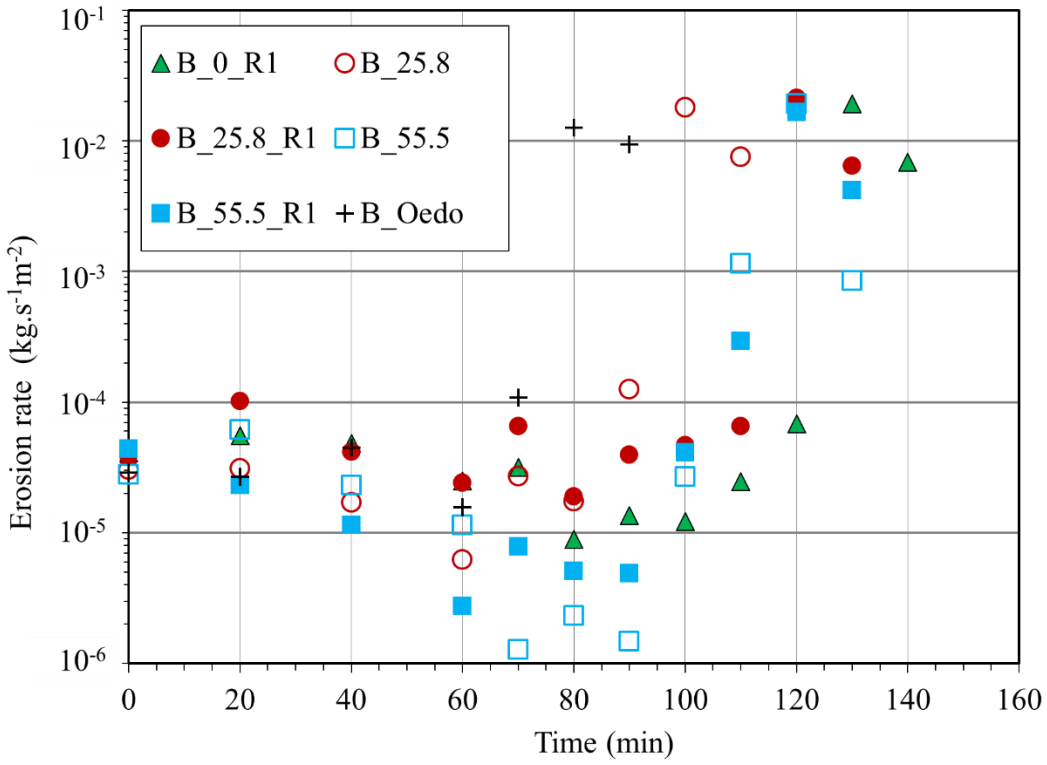

Figure 4.13 Time evolution of erosion rate, for soil B and different stress states

To summarize, fine content substantially influences the onset of suffusion as opposed to the stress state. Nonetheless, it is imperative to underscore that the variability of this parameter is influenced by the seepage length of the specimen (Zhong et al., 2018) and the hydraulic loading path (Rochim et al., 2017), necessitating its cautious application.

One alternative parameter to the critical hydraulic gradient i_{SB} is the critical Darcy velocity (Côté, 2010) that may be compared directly against the in-situ flow velocity when a salt tracer method can be used. Following the work of Stéphane Côté (2010), the Darcy velocity corresponding to the onset of suffusion v_{onset} may be directly estimated from the porosity n and the permeability K (cm⁄s):

$$v_{onset}\ (cm/s) = 0.399 * n * K^{0.586} \quad (4\text{-}5)$$

Figure 4.14 compares the experimentally obtained Darcy velocity against the above prediction for all tests. Details are provided in Appendix D. When the onset defined by Skempton and Brogan (1994) was observed, the corresponding experimental velocity is used. Alternatively, the initial experimental velocity is used. For all tests, the experimental Darcy velocity corresponding to the initiation of suffusion is found smaller than the one predicted with equation 4-5. Hence, the formula proposed by Stéphane Côté was determined was determined from tests carried out on soils which are a priori resistant since they are present in earth-structures. It should therefore be used with caution because it does not seem conservative.

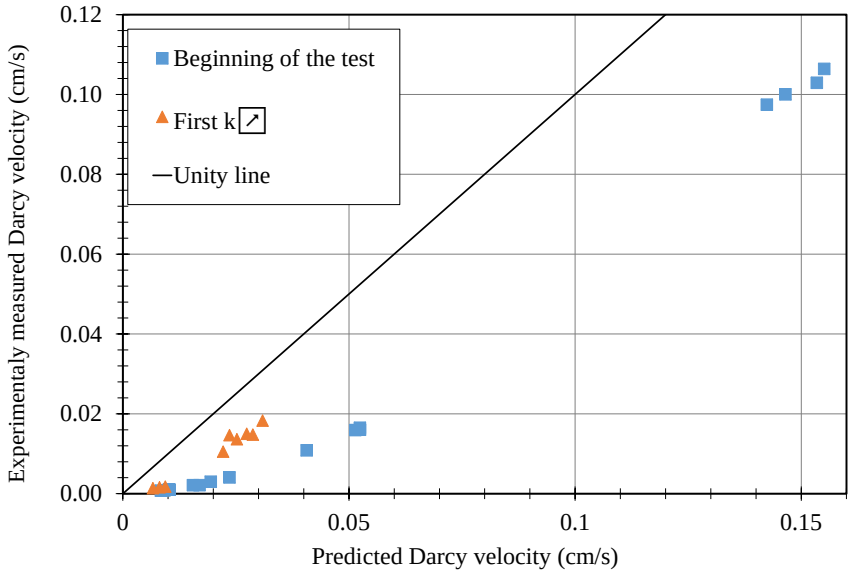

Figure 4.14 Experimental versus predicted Darcy velocity at the initiation of the suffusion process

4.4.2 Effect of the stress state on the self-filtration

The self-filtration process is primarily influenced by two key factors: (1) the nature of micro-structure i.e. underfilled, overfilled or in transition (Prasomsri and Takahashi, 2020) and (2) the stress state.

(1) In the underfilled condition, soil A (15% fine content) exhibits the lowest variation of normalized hydraulic conductivity (Figure 4.15). This outcome can be attributed to the prevailing washout of fine particles through pore throats, where coarse particles primarily dominate the soil matrix and finer particles contribute modestly. In contrast, the overfilled soil D demonstrates a slightly larger self-filtration amplitude due to the interplay between localized clogging and the detachment of fine particles. In such cases, finer particles, which bear a significant portion of the stress, show less susceptibility to detachment and subsequent self-filtration. However, the relatively small constriction sizes within this mixture likely facilitate the self-filtration of the detached particles, possibly prolonged by the duration of this phase. Within the transitional zone occupied by soils B and C, the competition between clogging and fine particle detachment results in a more pronounced self-filtration amplitude. These observations highlight the intricate interrelationship between the detachment and transportation of fines, underscoring the complexity of the phenomenon. When comparing soils, A and B, the latter displays a slightly higher intercoarse void ratio (Table 4.3), which facilitates fines' transport, contributing further to self-filtration. In Figure 4.15, the dotted lines represent the ranges of normalized hydraulic conductivity from the repeatability tests. The average is visually represented by a symbol.

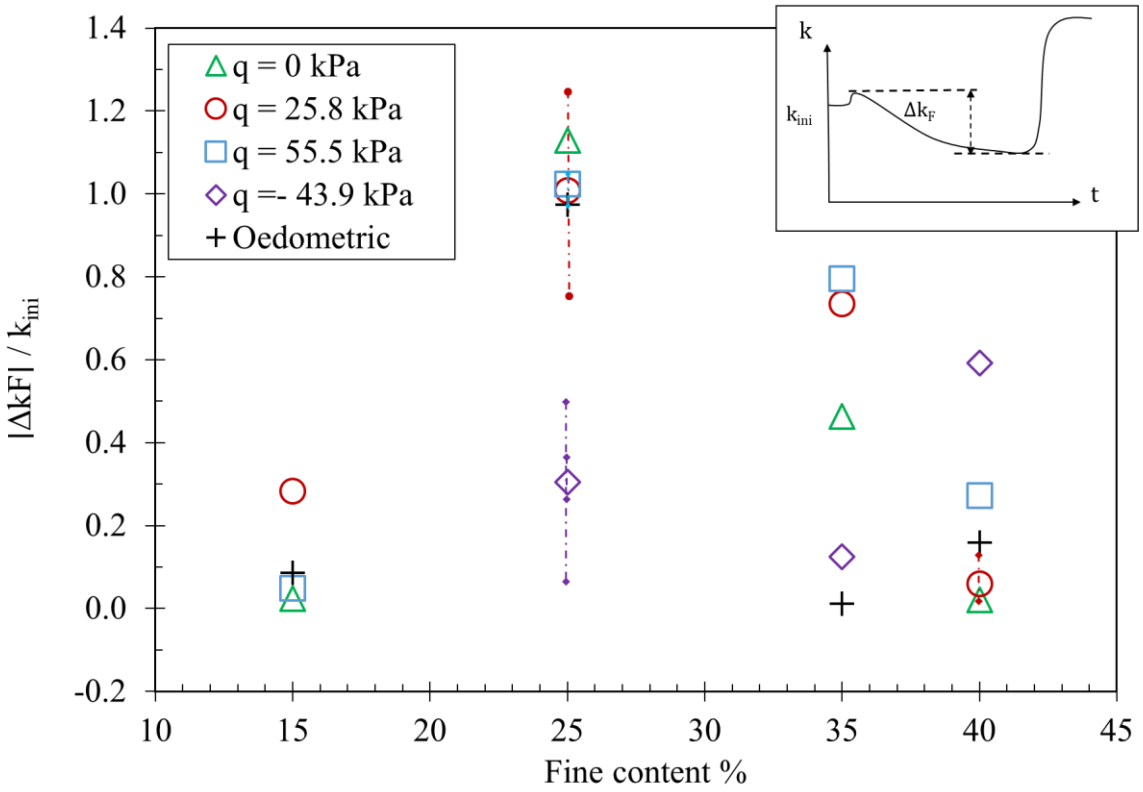

Figure 4.15 Normalized hydraulic conductivity variation during self-filtration with fine content

(2) The influence of the stress state on the self-filtration phase requires careful analysis alongside micro-structural considerations. Upon detachment, the subsequent self-filtration of fine particles is predominantly controlled by the orientations of pores and constrictions within the soil (Seblany et al., 2021). It is noteworthy that elongated pores tend to form along axial directions under positive deviatoric stresses and horizontally under negative deviatoric stresses (Chang and Zhang, 2013a).

Turning our attention to tests conducted under triaxial stress states, the deviatoric stress alone does not consistently impact self-filtration, at least within the range of tested peak stress ratios q/q_{peak}. In the case of triaxial tensile stress states with 25% sand content (soil B), it is observed that the initial hydraulic conductivity surpasses that under triaxial compressive stress states, indicating a distinct micro-structural configuration. This difference is due to elongated pores aligning radially, leading to larger constrictions perpendicular to the vertical direction, thereby promoting flow. Soil B, classified as a filled soil, exhibits lower self-filtration amplitudes under negative deviatoric stress in comparison to other stress states. This is because pores primarily elongated radially encourage horizontal displacement of detached particles, with minimal effect on self-filtration. In contrast, for the underfilled soil A and the overfilled soil D, the main stress minimally influences overall hydraulic conductivity evolution. This suggests a limited impact of the stress state on the pore orientations and subsequent constriction dimensions and orientations. Soil C, however, exhibits an intermediary response, falling between the behaviors of soils B and D.

In the context of tests conducted under oedometric stress states, it is clearly observed that the self-filtration phase's duration is shorter compared to the compressive triaxial stress states for soils B (Figure 4.12 & Figure 4.13) and C (Figure 4.16). This distinction arises due to the emergence of preferential flow paths that localize at the specimen's circumference in the oedometric configuration (Figure 4.17). Such circumferential flow localization contributes to a faster resolution of the self-filtration process. However, this effect is not predominant for soils A and D, where the nature of micro-structure takes precedence over the impact of the stress state.

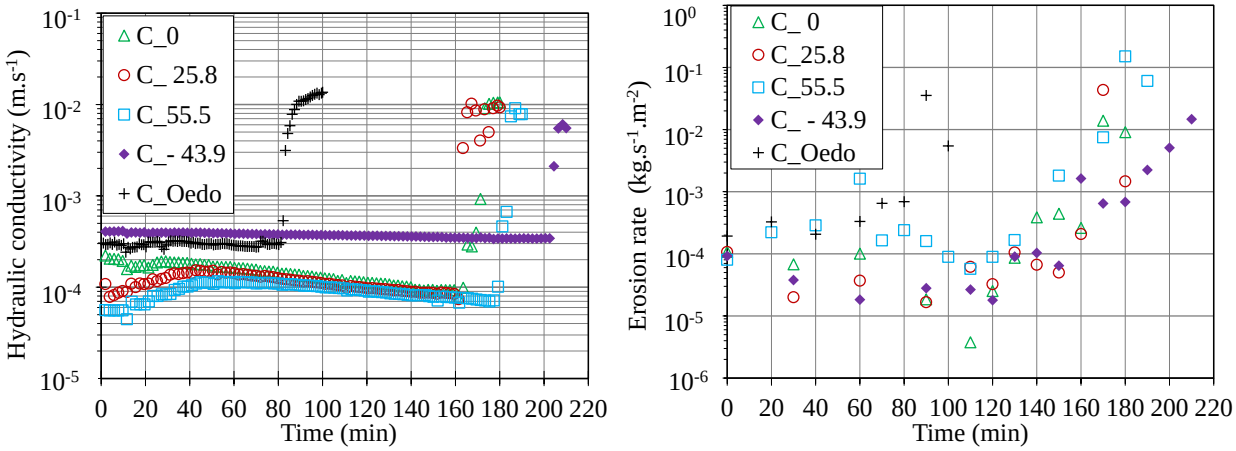

Figure 4.16 Time evolution of hydraulic conductivity [a] and erosion rate [b], for soil C under different stress state

Figure 4.17 Post-suffusion specimen under oedometric state [a] and compressive triaxial stress state q = 55.5 kPa [b], for soil B

4.4.3 Effect of the stress state on the blow-out

Analogous to the self-filtration phenomenon, the dynamics of the blow-out are principally influenced by the intrinsic micro-structural attributes and the prevailing stress state. In the context of the underfilled microstructure, exemplified by soil A, both parameters i_{MVE} and E_{MVE} exhibit relatively low values across the spectrum of tested soils, displaying a limited sensitivity to variations of the stress state (Figure 4.18 and Figure 4.19). This behavior is underpinned by the different role that coarse and fine particle fractions play within the soil matrix: coarse particles shoulder the primary load and govern the course of seepage, while the contribution of fine particles is less significant.

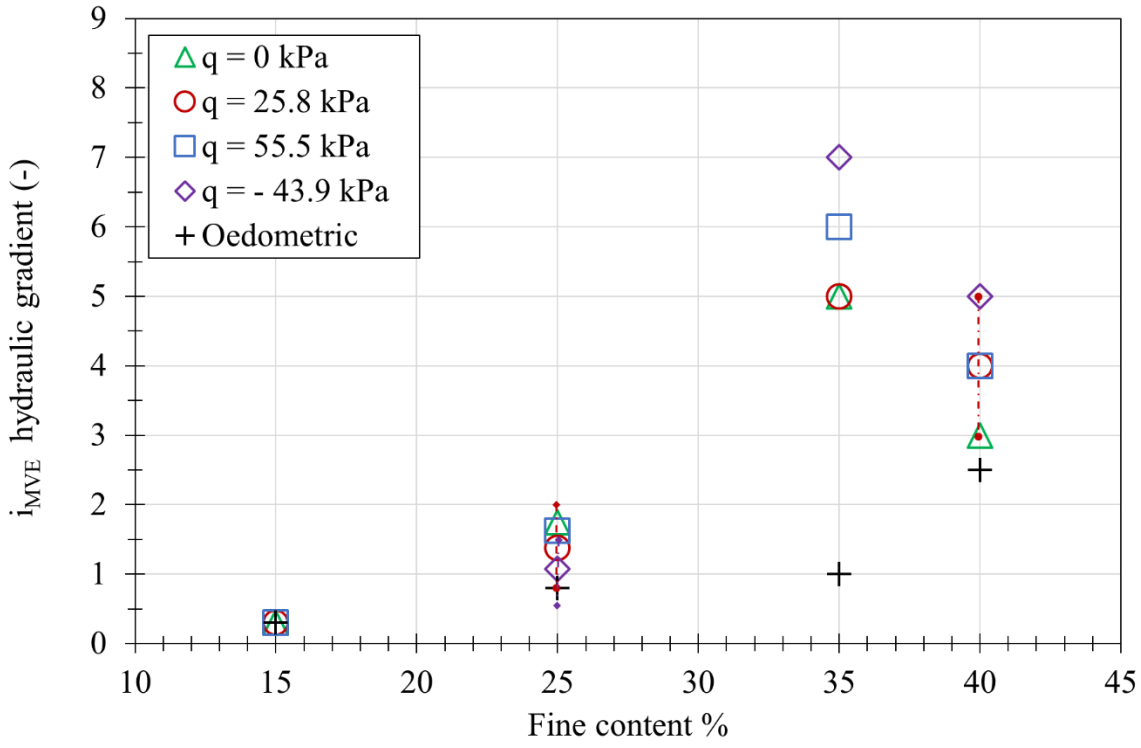

Figure 4.18 Variation in blow-out hydraulic gradient with the fine content under different stress states

Considering the remaining soils — B, C and D — suffusion tests executed in oedometric stress conditions display lower blow-out magnitudes in terms of hydraulic gradient and cumulative energy dissipation, relative to tests conducted under triaxial stress conditions. This pattern is intrinsically tied to the expedited mitigation of self-filtration within the oedometric stress regime. Indeed, when evaluating a soil's vulnerability to blow-out by quantifying the hydraulic loading necessitated to initiate it, the oedometric configuration emerges as a more conservative approach. Diverging from soil A, the blow-out parameters for soil C manifest notable sensitivity to the applied stress regime, likely due to a more balanced distribution of load and flow control between coarse and fine particle constituents. In agreement with soils A and C, soil B exhibits an intermediate response. Specifically for soil C, a higher degree of fine particle participation in compressive force chains is expected relative to soil B. Moreover, the average constriction size in soil C is presumably smaller than in soil B. This supposition is coherent with the observation that

the magnitude of hydraulic loadings required to surmount local obstructions is elevated for soil C in contrast with soil B, across the spectrum of tested deviatoric stress levels.

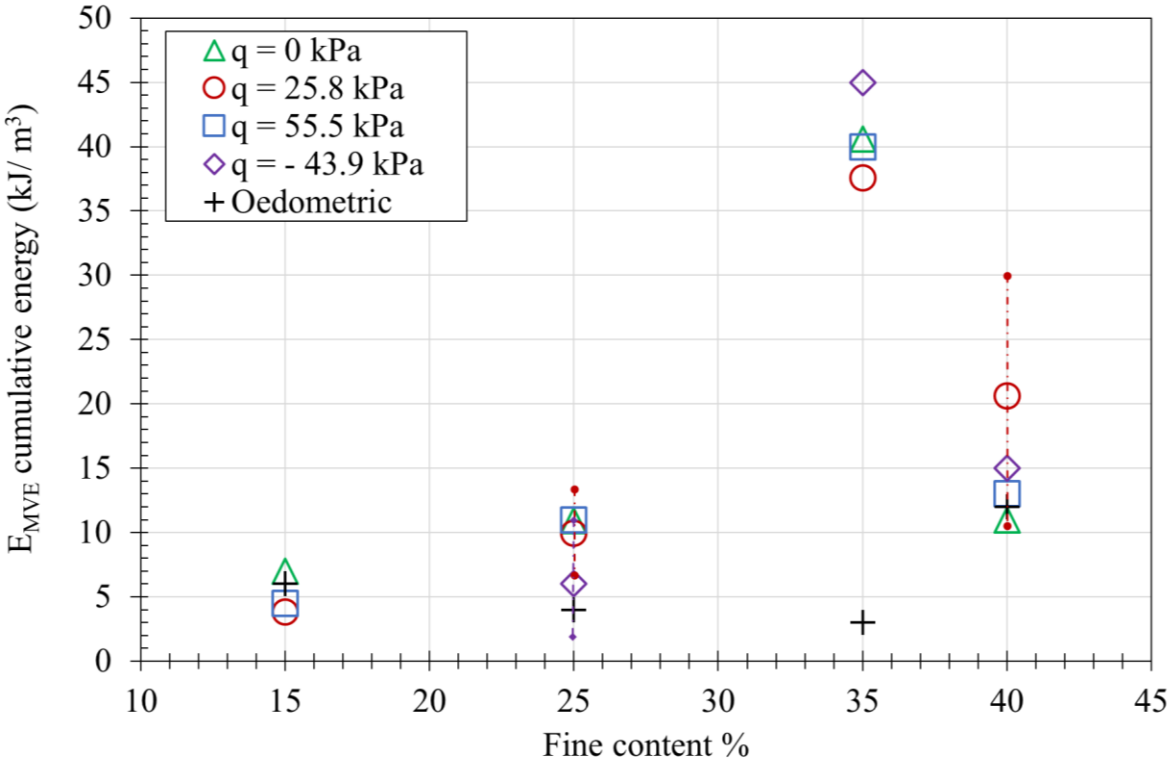

Figure 4.19 Variation in blow-out cumulative energy with the fine content under different stress states

Finally, soil D's susceptibility to stress-induced blow-out sensitivity is comparatively lower than that of soil C. This is due to the overfilled micro-structure of soil D, where finer particles play a more significant role in stress transfer and flow dynamics. Notably, the stress states have a smaller influence on self-filtration dynamics and, consequently, on the hydraulic loading required to mitigate localized clogs.

4.4.4 Effect of the stress state on the steady state

The steady state of suffusion, which is characterized by a stabilization of the hydraulic conductivity accompanied by a diminishing erosion rate, was reached for all the presented specimens to the exception of specimen D_55.5. The inability to elevate the hydraulic gradient beyond 8.0 accounts for this anomaly. This stabilization occurs subsequent to the blow-out event and the application of the hydraulic loading path. To comprehensively characterize this definitive steady state, attention can be directed towards four distinct aspects: (1) the quantification of eroded mass, (2) the measurement of flow dynamics and (3) the combination (1) and (2) assessments. Accordingly, we present the following metrics: the percentage of eroded mass in relation to the initial fine content, the Darcy velocity and the erosion resistance index.

(1) In characterizing the steady state regarding to the eroded mass, our analysis encompasses distinct stages within the suffusion kinetics: the pre-suffusion phase (post sample preparation,

saturation and consolidation), the blow-out onset and the ultimate steady state, as illustrated in Figure 4.20. Our focus lies on the percentage of eroded mass, evaluated within triaxial stress conditions (q = 25.8 kPa) — a specific stress state chosen for the analysis.

Initially, an observable trend emerges where the percentage of eroded mass lost prior to the initiation of the suffusion test displays a positive correlation with the initial fine content. Furthermore, a prominent pattern surfaces: a notable proportion of eroded mass is lost during the blow-out phase. This observation suggests that the blow-out event probably exert a more substantial influence than the suffusion initiation itself. Lastly, it is noted that the final eroded mass percentage also displays a pseudo-linear correlation with the initial fine content proportion. This observation potentially stems from the necessity of eroding a greater quantity of fine particles to establish the preferential flow pathways that characterize the ultimate steady state post-blow-out. The substantial 40% mass loss in soil D, relative to the initial sand mass, contrasts with a modest average 4% decrease in dry density. This result can be explained by acknowledging the joint impact of mass loss and volume variation. Indeed, specimens experience both axial and volumetric contractive strains (Figure 4.24).

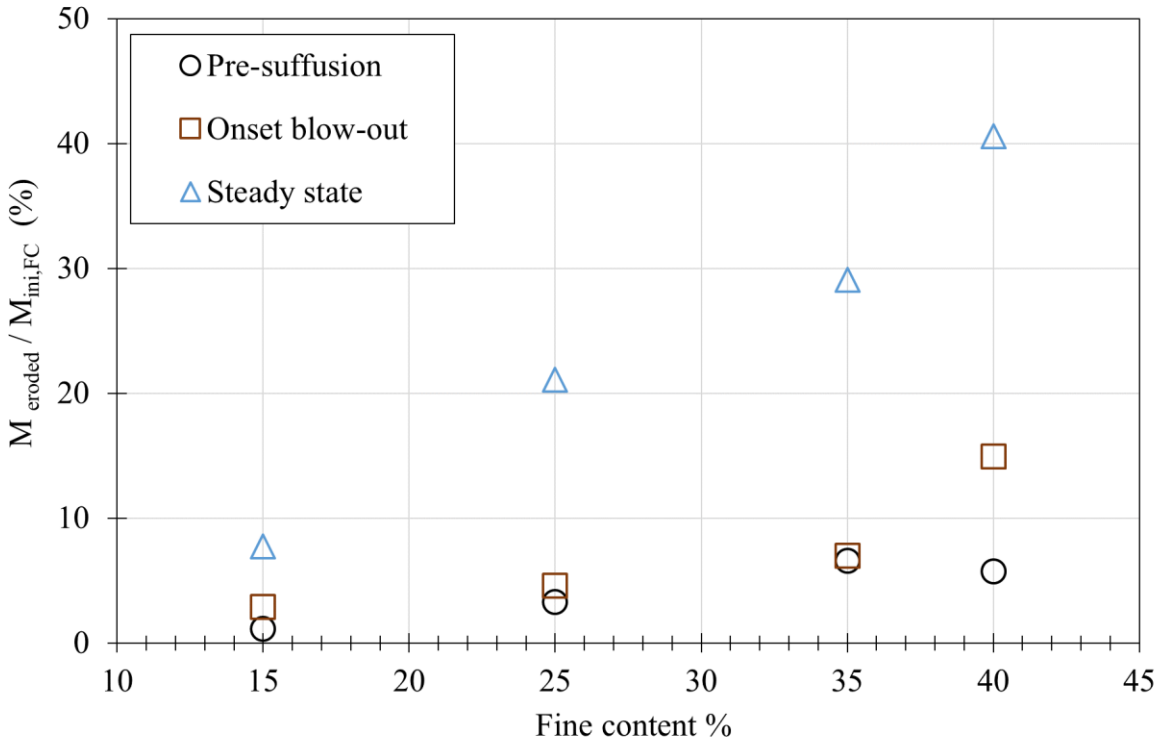

Figure 4.20 Normalized cumulative eroded mass vs. initial fine content under triaxial compression stress (q = 25.8 kPa)

(2) The changes in Darcy velocity over time are shown for different stress conditions and for soils B and C (Figure 4.21). When considering an oedometric stress state, both soils B and C reach a consistent Darcy velocity of approximately 0.4 cm/s. Under all triaxial conditions, soil B reaches a Darcy velocity of about 0.5 cm/s, while soil C experiences a slightly higher steady state velocity of 0.58 cm/s. Notably, the oedometric configuration demonstrates a more conservative behavior in both scenarios, with a steady state difference of 0.11 cm/s for soil B and 0.17 cm/s for soil C. A compelling informative observation arises from the fact that these magnitudes are roughly 50% of

the threshold velocity for the initiation of contact erosion, which stands at 1 cm/s as stated by Beguin et al., (2013). This underlines the significance of this experimental study and highlights the cautious nature of parameters obtained under an oedometric stress state.

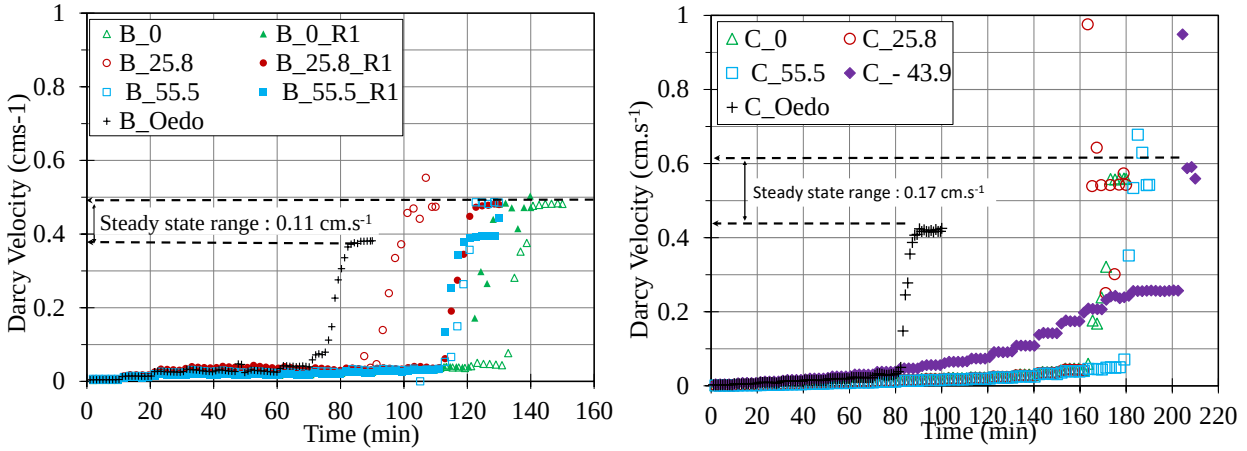

Figure 4.21 Time evolution of Darcy velocity, for soil B [a] and soil C [b]

(3) The characterization of suffusion may be achieved through the energy approach (Marot et al., 2016) that combines the mass eroded due to seepage and the energy expended by this flow. The authors introduce an erosion resistance index I_α that quantifies soil's susceptibility to suffusion (Section 2.2.3). This index was computed out for all tested specimens. Figure 4.22 specifically illustrates this computation for soils B and C, while the details for the other soils are provided in the appendix C. Importantly, the erosion resistance index I_α is always computed at the steady state of suffusion which corresponds to the last point of each tests presented in Figure 4.23.

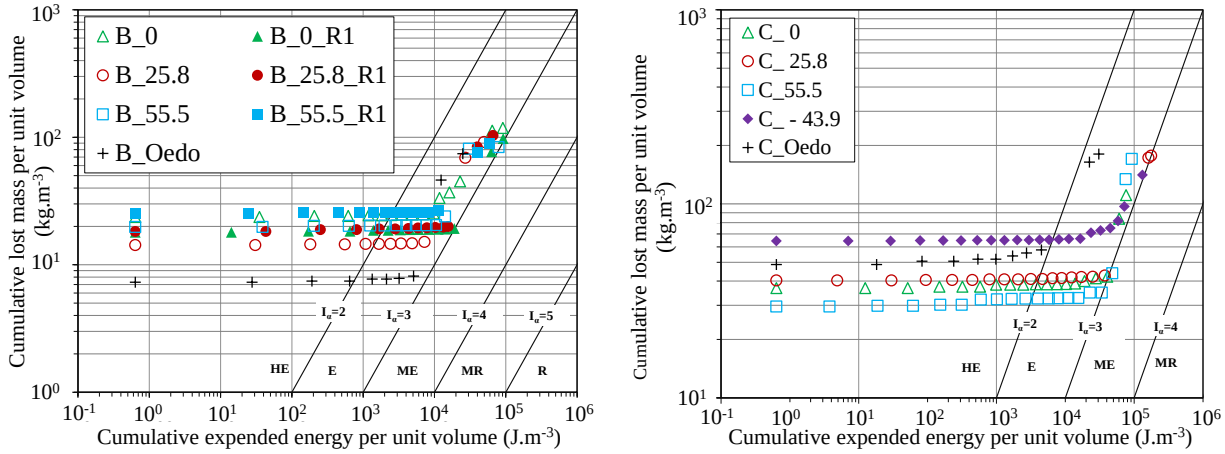

Figure 4.22 Cumulative lost mass versus cumulative expended energy, for soil B [a] and soil C [b]

Figure 4.23 presents the erosion resistance index for all tested soils under different stress conditions. Among the tested soils, stress state appears to have a limited influence on the erosion resistance index. Soils B, C and D are all classified as erodible, falling within the range of $2 \leq I_\alpha < 3$. Soil A demonstrates slightly higher resistance and is moderately erodible, ranging from

$3 \leq I_\alpha < 4$. This difference might stem from a lower intercoarse void ratio and the need for fewer eroded particles to establish preferred flow paths and attain a stable erosion state.

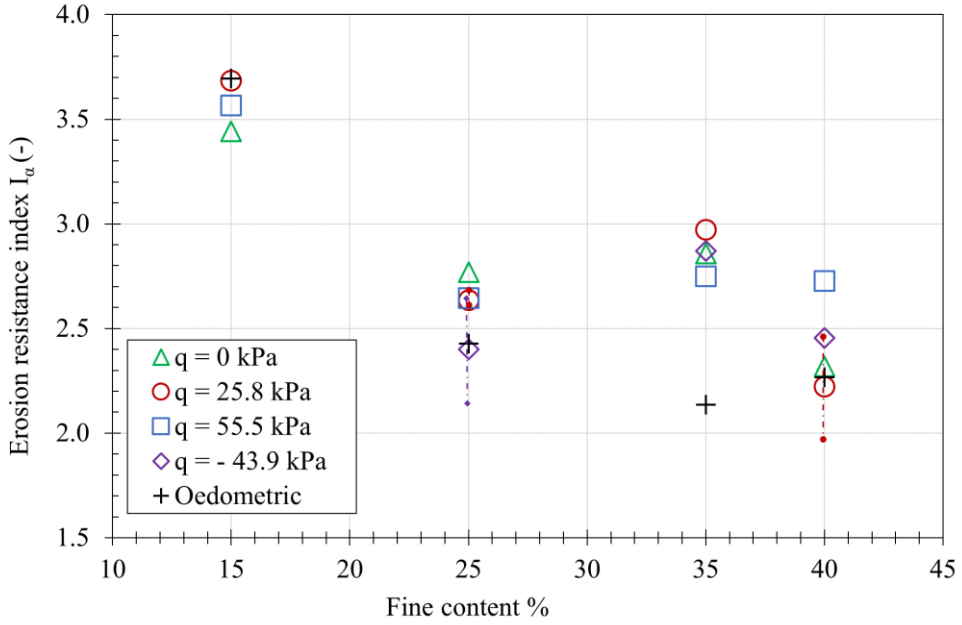

Figure 4.23 Variations in erosion resistance index I_α with the fine content under different stress states

In terms of axial strain behavior, it is noteworthy that soils under underfilled and transitional conditions exhibit minimal changes in axial strain. On the other hand, in cases of overfilled conditions, specimens undergo significant axial deformation, up to 17 %, as depicted in Figure 4.24. This aligns with findings from (Chang and Zhang, 2013a), where axial strains of tests conducted under triaxial stress state ranges with 6 to almost 20%.

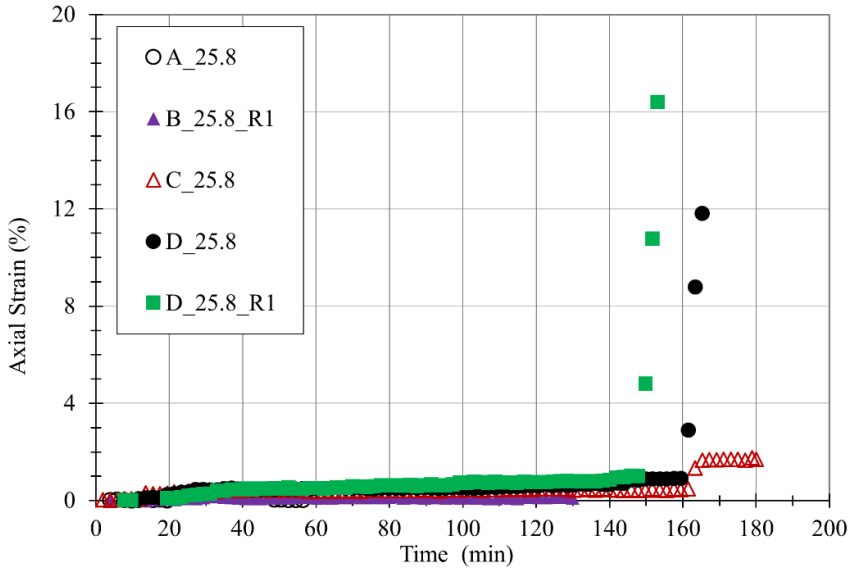

Figure 4.24 Time evolution of the axial strain under a triaxial compression (q = 25.8 kPa) in four different soils

Soil B is chosen to illustrate the effect of the stress state on the post-suffusion microstructure. In particular, the triaxial compression and oedometric stress conditions are compared.

The upstream and downstream post-suffusion slices of the oedometric specimen are shown in Figure 4.25, top. We observe that sand loss mainly concentrates on the outer boundary of the specimen, indicating circumferential preferential flow paths. This observation aligns with X-ray tomography findings by Nguyen et al., (2019). Conversely, when subjected to compression stress states, the flow follows a concentric pattern that eventually leads to a stable state (Figure 4.25, below).

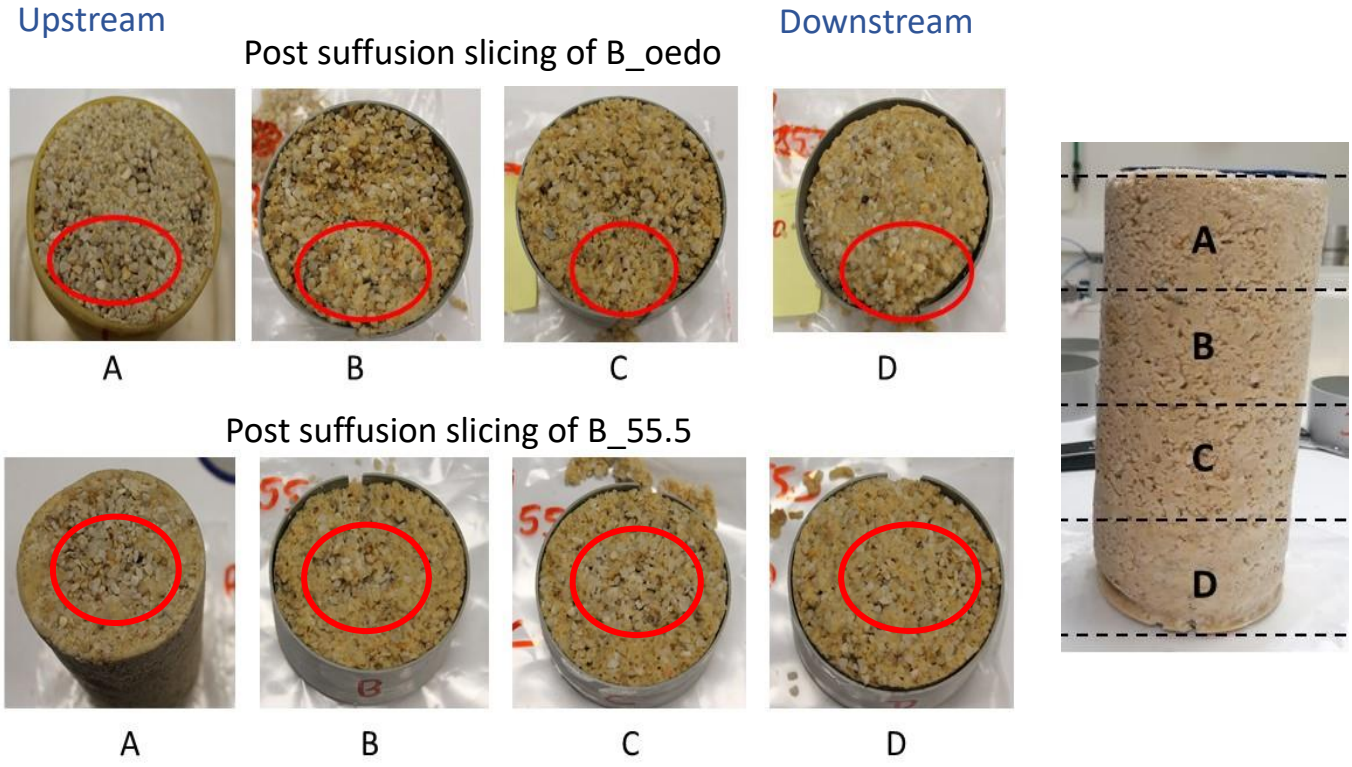

Figure 4.25 Post-suffusion slicing of oedometric stress and triaxial compression stress state specimen

Moving to Figure 4.26, which presents the vertical profile of fine particle percentage after the suffusion process, a clear trend emerges: the overall mass retention decreases from upstream to downstream. However, in the context of oedometric conditions, particle retention is notably higher compared to triaxial compression. This difference can be attributed to the localized erosion occurring along the circumference in the oedometric configuration which tends to limit the total amount of eroded mass.

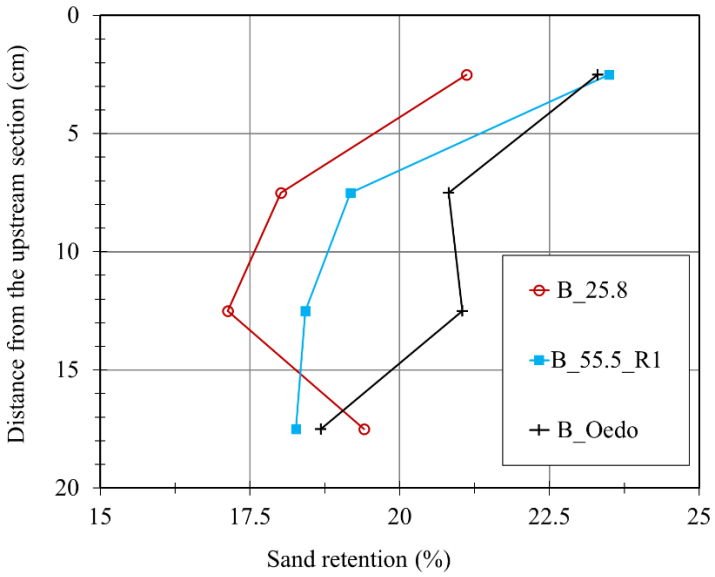

Figure 4.26 Sand retention vertical profile for soil B

4.5 Implication for engineering practices

The practical demands emphasized by (Courivaud, 2023) hold important implications for the landscape of engineering practices. These demands cover crucial domains including the characterization of soil resistance to suffusion (Marot et al., 2016), identification of risk-prone zones within structurally heterogenous zones (Zhang et al., 2019), validation of behavior laws governing suffusion kinetics (Kodieh et al., 2021; Gelet and Marot, 2022) and the estimation of the hydro-mechanical response due to suffusion (Rousseau et al., 2020). In the context of these demands, a set of key observations are now proposed, each contributing to improve both maintenance strategies and the precision of design methodologies applicable to hydraulic structures constructed with earth materials.

1. **Comprehensive testing approach**: Employing both oedometric and triaxial tests covers a wider spectrum of stress states, offering a more complete assessment of the soil's hydro-mechanical behavior. Oedometric tests yield conservative behavior, while under certain triaxial conditions, the impact of the deviatoric stress is limited, particularly when stress states are significantly distant from failure conditions ($0 < q/q_{peak} < 26\%$).

2. **Critical hydraulic gradient**: The applicability of the Skempton and Brogan (1994) critical hydraulic gradient is a limited concept since this threshold could not be measured for all cases. In cases where the self-filtration phase's influence on the hydraulic conductivity is limited, especially in highly underfilled microstructures (Figure 4.10), measuring this gradient becomes challenging. On the other hand, when the self-filtration phase dominates, as observed in overfilled microstructures (Figure 4.11), grasping and quantifying this gradient's significance becomes complex.

3. **Critical Darcy velocity**: The critical velocity prediction proposed by Côté (2010) was found to be greater than the experimentally measured one for all tests (Figure 4.14) which implies that this formula may underestimate the onset of the suffusion phenomenon.

4. **Transition zone sensitivity**: Soils in the transition zone, i.e. in the boundary between underfilled and overfilled states, are more susceptible to the self-filtration phenomenon.

5. **Complex assessment of the erosion resistance**: Quantifying a soil's relative resistance to internal erosion necessitates defining specific criteria based on stakeholders' requirements for each hydraulic structure. Different criteria may yield to different interpretation. For example, underfilled soils may be found quite resistant when focusing on criteria like the eroded mass percentage (Figure 4.20) and the axial deformation (Figure 4.24). Furthermore, if the erosion resistance index (I_α) is chosen as the sole indicator, it reaffirms that highly underfilled soils exhibit the highest resistance (Figure 4.23). Conversely, when attention turns to the hydraulic load required to trigger a blow-out event, overfilled soils emerge as more resilient than their underfilled counterparts (Figure 4.18). These criteria-based interpretations should empower engineers to fine-tune their strategies, optimizing both the design and maintenance approaches for hydraulic structures.

6. **Significance of blow-out events**: The blow-out event, involving a considerably larger loss of eroded mass compared to pre-blow-out losses, holds greater importance than the initiation of suffusion. Consequently, more efforts should be developed in estimating the hydraulic loadings characterizing this threshold.

7. **Parameter scale consideration**: Contextualizing relevant parameters within their measurement scales holds significant importance. A clear illustration of this emerges when we examine Darcy velocity. In laboratory conditions, the Darcy velocity obtained at the steady state is approximately 0.5 cm/s, which interestingly is half the value employed in field settings to characterize the onset of contact erosion at around 1 cm/s (Beguin et al., 2013). This disparity underscores the necessity of appreciating the scale at which parameters are evaluated in practical scenarios.

4.6 Summary

In an effort to advance our understanding of suffusion kinetics under complex stress conditions and the influence of stress states on relevant parameters, a comprehensive experimental program was undertaken involving four distinct soil types. This investigation involved four specific stress states: triaxial isotropic, triaxial compression, triaxial extension and oedometric. Analyzing the results from 25 specimens, several key conclusions can be drawn.

Firstly, to mitigate variations in initial micro-structure and subsequent suffusion behavior, a systematic approach involving controlled hydraulic head adjustments during saturation and loading is recommended. Secondly, the suffusion process unfolds in four distinct phases: initiation, self-filtration, blow-out and steady state. Initiation is characterized by an initial rise in hydraulic conductivity as per Skempton and Brogan (1994). Self-filtration is marked by a reduction of the hydraulic conductivity and the erosion rate. The blow-out entails a simultaneous increase in

hydraulic conductivity and erosion rate, while the steady state of suffusion is reached for a stabilized hydraulic conductivity and a diminishing erosion rate.

Each phase can be characterized by one or more specific parameters. Traditionally, the initiation is represented by the critical hydraulic gradient. The amplitude of the self-filtration is encapsulated by a normalized hydraulic conductivity variation. The blow-out is currently best defined at the turning point of the cumulative mass versus cumulative expended energy curve, by either one of the two following hydraulic loads: the blow-out hydraulic gradient and the blow-out cumulative expended energy. The steady state of suffusion may be characterized by several factors such as the percentage of eroded mass relative to initial mass, the erosion resistance index, the Darcy velocity and the axial strain.

The critical hydraulic gradient is challenging to measure in tensile triaxial conditions, emphasizing our preference for compressive triaxial, isotropic or oedometric stress states. It is noteworthy that the critical hydraulic gradient's sensitivity to stress state is limited across the four soil types investigated.

Furthermore, both the micro-structure categorization (underfilled, overfilled, transitional) and the stress state exert an influence over the self-filtration phase. The orientation of small constriction sizes with respect to flow direction, along with the role of sand grains in stress distribution, impact self-filtration behavior. Most notably, transitional soils exhibit the most pronounced self-filtration amplitudes, reflecting the equilibrium between localized clogging and fine particle detachment. Specific to oedometric conditions, circumferential flow paths shorten self-filtration development.

Moreover, highly underfilled soils demonstrate stress state-insensitive blow-out behavior due to the secondary role of fine particles in force transmission. Conversely, in other soils where both coarse and fine particles contribute to load and seepage control, blow-out parameters are more susceptible to stress state variation. In oedometric conditions, circumferential flow paths mitigate the magnitude of blow-out parameters.

Lastly, the influence of the stress state on the erosion resistance index appears to be constrained across all tested soils. In soils transitioning between micro-structural states, the steady Darcy velocity under oedometric conditions exhibits slightly reduced magnitude compared to triaxial stress states.

Chapter 5

5 Influence of complex hydraulic loadings on the suffusion process

5.1 Introduction and objectives

As detailed in Chapter 2, tests described in literature were performed under various hydraulic conditions: single-staged hydraulic gradients, multi-staged-hydraulic gradients or under constant flow rate. However, there is no clear description of the influence of the hydraulic loading path on the initiation and the development of suffusion. Even with the same type of hydraulic loading (i.e., hydraulic-gradient controlled conditions), Luo et al.,(2013) showed that the suffusion susceptibility seems to be influenced by both the increment of the hydraulic gradient and the duration of each stage. Rochim et al., (2017) also showed that the history of the hydraulic loading can substantially modify the value of the critical hydraulic gradient at which suffusion initiates.

With the objective of following the development of all suffusion phases (detachment, transport and filtration, which in particular depend on the history of the hydraulic loading), tests must be realized by increasing the applied hydraulic gradient, which should be carried on until the stabilization of the hydraulic conductivity (Marot et al., 2016; Rochim et al., 2017; Takahashi 2023). However, it is worth noting that, all aforementioned tests were performed under a constant or an increasing hydraulic loading, while in-situ the hydraulic loading path can be more complex. This complexity can be observed in diverse contexts, where water levels experience significant changes on a daily, seasonal and yearly basis. An illustrative instance lies in pumped storage hydropower systems, where water levels undergo extensive adjustments to meet energy demands.

These cyclic variations in hydraulic load induce fluctuations in the forces acting on the soil particles. During phases of higher hydraulic gradients or velocities, particles are exposed to increased hydraulic forces, making them more susceptible to detachment and transportation. Subsequent phases characterized by lower hydraulic gradients could provide the opportunity for particles to settle or redistribute. These movement and redistribution of particles can lead to the formation of preferential pathways for water flow, thereby amplifying the potential for suffusion mechanisms to initiate and progress. However, despite the potential importance of these cyclic effects, limited investigation has been conducted on the implications of cyclic loading paths. We can mention the recent study of Chen and Zhang (2023), dedicated to the influence of a cyclic hydraulic gradient on a widely graded soil and on a gap graded soil with 35% fine content. Yet, the experimental campaign was realized with an exceptionally high reference hydraulic gradient (i = 9) and an extreme mean hydraulic gradient of i = 41. Critically, these exaggerated loading conditions hold limited practical relevance for embankment dams due to the unrealistic order of magnitude of the initial gradient.

Consequently, the significance of understanding the impact of the cyclic starting point on suffusion process is underscored.

In this context, this study examines the influence of cyclic loading paths on a gap-graded suffusive soil. The specific objectives of the study are:

1. To investigate the influence of the imposed initial hydraulic gradient of the cyclic loading
2. To analyze the impact of the amplitude of applied cyclic loading
3. To assess the influence of the number of loading cycles

5.2 Testing program

The specimen preparation process and methodology remain consistent with the method detailed in Chapter IV. To explore the impact of complex mechanical loading, we used soil B, but unwanted variations in the material obtained from the Sablière Palvadeau quarry in (France) involved the use of a slightly modified gap-graded soil (referred to as B_M), which incorporates a 25% fine fraction as shown in Figure 5.1.

To determine the suitability of the chosen soil gradation, we initially employed geometric criteria, drawing inspiration from established benchmarks such as those proposed by the U.S. Army (1953) and Isotomia (1957). Focusing on the uniformity coefficient (C_u), which plays a key role in these criteria, the selected soil gradation (C_u = 15) demonstrates internal stability, falling below the threshold of 20. Moreover, in accordance with Chang and Zhang (2013)'s criterion, the gradation closely approaches the stability limits. However, when evaluated against the guidelines presented by Kenney and Lau (1985), the selected soil gradation is defined as internal instable.

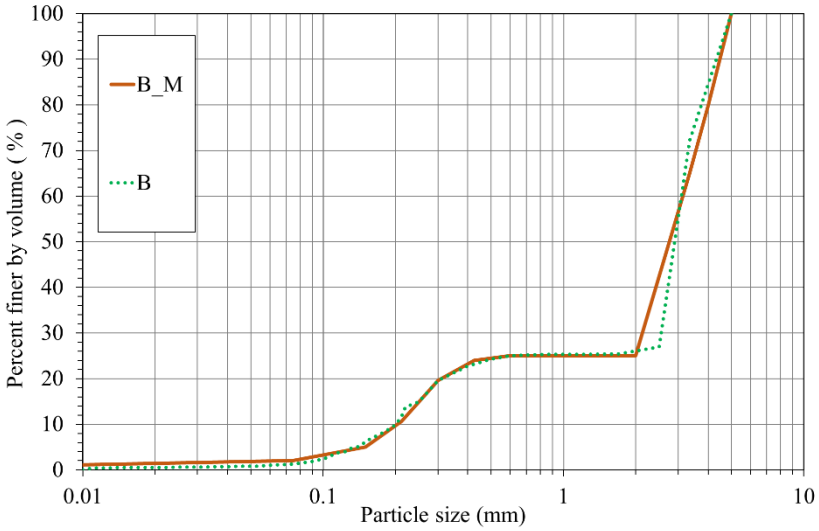

Figure 5.1 Particle size distribution of the tested soils for the studies of the influence of (B_M) complex hydraulic loadings and (B) complex stress states, on the suffusion process

Specimen labelling

The test specimen nomenclature follows a specific format: **Hydraulic loading path_i_0_i_u_number of cycles_ repeatability**. Here is the concise breakdown of each item:

Hydraulic loading path: this indicates the type of hydraulic loading path, categorized as either Multistage hydraulic loading (MHL) or Multistage hydraulic loading followed by a cyclic loading (C). The first type of loading path, i.e. MHL, is viewed as a reference.

i_0: refers to the hydraulic gradient chosen to initiate the cyclic loading (Figure 5.2)

i_u: represents the minimum hydraulic gradient value within the cycle (Figure 5.2)

Number of cycles: denotes the count of cycles applied. This number is equal to 1 or 2

Repeatability: Indicates if the test is a repeatability test.

Proposed hydraulic loading paths

Following the specimen preparation phase, all specimens were first isotropically consolidated to 51.5 kPa; then the targeted deviatoric stress q = 55.5 kPa was maintained, establishing a mean effective stress of p' = 70 kPa. Afterward the suffusion was triggered based on the proposed two hydraulic loading paths as shown in Figure 5.2.

For the first path, the applied multi-stage hydraulic gradient is the same as discussed in chapter IV: it is increased till the specimen reaches the steady state after the development of blow-out event. This test is the reference test to analyze the influence of the cyclic hydraulic loading.

During the 2nd path, first the multi-stage hydraulic gradient is increased up to a value named i_0. This phase is followed by a cyclic hydraulic load. If the blow-out event is not achieved at the end of the cyclic path, then the multistage hydraulic loading path is continued.

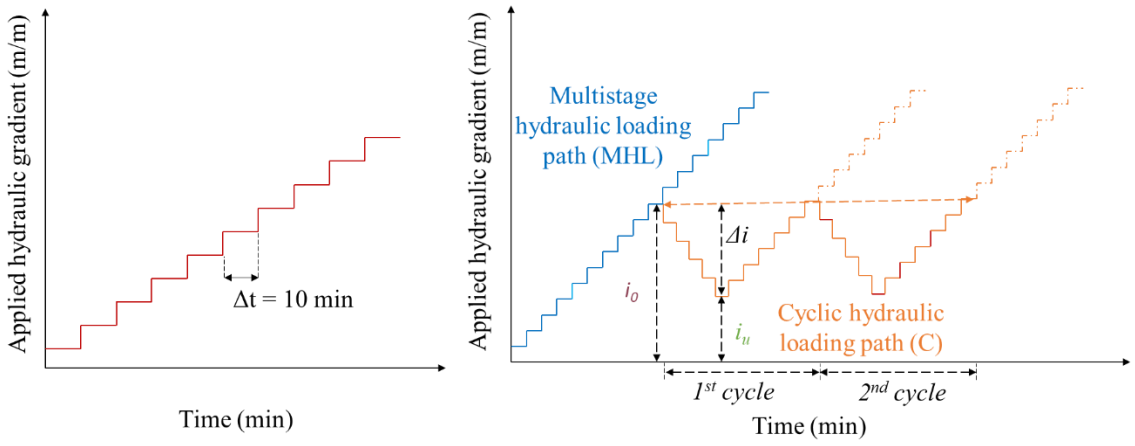

Figure 5.2 (a) Multistage hydraulic loading (b) Cyclic hydraulic loading

The Table 5.1 details for all performed tests, the values of hydraulic gradients: i_0 which corresponds to the initiation of the cyclic path, i_u which is the minimal value applied during the cycle and Δi which is the amplitude of the applied hydraulic gradient during the cycle.

Table 5.1 Summary of test program

Specimen	Hydraulic gradient chosen to initiate the cycle, i_0	Unloaded value of hydraulic gradient, i_u	Amplitude of the cycle $\Delta i = i_0 - i_u$	Testing scheme	Remarks
MHL	-	-	-	Multistage hydraulic loading path (M)	Reference test to characterize the initiation, the development and the steady state of suffusion
C_1.5_0.4_1	1.5	0.4	1.1	Multistage followed by cyclic (C)	To investigate the influence of i_0, amplitude of cyclic loading Δi and the number of cycles
C_2.5_1.4_1	2.5	1.4	1.1		
C_2.5_0.4_1	2.5	0.4	2.1		
C_2.5_1.4_2	2.5	1.4	1.1		
C_4_2.9_1	4	2.9	1.1		
C_4_2.9_2	4	2.9	1.1		
C_5_3.9_1	5	3.9	1.1		
C_5_3.9_1_R3	5	3.9	1.1		

Figure 5.3 and Figure 5.4 show the time evolution of the hydraulic gradients applied on the specimens of soil B_M. Tests with a single cycle have a shorter duration of approximately 330 minutes (C_1.5_0.4_1, C_2.5_1.4_1, C_4_2.9_1, C_5_3.9_1, and C_5_3.9_1_R3), while other tests with double cycles and higher amplitudes have longer durations (C_2.5_0.4_1, C_2.5_1.4_2, and C_4_2.9_2). Data corresponding to the MHL test is included in both figures for easier comparison with the other tests.

In Chapter 4, the suffusion process can be decomposed into (at most) four phases: onset, self-filtration, blow-out and steady state. To characterize the effect of the stress state on each of these phases, several parameters are proposed. In the same way, the influence of complex hydraulic loading paths is first studied while using the same parameters, which are all detailed in Table 5.2.

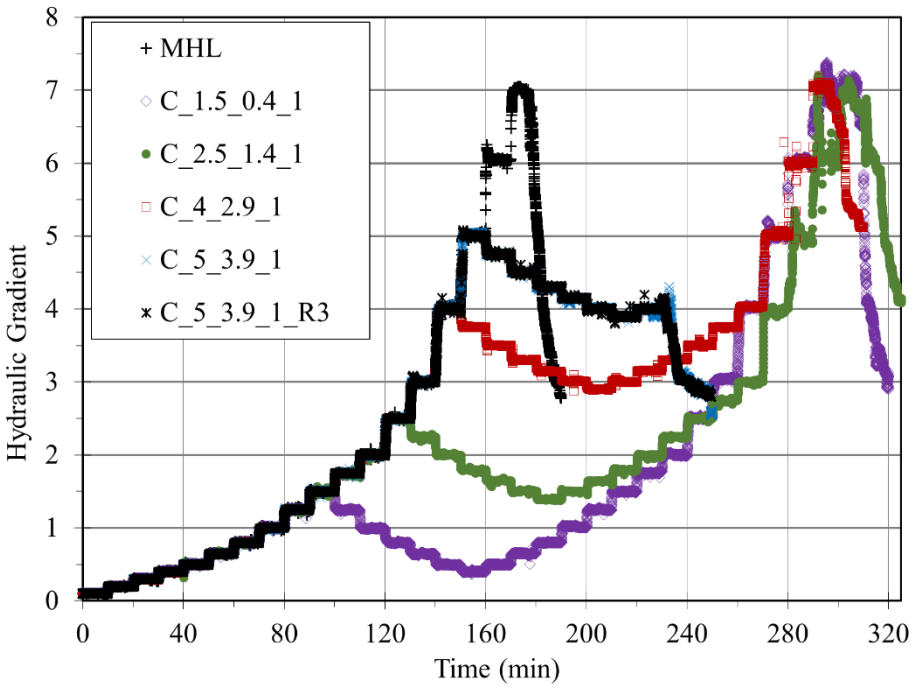

Figure 5.3 Time evolution of the applied hydraulic gradients for tests: MHL, C_1.5_0.4_1, C_2.5_1.4_1, C_4_2.9_1, C_5_3.9_1 and C_5_3.9_1_R3

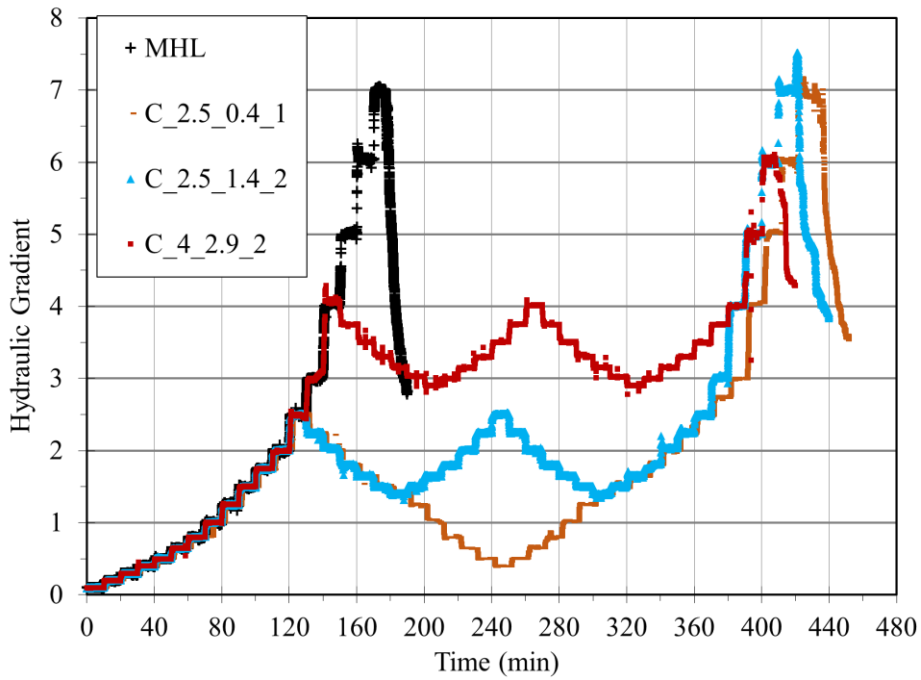

Figure 5.4 Time evolution of the applied hydraulic gradients for tests: MHL, C_2.5_0.4_1, C_2.5_1.4_2 and C_4_2.9_2

Table 5.2 Parameters characterizing the four suffusion phases for all tested specimens

Specimen identity	Onset	Self-filtration	Blow-out characterization								Steady state			
			Strong increase in hydraulic conductivity		1st increase in erosion rate		2nd increase in erosion rate		Turning point of M VS E curve					
	i_{SB}	$\lvert\Delta k_F\rvert / k_{ini}$	i_{HC}	E_{HC}	i_{RE}	E_{RE}	i_{RE2}	E_{RE2}	i_{MVE}	E_{MVE}	$M_{eroded}/M_{ini,FC}$	$v_{F,steady}$	$\lvert\varepsilon_{z,steady}\rvert$	I_α
	(-)	(-)	(-)	(kJ/m^3)	(-)	kJ/m^3)	(-)	(kJ/m^3)	(-)	(kJ/m^3)	(%)	(cm/s)	(%)	SI
MHL	0.1	0.88	7.00	123.89	1.25	7.56	*	*	6.00	108	12.06	0.44	0.06	3.52
C_1.5_0.4_1	0.1	0.90	7.00	143.38	1.75	20.44	*	*	6.00	115	17.71	0.45	0.20	3.40
C_2.5_1.4_1	0.1	0.89	7.00	210.13	1.50	46.63	4	83.52	6.00	152	13.73	0.41	0.06	3.61
C_2.5_0.4_1	0.1	0.91	7.00	220.25	1.40	58.26	*	*	6.00	170	14.47	0.45	0.14	3.71
C_2.5_1.4_2	0.1	0.86	7.50	250.59	1.50	100.09	5	168.31	7.00	251	12.67	0.42	0.18	3.90
C_4_2.9_1	0.1	0.88	7.00	292.72	2.00	19.91	4	224.13	5.00	250	10.50	0.35	0.06	3.98
C_4_2.9_2	0.1	0.86	6.00	384.02	2.00	34.27	5	368.41	3.75	370	14.74	0.46	0.08	3.90
C_5_3.9_1	0.1	0.83	4.00	181.83	3.00	27.84	4	181.83	4.00	175	19.00	0.44	0.12	3.61
C_5_3.9_1_R3	0.1	0.82	4.15	202.44	2.50	28.51	4	182.46	4.00	179	17.32	0.43	0.12	3.67

Notes: i_{SB} = the critical hydraulic gradient corresponding to the first increase of hydraulic conductivity (Skempton and Brogan, 1994); $\lvert\Delta k_F\rvert/k_i$ = normalized relative variation of hydraulic conductivity; i_{HC} = the hydraulic gradient corresponding to the strong increase in hydraulic conductivity as discussed in Chapter 4 (Figure 4.5) and its corresponding cumulative expended energy per unit volume denoted as E_{HC}; i_{RE} = the hydraulic gradient corresponding to the first increase in erosion rate as discussed in Chapter 4 (Figure 4.6) and its corresponding cumulative expended energy per unit volume denoted as E_{RE}; i_{RE2} = the hydraulic gradient corresponding to the second increase in erosion rate and its corresponding cumulative expended energy per unit volume denoted as E_{RE2}; i_{MVE}= the hydraulic gradient corresponding to the turning point of the curve cumulative lost mass per unit volume vs cumulative expended energy per unit volume and its corresponding cumulative expended energy per unit volume denoted E_{MVE}; $M_{eroded}/M_{ini,FC}$ = the percentage of total lost mass with respect to the initial mass of sand; I_α = the erosion resistance index (Marot et al., 2016); $v_{F,steady}$ = the Darcy velocity at the steady state; $\varepsilon_{z,steady}$ = the axial strain at the steady state. * = not observed.

5.3 Influence of the hydraulic gradient chosen to initiate the cyclic loading i_0

To investigate the influence of the cycle starting point i_0, five tests are conducted, including four with different i_0 values (1.5, 2.5, 4 and 5), as well as one repeatability test (see Table 5.2 for details). Throughout the whole experimental program, the stress state is kept constant, allowing us to isolate the specific impact of the cyclic hydraulic loading path. Analyzing these dedicated tests alongside the reference test (MHL) provides valuable insights on the impact of the cycle starting point i_0 on the different suffusion phases.

Figure 5.5 [a] shows the time evolution of the hydraulic conductivity, while Figure 5.5 [b] displays the erosion rate.

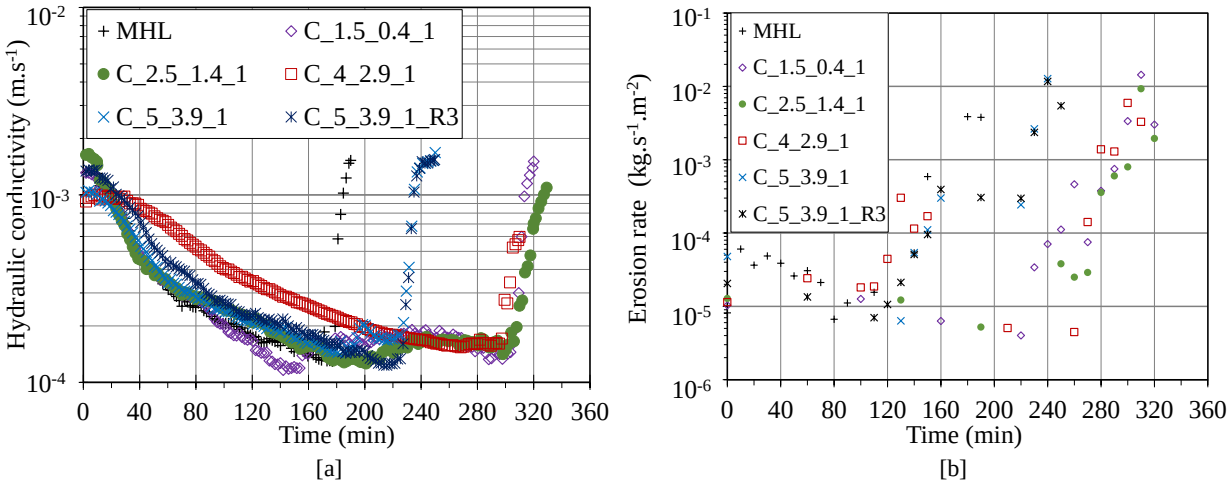

Figure 5.5 Time evolutions of [a] the hydraulic conductivity and [b] the erosion rate, for soil B_M

The cumulative lost mass versus cumulative expended energy for these six tests are illustrated in Figure 5.6.

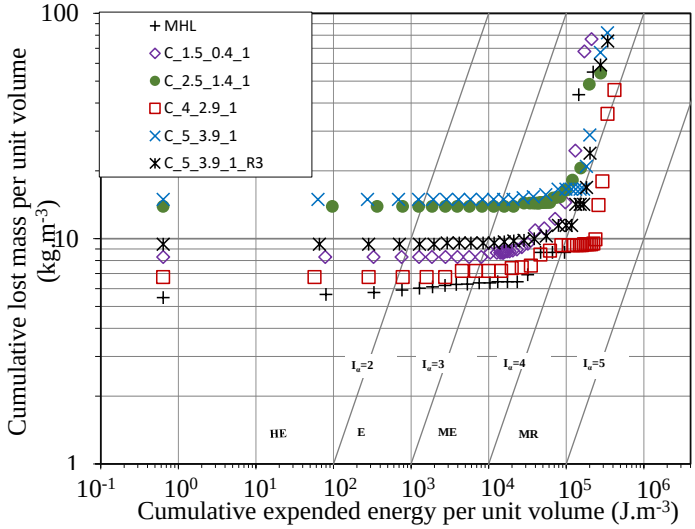

Figure 5.6 Cumulative lost mass versus cumulative expended energy for soil B_M

5.3.1 Influence of i_0 on the onset and self-filtration phases

The study reveals that the initiation phase, marked by a slight increase in hydraulic conductivity, occurs at a critical gradient i_{SB} of 0.1 for both the reference MHL test and all cyclic tests (see Table 5.2). Subsequently, the second phase quantifies the self-filtration for which the MHL test demonstrates a relative variation of hydraulic conductivity of $|\Delta k_F|/ k_{ini} = 0.88$.

The cyclic hydraulic gradient initiation value i_0 influences the self-filtration dynamics within the suffusion mechanism, as shown in Figure 5.7. Lower i_0 values are correlated with an increased $|\Delta k_F|/k_{ini}$, and conversely. The transition of i_0 from 4 to 5 reveals a stronger decrease of the self-filtration behavior. While, i_0 values lower than 4 seems to favor intensified suffusion-driven self-filtration, i_0 values higher than 4 lead to diminish self-filtration before the strong increase in hydraulic conductivity.

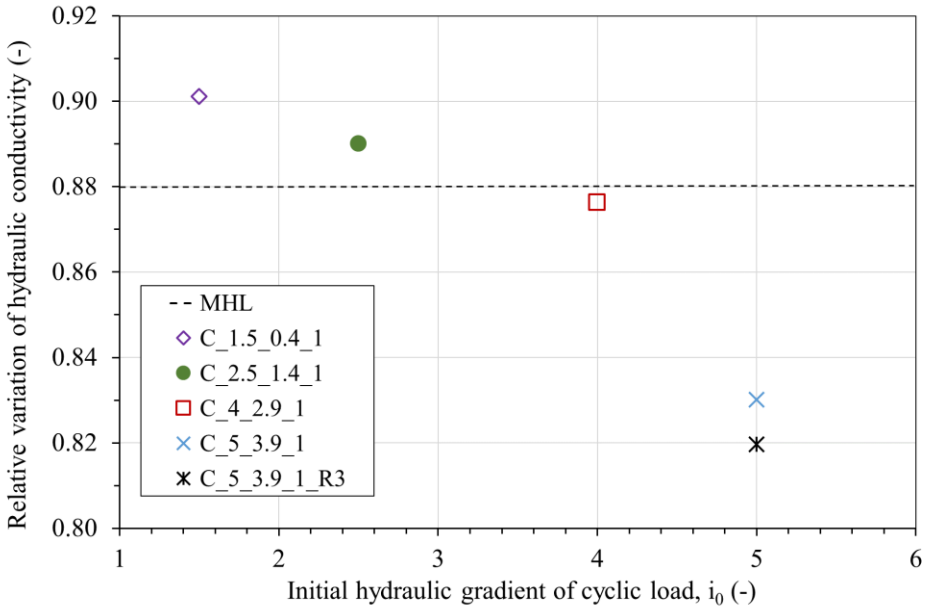

Figure 5.7 Relative variation of hydraulic conductivity $|\Delta k_F|/ k_i$ versus hydraulic gradient chosen to initiate the cyclic loading i_0.

5.3.2 Influence of i_0 on the blow-out phase

The blow-out phase is distinctly marked by substantial increases in both hydraulic conductivity and erosion rate. It can also be identified by the turning point on the cumulative mass versus cumulative expended energy curve. For the reference test MHL, the blow-out occurs at $i_{HC} = 7$, $i_{RE} = 1.25$ and $i_{MVE} = 6$.

Unfortunately, the acquisition frequency of the erosion rate doesn't permit to clearly identify its first increase for tests C_1.5_0.4_1 and C_2.5_1.4_1 (see Figure 5.5 [b]). For the other tests, this first increase of erosion rate appears simultaneous with that of the test MHL. At the end of cyclic load, a second increase of the erosion rate can be observed similarly to the first one. This second erosion rate increase occurs much earlier for tests C_5_3.9_1 and C_5_3.9_1_R3, however the Figure 5.8 permits to note that this second erosion rate increase is triggered for all tests under the same hydraulic gradient ($i_{RE2} = 4$).

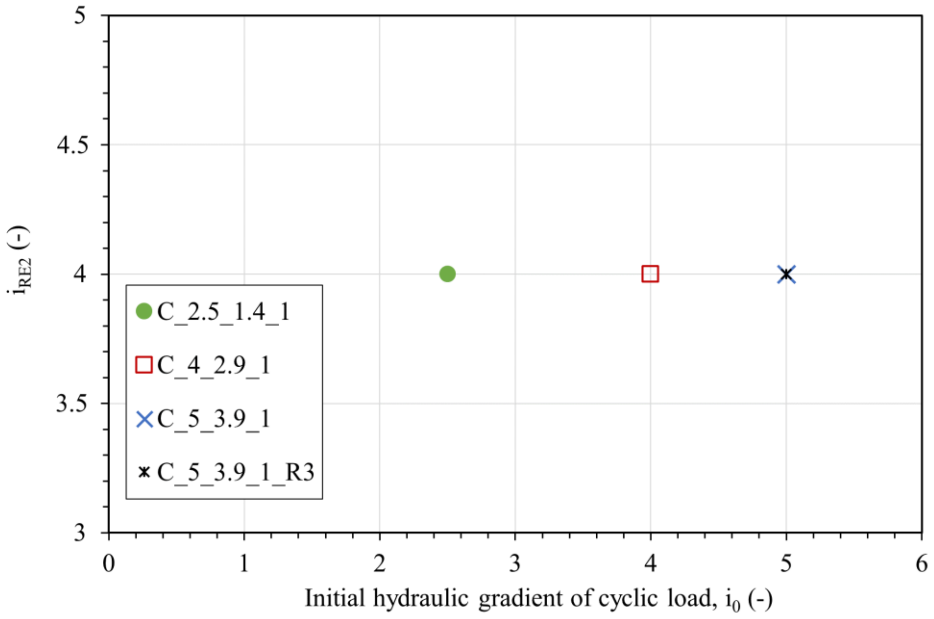

Figure 5.8 Blow-out hydraulic gradient i_{RE2} versus the hydraulic gradient chosen to initiate the cyclic loading i_0

The critical hydraulic gradients, corresponding to the strong increase in hydraulic gradient i_{HC}, have been documented in Table 5.2 for all tests conducted under cyclic hydraulic loading conditions. Notably, it is important to emphasize that with i_0 values of 1.5, 2.5 and 4, i_{HC} is equal to 7, i.e. the same value as for test MHL (see Figure 5.9). In contrast, for tests C_5_3.9_1 and C_5_3.9_1_R3, i_{HC} is lower, i.e. around 4. This observation underscores the influence of the initiation of the cyclic loading on the soil's resistance to the blow-out event. When i_0 is lower than 5, the influence of the cycle appears limited, whereas when i_0 equals to 5, the cycle seems to favor preferential flow paths which could result in a significant increase in hydraulic conductivity and in turn a decrease of i_{HC}.

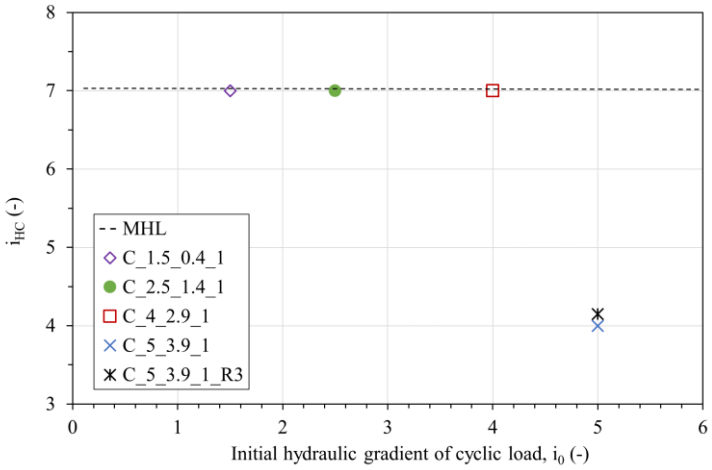

Figure 5.9 Blow-out hydraulic gradient i_{HC} versus the hydraulic gradient chosen to initiate the cyclic loading i_0

In Appendix D, the hydraulic gradient i_{MVE} and the corresponding energy E_{MVE} are plotted as a function of the initial hydraulic gradient of the cyclic load.

Figure 5.10 shows the erosion rate as a function of the applied hydraulic gradient. For hydraulic gradients lower than 1.5, the erosion rate decreases by a factor of 10. For larger values of hydraulic gradient, the erosion rate increases quite linearly with the hydraulic gradient and its final values lie between $3*10^{-3}$ and 10^{-2} $kg.s^{-1}.m^{-2}$. However, in the case of test C_4_2.9_1, it can be noted that for a given value of hydraulic gradient between 3 and 4, the corresponding rate of erosion can vary by a factor of 20. Moreover, this factor can reach 100 for tests C_5_3.9_1 and C_5_3.9_1_R3.

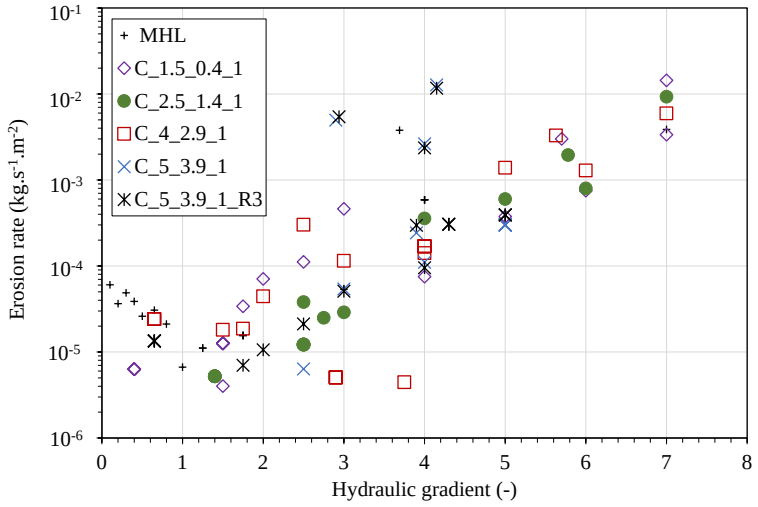

Figure 5.10 Erosion rate versus applied hydraulic gradient (Tests: MHL, C_1.5_0.4_1, C_2.5_1.4_1, C_4_2.9_1, C_5_3.9_1 and C_5_3.9_1_R3)

Now, by considering the power expended by the flow, it is possible to limit this discrepancy as shown by Figure 5.11.

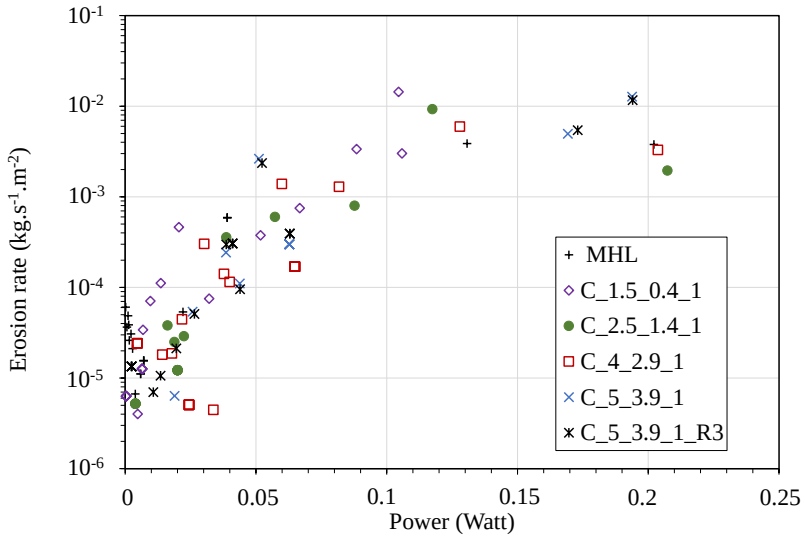

Figure 5.11 Erosion rate versus flow power (Tests: MHL, C_1.5_0.4_1, C_2.5_1.4_1, C_4_2.9_1, C_5_3.9_1 and C_5_3.9_1_R3)

Nevertheless, if we consider the tests C_4_2.9_1, C_5_3.9_1 and C_5_3.9_1_R3, for a power around 0.07 W, the rate of erosion can vary by a factor of 10. Furthermore, when the power exceeds 0.13 W, the erosion rate is slightly decreasing, except for tests C_5_3.9_1 and C_5_3.9_1_R3.

In Figure 5.6, or more clearly in Figure 5.12 [a] and Figure 5.12 [b] (in these figures, both axes are in linear scale) it is possible to note that in the case of test C_4_2.9_1, the rough increase of cumulative lost mass starts for a larger expended energy in comparison with other tests (i.e. 2.4 *10^5 J.m^{-3} for test C_4_2.9_1 and between 10^5 and 1.8 *10^5 J.m^{-3} for other tests)

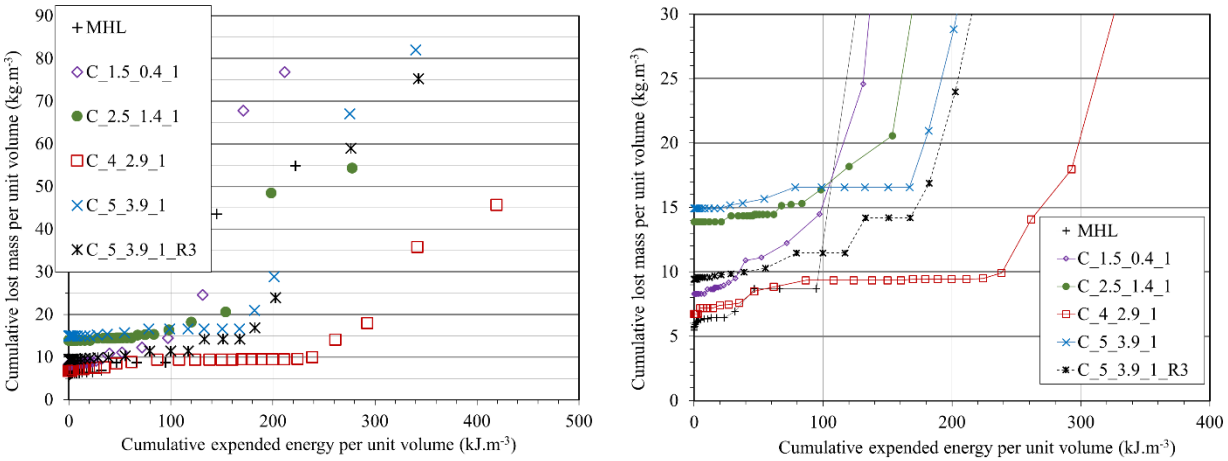

[a] [b]

Figure 5.12 Cumulative lost mass per unit volume versus cumulative expended energy per unit volume, [a] full linear scales, [b] lost mass per unit volume lower than 30 kg.m^{-3} and expended energy lower than 400 kJ.m^{-3}

With the objective to improve our understanding of the previous observation, the cumulative lost mass per unit volume is represented as a function of: applied hydraulic gradient in Figure 5.13 [a] and power in Figure 5.13 [b].

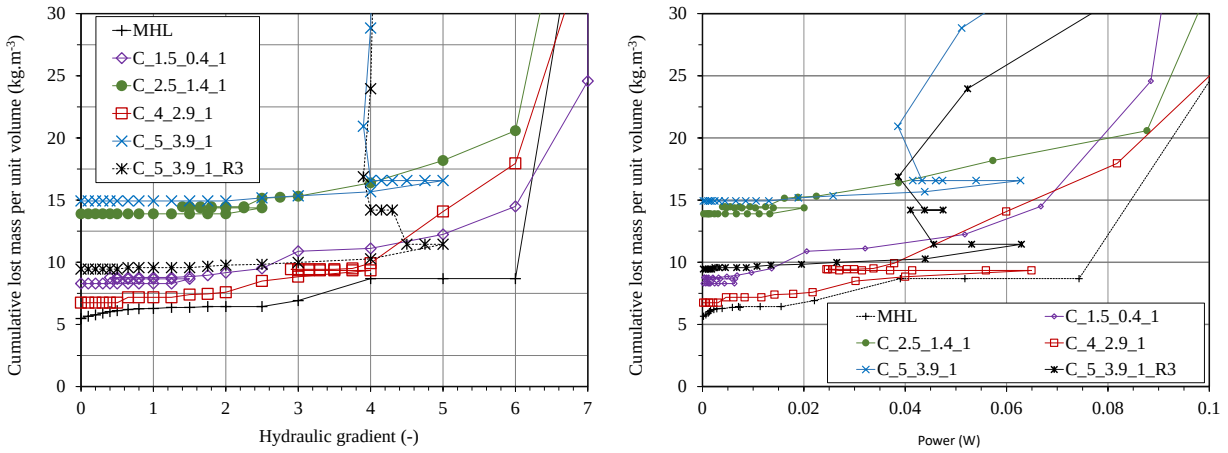

[a] [b]

Figure 5.13 Cumulative lost mass per unit volume versus: [a] applied hydraulic gradient, [b] power expended by the flow

Thanks to these figures, it is possible to distinguish two different behaviors: for tests MHL, C_1.5_0.4_1 and C_2.5_1.4_1, on the one hand and for tests C_4_2.9_1, C_5_3.9_1 and C_5_3.9_1_R3, on the other hand.

- For tests MHL, C_1.5_0.4_1 and C_2.5_1.4_1, the increase of cumulative lost mass per unit volume is more intense when the applied hydraulic gradient exceeds 2.5. The corresponding power is between 1.35 $*10^{-2}$ W (test C_1.5_0.4_1) and 1.89 $*10^{-2}$ W (test C_2.5_1.4_1). It is worth noting that the cumulative lost mass only increases, when the hydraulic load becomes more intense. In other terms, no increase of cumulative lost mass is measured during the decreasing phase of cyclic hydraulic loading.
- For test C_4_2.9_1, a small increase of cumulative lost mass is measured during the decreasing phase (when the hydraulic gradient is decreased from 4 to 3 and the corresponding power from 6.5 $*10^{-2}$ W to 2.7 $*10^{-2}$ W). This increment of cumulative lost mass is more obvious during tests C_5_3.9_1 and C_5_3.9_1_R3 (when the hydraulic gradient is decreased from 5 to 4 and the power from 6.3 $*10^{-2}$ W to 3.9 $*10^{-2}$ W).

Figure 5.13[a] shows that under a hydraulic gradient larger than 4, the growth of cumulative lost mass has globally the same order of magnitude for tests MHL, C_1.5_0.4_1, C_2.5_1.4_1 and C_4_2.9_1. Whereas for tests C_5_3.9_1 and C_5_3.9_1_R3, under the hydraulic gradient equals to 4, the cumulative lost mass strongly increases. By considering Figure 5.13[b], it is possible to note that after reaching 6.5 $*10^{-2}$ W, if the power decreases until reaching 2.5 $*10^{-2}$ W (i.e. test C_4_2.9_1), the growth of cumulative lost mass has globally the same order of magnitude as for tests MHL, C_1.5_0.4_1, C_2.5_1.4_1. Yet if the power is only decreasing from 6.5 $*10^{-2}$ W to 4 $*10^{-2}$ W, the cumulative lost mass strongly increases.

All these observations suggest that if i_0 is smaller or equal to 4, the effect of single cycle appears limited on the cumulative lost mass. However, if i_0 is larger than 4, the cumulative lost can increase even during the decreasing phase of the cyclic hydraulic load. Now, the computation of the power permits to highlight the effect of the decreasing phase of the cyclic hydraulic load. For the three tests C_4_2.9_1, C_5_3.9_1 and C_5_3.9_1_R3, the decreasing phase starts from 6.5 $*10^{-2}$ W. But in tests C_5_3.9_1 and C_5_3.9_1_R3, this phase is limited to 4 $*10^{-2}$ W and the growth of lost mass is much more intense than in the case of test C_4_2.9_1 (i.e. with a minimal power during the cycle equals to 2.5 $*10^{-2}$ W).

Finally, by drawing a parallel between the soil behavior under a mechanical load and a hydraulic load, we can observe a kind of "plasticity effect" or "hydraulically-induced-damage". In other terms, the suffusion resistance of a soil could progressively deteriorate if the cyclic load overpasses a given threshold and this process seems to also depend on the decreasing phase.

5.3.3 Influence of i_0 on the steady state phase

For the MHL test, the steady state results in the erosion of approximately 12% of the initial fine content, with the Darcy velocity $v_{F,steady}$ stabilizing at around 0.44 cm/s and a negligible axial

deformation of 0.12%. Furthermore, the erosion resistance index I_α is equal to 3.52 which leads to the classification of a moderately erodible soil ($3 < I_\alpha < 4$).

The comparison of cyclic test results with those of the MHL test shows that the axial deformation is negligible for all cyclic tests (axial strain generally lower than 0.2%, see Figure 5.14[a]). Figure 5.14 [b] shows that the steady state Darcy velocity $v_{F,\text{steady}}$ is in the same order of magnitude (between 0.41 and 0.45 cm/s), except for test C_4_2.9_1 with $v_{F,\text{steady}}$ equals to 0.31 cm/s. Test C_4_2.9_1 is also distinguished by a value of erosion resistance index equals to 3.98, which is the greatest value obtained for all cyclic tests (see Figure 5.15). So, based on the results of this test, the soil appears slightly more resistant, with a sensibility classification very closed to moderately resistant (see Figure 5.6).

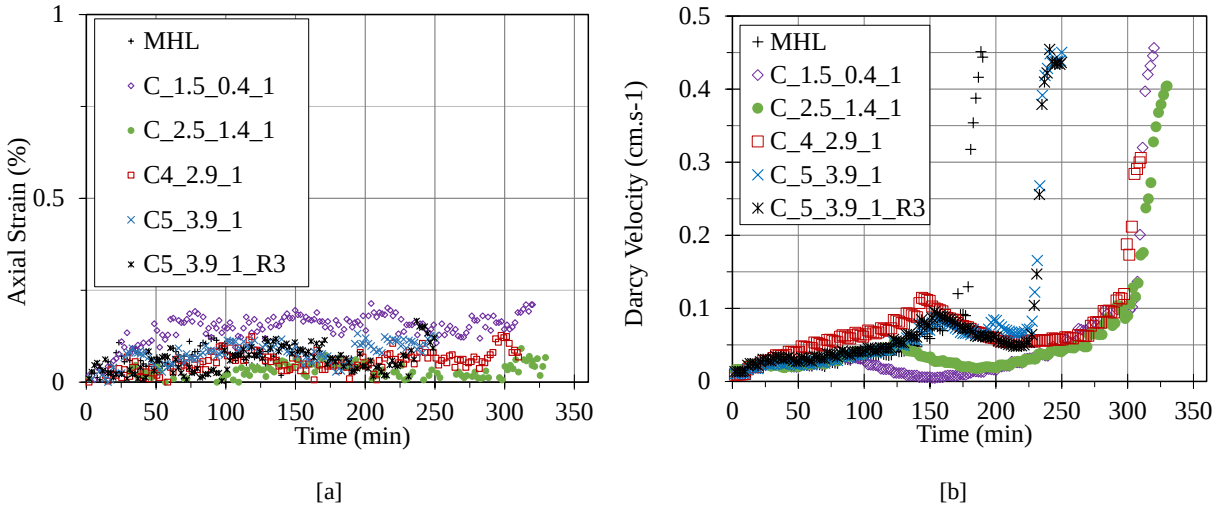

Figure 5.14 Time evolution of: [a]axial strain and [b] Darcy velocity

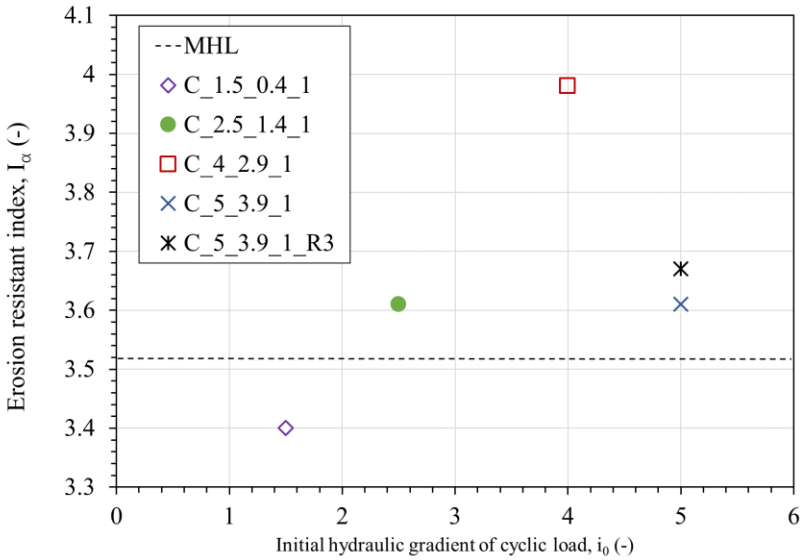

Figure 5.15 Erosion resistance index versus the hydraulic gradient chosen to initiate the cyclic loading i_0

Consequently, the soil's resistance based on the test MHL results appears slightly underestimated in comparison with results of test C_4_2.9_1.

By considering the time evolution of hydraulic conductivity (see Figure 5.5 [a]) (or even under a same hydraulic gradient by considering the Darcy velocity, see Figure 5.14 [b]) it can be noted that the steady state characterized by a constant hydraulic conductivity is not reached at the end of tests C_1.5_0.4_1 and C_2.5_1.4_1. In conclusion for these two tests, the value of I_α is probably underestimated.

5.4 Influence of the cycle amplitude Δi on the suffusion process

Test C_2.5_0.4_1 was performed with an amplitude of the cyclic load of Δi = 2.1. A comparative analysis is conducted with its counterpart, the C_2.5_1.4_1 test, characterized by a smaller amplitude of Δi = 1.1.
It can be noted in Table 5.2 that the values of i_{HC}, i_{RE}, i_{MVE} and their corresponding energy values (E_{HC}, E_{RE} and E_{MVE}), remain remarkably consistent, despite the variation in amplitude from Δi = 1.1 to Δi = 2.1. The difference in relative variation of hydraulic conductivity $|\Delta k_F|/k_i$ is also limited: 1.46 $*10^{-3}$ (test C_2.5_1.4_1) and 1.24 $*10^{-3}$ (test C_2.5_0.4_1).

For both tests, the erosion rate is plotted as a function of hydraulic gradient in Figure 5.16 and as a function of power in Figure 5.17.

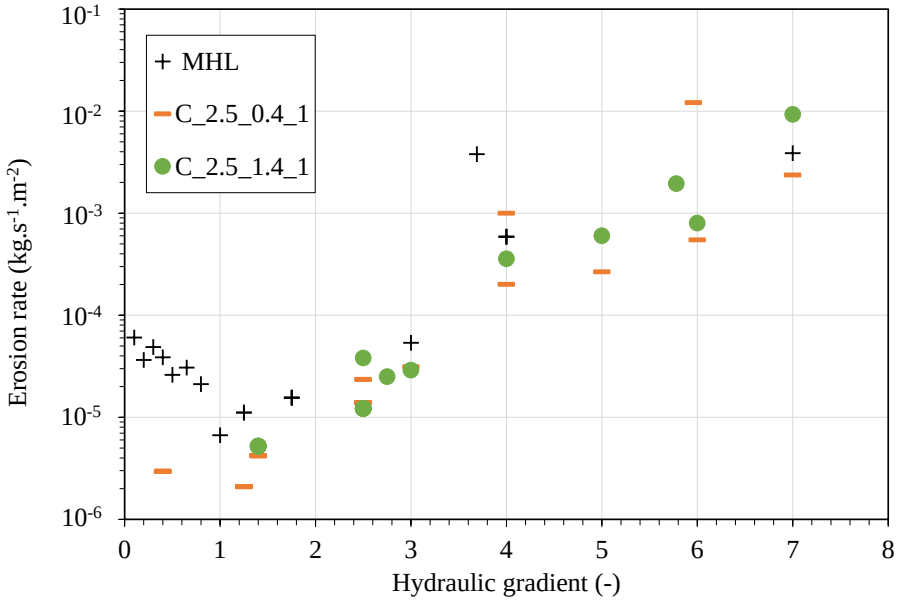

Figure 5.16 Erosion rate versus hydraulic gradient, for two amplitudes of Δi

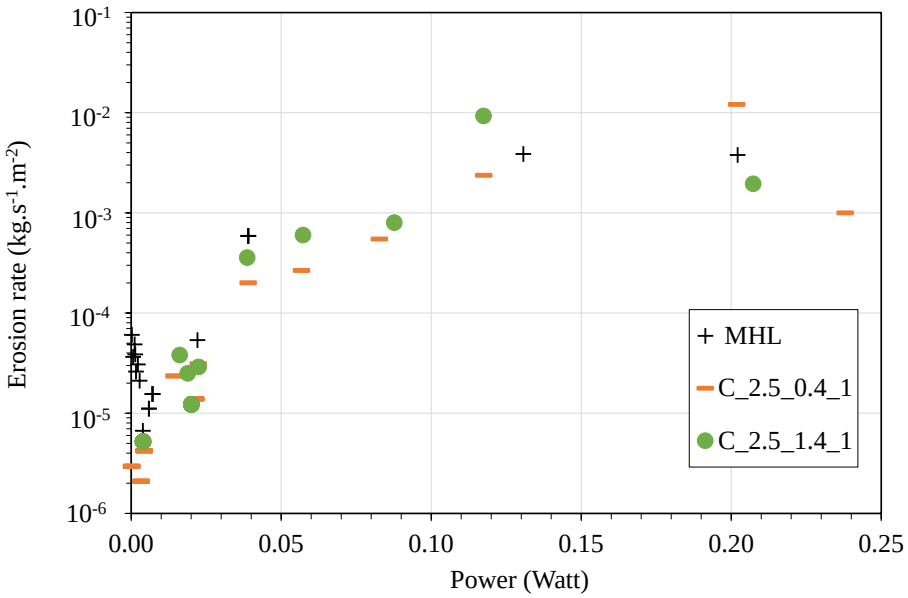

Figure 5.17 Erosion rate versus power, for two amplitudes of Δi

Thanks to these figures, it is possible to note that the influence of cycle amplitude is low and this conclusion is corroborated by the Figure 5.18, which represents the cumulative lost mass per unit volume versus the cumulative expended energy per unit volume.

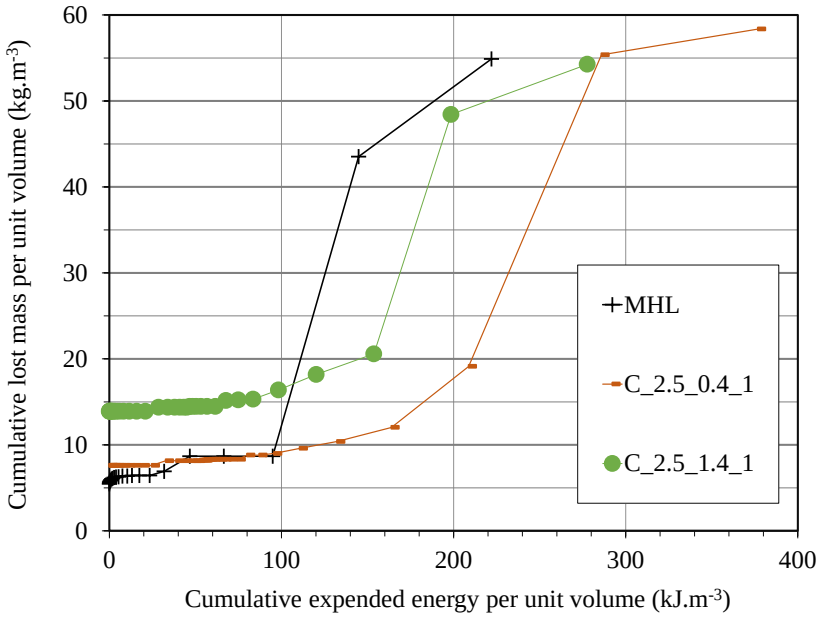

Figure 5.18 Cumulative lost mass per unit volume versus cumulative expended energy per unit volume, for two amplitudes of Δi

5.5 Influence of the number of cycles on the suffusion process

The experimental setup imposed certain limitations, notably a maximum of only two cycles due to the constraints of the experiment's duration. To explore this topic further, two double cyclic hydraulic loading paths were selected, maintaining the same amplitude ($\Delta i = 1.1$) while varying the initial hydraulic gradient of the cyclic loading, specifically at $i_0 = 2.5$ and 4. These dedicated tests are denoted as C_2.5_1.4_2 and C_4_2.9_2, respectively. The influence of the double cycle is studied by plotting the erosion rate as a function of the hydraulic gradient for tests C_2.5_1.4_1 and C_2.5_1.4_2 (see Figure 5.19 [a]) on the one hand and for tests C_4_2.9_1 and C_4_2.9_2 (see Figure 5.19 [b]) on the other hand. Moreover the erosion rate is plotted versus the power in Figure 5.20 [a] for tests C_2.5_1.4_1 and C_2.5_1.4_2 and in Figure 5.20 [b] for tests C_4_2.9_1 and C_4_2.9_2. For both tests with a double cycle, the fluctuation is slightly amplified, however the general trend is the same and the influence of the double cycle appears to be limited. The double cyclic influence is also small on the filtration phase as exhibited by the low discrepancy between values of $|\Delta k_F|/k_i$, i.e. 1.46 $*10^{-3}$ and 1.26 $*10^{-3}$ for tests C_2.5_1.4_1 & C_2.5_1.4_2 and 8.26 $*10^{-4}$ and 8.79 $*10^{-4}$ for tests C_4_2.9_1 & C_4_2.9_2, respectively (see Table 5.2).

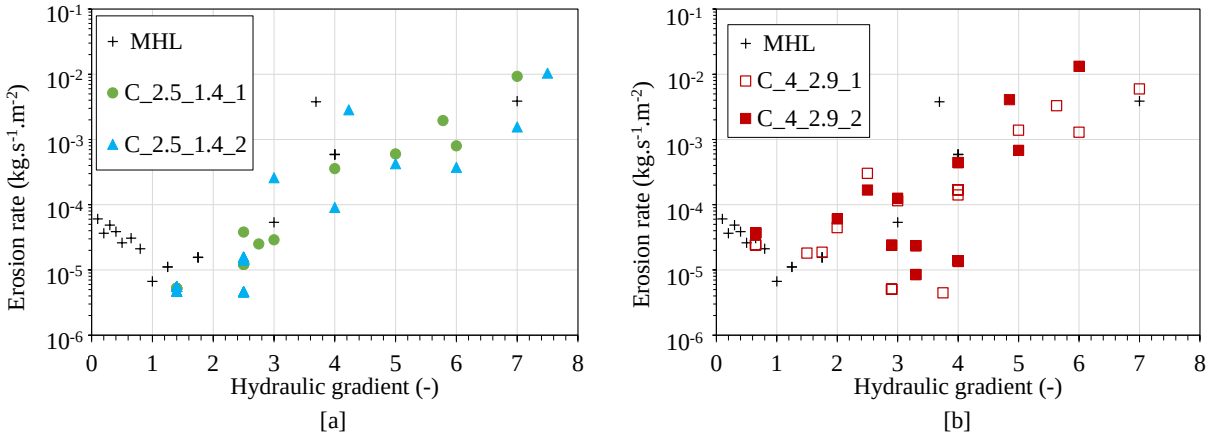

Figure 5.19 Erosion rate versus hydraulic gradient, for one and two of cycles, with i_0 equals to [a] 2.5 and [b] 4

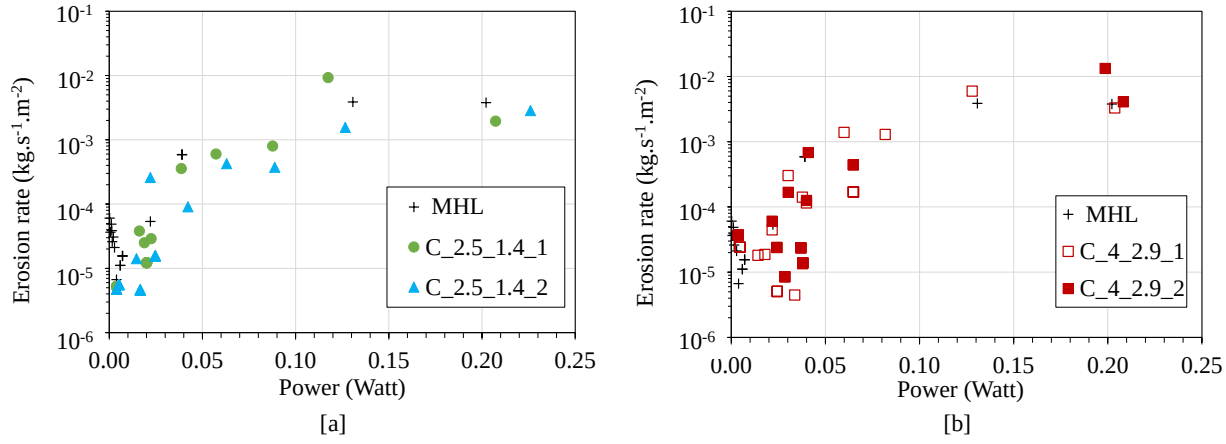

Figure 5.20 Erosion rate versus power, for one and two cycles, with i_0 equals to [a] 2.5 and [b] 4

Figure 5.21 [a] and Figure 5.21 [b] shows the cumulative lost mass per unit volume versus the cumulative expended energy per unit volume, for pair tests C_2.5_1.4_1 & C_2.5_1.4_2 and C_4_2.9_1 & C_4_2.9_2, respectively. Only few differences are observed and the global trend is the same. Logically, the cumulative expended energy is greater for tests with two cycles than for tests with one cycle since these tests last for a longer time and the power expended by the flow remains at the same order of the magnitude. Furthermore, it can be noted that the difference in values of the erosion resistance index I_α is very limited: 0.08 for tests C_2.5_1.4_1 & C_2.5_1.4_1 and 0.29 for tests C_4_2.9_1 & C_4_2.9_2 (Table 5.2 details the values of I_α).

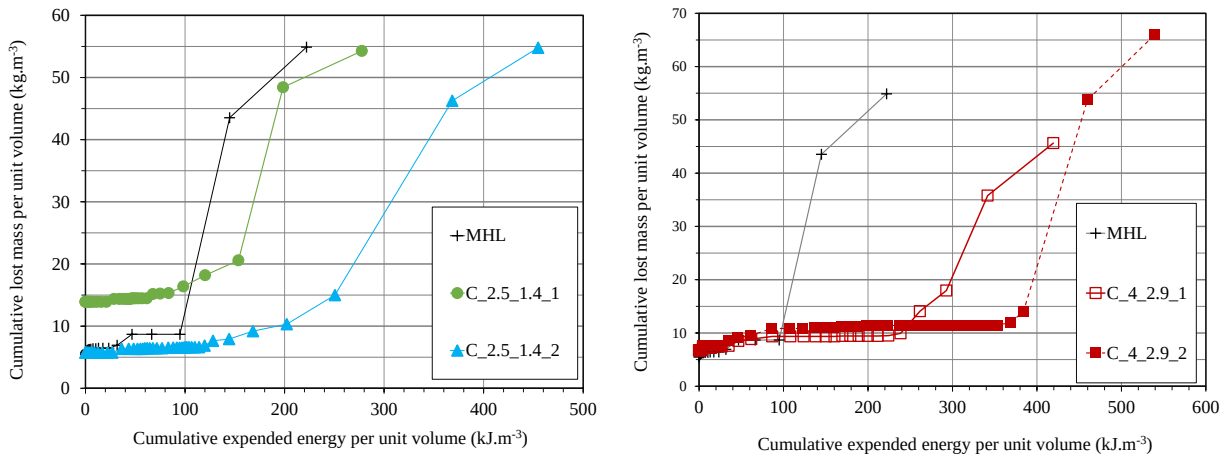

Figure 5.21 Cumulative lost mass versus cumulative expended energy per unit volume, for one and two cycles, with i_0 equals to [a] 2.5 and [b] 4

5.6 Synthesis and implication for engineering practices

This chapter is dedicated to the study of the influence of complex cyclic hydraulic loading patterns. The specific objectives of this study are comprising the investigation of the initial hydraulic gradient of the cycle, the amplitude of the cycle and the number of loading cycles. The suffusion erodibility of one gap graded cohesionless soil was characterized by performing: one test under multi staged hydraulic gradient and eight tests under various cyclic hydraulic loading paths. The comparative analysis of all obtained results permits to draw the following conclusions:

1. For an initial hydraulic gradient of the cycle i_0 = 2.5 and the tested range of **cycle amplitudes** (Δi = 1.1 and 2.1), this latter parameter does not significantly affect the four phases of suffusion (initiation, self-filtration, blow-out and steady state).

2. In this study, the **number of cycles** is equal to one or two. For two different initial hydraulic gradient values, the test results show that the number of cycles has a limited influence on the suffusion process.

3. Four different **initial hydraulic gradient** values, i_0 = 1.5, 2.5, 4, or 5, were used in the study. The results reveal that for the tested soil, when i_0 is smaller than or equal to 4, the influence of one or two cycles on the suffusion process is limited. However, if the cycle starts with i_0 greater than 4, an increase in cumulative lost mass per unit volume is observed, even during the decreasing phase of the cycle. It is worth noting that, even if the maximum power reached before the decreasing phase of the cycle remains the same (i.e., $6.5 * 10^{-2}$ W), the growth of lost mass depends on the minimum power reached. Specifically, if the minimum power during the cycle, $P_{min} = 2.5 * 10^{-2}$ W, the increase in lost mass is of the same order of magnitude as in other tests but much more significant if $P_{min} = 4 * 10^{-2}$ W.

4. Particular attention should be given to the approach based on critical hydraulic gradients, i_{HC} and i_{MVE}. i_{HC} represents the point of a strong increase in hydraulic conductivity, while i_{MVE} corresponds to the turning point on the cumulative lost mass per unit volume vs. cumulative expended energy per unit volume curve. Notably, for cyclic tests with i_0 = 5, their values are lower compared to those of the MHL test, which is conducted under multi staged hydraulic gradients and without cycles. In other words, this interpretative method suggests that the soil exhibits greater resistance in the results of the MHL test.

5. The erosion resistance index is slightly lower for the MHL test compared to cyclic tests. As a result, the suffusion susceptibility classification based on the MHL test is slightly more conservative.

Conclusions and Perspectives

Conclusions

This chapter presents the key findings and insights drawn from the research conducted in this PhD thesis. The research was primarily centered around the development of a modified triaxial apparatus and the investigation of two related subjects: (i) the influence of the stress state, on one hand and (ii) the impact of complex hydraulic loadings, on the other hand, on the initiation and the development of suffusion.

The modified triaxial apparatus was designed to provide precise control over hydraulic and mechanical conditions during experiments. Key modifications were made to the triaxial chamber's top cap and base pedestal, enabling controlled water inflow and soil particle collection during experiments. The apparatus allows an independent control of compressive or tensile deviatoric stress, including automated saturation, consolidation, erosion and post-suffusion analysis. The instrumentation system, featuring pressure transducers and sensors ensured reliable data acquisition. Validation tests confirmed the apparatus's reliability and accuracy, making it a valuable tool for the study of suffusion behavior under stress-controlled and hydraulic loading path-controlled conditions.

The investigations focused on gap-graded cohesionless soils, which are significant in the construction of embankment dams and dikes but are susceptible to suffusion. To this end, four binary mixtures were carefully prepared, consisting of well-graded fine sand (designated as P-S1) and uniformly-graded coarse gravel (referred to as P-G3), sourced from the Sablière Palvadeau quarry in France. Four distinct gap-graded mixtures (with the fine sand contents of 15%, 25%, 35% and 40%) were subjected to a comprehensive analysis to understand the initiation and progression of the suffusion phenomenon. These investigations were conducted under various stress states: oedometric, triaxial isotropic, triaxial compressive (with the principal stress in the vertical direction) and triaxial tensile (with the principal stress in the horizontal direction). Furthermore, a significant attention was devoted to ensure the repeatability of the experimental procedure, which was validated by comparing the temporal evolution of the hydraulic conductivity, the erosion rate, the cumulative lost mass and the cumulative expended energy.

Throughout this work, a systematic approach was rigorously employed to comprehensively characterize the diverse phases of the suffusion process, grounded in the temporal evolution of the hydraulic conductivity and the erosion rate. These phases are referred to as initiation, self-filtration, blow-out and steady state. The initiation of suffusion is identified thanks to a slight but marked increase of the hydraulic conductivity (Skempton and Brogan, 1994). Subsequently, the second phase prominently features a phenomenon of self-filtration, supported by the reduction in erosion rate which may be concomitant with a reduction of the hydraulic conductivity. The self-filtration amplitude is synthesized by the normalized hydraulic conductivity variation. The third phase manifests as a distinct surge in the erosion rate, which may be followed by a marked increase in hydraulic conductivity. Termed the "blow-out" event, this phase is primarily attributed to the detachment and transportation of solid particles. The blow-out is best defined at the turning point

of the cumulative mass versus the cumulative expended energy curve to favor a global approach. In the fourth and final phase, the hydraulic conductivity converges towards stability, while the erosion rate experiences a diminishing trend. This behavior can be explained by the presence of one or more preferential flow pathways created by the erosion process, ultimately culminating in a state of equilibrium. This "steady state" of suffusion can be characterized by several relevant parameters such as the final vertical deformation, the erosion resistance index, the Darcy velocity and the percentage of lost mass.

The methodology outlined by Skempton and Brogan (1994) for analyzing the initiation hydraulic gradient i_{SB} across various test conditions was employed. Specifically, in some tests conducted under isotropic or compressive deviatoric stress states, a unique initiation hydraulic gradient of 0.2 was observed, which indicates that the critical hydraulic gradient i_{SB} is probably little influenced by the stress state. However, under a tensile stress state, the initiation as defined by Skempton and Brogan (1994) could not be observed. Under this stress state, the downward vertical flow aims to establish vertically elongated pores. Yet the applied stresses favor horizontal principle force chains and horizontally elongated pores that counteract the effect of the flow. This competition tends to favor local heterogeneities and hence an increased variability of the suffusion kinetics. Having this in mind, compressive triaxial, isotropic or oedometric stress states should be favored to measure onset related parameters (critical hydraulic gradients or critical Darcy velocities).

Also, this research highlighted the combined influence of both the micro-structure (underfilled, in transition or overfilled) and the stress state on both the self-filtration and the blow-out phases. It was observed that self-filtration is hindered when either the gravels or the sand grains bear a large portion of the stress, i.e. for highly underfilled or highly overfilled soils. On the other hand, transitional soils were found to exhibit large self-filtration amplitudes which is attributed to a competition between clogging and fine particle detachment. Noteworthy differences emerged when comparing tests conducted under oedometric and compressive triaxial stress states. Consistently, the self-filtration phase is shorter in the oedometric configuration, enabling an earlier blow-out event and thereby indicating the conservative behavior of this stress state. A detailed analysis of post-suffusion grain size distributions and cross-sectional slices revealed that oedometric stress conditions promote circumferential preferential flow pathways, resulting in a shortened timeframe to reach the blow-out. As explained above, under a tensile stress state, the variability of the suffusion kinetics increases and the blow-out initiates for a rather large variety of hydraulic loadings. Specific to highly underfilled soils, the initiation of the blow-out is not influenced by the stress state due to the secondary role played by the fine particles in the force chains.

The influence of stress state on the steady state of suffusion was explored, revealing a limited sensitivity across all tested soils in front of the influence of the microstructure. In soils transitioning between micro-structural states, slight reductions in the steady Darcy velocity under oedometric conditions were observed compared to triaxial stress states.

The comprehensive investigation of the influence of complex cyclic hydraulic loadings on the suffusion process has yielded valuable insights for engineering practices. One significant finding is the key role played by the cyclic loading initiation point i_0 that significantly influences the blow-out when the hydraulic load used for the cycle (expressed in gradient or in power) exceeds a

threshold (i_0 = 4). When i_0 is lower than this threshold, the impact of the cycle on the overall behavior is small in comparison with a reference multi-stage hydraulic loading. Conversely, as the hydraulic load exceeds this threshold during the cycle, a damage-like behavior is observed, i.e. the blow-out is triggered for a smaller hydraulic load than the reference test.

The exploratory study of the influence of the loading amplitude Δi revealed that the two tested amplitudes (1.1 to 2.1) did not exert a substantial influence on the blow-out event nor on the overall suffusion behavior. Furthermore, the influence of the number of loading cycles (1 or 2) on the overall suffusion phenomenon and on the related parameters appears also limited.

Perspectives

This thesis report investigates the impact of complex stress states on the initiation and the development of suffusion on several unstable gap-graded soils, shedding light on a critical aspect often overlooked in existing research. The scientific community primarily compares the mechanical behavior of non-eroded soil samples with their eroded counterparts, disregarding the degree of erosion inherent to these materials (Chang and Zhang, 2011; Chang et al., 2014; Ke and Takahashi, 2014a, 2014b, 2015; Mehdizadeh et al., 2017; Mehdizadeh, 2018). A key consideration in this context is the establishment of parameters to characterize each phase of the suffusion process, thereby improving post-suffusion mechanical comparison for various degrees of suffusion. Also, the post-suffusion homogeneity of each specimen should be characterized before performing a post-suffusion mechanical test since both the degree of suffusion and the degree of homogeneity may affect the post-suffusion mechanical behavior.

Up to date, no standards exists regarding the choice of the outlet grid or screen that is placed at the downstream end of the specimen. Often, this opening is selected to allow the detachment of the finer particles and to retain the coarser ones. Yet, on site, many representative elementary volumes (REV) are located in the body of the hydraulic structure and are subjected to a much finer outlet opening, i.e. the REV that is just downstream of the one at hand. Hence, suffusion should probably be analyzed for a representative range of outlet openings that could be computed from the mean constriction size (Seblany et al., 2021) . In addition, great care should be taken when maintaining this opening during post-suffusion mechanical characterization, as an increase of deviatoric stress may cause part of the specimen to extrude through this grid.

Also, future investigations should focus on the analysis of suffusion related parameters that need to be challenged with respect to the size of the specimen, the hydraulic loading path and the flow orientation with respect to gravity. In other words, the intrinsic character of these parameters should be assessed, or at least their range of validity should be clearly specified. Such investigations would allow a more informed usage of these parameters in behavior laws (Kodieh et al., 2021; Gelet and Marot, 2022).

So far, repeatability tests are seldom performed and are often mainly used to check the validity of a given experimental procedure. Yet, repeatability tests can also be used to measure the amount of variation or dispersion of a set of parameters. For the parameters that will be found to be intrinsic or reliable for a given range of boundary conditions, it would be informative to perform many

repeatability tests to better assess the dispersion of these parameters, in particular the standard deviation with respect to the mean. This type of information would improve our interpretations on the influence of the stress state on suffusion related parameters.

The scientific community would benefit from proposing a standardization for suffusion tests. Such standards would allow (i) a better comparison between several studies, (ii) a rigorous commissioning of new apparatuses and (iii) could serve as reference for validating constitutive laws. Currently, there is a lack of universally accepted standards in this regard. For example, if no eroded mass is collected, the erosion resistance index cannot be obtained. The main objective of such research endeavors would be to actively participate in and contribute to the creation of an international benchmark for suffusion testing. This benchmark would serve to define a consistent and rigorous procedure for conducting suffusion tests. Upon these benchmark tests, the raw data could be published in open access and several interpreting methods could be proposed (Marot and Bowman, 2022).

Regarding the influence of cyclic hydraulic loading paths on the suffusion overall behavior, the obtained results remain exploratory so that a large variety of configurations remain to be explored. For example, the obtained results need to be confirmed for other percentages of fines and other stress states. Also, the memory effect related to the greatest hydraulic load applied to the specimen (expressed in hydraulic gradient or in power dissipated by the flow) needs to confirmed by additional tests. Last but not least, our laboratory tests are often realized within a few hours whereas, on site, soils may be subjected to floods over several days. Hence, the validity of our observations should be confirmed by performing long-term tests.

By focusing on these research objectives, future studies can significantly advance our understanding of the suffusion process and contribute to the development of standardized procedures to enhance the consistency and reliability of suffusion testing protocols. These perspectives collectively aim to enhance the rigor and consistency of research in this domain, ultimately yielding more reliable and comprehensive insights into the coupled hydro-mechanical behavior of suffusive soil.

List of publications

Paper submitted to International Journals

Marot, D., Oli, B., Gelet, R., Bendahmane, F., 2023. A hydraulic Loading path controlled and stress-controlled Erosion Apparatus for assessing soil Internal Erosion. *Geotechnical Testing Journal. (Submitted)*

Oli, B., Gelet, R., Marot, D., Bendahmane, F., Coubard, G., 2023. Characterizing the initiation and the development of internal erosion under complex stress states. *Acta Geotechnica. (Submitted)*

Paper published in International conference proceedings

Oli, B. (2023). Suffusion under different stress states. Presented at the Congrès Français du Génie Civil, *Academic Journal of Civil Engineering*, Paris-Saclay, France, May 23-25.

Oral presentation in International conferences

Oli, B. (2022). Suffusion under different stress states for one gap graded soil. Presented at the *28th European Working Group on Internal Erosion in Embankment Dams, Levees and Dikes and their Foundations*, Sheffield, United Kingdom, July 18-21.

Oli, B., Marot, D., Gelet, R., & Bendahmane, F. (2023). Stress-state-controlled and hydraulic-loading-controlled suffusion test. Presented at the *29th European Working Group on Internal Erosion in Embankment Dams, Levees and Dikes and their foundations*, Lyon, France, July 3-5.

Paper in preparation to International Journals

Oli, B., Marot, D., Gelet, R., & Bendahmane, F. (2023). Understanding suffusive soil response to cyclic hydraulic loading paths in stress-induced environments. XXX, (In preparation).

Bibliography

Åberg, B. (1993) ‘Washout of Grains from Filtered Sand and Gravel Materials’, *Journal of Geotechnical Engineering*, 119(1), pp. 36–53.

Ahlinhan, M.F. and Achmus, M. (2010) ‘Experimental Investigation of Critical Hydraulic Gradients for Unstable Soils’, in *Scour and Erosion. International Conference on Scour and Erosion (ICSE-5) 2010*, San Francisco, California, United States: American Society of Civil Engineers, pp. 599–608.

Ahlinhan, M.F. and Achmus, Martin (2010) ‘Experimental investigation of critical hydraulic gradients for unstable soils’, in *Scour and erosion*, pp. 599–608.

Ataii, S. and Fannin, J. (2022) ‘A Triaxial Permeameter to Study the Mechanical Consequences of Internal Erosion’.

Beguin, R. *et al.* (2012) ‘Contact erosion between two soils’, in *Erosion of Geomaterials, Bonelli S. (ed.), Wiley/ISTE, Londres, 2012*. ISTE/Wiley, pp. 115–154.

Beguin, R., Philippe, P. and Faure, Y.-H. (2013) ‘Pore-Scale Flow Measurements at the Interface between a Sandy Layer and a Model Porous Medium: Application to Statistical Modeling of Contact Erosion’, *Journal of Hydraulic Engineering*, 139(1), pp. 1–11.

Bendahmane, F., Marot, D. and Alexis, A. (2008) ‘Experimental Parametric Study of Suffusion and Backward Erosion’, *Journal of Geotechnical and Geoenvironmental Engineering*, 134(1), pp. 57–67.

Bishop, A.W.T. and Donald, I.B. (1961) ‘Experimental study of partly saturated soil in the triaxial apparatus’, in *Proc. 5th International Conference on Soil Mechanics and Foundation Engineering, Paris, 1961*. Paris, Dunod, pp. 13–21.

Bonelli, S. (2012) *Erosion of geomaterials*. John Wiley & Sons.

Bonelli, S. (ed.) (2013) *Erosion in geomechanics applied to dams and levees*. 1. publ. London: ISTE (Civil engineering and geomechanics series).

Bradshaw, A.S. and Baxter, C. (2007) ‘Sample Preparation of Silts for Liquefaction Testing’, *Geotechnical Testing Journal*, 30, pp. 1–9.

Brown, A. and Gosden, J. (2008) ‘Defra research into internal erosion’, in. *Ensuring reservoir safety into the future: Proceedings of the 15th Conference of the British Dam Society at the University of Warwick from 10–13 September 2008*, Thomas Telford Publishing, pp. 39–50.

Burenkova, V.V. (1993) ‘Assessment of suffusion in non-cohesive and graded soils’, *Filters in geotechnical and hydraulic engineering. Balkema, Rotterdam*, pp. 357–360.

Carraro, J.A.H. and Prezzi, M. (2008) ‘A new slurry-based method of preparation of specimens of sand containing fines’, *Geotechnical Testing Journal*, 31(1), p. 467.

Chang, D. and Zhang, L. (2011) 'A Stress-controlled Erosion Apparatus for Studying Internal Erosion in Soils', *Geotechnical Testing Journal*, 34(6), pp. 579–589.

Chang, Dongsheng and Zhang, L. (2011) 'A stress-controlled erosion apparatus for studying internal erosion in soils', *Geotechnical Testing Journal*, 34(6), pp. 579–589.

Chang, D., Zhang, L. and Cheuk, J. (2014) 'Mechanical consequences of internal soil erosion', *HKIE Transactions*, 21(4), pp. 198–208.

Chang, D.S., Zhang, L. and Xu, T.H. (2012) 'Laboratory investigation of initiation and development of internal erosion in soils under complex stress states', in *Proceedings of the Sixth International Conference on Scour and Erosion*. ISSMGE Paris, pp. 895–902.

Chang, D.S. and Zhang, L.M. (2013a) 'Critical Hydraulic Gradients of Internal Erosion under Complex Stress States', *Journal of Geotechnical and Geoenvironmental Engineering*, 139(9), pp. 1454–1467.

Chang, D.S. and Zhang, L.M. (2013b) 'Extended internal stability criteria for soils under seepage', *Soils and Foundations*, 53(4), pp. 569–583.

Chen, C. and Zhang, L. (2023) 'Hydro-mechanical behaviour of soil experiencing seepage erosion under cyclic hydraulic gradient', *Géotechnique*, 73(2), pp. 115–127.

Chen, C., Zhang, L.M. and Chang, D.S. (2016) 'Stress-Strain Behavior of Granular Soils Subjected to Internal Erosion', *Journal of Geotechnical and Geoenvironmental Engineering*, 142(12), p. 06016014.

Chen, L. *et al.* (2019) 'Influence of the Initial Relative Density on the Drained Strength Properties of Soils Subjected to Internal Erosion', *Soil Mechanics and Foundation Engineering*, 56(4), pp. 273–279.

Côté, S. (2010) *Critères de stabilité interne pour des matériaux de faible plasticité soumis à l'écoulement de l'eau*. PhD Thesis. Université Laval.

Courivaud, J.R. (2023) 'Feed-back from 18 years of internal erosion risk assessment practice at edf since the Aussois workshop in 2005: what are the gaps which still need to be filled', in. *The 28th annual meeting of the European Working Group on Internal Erosion in Embankment Dams, 498 Levees and Dikes, and their Foundations (EWG-IE)*, Lyon, France.

Engemoen, W. and Redlinger, C. (2009) 'Internal erosion incidents at Bureau of Reclamation dams', in. *Proceeding of USSD Annual Conference, Nashville Tennessee*.

Engemoen, W.O. (2011) 'Bureau of Reclamation experiences with internal erosion incidents', in. *Proc. of Workshop on Internal Erosion in embankment dams and their foundations*, pp. 11–18.

Fell, R. and Fry, J.J. (eds) (2007) *Internal erosion of dams and their foundations: selected and reviewed papers from the Workshop on Internal Erosion and Piping of Dams and Their Foundations, Aussois, France, 25 - 27 April 2005*. *Workshop on Internal Erosion and Piping of Dams and Their Foundations*, London: Taylor & Francis (BALKEMA - Proceedings and Monographs in Engineering, Water and Earth Science).

Fell, R. and Fry, J.-J. (2007) 'The state of the art of assessing the likelihood of internal erosion of embankment dams, water retaining structures and their foundations', *Internal Erosion of Dams and their Foundations*, pp. 1–23.

Fell, R. and Fry, J.-J. (2013) 'State of The Art on the Likelihood of Internal Erosion of Dams and Levees by Means of Testing', in *Erosion in Geomechanics Applied to Dams and Levees*. John Wiley & Sons, Ltd, pp. 1–99.

Foster, M. and Fell, R. (2001) 'Assessing Embankment Dam Filters That Do Not Satisfy Design Criteria', *Journal of Geotechnical and Geoenvironmental Engineering*, 127(5), pp. 398–407.

Foster, M., Fell, R. and Spannagle, M. (2000) 'The statistics of embankment dam failures and accidents', *Canadian Geotechnical Journal*, 37(5), pp. 1000–1024.

Foster, M.A., Spannagle, M. and Fell, R. (1998) *Analysis of embankment dam incidents*. University of New South Wales, School of Civil Engineering.

Frost, J.D. and Park, J.-Y. (2003) 'A Critical Assessment of the Moist Tamping Technique', *Geotechnical Testing Journal*, 26(1), pp. 57–70.

Fry, J.-J. *et al.* (2012) 'Dam failures by erosion: lessons from ERINOH data bases', *ICSE6 Paris*, pp. 273–280.

Garner, S. and Fannin, R. (2010) 'Understanding internal erosion: a decade of research following a sinkhole event', *The international journal on hydropower & dams*, 17(3), p. 93.

Garner, S.J. and Sobkowicz, J.C. (2002) 'Internal instability in gap-graded cores and filters', in. *Canadian Dam Association Annual Conference*, Canada.

Gaucher, J., Marche, C. and Mahdi, T.-F. (2010) 'Experimental Investigation of the Hydraulic Erosion of Noncohesive Compacted Soils', *Journal of Hydraulic Engineering*, 136(11), pp. 901–913.

Gelet, R. *et al.* (2021) 'Analysis of volumetric internal erosion in cohesionless soils: Model, experiments and simulations', *International Journal for Numerical and Analytical Methods in Geomechanics*, 45(18), pp. 2780–2806.

Gelet, R. and Marot, D. (2022) 'Internal erosion by suffusion on cohesionless gap-graded soils: Model and sensibility analysis', *Geomechanics for Energy and the Environment*, 31, p. 100313.

Griffiths, D.V. and Fenton, G.A. (2004) 'Probabilistic Slope Stability Analysis by Finite Elements', *Journal of Geotechnical and Geoenvironmental Engineering*, 130(5), pp. 507–518.

Holtz, R.D., Kovacs, W.D. and Sheahan, T.C. (1981) *An introduction to geotechnical engineering*. Prentice-Hall Englewood Cliffs.

ICOLD (1995) 'Dam Failures Statistical Analysis.', in. *Bulletin 99, International Commission on Large Dams, Paris.*

ICOLD (2015) ‘Internal erosion of existing dams, levees and dikes, and their foundations.’, in. *Bulletin 164, International Commission on Large Dams, Paris*.

Indraratna, B., Israr, J. and Rujikiatkamjorn, C. (2015) ‘Geometrical Method for Evaluating the Internal Instability of Granular Filters Based on Constriction Size Distribution’, *Journal of Geotechnical and Geoenvironmental Engineering*, 141(10), p. 04015045.

Indraratna, B., Nguyen, V.T. and Rujikiatkamjorn, C. (2011) ‘Assessing the Potential of Internal Erosion and Suffusion of Granular Soils’, *Journal of Geotechnical and Geoenvironmental Engineering*, 137(5), pp. 550–554.

Indraratna, B. and Radampola, S. (2002) ‘Analysis of critical hydraulic gradient for particle movement in filtration’, *Journal of Geotechnical and Geoenvironmental Engineering*, 128(4), pp. 347–350.

Indraratna, B., Raut, A.K. and Khabbaz, H. (2007) ‘Constriction-Based Retention Criterion for Granular Filter Design’, *Journal of Geotechnical and Geoenvironmental Engineering*, 133(3), pp. 266–276.

Istomina, V.S. (1957) ‘Filtration stability of soils’, *Gostroizdat, Moscow, Leningrad*, 15.

Jones, J.A.A. (1981) ‘The nature of soil piping-a review of research’, *BGRG research monograph* [Preprint].

Ke, L. *et al.* (2016) ‘Soil deformation due to suffusion and its consequences on undrained behavior under various confining pressures’, *Japanese Geotechnical Society Special Publication*, 2(8), pp. 368–373.

Ke, L. and Takahashi, A. (2012a) ‘Influence of internal erosion on deformation and strength of gap-graded non-cohesive soil’, in *Proceedings of the Sixth International Conference on Scour and Erosion, Paris*, pp. 847–854.

Ke, L. and Takahashi, A. (2012b) ‘Strength reduction of cohesionless soil due to internal erosion induced by one-dimensional upward seepage flow’, *Soils and Foundations*, 52(4), pp. 698–711.

Ke, L. and Takahashi, A. (2014a) ‘Experimental investigations on suffusion characteristics and its mechanical consequences on saturated cohesionless soil’, *Soils and Foundations*, 54(4), pp. 713–730.

Ke, L. and Takahashi, A. (2014b) ‘Triaxial Erosion Test for Evaluation of Mechanical Consequences of Internal Erosion’, *Geotechnical Testing Journal*, 37(2), pp. 347–364.

Ke, L. and Takahashi, A. (2015) ‘Drained Monotonic Responses of Suffusional Cohesionless Soils’, *Journal of Geotechnical and Geoenvironmental Engineering*, 141(8), p. 04015033.

Kenney, T.C. and Lau, D. (1985) ‘Internal stability of granular filters’, *Canadian Geotechnical Journal*, 22(2), pp. 215–225.

Kenney, T.C. and Lau, D. (1986) ‘Internal stability of granular filters: Reply’, *Canadian Geotechnical Journal*, 23(3), pp. 420–423.

Kezdi, A. (1969) ‘Increase of protective capacity of flood control dikes’, *Department of Geotechnics, Technical University of Budapest, Report* [Preprint], (1).

Kodieh, A. *et al.* (2021) ‘A study of suffusion kinetics inspired from experimental data: comparison of three different approaches’, *Acta Geotechnica*, 16(2), pp. 347–365.

Kolbuszewski, J. and Frederick, M.R. (1963) ‘The significance of particle shape and size on the mechanical behaviour of granular materials’, in *European Conference on Soil Mechanics and Foundation Engineering*, pp. 253–263.

Kuerbis, R. and Vaid, Y.P. (1988) ‘Sand Sample Preparation-the Slurry Deposition Method’, *土質工学会論文報告集*, 28(4), pp. 107–118.

Kulhawy, F.H. and Duncan, J.M. (1972) ‘Stresses and Movements in Oroville Dam’, *Journal of the Soil Mechanics and Foundations Division*, 98(7), pp. 653–665.

Ladd, R.S. (1978) ‘Preparing Test Specimens Using Undercompaction’, *Geotechnical Testing Journal*, 1(1), pp. 16–23.

Lafleur, J., Mlynarek, J. and Rollin, A.L. (1989) ‘Filtration of Broadly Graded Cohesionless Soils’, *Journal of Geotechnical Engineering*, 115(12), pp. 1747–1768.

Lane, E.W. (1935) ‘Security from under-seepage-masonry dams on earth foundations’, *Transactions of the American Society of Civil Engineers*, 100(1), pp. 1235–1272.

Le, V.T. *et al.* (2018) ‘Suffusion susceptibility investigation by energy-based method and statistical analysis’, *Canadian Geotechnical Journal*, 55(1), pp. 57–68.

Li, M. (2008) *Seepage induced instability in widely graded soils*. University of British Columbia.

Li, M. and Fannin, R. j. (2012) ‘A theoretical envelope for internal instability of cohesionless soil’, *Géotechnique*, 62(1), pp. 77–80.

Li, M. and Fannin, R.J. (2008) ‘Comparison of two criteria for internal stability of granular soil’, *Canadian Geotechnical Journal*, 45(9), pp. 1303–1309.

Li, S., Russell, A.R. and Muir Wood, D. (2020) ‘Influence of particle-size distribution homogeneity on shearing of soils subjected to internal erosion’, *Canadian Geotechnical Journal*, 57(11), pp. 1684–1694.

Liang, Y. *et al.* (2017) ‘Onset of suffusion in upward seepage under isotropic and anisotropic stress conditions’, *European Journal of Environmental and Civil Engineering*, 23(12), pp. 1520–1534.

Liang, Y. *et al.* (2019) ‘Particle erosion in suffusion under isotropic and anisotropic stress states’, *Soils and Foundations*, 59(5), pp. 1371–1384.

Luo, Y., Wu, Q., *et al.* (2013) ‘Hydro-mechanical coupling experiments on suffusion in sandy gravel foundations containing a partially penetrating cut-off wall’, *Natural Hazards*, 67(2), pp. 659–674.

Luo, Y., Qiao, L., *et al.* (2013) 'Hydro-mechanical experiments on suffusion under long-term large hydraulic heads', *Natural Hazards*, 65(3), pp. 1361–1377.

Luo, Y., Luo, B. and Xiao, M. (2020) 'Effect of deviator stress on the initiation of suffusion', *Acta Geotechnica*, 15(6), pp. 1607–1617.

Marot, D. *et al.* (2009) 'Internal Flow Effects on Isotropic Confined Sand-Clay Mixtures', *Soil and Sediment Contamination: An International Journal*, 18(3), pp. 294–306.

Marot, D. *et al.* (2016) 'Assessing the susceptibility of gap-graded soils to internal erosion: proposition of a new experimental methodology', *Natural Hazards*, 83(1), pp. 365–388.

Marot, D. *et al.* (2020) 'Multidirectional Flow Apparatus for Assessing Soil Internal Erosion Susceptibility', *Geotechnical Testing Journal*, 43(6), pp. 1481–1498.

Marot, D., Bendahmane, F. and Konrad, J.-M. (2011) 'Multichannel optical sensor to quantify particle stability under seepage flow', *Canadian Geotechnical Journal*, 48(12), pp. 1772–1787.

Marot, D., Bendahmane, F. and Nguyen, H.H. (2012) 'Influence of angularity of coarse fraction grains on internal erosion process', *La Houille Blanche*, (6), pp. 47–53.

Marot, D. and Bowman, E. (2022) 'Internal Erosion by Suffusion – Round Robin Testing program proposal', in *EWG-IE : 28th Annual Meeting*. *European Working Group on Internal Erosion in Embankment Dams, Levees and Dikes and their Foundations*, Sheffield, United Kingdom, pp. 42–44.

Marot, D., Regazzoni, P.-L. and Wahl, T. (2011) 'Energy-Based Method for Providing Soil Surface Erodibility Rankings', *Journal of Geotechnical and Geoenvironmental Engineering*, 137(12), pp. 1290–1293.

McClelland, V.A. (2020) *On the critical state of gap-graded sandy soil*. University of British Columbia.

Mehdizadeh, A., Disfani, M.M., *et al.* (2017) 'Mechanical Consequences of Suffusion on Undrained Behaviour of a Gap-Graded Cohesionless Soil - An Experimental Approach', *Geotechnical Testing Journal*, 40(6), p. 20160145.

Mehdizadeh, A., Evans, R., *et al.* (2017) 'Mechanical consequences of suffusion on undrained behaviour of a gap-graded cohesionless soil-an experimental approach', *Geotechnical Testing Journal*, 40(6), pp. 1026–1042.

Mehdizadeh, A. (2018) *Multi scale investigation of post-erosion mechanical behaviour of granular material*. Swinburne University of Technology Melbourne, Australia.

Moffat, R. and Fannin, J. (2006) 'A Large Permeameter for Study of Internal Stability in Cohesionless Soils', *Geotechnical Testing Journal*, 29(4), p. 100021.

Moffat, R. and Fannin, R.J. (2011) 'A hydromechanical relation governing internal stability of cohesionless soil', *Canadian Geotechnical Journal*, 48(3), pp. 413–424.

Moffat, R., Fannin, R.J. and Garner, S.J. (2011) 'Spatial and temporal progression of internal erosion in cohesionless soil', *Canadian Geotechnical Journal*, 48(3), pp. 399–412.

Moffat, R. and Herrera, P. (2015) 'Hydromechanical model for internal erosion and its relationship with the stress transmitted by the finer soil fraction', *Acta Geotechnica*, 10(5), pp. 643–650.

Nguyen, C.D. *et al.* (2019) 'Experimental investigation of microstructural changes in soils eroded by suffusion using X-ray tomography', *Acta Geotechnica*, 14(3), pp. 749–765.

Nguyen, H.H., Marot, D. and Bendahmane, F. (2012) 'Erodibility characterisation for suffusion process in cohesive soil by two types of hydraulic loading', *La Houille Blanche*, (6), pp. 54–60.

Oli, B. (2020) *Internal Erosion within Hydraulic Earth Structures and Eroded Soil Behavior Subjected to Complex Hydro-Mechanical Loading*. Master's thesis. Grenoble INP-ENSE3, UGA.

Ouyang, M. and Takahashi, A. (2015) 'Influence of initial fines content on fabric of soils subjected to internal erosion', *Canadian Geotechnical Journal*, 53(2), pp. 299–313.

Pachideh, V. and Hosseini, S.M.M.M. (2019) 'A New Physical Model for Studying Flow Direction and Other Influencing Parameters on the Internal Erosion of Soils', *Geotechnical Testing Journal*, 42(6), pp. 1431–1456.

Prasomsri, J., Shire, T. and Takahashi, A. (2021) 'Effect of fines content on onset of internal instability and suffusion of sand mixtures', *Géotechnique Letters*, 11(3), pp. 209–214.

Prasomsri, J. and Takahashi, A. (2020) 'The role of fines on internal instability and its impact on undrained mechanical response of gap-graded soils', *Soils and Foundations*, 60(6), pp. 1468–1488.

Prasomsri, J. and Takahashi, A. (2021) 'Experimental study on suffusion under multiple seepages and its impact on undrained mechanical responses of gap-graded soil', *Soils and Foundations*, 61(6), pp. 1660–1680.

Richards, K.S. and Reddy, K.R. (2007) 'Critical appraisal of piping phenomena in earth dams', *Bulletin of Engineering Geology and the Environment*, 66(4), pp. 381–402.

Robbins, B.A. and Griffiths, D.V. (2018) 'Internal Erosion of Embankments: A Review and Appraisal', in *Rocky Mountain Geo-Conference 2018*. *Rocky Mountain Geo-Conference 2018*, Golden, Colorado: American Society of Civil Engineers, pp. 61–75.

Rochim, A. *et al.* (2017) 'Effects of Hydraulic Loading History on Suffusion Susceptibility of Cohesionless Soils', *Journal of Geotechnical and Geoenvironmental Engineering*, 143(7), p. 04017025.

Rönnqvist, H. and Viklander, P. (2015) 'Applying Empirical Methods to Assess the Internal Stability of Embankment Dam Cores of Glacial Till', *Geomaterials*, 05(01), pp. 1–18.

Rousseau, Q. *et al.* (2020) 'Modelling the poroelastoplastic behaviour of soils subjected to internal erosion by suffusion', *International Journal for Numerical and Analytical Methods in Geomechanics*, 44(1), pp. 117–136.

Sail, Y. *et al.* (2011) 'Suffusion tests on cohesionless granular matter', *European Journal of Environmental and Civil Engineering*, 15(5), pp. 799–817.

Seblany, F., Vincens, E. and Picault, C. (2021) 'Determination of the opening size of granular filters', *International Journal for Numerical and Analytical Methods in Geomechanics*, 45(9), pp. 1195–1211.

Sherard, J.L. (1979) 'Sinkholes in dams of coarse, broadly graded soils. 13th Int', in *Congress on Large Dams, New Delhi Q*, p. R2.

Sherard, J.L., Dunnigan, L.P. and Talbot, J.R. (1984) 'Basic Properties of Sand and Gravel Filters', *Journal of Geotechnical Engineering*, 110(6), pp. 684–700.

Shire, T. *et al.* (2014) 'Fabric and Effective Stress Distribution in Internally Unstable Soils', *Journal of Geotechnical and Geoenvironmental Engineering*, 140(12), p. 04014072.

Shire, T., O'Sullivan, C. and Hanley, K.J. (2016) 'The influence of fines content and size-ratio on the micro-scale properties of dense bimodal materials', *Granular Matter*, 18(3), p. 52.

Shwiyhat, N. and Xiao, M. (2010) 'Effect of Suffusion on Mechanical Characteristics of Sand', in, pp. 378–386.

Sibille, L., Marot, D. and Sail, Y. (2015) 'A description of internal erosion by suffusion and induced settlements on cohesionless granular matter', *Acta Geotechnica*, 10(6), pp. 735–748.

Skempton, A.W. and Brogan, J.M. (1994) 'Experiments on piping in sandy gravels', *Géotechnique*, 44(3), pp. 449–460.

Slangen, P. and Fannin, R.J. (2017) 'A Flexible Wall Permeameter for Investigating Suffusion and Suffosion', *Geotechnical Testing Journal*, 40(1), p. 20150287.

Slangen, P.H.H. (2015) *On the influence of effective stress and micro-structure on suffusion and suffosion*. University of British Columbia. Available at: https://doi.org/10.14288/1.0166340.

Soroush, A. and Pourakbar, M. (2022) 'Evaluation of Low Stress and Cracking Zones in the Core of a High Rockfill Dam in a Relatively Narrow Canyon Using 3D Numerical Modeling', *International Journal of Geomechanics*, 22(3), p. 04021299.

Sterpi, D. (2003) 'Effects of the Erosion and Transport of Fine Particles due to Seepage Flow', *International Journal of Geomechanics*, 3(1), pp. 111–122.

Takahashi, A. (2023) 'Observation of internal erosion in the triaxial cell and physical models How to mimic the realistic situation in the lab'. *IRNGeoMech Workshop 2023*.

Tanaka, T. and Toyokuni, E. (1991) 'Seepage—Failure Experiments on Multi—Layered Sand Columns: —Effects of Flow Conditions and Residual Effective Stress on Seepage-Failure Phenomena—', *Soils and Foundations*, 31(4), pp. 13–36.

Terzaghi, K. (1925) 'Principles of soil mechanics. IV. Settlement and consolidation of clay', *Engineering News-Record*, 95, p. 874.

Terzaghi, K. (1939) ‘Soil mechanics - a new chapter in engineering science’, *Journal of the Institution of Civil Engineers*, 12(7), pp. 106–142.

Thevanayagam, S. *et al.* (2002) ‘Undrained Fragility of Clean Sands, Silty Sands, and Sandy Silts’, *Journal of Geotechnical and Geoenvironmental Engineering*, 128(10), pp. 849–859.

Thevanayagam, S. (2007) ‘Intergrain contact density indices for granular mixes—I: Framework’, *Earthquake Engineering and Engineering Vibration*, 6(2), pp. 123–134.

U.S. Army (1953) *Filter experiments and design criteria*. Technical Memorandum No. 3-360, Waterways Experiment Station, Vicksburg, MS.

Wan, C. and Fell, R. (2007) ‘Investigation of internal erosion by the process of suffusion in embankment dams and their foundations’, *Internal erosion of dams and their foundations (eds R. Fell and JJ Fry)*, pp. 219–234.

Wan, C.F. and Fell, R. (2004) *Experimental investigation of internal instability of soils in embankment dams and their foundations*. University of New South Wales, School of Civil and Environmental Engineering.

Wan, C.F. and Fell, R. (2008) ‘Assessing the Potential of Internal Instability and Suffusion in Embankment Dams and Their Foundations’, *Journal of Geotechnical and Geoenvironmental Engineering*, 134(3), pp. 401–407.

Wautier, A., Bonelli, S. and Nicot, F. (2019) ‘DEM investigations of internal erosion: Grain transport in the light of micromechanics’, *International Journal for Numerical and Analytical Methods in Geomechanics*, 43(1), pp. 339–352.

Xiao, M. and Shwiyhat, N. (2012) ‘Experimental Investigation of the Effects of Suffusion on Physical and Geomechanic Characteristics of Sandy Soils’, *Geotechnical Testing Journal*, 35, p. 104594.

Xu, Z.D. *et al.* (2022) ‘Experimental Study of Internal Erosion in Granular Soil Subject to Cyclic Hydraulic Gradient Reversal’, *Journal of Geotechnical and Geoenvironmental Engineering*, 148(5), p. 04022014.

Zhang, L. *et al.* (2019) ‘A method to assess the suffusion susceptibility of low permeability core soils in compacted dams based on construction data’, *European Journal of Environmental and Civil Engineering*, 23(5), pp. 626–644.

Zhong, C. *et al.* (2018) ‘Investigation of Spatial Scale Effects on Suffusion Susceptibility’, *Journal of Geotechnical and Geoenvironmental Engineering*, 144(9), p. 04018067.

Appendices

A Study on effluent Tank

A.1 Perturbation and noise on load cell

The accuracy of eroded mass measurement, as reported in various studies, provides valuable insights into the precision achieved using different devices. For instance, Ke and Takahashi (2014a) achieved a remarkable level of accuracy with a load resolution of 0.015 [g]. This reference value serves as a benchmark for desired accuracy in subsequent measurements, as mentioned later in the discussion. A summary of accuracy values for eroded mass measurements in different studies is presented in Table_Appx. A.1, offering a comprehensive view of the range of precision attainable in this field.

Table_Appx. A.1 Accuracy of eroded mass measurement

S.N.	Authors	Fine content [%]	Fm_d [g]	Δm [g]	± Accuracy [%]
1	Ke and Takahashi (2014a)	35	328,66	0,015	0,00456
2	Mehdizadeh et al., (2017)	25	295,20	10	3,38752
3	Chang and Zhang (2011)	35	559,03	0,2	0,03578
4	Zhong et al., (2018)	25	85,06	0,002	0,00235
5	Rochim et al., (2017)	25	87,02	0,02	0,02298
6	Marot et al., (2019)	25	778,77	0,02	0,00257
7	Pachideh & Mir (2019)	25	4995,90	2	0,04003

Note: Fm_d represents initial dry mass of fine content and Δm is resolution of the load cell.

Figure_Appx. A.1 illustrates the initial version of the developed effluent tank, specifically designed for studying the effects of inflow on a dedicated submersible load measuring cell used for continuous mass measurement. The figure provides a visual representation of the configuration, allowing for a comprehensive examination of the influence of inflow conditions on the load measuring cell.

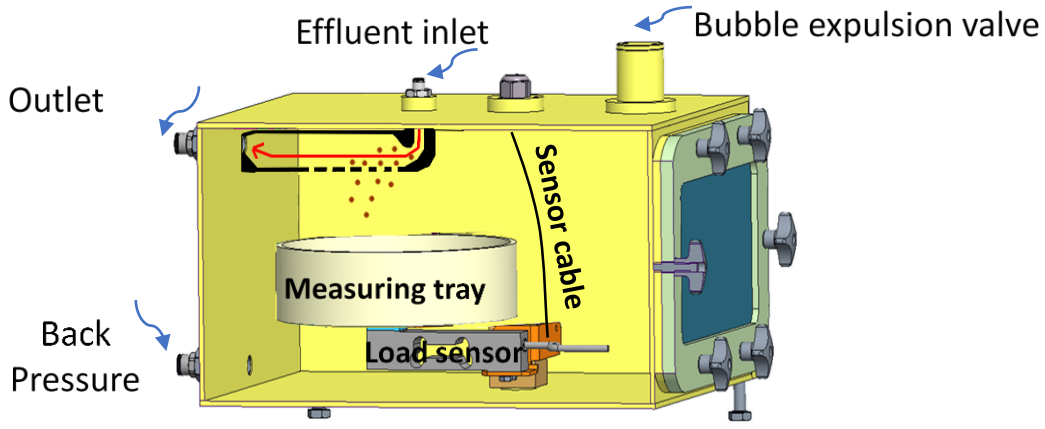

Figure_Appx. A.1 First version of effluent tank

During the stationary flow condition, it was observed that the noise on the load cell was measured to be 0.3 g. To further evaluate the perturbation caused by the inlet flow, an experimental test was conducted within the range of 0 l/min to 3.5 l/min, as depicted in Figure_Appx. A.2. In the experiment, the inflow was gradually increased up to the maximum value of 3.3 l/min (represented by the orange curve), while the mass effluent was simultaneously measured using the load cell (represented by the blue curve). The results indicated that the perturbation on the load cell increased progressively with the rise in inflow due to the impact of the jet.

For inflow rates below 0.2 l/min, the observed perturbation was approximately 0.7 g, which is considered acceptable for such low flow rates. Thus, the current device configuration can be used effectively under these specific conditions. However, it should be noted that the desired accuracy cannot be attained with the presented tank configuration, highlighting the need for further improvements.

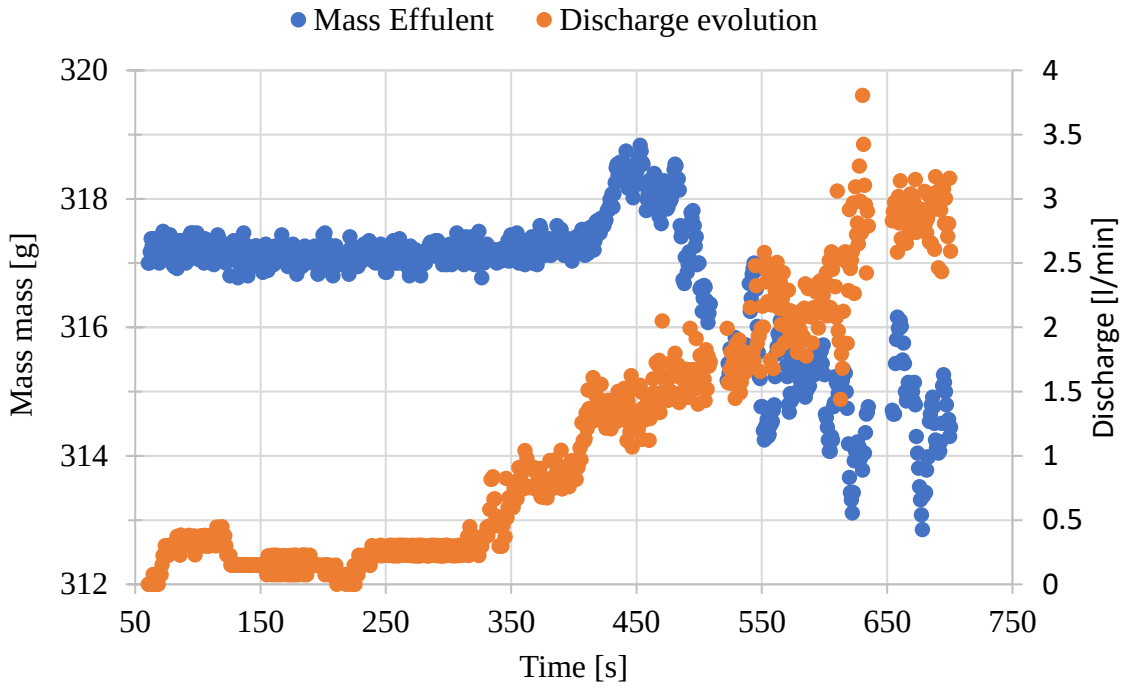

Figure_Appx. A.2 Effect of injected flow on mass measurement

A.2 Delay test

To evaluate the transportation delay of eroded particles, their travel was assumed to be a combination of settling velocity and flow velocity. The pathway from the specimen outlet to the measuring tray plays a crucial role in this delay. Although literature often overlooks these parameters when studying suffusion onset, their consideration is important for accuracy.

The accuracy of suffusion characterization depends on factors like the hydraulic loading path, time evolution of hydraulic conductivity and erosion rate, as shown in Figure_Appx. A.3 by Rochim et al. (2017). A significant time gap between specimen exit and recorded time can lead to misinterpretation. To address this issue, tests were conducted on Fontainebleau sand specimens under two conditions: (i) without flow and (ii) with flow. These tests aim to provide insights into the significance of transportation delay and enhance the accurate interpretation of suffusion phenomena.

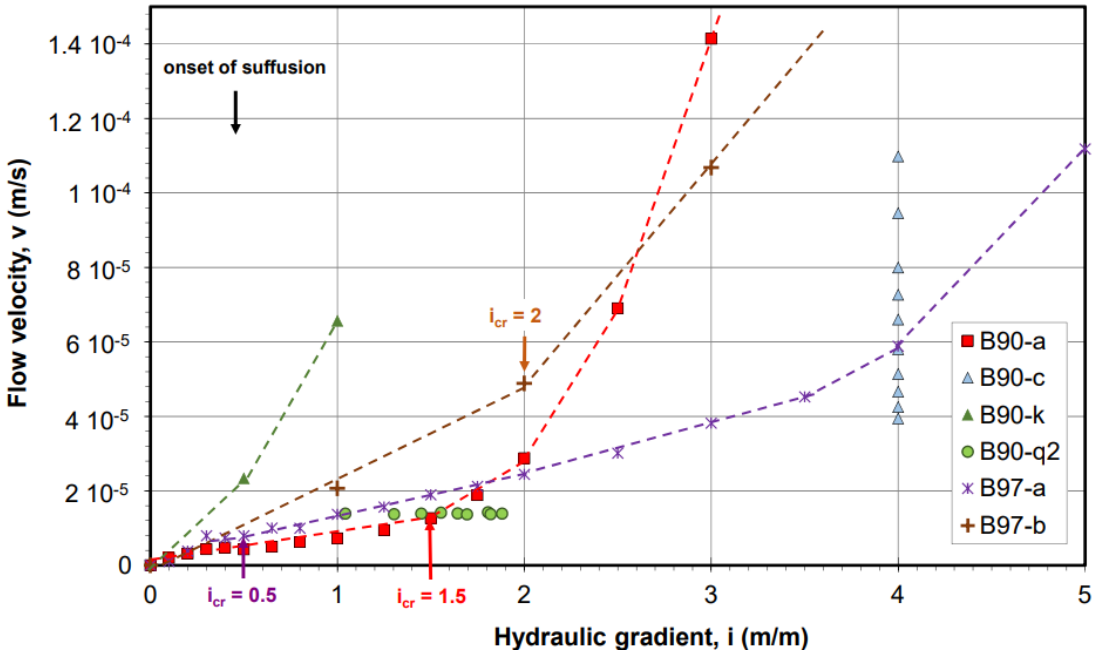

Figure_Appx. A.3 Flow velocity vs hydraulic gradient by Rochim et al., (2017)

Without flow

To analyze the impact of the "cloud of particles" size, seven experimental tests were conducted with different mass quantities. The delay in particle detection increased as the injected mass amount increased. This delay can be attributed to various factors, such as hydrodynamic interactions, particle size, arrangement and segregation within the particle cloud. On average, the delay without flow conditions was 42.13 seconds.

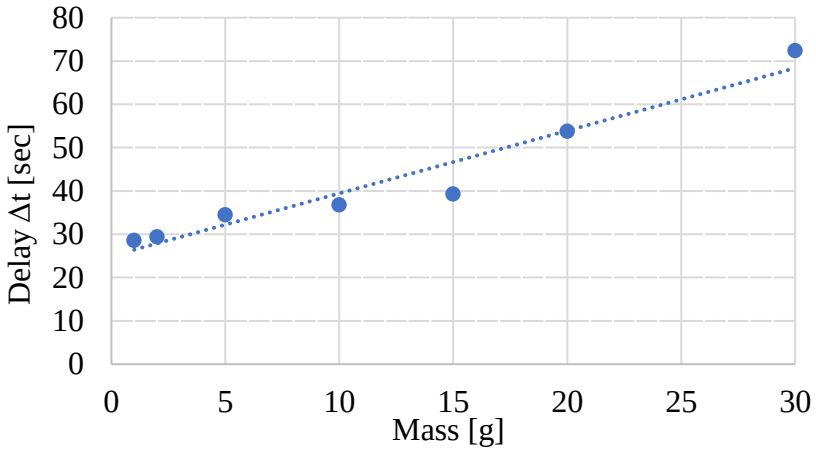

Figure_Appx. A.4 Delay Test without flow condition

The theoretical settling time was calculated to be 11.42 seconds, resulting in a discrepancy of 30.71 seconds compared to the average experimental value. This difference can be attributed to two possible factors. Firstly, the theoretical calculation (based on the Stokes's settling velocity) assumes isolated particles and does not consider hydrodynamic interactions among them. Secondly, the simplified theoretical flow path, which assumes a purely vertical trajectory, may not accurately represent the actual flow behavior. The flow momentum in reality can transition between vertical and horizontal directions, as depicted in Figure_Appx. A.4.

With flow

When transporting particles, two primary physical phenomena are involved: settling velocity and inflow velocity. It has been observed that the transportation delay decreases by approximately 42% when the inflow velocity is introduced (see Figure_Appx. A.5) which further supports this observation, indicating a decrease in the delay with increasing inflow velocity. Conversely, an increase in the eroded mass leads to a longer settling time due to the reasons mentioned earlier.

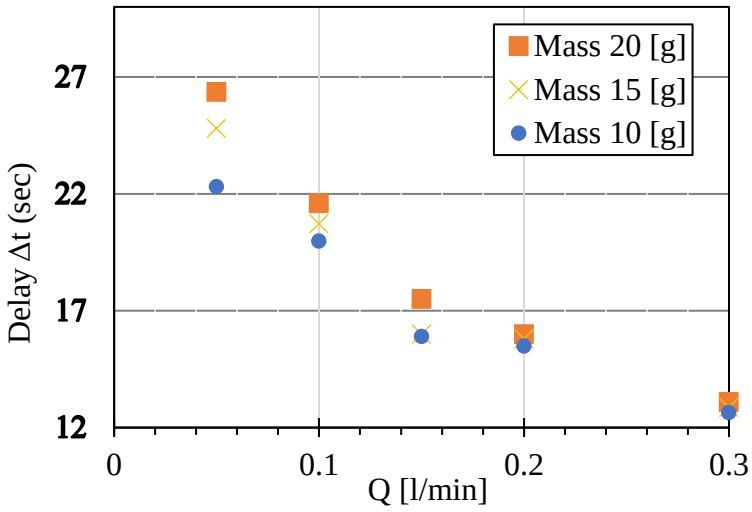

Figure_Appx. A.5 Delay of particle detection as a function of injected flow and eroded mass

A.3 Effluent tank development

After the initial version of the effluent tank failed to meet the desired accuracy, a second version was proposed, as depicted in Figure_Appx. A.6. However, this new configuration proved to be highly sensitive to vibrations, resulting in flow perturbations equivalent to 1 g and difficulties in accurately measuring the eroded mass.

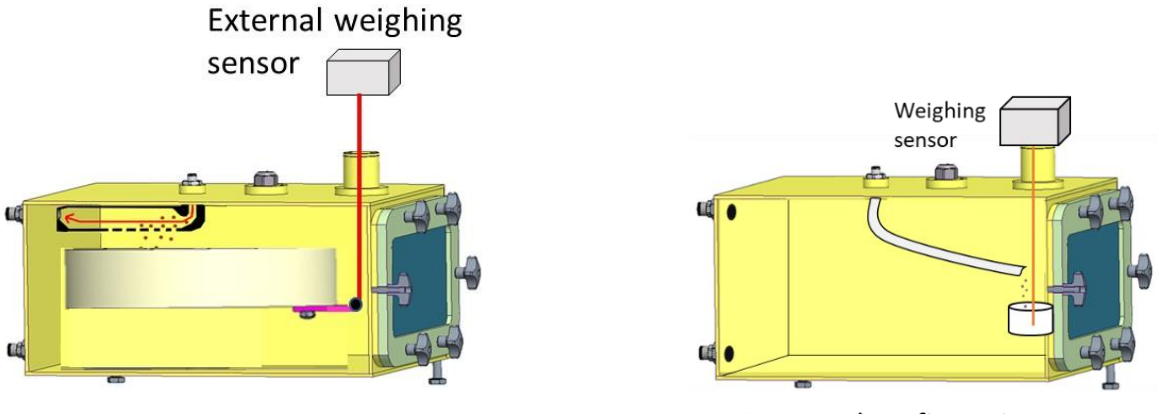

Figure_Appx. A.6 [a] 2nd version of effluent tank [b] 3rd version of effluent tank

In an attempt to address these challenges, a third version of the effluent tank was tested. This version featured an inclined transportation tube and a hanging measuring sensor placed outside the collection tank, as shown in Figure_Appx. A.6 [b]. While this version was capable of measuring a dry mass of 0.1 g, it experienced increased detection delay due to the longer pathway and generated flow perturbations.

None of the presented versions were able to achieve the desired accuracy. As a result, the previous developed rotation collection unit with 8 buckets was slightly modified to include 16 buckets, as represented in Figure_Appx. A.7. The modified configuration was used for the entirety of this thesis program. It offers a higher precision in measuring the eroded mass and the possibility to measure the size of the loss particles, although the main limitation remains the discontinuous measurement of the eroded mass.

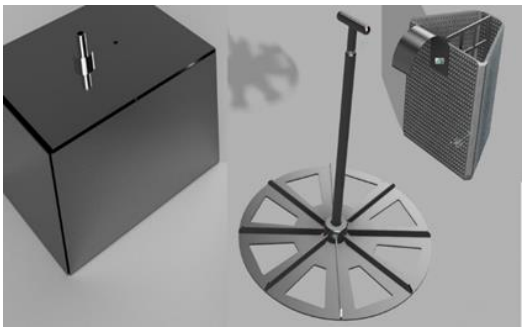

Figure_Appx. A.7 Enhanced effluent tank with rotational configuration and partitioned collection buckets

B Data acquisition

The developed LabVIEW code, along with the calibration process for input/output sensors and signals, is thoroughly explained and documented in Appendix B.

DATA acquisition

Figure_Appx. B.1 shows the front panel where all the measured parameters can be monitored graphically and multiple windows can be switched to visualize the evolution with time.

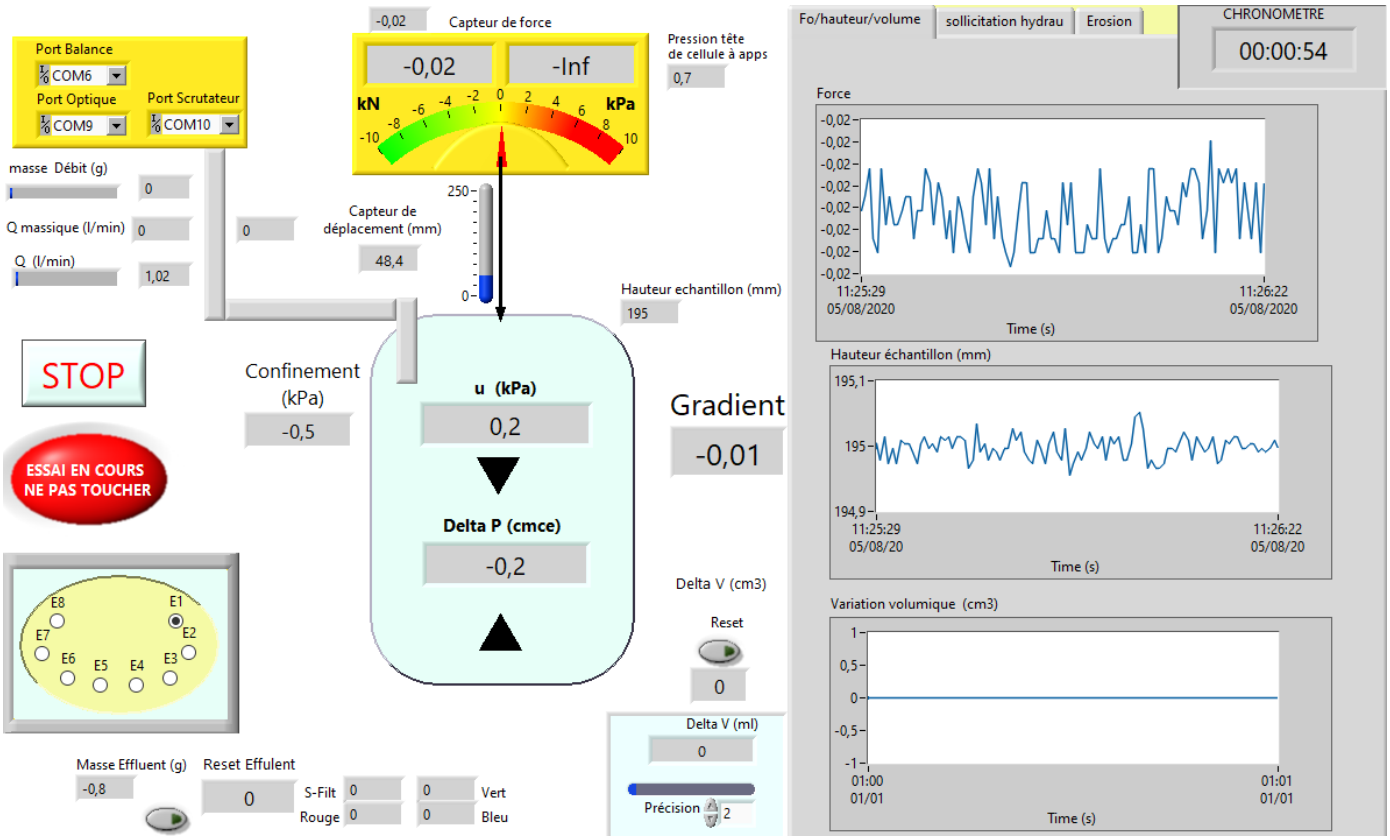

Figure_Appx. B.1 LabVIEW front panel for real time monitoring

Indicators are also integrated into the programming to avoid any damage and for alert notification. The block diagram of all the graphical code is summarized below.

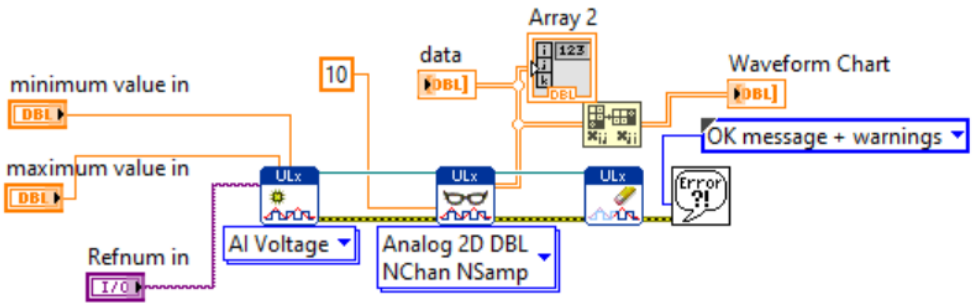

Figure_Appx. B.2 Principle palettes used to read the signal in LabVIEW block diagram

The code is very large and Figure_Appx. B.2 is only a representation of its working principle. Each sensor transmits a voltage that is centralized by LabVIEW by creating a channel from the corresponding port. Then the code reads the task from the respective block that contains one or more analog input channel. Depending on the need, the data are formatted into different data types such as floating point, long integer, array etc. All errors are systematically signaled: an error message will pop up to find and solve the issue, even during monitoring.

Figure_Appx. B.3 represents one of the sub-modules to record a specific parameter. The various sensors are arranged in column with their corresponding heading and event time.

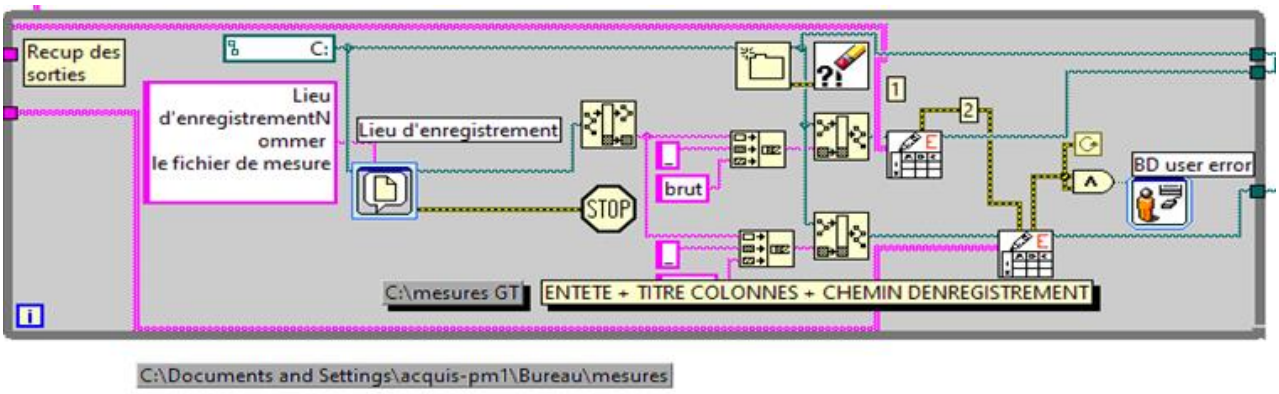

Figure_Appx. B.3 Main dialog for writing a text file in LabVIew block diagram

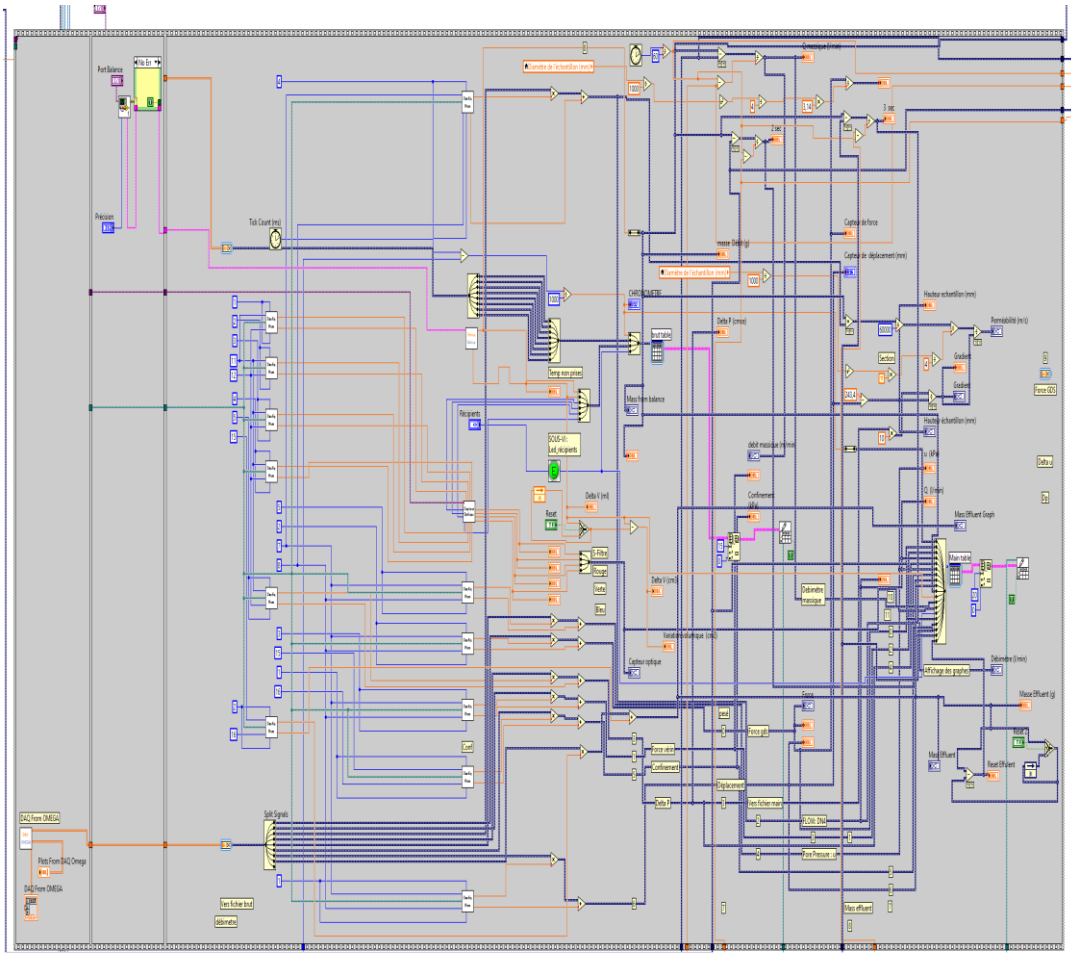

Figure_Appx. B.4 Main block diagram for DAQ

The input signal is calibrated and converted to an appropriate digital data. All the graphical plots are computed at this section and can be monitored from the front panel during the running time of the program.

B.1 Calibration and validation of input/output sensors and signals

A rigorous and precise calibration procedure is crucial to achieve the intended measurement. Calibration consists of comparing the output of a sensor with that of a known instrument, providing that the same input was applied to both. The input analog signal is transferred to the OMEGA DAQ and measured in Volt (max. range ± 10 V). The Volt values are next converted in numerical values. Therefore, two calibrations are required: (a) between each sensor and DAQ device and (b) between each sensor and monitoring display unit. By performing numerous tests, each sensor was calibrated. The appropriate coefficients/constants for each of the following instruments are provided in Figure_Appx. B.5 to Figure_Appx. B.7:

[a] Load sensors: The load is measured by two different sensors, one at the top of the piston and one at the interface between the piston and the specimen. The difference between these two values will provide information on the amount of friction induced by the piston on the cell.

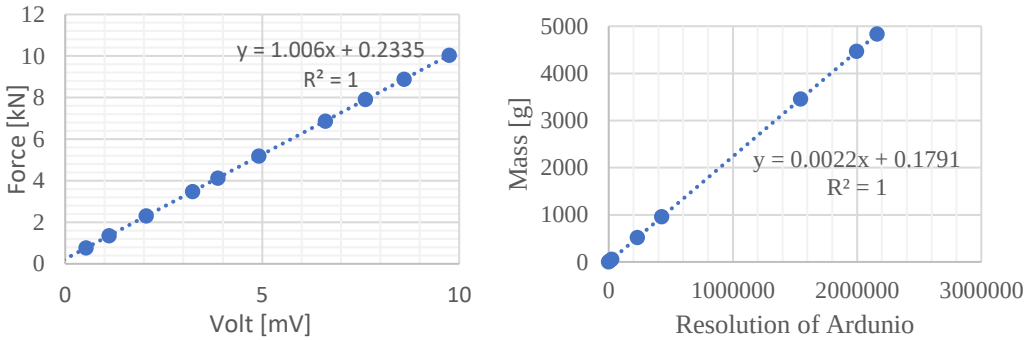

[a] *[b]*

Figure_Appx. B.5 Calibration of load sensors[a] and mass balance sensor [b]

[b] Mass balance from Arduino: For the measurement of low outflows, a mass balance technique is used. The 1-bit resolution of this device is equivalent to 4.88 mV.

[c] Flow meter: For large outflows measurements, a flow meter is used.

[d] Pressure transducer: To measure the differential pressure of specimen.

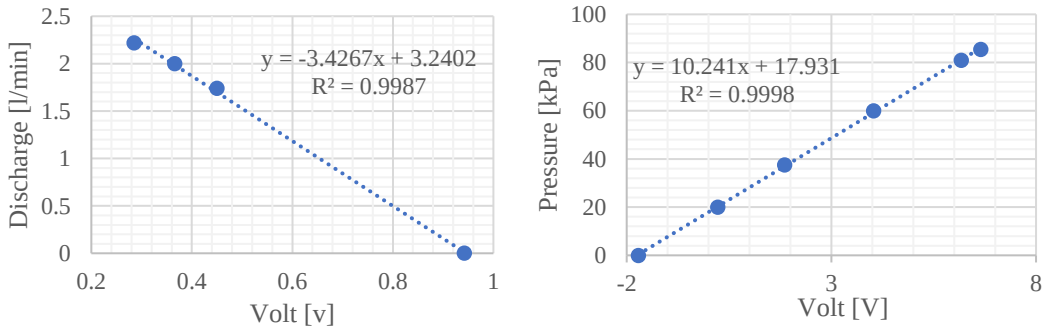

[c] *[d]*

Figure_Appx. B.6 Calibration of flow meter [c] and pressure transducer [d]

[e] Displacement: To measure the axial displacement and strain of the specimen.

[f] Mass effluent: The eroded mass is collected in a submerged unit

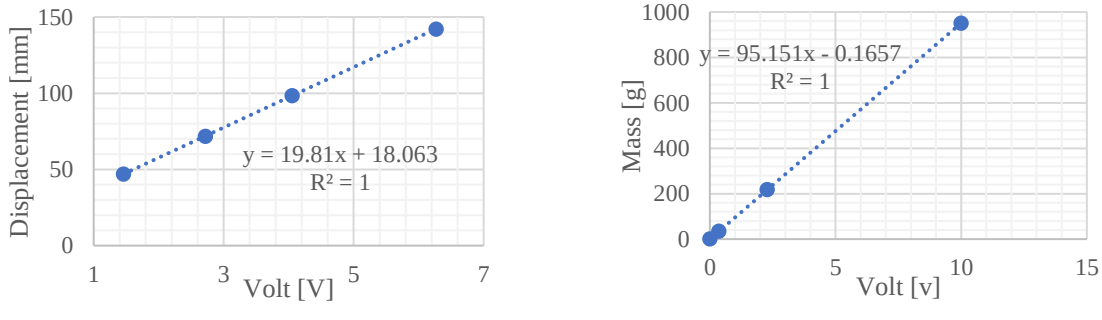

[e] *[f]*

Figure_Appx. B.7 Calibration for displacement [e] and mass effluent [f]

C Study on influence of stress state

C.1 Test result on soil A

The temporal changes in hydraulic conductivity and erosion rate within the sample containing 15% fine content exhibit limited fluctuations despite the escalation of deviatoric stress. This phenomenon can be attributed to the underfilled conditions, wherein self-filtration plays a negligible role, allowing the erosion rate to persistently rise and ultimately reach equilibrium within a brief timeframe, as depicted in the figure below. Consequently, the erosion resistance index falls within the category of moderately erodible.

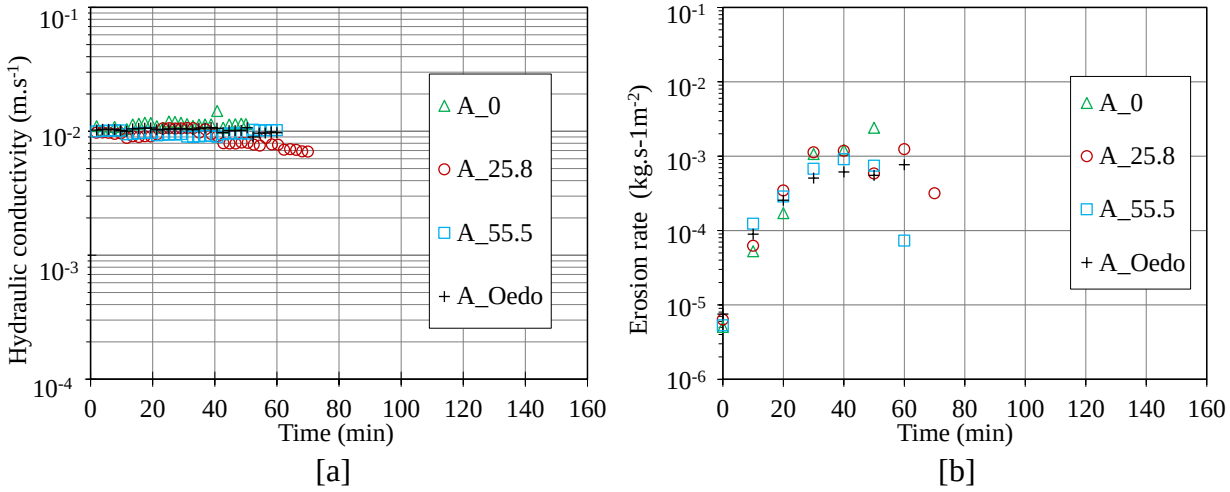

Figure_Appx. C.1 Time evolution of hydraulic conductivity [a] and erosion rate [b], for soil A under different stress state

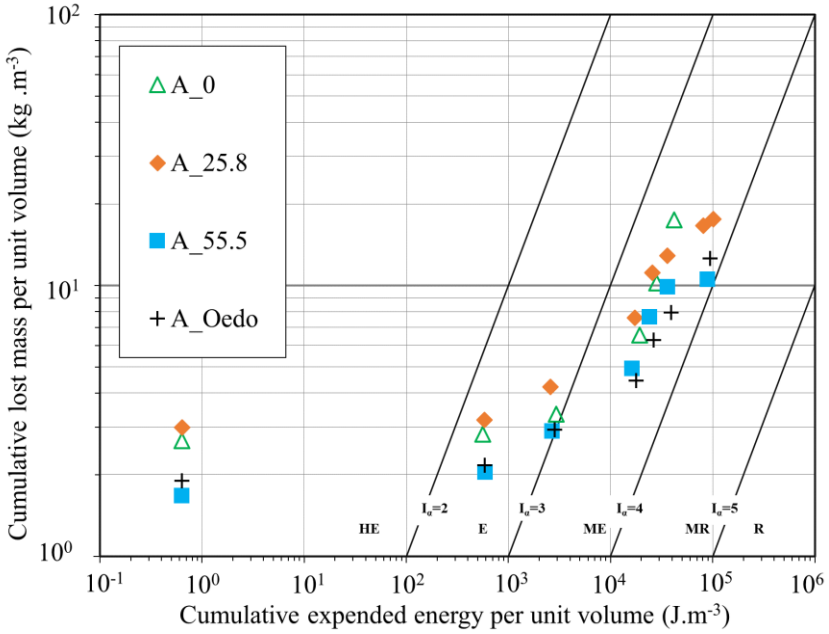

Figure_Appx. C.2 Cumulative lost mass versus cumulative expended energy, for soil A under different stress state

C.2 Test results on soil D

In the case of overfilled conditions with 40% fine content, the initial hydraulic conductivity experiences a substantial reduction when compared to the underfilled microstructures. During this phase, self-filtration emerges as the dominant process until the blow-out phase is triggered, as illustrated in the figure below.

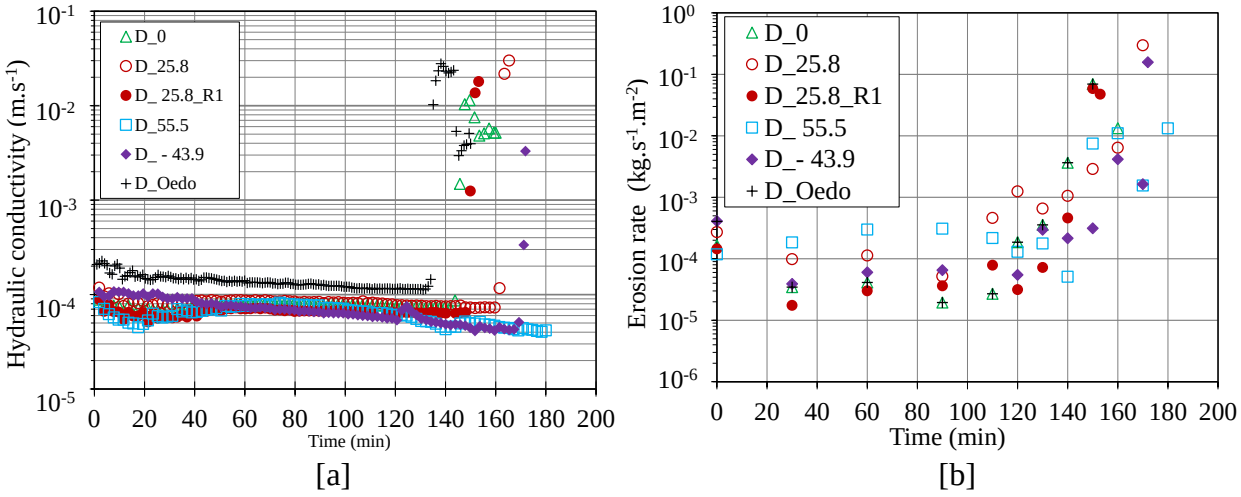

Figure_Appx. C.3 Time evolution of hydraulic conductivity [a] and erosion rate [b], for soil D under different stress state

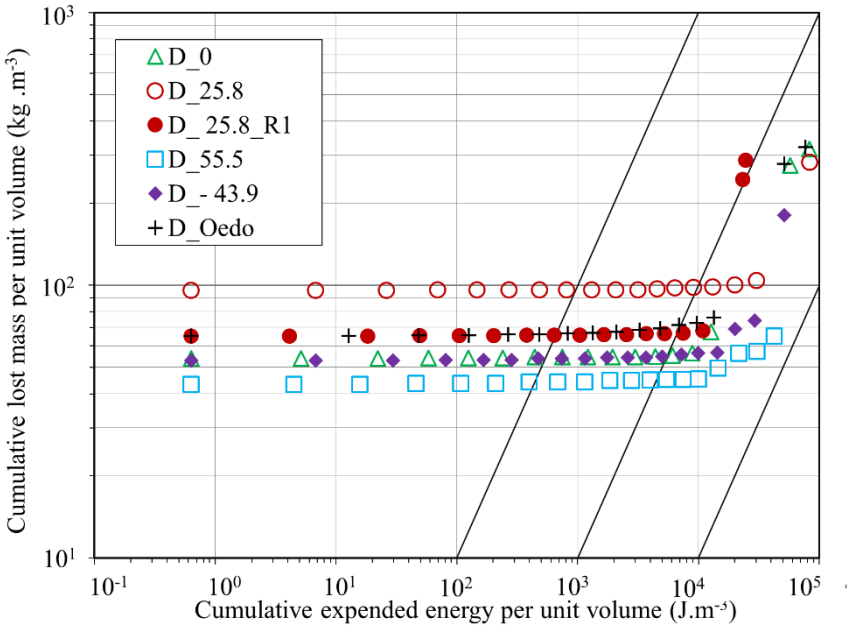

Figure_Appx. C.4 Cumulative lost mass versus cumulative expended energy, for soil D under different stress state

C.3 Triaxial consolidated drain test on soil A, B, C and D

Consolidated drained triaxial tests were conducted on all selected soils to ascertain their peak strength and to meticulously select the stress state for the suffusion tests. This selection ensures that the chosen stress state does not correspond to the condition where shear bands are incompletely developed. Notably, the soil with the lowest fine content, soil A, exhibits a high peak strength.

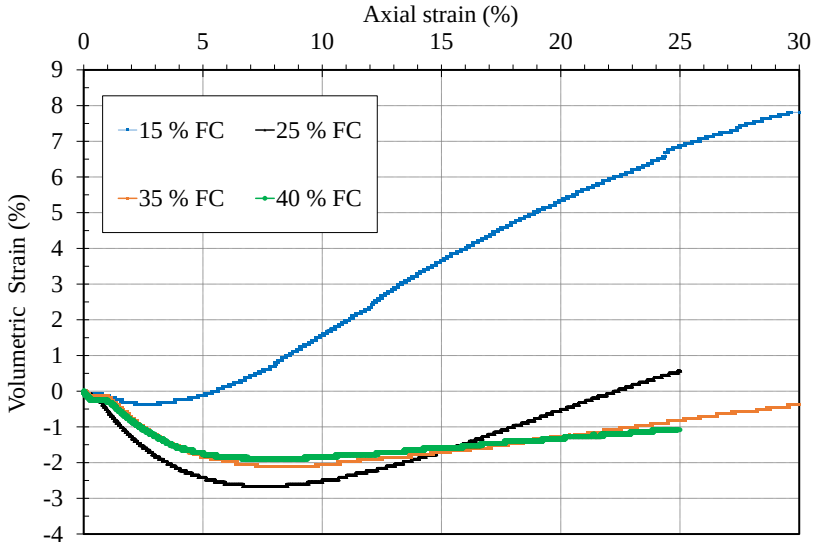

Figure_Appx. C.5 Consolidated drained triaxial test result: volumetric strain curves

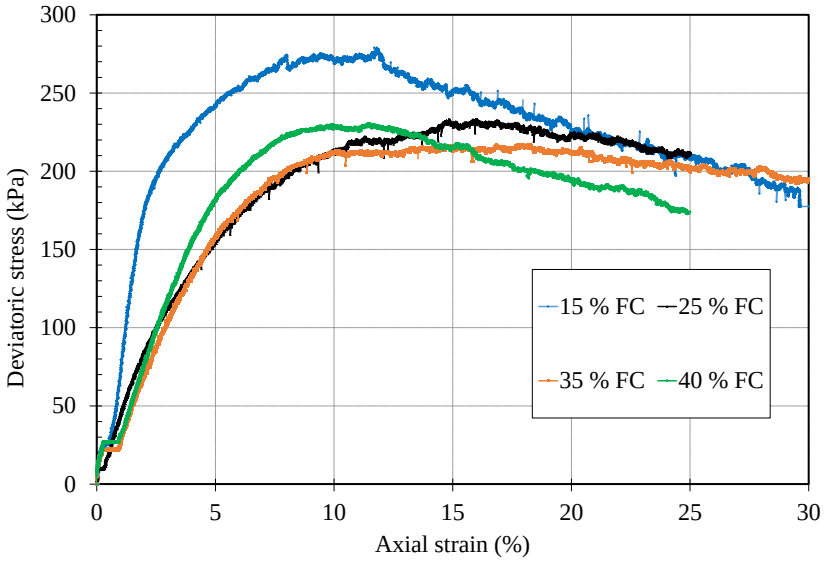

Figure_Appx. C.6 Consolidated drained triaxial test result: stress-strain curves

C.4 Experimental versus predicted Darcy velocity

This appendix contains a computation table presenting numeric values of Darcy velocities. These values are obtained through analysis, comparing experimentally observed Darcy velocities with predictions based on the formula proposed by Stéphane Côté (2010). Additionally, the appendix offers insights into the onset criteria and the conservatism of the formula.

Table_Appx. C.1 Computation of experimental versus predicted Darcy velocity at the initiation of the suffusion process

Specimen	% of sand	Pre-suffusion state		First 4 min of the test		(First k↗)			Stéphane Côté (2010)	
		Dry unit weight (kN/m^3)	Porosity (-)	Permeability (cm/s)	Darcy velocity (cm/s)	i_{SB}	Permeability (m/s)	Dacry velocity (cm/s)	Critical velocity (cm/s)	Comparison
A_55.5	15	16.77	0.367	1.000	0.100	NA		NA	0.147	OK
A_25.8	15	16.90	0.362	0.975	0.097	NA		NA	0.142	OK
A_0	15	16.57	0.375	1.064	0.106	NA		NA	0.155	OK
A_oedo	15	16.48	0.378	1.029	0.103	NA		NA	0.153	OK
B_55.5	25	17.27	0.348	0.068	0.007	0.200	7.40E-04	0.015	0.029	OK
B_25,8	25	17.03	0.357	0.052	0.005	0.200	6.82E-04	0.014	0.025	OK
B_0	25	16.83	0.365	0.058	0.006	0.200	7.50E-04	0.015	0.027	OK
B_-43.9	25	16.31	0.385	0.160	0.016	NA		NA	0.052	FAUX
B_oedo	25	16.99	0.359	0.046	0.005	0.200	7.33E-04	0.015	0.024	OK
B_55.5_R1	25	17.05	0.357	0.042	0.004	0.200	5.27E-04	0.011	0.022	FAUX
B_25.8_R1	25	16.91	0.362	0.072	0.007	0.200	9.15E-04	0.018	0.031	OK
B_-43.9_R1	25	16.50	0.377	0.165	0.017	NA		NA	0.052	FAUX
B_-43.9_R2	25	16.48	0.378	0.159	0.016	NA		NA	0.051	FAUX
B_-43,9_R3	25	16.59	0.374	0.109	0.011	NA		NA	0.041	FAUX
C_55.5	35	17.28	0.348	0.006	0.001	0.200	6.93E-05	0.001	0.007	FAUX
C_25.8	35	16.85	0.364	0.009	0.001	0.200	8.87E-05	0.002	0.009	FAUX
C_0	35	16.70	0.370	0.021	0.002	NA		NA	0.015	FAUX
C_-43.9	35	16.27	0.386	0.041	0.004	NA		NA	0.024	FAUX
C_oedo	35	16.40	0.381	0.030	0.003	NA		NA	0.019	FAUX
D_55.5	40	17.18	0.352	0.008	0.001	0.300	5.31E-05	0.002	0.008	FAUX

D_25,8	40	16.85	0.364	0.011	0.001	NA	NA	0.010	FAUX
D_0	40	16.31	0.385	0.008	0.001	NA	NA	0.009	FAUX
D_-43.9	40	16.36	0.383	0.010	0.001	NA	NA	0.010	FAUX
D_oedo	40	15.71	0.407	0.021	0.002	NA	NA	0.017	FAUX
D_25.8_R1	40	16.86	0.364	0.008	0.001	NA	NA	0.008	FAUX

D Study on influence of cyclic hydraulic paths

For the reference test MHL and tests with i0 values of 1.5 and 2.5, the occurrence of i_{MVE} was observed at a gradient of 7, following the completion of the cyclic load. In contrast, in the case of tests C_5_3.9_1 and its repeatability test C_5_3.9_1_R3, both conducted with an i_0 value of 5, i_{MVE} was observed during the first half of the applied cyclic loading path, at approximately i_{MVE} = 4, as depicted in Figure_Appx. D.1. Additionally, with an i0 value of 4, there is a transitional phase at i_{MVE} = 5. When i_0 values are below this threshold, the cyclic load exerts a minimal influence on the overall behavior compared to a reference multi-stage hydraulic loading. Conversely, when the hydraulic load exceeds this threshold during the cycle, it leads to a damage-like behavior, triggering blow-out at a hydraulic load smaller than that of the reference test.

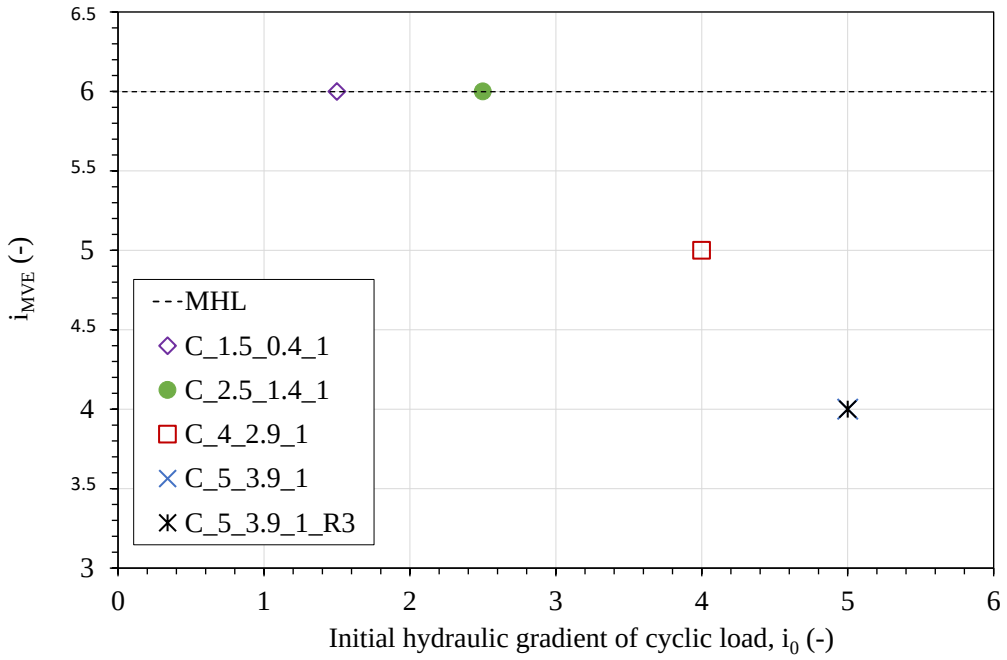

Figure_Appx. D.1 Variation in critical hydraulic gradient (i_{MVE}) with the initial hydraulic gradient of cyclic load (i_0)

Upon examining the corresponding cumulative expended energy per unit volume (referred to as E_{MVE}) at i_{MVE}, a distinct pattern becomes evident. In tests with i_0 values of 1.5, 2.5, and 4, where i_0 is far lower than threshold, the cumulative expended energy, E_{MVE}, exhibits a linear increase with the incremental initiation of the cyclic hydraulic path. However, this pattern undergoes a significant shift as i_0 approaches the threshold. Specifically, E_{MVE} demonstrates a noticeable decrease, as illustrated in Figure_Appx. D.2.

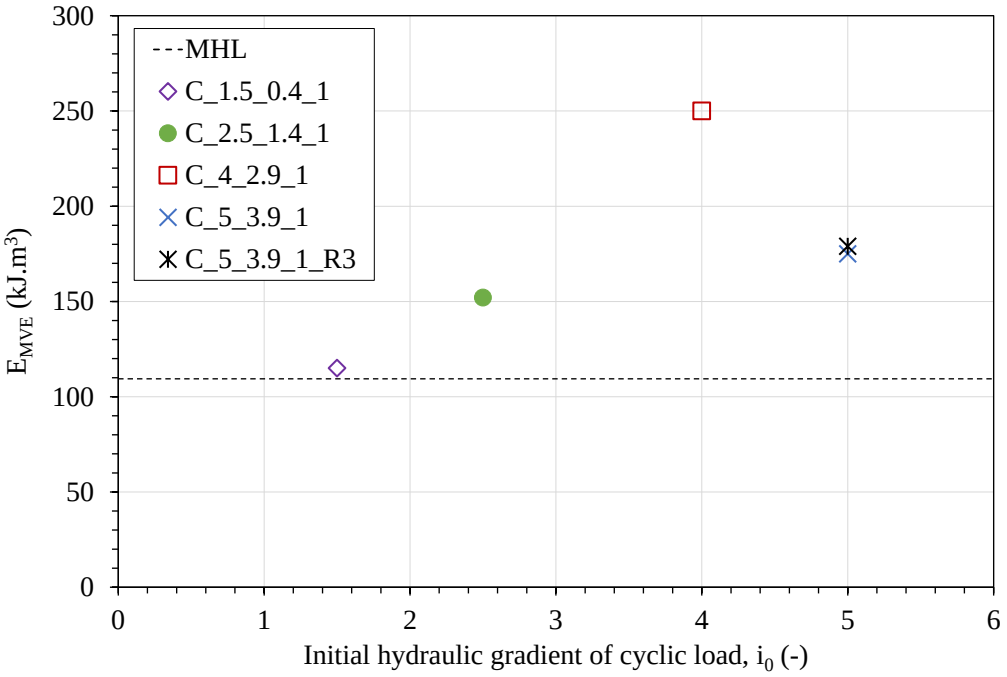

Figure_Appx. D.2 Variation in cumulative expended energy (E_{MVE}) with the initial hydraulic gradient of cyclic load (i_0)

Titre : Érosion interne dans les ouvrages hydrauliques en terre et comportement des sols sous chargements hydro-mécaniques complexes

Mots clés : suffusion, état mécanique, chargement hydraulique cyclique, approche énergétique

Résumé : La suffusion est un mécanisme d'érosion interne, impliquant le détachement, le transport et la filtration partielle des particules fines dans un sol granulaire. Il génère d'importants problèmes de maintenance pour les structures hydrauliques en terre. Cette étude analyse le phénomène de suffusion grâce à un nouveau perméamètre triaxial, permettant le contrôle précis des chargements mécaniques et hydrauliques. L'influence sur la suffusion de deux facteurs importants est étudiée : l'état mécanique, et les chargements hydrauliques cycliques. En ce qui concerne la première étude, quatre sols lacunaires sont soumis à différents états mécaniques : œdométrique, isotrope triaxial, compression triaxale et extension triaxiale. L'état œdométrique est historiquement l'état de référence. Une approche systématique est utilisée pour characteriser chaque étape du processus de suffusion : l'initiation, l'auto-filtration, le débourrage et l'état permanent ; à partir des évolutions temporelles : de la conductivité hydraulique, du taux d'érosion, de la masse érodée cumulée et de l'énergie cumulée dissipée par l'écoulement. Finalement, l'impact de l'état mécanique sur l'état permanent de la suffusion apparait limité, devant l'impact de la microstructure. Toutefois l'état oedometrique accélère l'apparition du débourrage, grâce à des chemins d'écoulements préférentiels.
Pour la seconde étude, plusieurs chargements hydrauliques cycliques sont étudés et comparés au chargement hydraulique croissant par palier, couramment utilisé. Le point d'initiation du cycle influence significativement l'initiation du débourrage.

Title: Internal erosion in soil hydraulic structures and behavior of eroded soils under complex hydro-mechanical stresses

Keywords: suffusion, stress state, cyclic hydraulic loading, energy-based approach

Abstract: Suffusion is a complex internal erosion mechanism involving the dislodgment, transport, and partial filtration of fine particles within granular soils. It poses significant challenges in the maintenance of hydraulic earth-structures. This study analysis the suffusion behavior utilizing a newly developed triaxial permeameter capable of precise control over hydraulic and mechanical conditions. The influence of two important factors on the suffusion behavior is studied: the mechanical stress state and cyclic hydraulic loadings. Regarding the first study, four gap-graded cohesionless soils were subjected to various stress states: oedometric, triaxial isotropic, triaxial compressive and triaxial tensile conditions. The oedometric stress state is historically the reference stress state. A systematic approach was employed to characterize each suffusion phases: initiation, self-filtration, blow-out and steady state, from the temporal evolution of: the hydraulic conductivity, the erosion rate, the cumulative eroded mass and the cumulative expended energy. Notably, the impact of the stress state on the steady state proved limited compared to microstructural effects, although oedometric stress conditions accelerated the blow-out phase through circumferential preferential flow paths.
For the second study, complex cyclic hydraulic loadings are studied with respect to piecewise increasing multi-stage hydraulic loadings that are commonly used. Notably, the influence of initiation point of the cyclic loading was found significant.